NUMERICAL ANALYSIS OF CONJUGATE HEAT TRANSFER FROM HEAT EXCHANGE SURFACES

by

David Alan Gardner

Submitted in accordance with the requirements for
the degree of Ph.D.
The University of Leeds, Department of Chemical Engineering,
and Department of Applied Mathematics

October 1988

ACKNOWLEDGEMENTS

It is not possible to thank all the people by name who have helped me during my research, so to all those not mentioned, I apologise and thank them.

During this work my supervisors, Professor Peter Heggs and Professor Derek Ingham have been a constant source of help, both academic and personal, and have shown great patience.

Special thanks go to Brenda Glossop who has typed this thesis under rather unusual conditions. Also, I would like to thank Professor Colin McGreavey and the S.E.R.C. for allowing me to study at Leeds and for providing the financial backing over the three years.

Finally, I would like to thank all my family and especially my parents, who have always believed in me and have given me the support I needed to finish this thesis.

Summary

Conjugate heat transfer results when there is an interaction between conduction and convection at an interface where there is a change of phase. The study of conduction and convection heat transfer has been carried out for two centuries, but they have been considered separately for most of this time.

The current work has been undertaken in an attempt to combine the effect of conduction and convection heat transfer theoretically. This involves having to derive fluid flow equations with one set of boundary conditions at the interface where heat fluxes are equated.

Several problems and geometries are studied, and results derived in one section used further to simplify other problems. The first situation considered is one in which a plane wall is heated by a well defined heat source. The wall in turn heats a colder fluid by natural convection. An integral analysis is used from which an explicit relationship for the boundary layer thickness is found.

The second problem investigates a downward projecting fin heating a fluid by natural convection. Again an integral analysis is used and several solution procedures are used depending on the assumptions used in defining the problem.

The third and fourth cases studied investigate a fin heating a fluid by mixed convection. One fin is immersed in a free fluid while the other is surrounded by a saturated porous medium.

The final problem studied looks at the plane wall, but this time two-dimensional conduction is assumed. The convection in the fluid is represented using the relationship for the boundary layer thickness found in the first problem.

LIST OF CONTENTS

Contents continued.

Contents continued. Page

Contents continued.

LIST OF TABLES

List of Tables continued

List of Tables continued

LIST OF FIGURES

List of Figures continued

List of Figures continued.

Nomenclature

A	cross-sectional or surface area	(m^2)
b	thickness of fin	(m)
Cp	specific heat capacity	(J/kg K)
d	diameter of porous material	(m)
g	acceleration due to gravity	(m/s^2)
h	heat transfer coefficient	(W/m^2K)
$I_{o, \text{ or } 1}$	Bessel function of zero or first order	
k	thermal conductivity	(W/mK)
K	permeability of porous material	(m^2)
L	length of fin	(m)
Lc	modified height of fin (see eqn. 4.39)	(m)
p	pressure	(Pa)
$\dot{Q}$	heat rate	(W)
$\dot{q}$	heat flux	(W/m^2)
T	temperature	(K)
U_o	overall heat transfer coefficient	(W/m^2K)
u	velocity in x-direction	(m/s)
U*	dimensionless velocity (eqn. 3.11)	
V	velocity in y-direction	(m/s)
WT	wall thickness	(m)
x	co-ordinate parallel to surface	
x*	dimensionless co-ordinate (eqn. 3.11)	
y	co-ordinate perpendicular to surface	

Greek Symbols

α	thermal diffusivity	(m^2/s)
β	coefficient of expansion	(/K)
β'	parameter for Bessel equation (eqn. 4.43)	

Γ	velocity term (eqn. 3.8)	(m/s)
δ	boundary layer thickness	(m)
δ^*	dimensionless boundary layer thickness (eqn. 3.11)	
ξ	dimensionless length in x-direction	
κ	ratio of thermal conductivity to heat transfer coefficient	(m)
λ	Forchheimer's coefficient $[1.75d/(150(1-\varepsilon))]$	
ψ	stream function (eqn. 2.18)	
η	similarity variable (eqn. 2.17)	
η_m	modified similarity variable (eqn. 5.16)	
ρ	density	(kg/m^3)
μ	dynamic viscosity	(kg/ms)
ν	kinematic viscosity	(m^2/s)
τ	shear stress	(N/m^2)
ε	porosity of medium	

Dimensionless Variables

CCP_m	convection conduction parameter for mixed convection ($\sqrt{\text{Re}}\, k_1 L/k_f b$)
Gr	Grashof number ($\beta g L^3 \Delta T/\nu^2$)
$\hat{Gr}$	modified Grashof number ($\lambda K \beta g (T_w - T_\infty)/\nu^2$
Gr_m	Grashof number for porous medium ($g\beta KL\Delta T/\nu^2$)
Nu	Nusselt number (hD/k)
Pe	Peclet number ($U_\infty L/\alpha$)
Pn_x	local no-slip parameter $\left(\left[\frac{K^2 \beta g (T_w - T_\infty)}{\varepsilon \nu \alpha x}\right]^{\frac{1}{2}}\right)$
Pr	Prandtl number ($\frac{Cp\mu}{k}$)
Ra	Rayleigh number (Gr.Pr)
Re	Reynolds number ($DV\rho/\mu$)

Subscripts

b	base of fin
f	fin
fl	fluid
l	liquid
ref	reference temperature
s	solid
0	interface (x=0)
∞	ambient

Constants

a_o, b_o, c_o, d_o

a_1, b_1, c_1, d_1

etc.

CHAPTER ONE

1. Introduction

Heat exchangers, both man-made and natural, can be found everywhere. The car radiator prevents an engine from overheating, whilst desert animals use an equivalent form of heat exchanger to survive. In all situations the transfer of heat between the heat source and heat sink occurs across a conjugate system. As can be seen from the above two examples the type of conjugate system can be fairly simple, in the case of the car radiator, or very elaborate, as is true for most living creatures. However, even some of the simplest systems have not been modelled accurately as solutions generally need to make a great number of assumptions before being calculated. This is because the mathematical description of the overall heat transfer must consider each element of the system, and any conjugate system is made up from a series of phases. As heat flows from one phase to the next the means by which the heat is transferred may change and this change will not always be smooth. In any problem a sudden change in a parameter will cause difficulties and heat transfer is no exception. If there is more than one interface through which the heat is transferred then the solution becomes even more difficult.

The means by which heat is transferred fall into three categories namely conduction, convection and radiation which, as already mentioned, are quite distinct from one another. Conduction heat transfer is due to the vibration of molecules being passed between adjacent points. Convection causes a fluid to move and thus a hot fluid moves to a colder area and so distributes the heat. Radiation is completely different in that the energy emitted by a hot body causes any colder body that is in line of sight to heat up provided the material is capable of accepting that energy. Convection heat transfer can be

split into two further components. Free convection is the result of fluids moving due to the temperature gradient alone, whilst in forced convection the fluid is, as the name suggests, forced to move by some external means such as a fan or pump. In all cases of forced convection some free convection will still be present and when both types of convection are of similar magnitude the type of convection is called mixed. As well as the two types of convection the flow which exists in the fluid can also be split into two parts, that is laminar and turbulent. Laminar flow is characterised by streamlines in the flow which do not mix, whilst in turbulent flow the position of one "packet" of fluid will move throughout the whole region. In the work considered here only laminar flow will be considered because efficient heat exchange equipment is often made with short elements (e.g. fins) over which only laminar flow occurs; and the modelling of the turbulent regime is very complex.

Attempts have been made to study the heat transfer over finned surfaces by both experimental [1] and theoretical means. To show the difficulties encountered, Figure 1.1 shows an early experiment involving annular fins. This figure shows a contour map of the mass transfer across a fin. The contours shown are not regular and cannot be predicted by any current model. Although this particular problem is not addressed here it graphically shows the difficulty that arises with virtually all fin problems. One of the common assumptions used in deriving heat transfer coefficients for fins is that the temperature gradient on the surface of the fin is known beforehand. In most cases this is not true but very few studies address the problem without assuming some known temperature or, a particular form of profile. It is in this area that the current research is directed and to show that the assumptions made concerning the temperature profile have

a great deal of influence on the final solution which is not desirable.

Clearly a cylinder with fins attached placed in a crossflow (which is the system used in [1]) is not an ideal problem to consider, so initially, a much simplified geometry is used. The simplest system, which contains all the features required, is shown in Figure 1.2. This consists of a constant temperature heat source with a constant heat transfer coefficient, heating a plane wall, which in turn heats a cold fluid which has a constant bulk temperature. The boundary layer marks the point where the velocity of the moving fluid adjacent to the hot wall falls to zero and so becomes part of the stationary bulk fluid. This is shown on Figure 1.2 as starting from the bottom of the wall. If the wall is colder than the bulk fluid the boundary layer would start from the top of the wall and the fluid would pass down the wall.

The region of most interest is at the interface between the plane wall and the cold fluid. Along this interface a temperature profile exists, but is not known. This is the problem encountered in all conjugate systems. In the case considered here the overall heat flow problem is simplifed as much as possible so that the cold fluid/wall interface can be studied more easily. It is the fact that a temperature profile along an interface is not known that deters many investigators. To solve a particular problem a temperature profile if not the heat transfer coefficient may be assumed. The simplest assumption to make is that the temperature and the heat transfer coefficient at the interface are constant. This greatly simplifies the calculations as the whole surface can be treated in one step. While such simplifications are very appealing the results are of dubious relevance to any practical situation. In this work temperature profiles and heat transfer coefficients are not assumed

at the interface, and so the results bear more resemblance to those that would be expected in a real situation.

By relating the heat flow through the conjugate network to the fluid flow it can be seen that the solution procedure will have to handle fluid flow equations simultaneously with the heat transfer equations. This clearly illustrates the intimate relationship between heat and fluid flow when convection is involved. Before, the need to solve the heat and fluid flow equations was avoided by using heat transfer coefficients. Whilst it seems that this is a good idea by removing complicated equations with a coefficient, it cannot be expected to result in accurate solutions. This can be illustrated by discussing some of the discrepancies which arise when heat transfer coefficients are adopted. To do this a history of the development of the concept of heat flow and how heat transfer coefficients resulted is given below.

In the seventeenth century Isaac Newton carried out a number of experiments with heated rods which were allowed to cool in air. From his observations he concluded that the heat flow was proportional to the temperature difference between the rod and the air. Thus, Newton's law of cooling is given by:

$$Q \propto (T_{rod} - T_{air}) \tag{1.1}$$

The constant of proportionality has since been given as the product of the heat transfer coefficient and the area available for heat transfer. Introducing these two parameters into equation (1.1) the following relationship can be written:

$$Q = hA\,(T_{rod} - T_{air}) \tag{1.2}$$

If a heat transfer coefficient for the whole rod is to be defined by equation (1.2) then the question arises, what value for the temperature of the rod is to be used? It cannot be assumed that the complete rod is at the same temperature, and yet some specified temperature must be given for equation (1.2) to be used. Even from this simple example it can be seen that the decision as to the temperature difference to be used in equation (1.2) is not a trivial one. In a more complicated system where several points at which the temperature could be defined exist, the choice of temperature becomes vital, and should always be specified in an answer. Such a choice is made when any heat transfer coefficient is calculated from experimental data. Therefore, when the derived heat transfer coefficient is used the temperature which was assumed initially must also be taken into account. If the same temperature difference does not exist in the new situation, how is that difference taken into account? The problem does not even disappear if the new application has the same average temperature as the initial experimental work as the way in which the temperature changes along a surface will greatly affect the heat flows. For example, an experiment is carried out to estimate a heat transfer coefficient from a plane heated wall to a fluid. In the experiment the wall is artificially maintained at $50^{o}C$. A relationship is found for the heat transfer coefficient and published. Later a designer calculates the required size of a heat exchanger which heats the same fluid as in the experimental work. The temperature down the interface varies between 0 and $100^{o}C$. Although the average temperature is the same, it would be incorrect to take the correlation found using the constant temperature surface. However, such correlations are used but usually not under such extreme conditions.

By using a given heat transfer coefficient at an interface, a conjugate problem (such as the plane wall already discussed) is decoupled. Once the system is decoupled each element (the heat source, intervening wall, and heat sink) is solved independently of the others. It is then necessary to combine the elements together again and this is usually done using the concept of the sum of resistances. Relationships for the heat flow through any one element can be written down and then equated with those for the other elements. From this an overall heat transfer coefficient can be found, for example, for the plane wall case:

$$\frac{1}{U_o A} = \Sigma R = \frac{1}{h_{hot} A} + \frac{WT}{k_w A} + \frac{1}{h_{cold} A} \qquad (1.3)$$

where U_o = overall heat transfer coefficient.

The three terms in the right hand side of equation 1.3 represent the individual resistances to heat flow on the heat source side, in the wall, and on the heat sink side respectively. By using the sum of resistance method, new temperatures can be found at the interfaces, which then give new values for the heat flow, and heat transfer coefficients, if these are dependent on temperature. This requires iterations to be carried out until calculated temperatures agree with estimated values taken at the beginning of the procedure.

The preceding discussion is valid for plane surfaces or large diameter vessels for which the effects of curvature may be ignored. The work presented in chapter three addresses this problem and compares the results found using the sum of resistance method with a solution found by considering the conjugate problem. It is also found that by using boundary layer theory in the cold fluid, variable physical

properties may be introduced. This analysis permits the properties of the fluid to change across the boundary layer, as well as in the direction of flow. This undoubtedly occurs but this effect has always been approximated. The approximation was achieved by assuming that some average temperature could be used at which all properties were calculated. The choice of this temperature can have a great affect on the final calculated heat flow.

When enhanced heat flow is required, fins may be attached to the side which has the greatest resistance to the flow of heat. A typical example is shown in Figure 1.3. The effect that attaching fins has on the heat flow has been studied previously [2], but the effect on the surrounding fluid is not so well documented when the temperature profile in the fin is not known, as was noted earlier. In the case of the plane wall it may be argued that some systems have constant temperatures, but no such argument can be put forward for fins. Therefore, analyses which use isothermal interfaces cannot be extended to fin calculations. Instead of constant temperature assumptions the heat transfer is assumed to remain constant. Harper and Brown [3] carried out an analytical study for a single fin which lost heat to the surroundings by convection alone. The results were presented using the idea of fin efficiency, η_{eff}, which they defined as:

$$\eta_{eff} = \frac{\text{heat dissipated by the fin}}{\text{heat dissipated by a fin at the same temperature as the fin base}} \qquad (1.4)$$

This work was performed in 1922, and, with the fin efficiency results produced by Gardner [4] in 1945, fin efficiencies have been determined analytically for a large range of fins provided they have constant heat transfer coefficients and constant surrounding fluid temperature.

The idea of fin efficiency and sum of resistances have been used in finding overall heat transfer coefficients for systems as illustrated in Figure 1.3. By using the electrical analogy, the resistance to heat flow is given by:

$$\frac{1}{U_o A} = \Sigma R = \frac{1}{h_{hot} A} + \frac{WT}{k_w A} + \left(\frac{1}{h_{cold} A_{surface} + \eta_{eff} h_{cold} A_{fin}}\right) \tag{1.5}$$

where $A_{surface}$ = area of the plane wall-base area of the fin

A_{fin} = area of fin

The last term on the right hand side of equation (1.5) is found by assuming that heat flow behaves like an electrical current. By making this assumption the idea of parallel resistances can be used. This method has only recently been shown to be valid by a mathematically rigorous method given by Manzoor [5]. However, the major assumption made in using equations (1.4) and (1.5) is that the heat transfer coefficients are constant. Even if this assumption were taken to be correct, the temperature difference to be used when calculating heat flow between two materials with varying temperatures is somewhat arbitrary.

In the current research the heat flow from fins is calculated in a similar way as for the plane wall. However, the constant temperature heat source, with a constant heat transfer coefficient, is replaced by a boundary condition which states that the base of the fin is maintained at a constant temperature. This then acts as the heat source from which the heat flows through the fin into the surrounding fluid. The heat flow from the fin/fluid interface is determined by solving the fluid flow equations. No assumptions need to be made

concerning the temperature of the fin, other than the base temperature. This makes the solution entirely general and hence applicable to many practical problems.

The solution for the fin problem can be extended further by considering a fin immersed in a saturated porous medium. As the fluid flow equations are employed in solving a fin immersed in a free fluid, the same procedure can be adopted. Again a base temperature is assumed to be known so that the region of interest, i.e. the fin/fluid interface, can be solved without having to couple the fin with the remainder of the heat exchanger surface.

Finally, a plane wall is examined again, but two-dimensional heat flow is assumed within the wall. The treatment of the problem is such that the wall itself is considered and the boundary conditions about it are assumed to be known. Iterations are required on the solution as the boundary layer flow must be re-calculated at every stage. The other boundary conditions are assumed to be constant.

The aim of the current research is to study the interaction between a solid and a fluid when no pre-conditions are imposed on the temperature profile at the interface. In doing this the errors introduced by making these assumptions can be investigated, and hence it can be decided whether the more complicated analysis presented here is necessary. Even if the approximations used do not produce large errors, the current research is useful in that it elucidates the complicated interaction that exists between the conduction in a solid and convection in the neighbouring fluid.

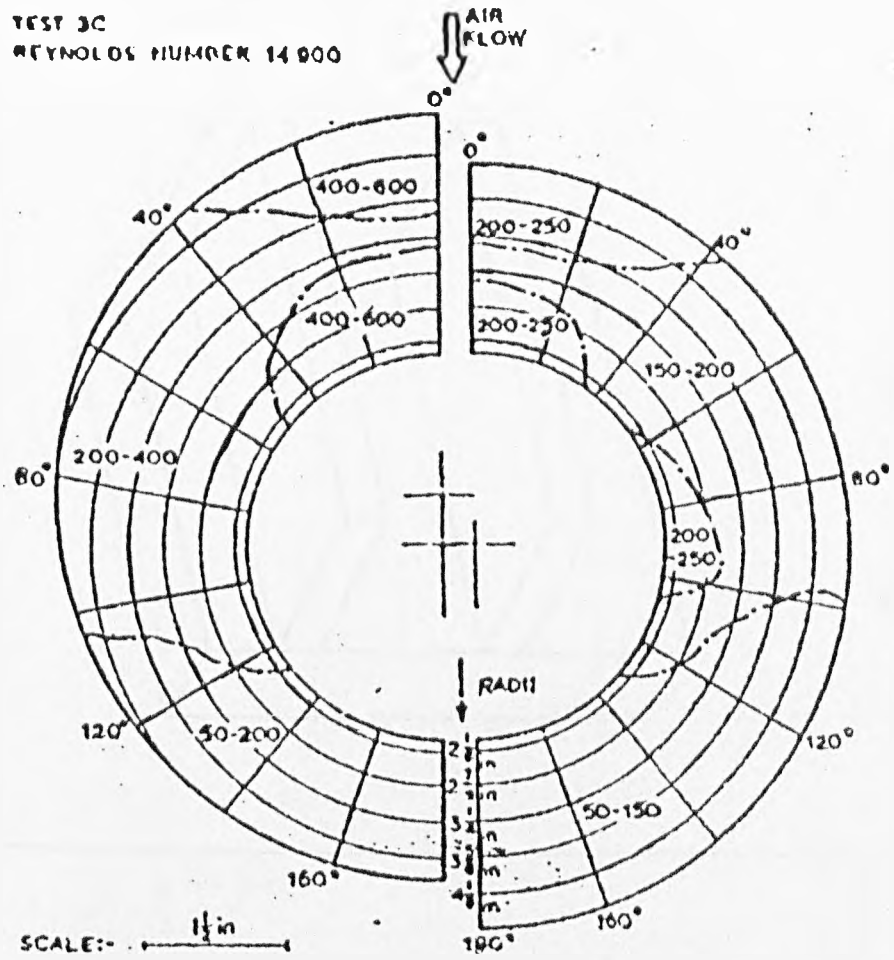

Fig. 1.1 Change of heat transfer coefficient about an annular fin

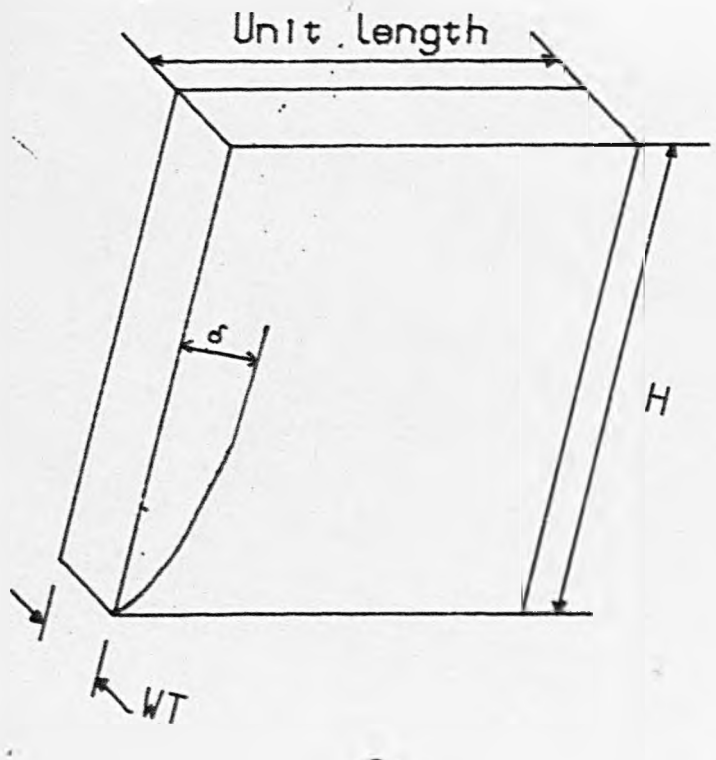

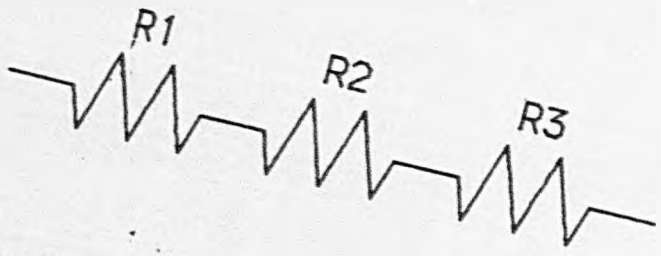

Figure 1.2 Resistance in plane wall

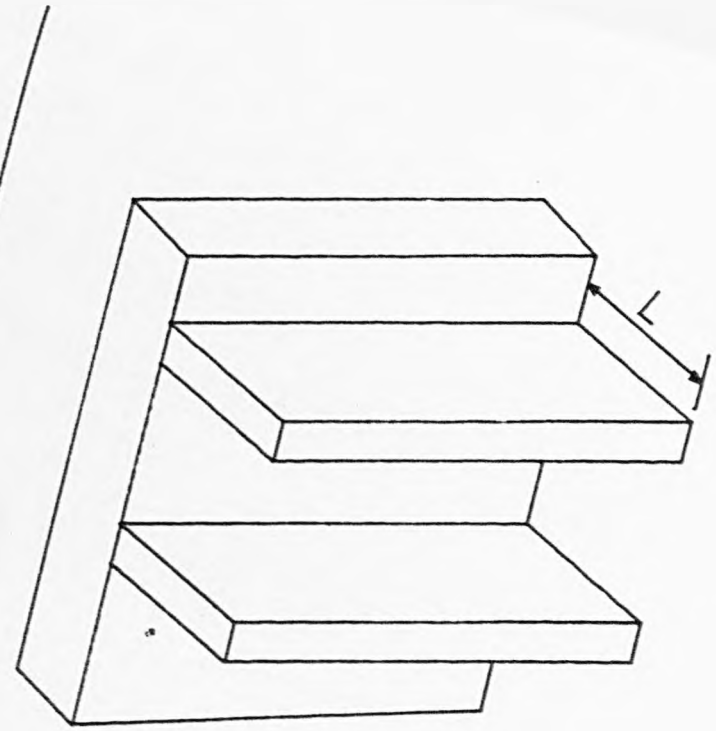

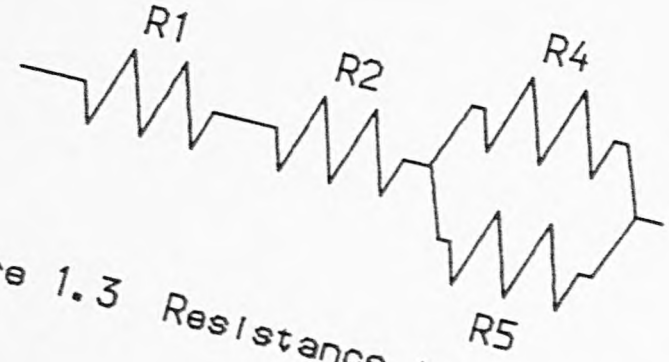

Figure 1.3 Resistance in extended surface

CHAPTER TWO

2. Review of Literature

2.1 Introduction

In this chapter the work of previous researchers will be discussed. Particular reference will be made of those studies which have moved some way to relaxing two standard assumptions, namely (i) a constant heat transfer coefficient; (ii) constant physical properties in the fluid. The value for the constant heat transfer coefficient which is used when it is assumed that (i) is true, is usually calculated by decoupling the system under investigation. This is done by ignoring all factors except those concerning the fluid being heated. The solution method which is adopted will obviously depend on the system considered (i.e. a plane surface or a fin and the boundary conditions imposed). When the heatflow is calculated for the whole system, the question is, how valid is the value for constant heat transfer coefficient already found?

The area of heat transfer from plane vertical surfaces and fins has been studied in great detail. Yet, despite all this work there is a large gap in the understanding of the heat flow between two points when the heat transfer coefficients or temperature profiles at the solid/fluid interface are not known a priori (either explicitly or implicitly in the form of a given value or a general, but known, profile).

The first section looks at how the idea of a heat transfer coefficient developed, and was then used as if it was a fundamental variable. Investigators in this area then noted that the treatment of convection problems was being oversimplified by the use of constant heat transfer coefficients and attempted to generalise the problems by introducing variable heat transfer coefficients. Whilst this went some way to representing the problem in a more realistic way the fundamental

situation of fluid flow was not being tackled.

Section 2.3 looks at boundary layer theory which developed alongside heat transfer theory. These two areas merge in the study of convection heat transfer from heated surfaces. Section 2.4 summarises the techniques available in solving this particular form of problem.

Sections 2.5 and 2.6 look at the specific problems of fins immersed in a free fluid and surfaces surrounded by a porous medium, respectively. They show how the emphasis has changed from using heat transfer coefficients to solving the fluid flow equations to find the rate of heat transfer from a hot surface.

In the last section a review is made of the problems which include the effect of variable physical properties in which calculations are made to find heat flow rates, to discover if such an exercise is just "fine tuning" for an established procedure.

2.2 Variable Heat Transfer Coefficients

The earliest work in the area of convection heat transfer was carried out by mathematicians. Perhaps the most famous, and earliest of these was Newton, who investigated the cooling of solids [6]. As a result of his work Newton wrote the following equations:

$$\dot{Q} \alpha (T_w - T_\infty) \qquad (2.1)$$

This equation shows that the heat flow from a hot body to the surroundings is proportional to the temperature difference between them. Only later was the proportionality constant given as the product of the area of the body and a factor h, now called the heat transfer coefficient. The determination of heat transfers coefficients from

experimental work has so dominated the study of heat transfer that their use has extended to areas of work that the initial assumptions did not cover. It is the use of general heat transfer coefficients which is challenged here.

In the nineteenth and early twentieth century mathematical analysis was carried out to formulate fluid flow and heat flow problems (e.g. [7], [8], [9]). It was the work by Prandtl [8], who introduced the idea of a boundary layer, which enabled later workers [10], [11], to solve the fluid flow equations and calculate heat flow rates from flat surfaces when subjected to natural or forced convection. Correlations are then found and can be expressed in terms of the Nusselt, Grashof, Reynolds and Prandtl numbers:

Forced convection $Nu = fn(Re,Pr)$

Natural convection $Nu = fn(Gr,Pr)$

These correlations are calculated at any point, x, along a surface, and they can then be integrated to find the relationship for the entire length of the surface under consideration. Unfortunately, the integrated expressions have been used, to a certain extent, to the exclusion of the relationships for point values of the Nusselt number. This way of thinking led to experimental work [12], [13] being carried out to obtain correlations for overall Nusselt numbers, rather than point values for the heat transfer coefficient. This resulted in correlations for a heat transfer coefficient for the particular system under consideration, and these correlations are then used for heat exchangers with similar geometries. The methods used for the presentation of the results suggested that the heat transfer coefficient has a single value for the entire length of a heat exchange surface.

The "re-discovery" of variable heat transfer coefficients occurred in the latter half ot the 1950's when it was recognised that the convective heat transfer coefficient is not uniform in ducts [14], [15].

Now, the treatment of variable heat transfer coefficients was different from that before, in that theoretical work started with a heat transfer coefficient as a fundamental variable, rather than deriving it as a result of more primary considerations (i.e. mass, momentum and heat balances).

A theoretical study was carried out by Han and Lefkowitz [16] to study the effect of allowing the heat transfer coefficient on the finned side of an assembly to vary. Later a similar study was carried out by Chen and Zyskowski [17]. In both these works a rectangular fin was studied (see Figure 2.1). Carrying out a heat balance on the fin, assuming a variable heat transfer coefficient along its surface, the following equation is obtained:

$$\frac{d^2T_s}{dx^2} - \frac{h(x)}{k_s b}\,(T_s - T_\infty) = 0 \qquad (2.2)$$

Both Han and Lefkowitz [16], and Chen and Zyskowski [17] assumed that the base of the fin is maintained at a constant temperature and that the fin is sufficiently long to assume that there is no heat loss from the fin tip and therefore the fin tip is adiabatic. Thus, the boundary conditions for the problem that they consider are:

$$T_s = T_o \quad \text{at} \quad x=0$$
$$\frac{dT_s}{dx} = 0 \quad \text{at} \quad x=L \qquad (2.3)$$

Even though the heat transfer coefficient is allowed to vary it is still forced to change in a particular way so that the solution may be found analytically. In [16], the change in the heat transfer coefficient is given by:

$$h(x) = h_{av} (a_1 + 1) (x/L)^{a1} \qquad (a_1 > 0) \qquad (2.4)$$

where h_{av} is an average heat transfer coefficient, which still needs to be assessed in someway. This representation of the heat transfer coefficient gives a value of zero at the fin tip. For this reason the later work of Chen and Zyskowski [17] represented the heat transfer coefficient by:

$$h(x) = h_{\infty} (1 - b_1^{-c_1 x/L}) \qquad (2.5)$$

where h_{∞} is the asymptotic value of the film coefficient as x approaches infinity. The values of b_1 and c_1 are arbitrary.

Both these problems can be solved analytically to find the heat flow, and hence the fin efficiencies. However, their use is limited to the cases when the heat transfer coefficient can be represented by the expressions given by equations 2.4 or 2.5 and when the values of h_{av}, h_{∞}, a, b_1 and c_1 are known. Thus, the problem of defining an appropriate constant value for the heat transfer coefficient is only replaced with that of defining a varying one. To overcome this difficulty it is necessary to study not the representation of a problem (which is what a heat transfer coefficient is), but the more fundamental situation. For heat transfer in a fluid we need to study fluid flow and the boundary layer theory.

2.3 Boundary Layer Theory

As already mentioned the heat transfer coefficient is a proportionality constant which is used to represent how the heat flows from a surface under complicated situations. While this is beneficial in many cases the designer of heat transfer equipment must realise that tables and charts produced using this idealisation are inherently incorrect, hence the use of 'safety factors' in final calculations. To gain an insight into the actual processes taking place in a heat transfer system then fluid flow and boundary layer theory must be studied.

Fluid flow about a surface can be described by carrying out heat, mass and momentum balances. However, if the resultant equations are not simplified a solution cannot be found [18]. By the introduction of the idea of a boundary layer [8], the infinite area of flow can be split into two distinct regions. The first, close to the surface, contains the flow of fluid in which all changes in temperature and velocity take place most rapidly; the second consists of the bulk fluid which has a constant temperature and velocity, in the case of natural convection the velocity is zero.

The temperature and velocity profiles have been investigated experimentally by many workers (e.g. [10], [19]). The first methods used fairly crude techniques which resulted in the disturbance of the boundary layer flows which were being measured [10]. Techniques are now available which enable an investigator to study the flow patterns without introducing artificial disturbances, such as laser doppler anenometry [19]. These workers have found temperature and velocity profiles for natural convection of the form shown in Figure 2.2.

The fluid and heat flow problem can be approximated by using the Navier-Stokes equation with the Boussinesq approximation. For

incompressible flow with a fluid that has constant physical properties the following set of four coupled differential equations is obtained [20].

$$\frac{\partial u}{\partial x} + \frac{\partial v}{\partial y} = 0 \tag{2.6}$$

$$u \frac{\partial u}{\partial x} + \nu \frac{\partial u}{\partial y} = - \frac{1}{\rho} \frac{dp}{\partial x} + \nu \left(\frac{\partial^2 u}{\partial x^2} + \frac{\partial^2 u}{\partial y^2}\right) - g \tag{2.7}$$

$$u \frac{\partial v}{\partial x} + \nu \frac{\partial v}{\partial y} = - \frac{1}{\rho} \frac{dp}{\partial y} + \nu \left(\frac{\partial^2 v}{\partial x^2} + \frac{\partial^2 v}{\partial y^2}\right) \tag{2.8}$$

heat transfer:

$$u \frac{\partial T_f}{\partial x} + \nu \frac{\partial T_f}{\partial y} = \alpha \left(\frac{\partial^2 T_f}{\partial x^2} + \frac{\partial^2 T_f}{\partial y^2}\right) \tag{2.9}$$

The above equations cannot be solved as they stand, despite over 200 hundred years work [18]. However, by applying the boundary layer theory to the equations (2.6 to 2.9) for the natural convection situation of a heated plate surrounded by a colder fluid, the problem can be simplified. Boundary layer theory suggests that the changes in the temperature and velocity of the fluid take place close to the solid fluid interface. This then becomes the region of interest and a scale analysis can be carried out on equation 2.5 to 2.9. If δ is the boundary layer thickness and H is the height of the solid, it is assumed that δ is very much less than H. Looking at the longitudinal momentum equation (2.7) the second differential for the velocity in the y-direction can be ignored by assessing the contribution from inertia, pressure, and friction. A similar

analysis is carried out on equation 2.8. This second analysis gives the relationship for the partial differential of the pressure in the x-direction in terms of a full differential. Combining the results of the scale analyses the boundary layer equations are given by:

$$\frac{\partial u}{\partial x} + \frac{\partial v}{\partial y} = 0 \tag{2.6}$$

$$\rho \left(u \frac{\partial u}{\partial x} + v \frac{\partial u}{\partial y}\right) = - \frac{dp}{dx} + \mu \frac{\partial^2 u}{\partial x^2} - \rho g \tag{2.10}$$

$$u \frac{\partial T_f}{\partial x} + v \frac{\partial T_f}{\partial y} = \alpha \frac{\partial^2 T_f}{\partial y^2} \tag{2.11}$$

These equations may be solved in a variety of ways and these methods will be discussed in the next section.

2.4 Solution of the Boundary Layer Equations for a Vertical Surface

In the following sections, three of the possible solution methods will be discussed. The three considered are the integral analysis, the similarity solution analysis, and numerical solution techniques. The first two were used to find solutions to general problems e.g. [21], [22], [23], but the similarity solution method is limited to a small range of boundary conditions [24], while the other two methods can be used more generally [22], [25].

2.4.1 Integral Analysis

Considering an element of fluid between an isothermal vertical surface and a plane at a distance $y=Y$ (such that $Y>\delta$, the boundary layer thickness) a momentum and energy balance can be carried out over that element (Figure 2.3). From these balances the integral

boundary layer equations for momentum and energy can be derived:

$$\frac{d}{dx}\int_0^Y u^2\,dy = -\nu\left(\frac{\partial u}{\partial x}\right)_{y=0} + g\beta\int_0^Y (T_f - T_\infty)dy \qquad (2.12)$$

energy balance

$$\frac{d}{dx}\int_0^Y u\,(T_\infty - T_f)dy = \alpha\left(\frac{dT_f}{dy}\right)_{y=0} \qquad (2.13)$$

Equations (2.12) and (2.13) can also be found by integrating equations (2.10) and (2.11) and replacing the integral of the pressure term with

$$\int_0^Y \frac{dP}{dx}\,dy = 0$$

The first time this method was used for natural convection was by Squire [21] and it was later repeated by Eckert and Jackson [22].

In all integral analyses, assumptions need to be made concerning the temperature and velocity profiles and the relative thickness of the two boundary layers (i.e. the velocity and the thermal boundary layers). In the work carried out by Squire [21] the two boundary layers were assumed to be of equal thickness, which is only true when the Prandtl number is equal to unity. He also assumed that the temperature and velocity profiles could be represented by polynomials in distance away from the surface, as this agreed well with previous experimental studies [10] and [26]. For an isothermal plate the temperature and velocity profiles were taken to be given by:

$$\frac{T_f - T_\infty}{T_o - T_\infty} = (1 - \frac{y}{\delta})^2 \qquad (2.14)$$

$$v = \Gamma \frac{y}{\delta} (1 - \frac{y}{\delta})^2 \qquad (2.15)$$

Substituting the temperature and velocity profiles (equations (2.14) and (2.15) respectively) into the momentum and energy equations (2.12) and (2.13) the Nusselt number can be predicted [21]:

$$Nu = 0.508 (Pr)^{\frac{1}{2}} (0.952 + Pr)^{-1/4} (Gr)^{1/4} \qquad (2.16)$$

Even though the approximation made by Squire concerning the boundary layer is only true when Pr=1, it is, in fact, found that results for the Nusselt number agree well with exact solutions over a wide range of the Prandtl number [27].

2.4.2 Similarity Solution

This technique is a result of realising that as a boundary layer grows the profiles between two points are similar (see Figure 2.4). In the case of natural convection over a vertical surface the parameter relating the profiles is given by [28].

$$\eta = \frac{x}{y} Ra_y^{1/4} \qquad (2.17)$$

where η is the similarity variable. The idea of a similarity solution was used by Pohlhausen [11] for the forced convection case. Ostrach [28] studied the natural convection situation in which a stream function is introduced. The stream function, ψ, is defined by the following equation:

$$u = \frac{\partial \psi}{\partial y}, \quad v = -\frac{\partial \psi}{\partial x} \tag{2.18}$$

where $\psi = \alpha \, Ra_y^{1/4} \, F(\eta, Pr)$

which automatically satisfies the continuity equation (2.6).

When using the stream function the boundary layer equations become:

$$\frac{3}{4} F \theta' = \theta'' \tag{2.19}$$

$$\frac{1}{Pr} \left(\tfrac{1}{2} F'^2 - \frac{3}{4} F F'' \right) = -F''' + \theta \tag{2.20}$$

Where primes denote differentiation with η.

These two equations can then be solved with the appropriate boundary conditions (which includes the assumption of a constant wall temperature).

It has been shown by Yang [29] that there is a limited range of the wall temperature profiles for which the similarity solution can be used. If none of these similarity profiles are appropriate for a particular problem then a solution cannot be found using the idea of similarity. When the similarity solution is used to find the heat flow from an isothermal wall the relationship between the Nusselt number and the Rayleigh number is given by:

$$Nu = 0.503 \, Ra_y^{1/4}, \text{ for } Pr \to \infty \tag{2.21}$$

$$Nu = 0.6 \, (Ra_y \, Pr)^{1/4}, \text{ for } Pr \to 0 \tag{2.22}$$

This can be compared with equation 2.16, the result found when using the integral analysis. Even though the integral analysis is only strictly true for a Prandtl number of one, and hence approximate near Pr = unity, the agreement between the values of the Nusselt number

given by equations (2.21) and (2.22) extends over a much wider range than might be expected.

2.4.3 Numerical Analysis

The two previously described solution methods provide accurate solutions for the situations when the temperature or heat flux are prescribed at the wall/fluid interface. However, they are not always able to solve the more specialised problems. For example, some problems contain boundary conditions which do not allow a similarity solution to be used, or employ fluids, such as liquid metals, which have Prandtl numbers varying significantly from unity.

With the advent of easily accessible powerful computers, numerical methods are utilised to solve heat transfer problems which contain more realistic, and hence more complicated, boundary conditions. Solutions can also be found for fluids that have Prandtl numbers which vary significantly from unity.

The full boundary layer equations (2.6, 2.10 and 2.11) are employed in numerical solution procedures. The method by which these equations are transformed into a suitable representation depends on the numerical technique to be employed. Possible methods are finite difference, finite element, boundary integral method, series truncation and collocation.

As already mentioned, the advantage of numerical methods is that once the equations for the fluid and heat flow have been formulated the boundary conditions can be changed to study very specific problems. For example, Kishinami and Seki [30] look at a numerical solution of an unheated vertical plate above an isothermal plate to study the effects of the plate-fluid thermal conductivity ratio. Also,

Suriano and Yang [31] looked at an isothermal fin to study the momentum and energy fields at a large distance from the solid/fluid interface for a range of Rayleigh and Prandtl numbers.

The effects of immersing a vertical surface in a porous medium has also been studied numerically, for example, [32], and will be discussed separately in section 2.6.

Numerical analysis can be used to study a wide variety of problems (e.g. [33]), and details of the pertinent works will be covered in detail in later chapters when used to compare the current research with immediately preceding studies of other investigators.

2.5 Solution of Heat Transfer From a Downward Projection fin in a Free Fluid

The first investigations in this area treated this problem as one of conduction with a convective boundary condition. This boundary condition can either be considered as a constant value [4] or as a pre-defined varying quantity [34], as discussed in section 2.2.

The first significant advance away from prescribing the heat transfer coefficient was proposed by Lock and Gunn [35]. In this work the authors assumed that a particular temperature profile existed along the fin, such that,

$$\theta_w = \theta_b \left(\frac{x}{L}\right)^n \quad (n > 0) \tag{2.23}$$

This profile was chosen so that the general similarity solution could be used. However, in the case of a fin used for any practical purpose it is normal to have a short fin, which means that the fin tip will not reach the same temperature as the surrounding

ambient fluid, which is the case in the paper by Lock and Gunn [35]. Later Kwon and Kuehn [36] also looked at the conjugate nature of heat transfer from a fin. They tackled the problem by solving the governing fluid flow equations numerically. Again, however, their boundary conditions assumed an infinitely long fin so that the fin tip temperature approached that of the surrounding ambient fluid. This particular area of research was extended by Tolpadi and Kuehn [37] to consider transerve fins, but infinitely long fins were used once again. Details of these studies will be discussed in the relevant chapters later.

2.6 Surfaces Immersed in a Porous Medium

The empirical law governing the isothermal vertical flow of water at low flow rate through a porous medium was first stated by Darcy [38]. When the Rayleigh number is sufficiently large there exists a thin boundary layer [39], as with flow about a surface in a free fluid. Under these conditions, boundary layer approximations can be made and an order of magnitude estimate results in the following equations [40]:

$$\frac{\partial u}{\partial x} + \frac{\partial v}{\partial y} = 0 \tag{2.24}$$

$$u = -\frac{K}{\mu}\left(\frac{dp}{\partial x} - \rho_{\infty} g\beta\,(T_f - T_{\infty})\right) \tag{2.25}$$

$$\frac{dp}{dy} = 0 \tag{2.26}$$

$$u\,\frac{\partial T_f}{\partial x} + v\,\frac{\partial T_f}{\partial y} = \alpha\,\frac{\partial^2 T_f}{\partial y^2} \tag{2.27}$$

Similarity solutions can be obtained when the wall temperature is prescribed as a power function of distance [41]. When the surface heat flux is prescribed, solutions can be found by a simple transformation of variables [42].

Work has been carried out to investigate the effects of the no-slip boundary condition, non-Darcian flow and thermal dispersion (e.g. [43], [44], [45]). However, in the current study only flows when Darcy's law hold are considered, and this is justified for the conditions investigated.

Only in 1986 have papers been written concerned with fins immersed in porous media [46], [47], [48]. Previous to this, the work on plane surfaces in a porous medium had to be adapted as best as possible when calculating heat flows from fins.

2.7 Variable Physical Properties

In natural convection heat transfer the flow present only occurs due to the change of density of a fluid with temperature. This change is usually the only variation of properties considered when looking at natural convection heat transfer. However, variation in properties for forced flow has been considered for some time [49], [50], [51]. The earliest theoretical work for natural convection was carried out by Hara [52] for air.

When calculating physical properties the average bulk temperature is usually used to evaluate all properties, which are then fixed at that value. However, other values for the reference temperature can be used. In the works of Sparrow and Gregg [53], and Minkowycz and Sparrow [54], a new reference temperature at which to evaluate physical properties was proposed.

The main thrust of research work has investigated the effects of variable viscosity. Perturbation solutions have been obtained for a variety of geometries and boundary conditions including a uniform flux wall [55]. Experimentally, Clausing and Kempka [56] have investigated variable property effects in nitrogen, but found virtually no influence in the laminar flow region. Further to this Clausing [57] has produced empirical relations for convective heat transfer from vertical isothermal surfaces to gases.

The interest in investigating variable physical properties is somewhat limited due to the idea that such an exercise only fine tunes a particular method [58]. However, this statement is never proven but merely stated as a belief. It is one of the aims in this research to investigate the effects of variable physical properties more methodically and so establish whether ignoring property changes with temperature provide sufficiently accurate solutions.

$$q = h(x)\ A(T-T_{\infty})$$

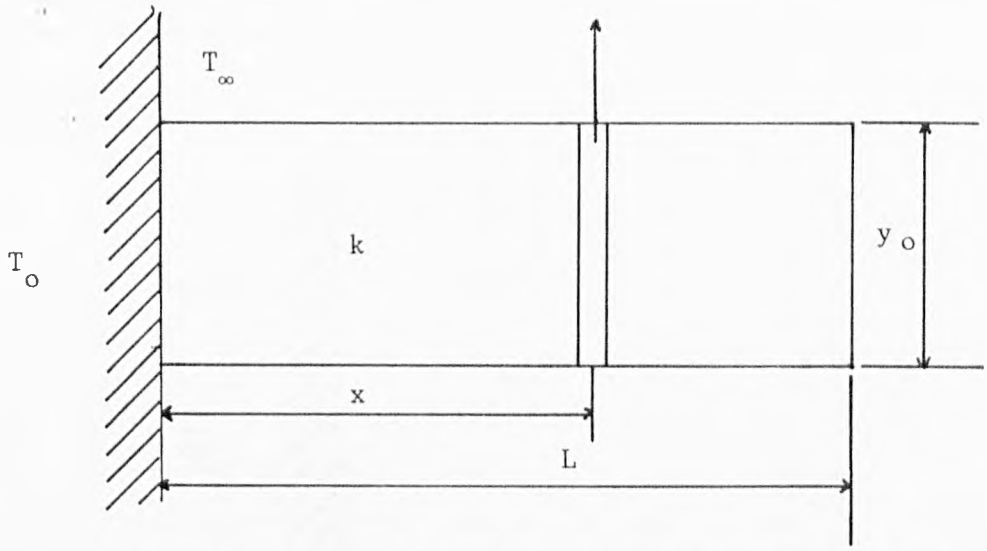

Fig. 2.1 Heat flow from a fin with a variable heat transfer coefficient

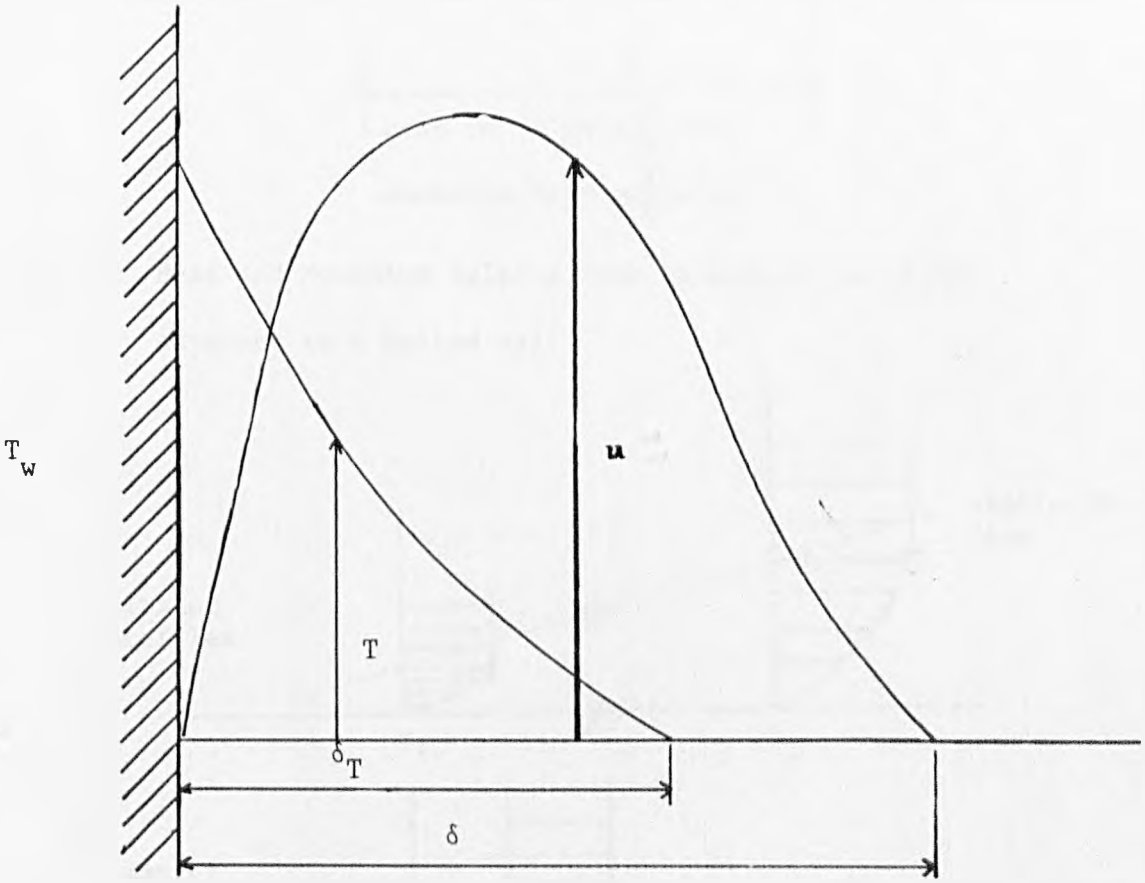

Fig. 2.2 Boundary layer profiles

heat out = $Cp\ \rho \int_0^Y u\theta\, dy + Cp\rho \frac{d}{dx} (\int_0^Y u\theta dy)\ \Delta x$

momentum out = $\rho \int_0^Y u^2\, dy + \rho \frac{d}{dx} \int_0^Y u^2 dy)\ \Delta x$

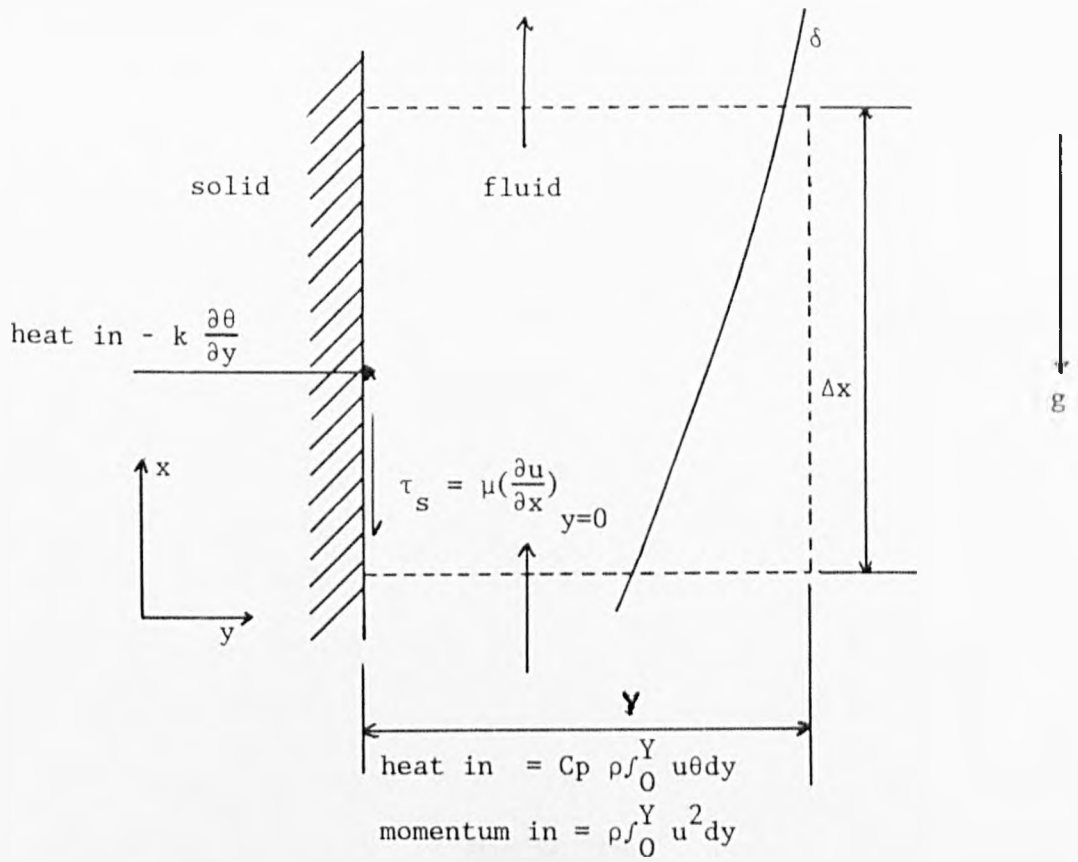

Fig. 2.3 Heat and Momentum Balance Over an Element in fluid Adjacent to a Heated Wall

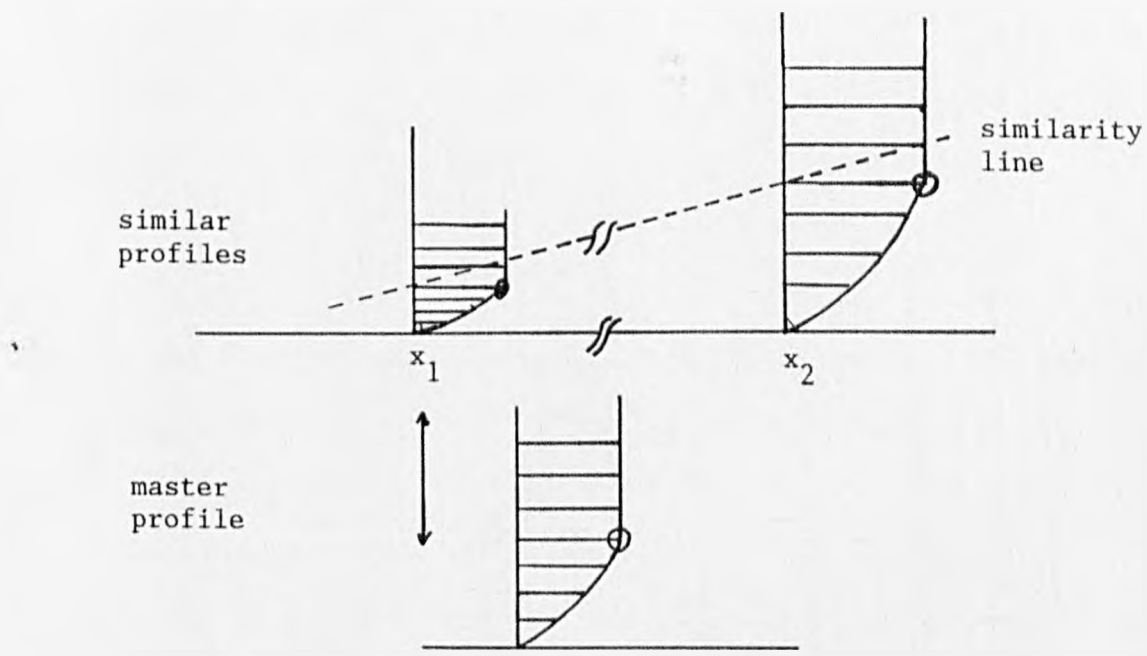

Fig. 2.4 Similarity Profiles for Boundary Layers

CHAPTER THREE

3. Natural Convection Heat Transfer from a Plane Vertical Surface with One-Dimensional Conduction

3.1 Introduction

This chapter investigates the heat flow through an indirect heating system. All indirect heating systems consist of a hot medium (heat source) an intervening wall and a cold fluid (heat sink). One particular arrangement is a hot fluid with a constant heat transfer coefficient heating a plane wall, which heats a cold fluid with a constant bulk temperature. If the cold fluid is not forced past the wall, heating occurs by natural convection (Figure 3.1).

The first direct solution for heat transfer by natural convection, in the laminar regime, was obtained by Schmidt and Beckman [10]. Since this, many investigations have been carried out utilising other solution methods which have allowed more practical situations to be considered.

A common example of heat transfer by natural convection which can be seen in everyday life is that of a radiator. Also on plant sites, the heat loss from pipework and vessels will need to be calculated. Free convection flows may also result from centrifugal forces, as in hollow gas turbine blades, as well as from gravitational forces. Increasingly more important is the heat dissipation from electronic equipment, which often falls into the area of natural convection heat flow.

The present solution technique considers the conjugate problem of a non-isothermal wall with a boundary layer on one side, for which the fluid considered can either have constant or variable physical properties. The boundary condition on the hot side of

the wall is that of a fluid at a known temperature with a constant heat transfer coefficient, although other boundary conditions could be used depending on the system being solved.

Non-isothermal walls have been studied using finite difference methods [59]. Integral solutions have been obtained [60], [61], [62] and similarity solutions found for the non-isothermal plate [63], [64]. For a smooth arbitrary temperature profile a technique has been developed which uses local similarity as a first approximation, and this is corrected by universal functions [65].

In all the aforementioned references a decoupling of the system occurs. In the work by Miyamoto et al [66], the system has a temperature or heat flux imposed on only one side of the wall, so that axial heat conduction can be studied. In this problem conjugate heat transfer is studied but the heat flow through a complete system is not investigated.

Kelleher and Yang [67] have looked at conjugate heat transfer in a heat generating slab. More recently Lock and Ko [68] and Anderson and Bejan [69] have looked at the coupling of convective systems through a wall. In [68] the wall thermal resistance is considered negligible, and in [69] the solution is dependent on the symmetry of the problem.

The integral analysis is used to find the heat flow and boundary layer thickness. Although the solution is only strictly valid for a Prandtl number of one an approximate solution can be obtained for fluids which have Prandtl numbers over a wider range. The two fluids considered in this chapter are air and water which both have Prandtl numbers which lie within a suitable range so that the integral analysis may be used.

For comparison, the heat flow is also found by using the integral analysis method, which assumes that the wall surface is at a constant temperature so that the conjugate nature and the effect of variable physical properties can be studied.

The height of the wall is restricted such that only the laminar regime of the natural convection flow is considered.

3.2 Statement of the Problem

In this problem the Navier-Stokes equations can be reduced to the standard boundary layer equations. These in turn can be integrated to give the integral boundary layer equations. An alternative path to the same equations is to study an elemental height across the boundary layer formed on the cold side of the system (see Figure 2.3). It is assumed that there is no heat loss by radiation from the surface of the wall to the surrounding fluid. The resulting equations are:

heat balance:

$$k_{fo} \left(\frac{\partial T_f}{\partial y}\right)_0 = \frac{d}{dx} \int_0^{\delta} (\rho Cp\ u\ (T_\infty - T_f))dy \qquad (3.1)$$

momentum balance:

$$\frac{d}{dx} \int_0^{\delta} \rho u^2 dy = -\mu_o \left(\frac{\partial u}{\partial y}\right)_0 + g(\delta\ \rho_\infty - \int_0^{\delta} \rho\ dy) \qquad (3.2)$$

To solve these integral equations the temperature and velocity profiles in the fluid need to be known. The form of the profiles used here are the same as those adopted by Squire [21] and later by Eckert and Jackson [22] who found that the profiles fitted the experimental data well. The profiles are polynomials in the y-direction,

the distance from the surface of the wall into the fluid being heated.

$$T_f - T_\infty = a_o + b_o\, y + c_o y^2 \tag{3.3}$$

$$u = a_1 + b_1\, y + c_1\, y^2 + d_1\, y^3 \tag{3.4}$$

Constants, a_o, b_o, c_o, a_1, b_1, c_1 and d_1 are found by using boundary conditions at the outer edge of the boundary layer, and at the wall.

The first boundary condition for the temperature profile is a result of carrying out a heat balance between the hot fluid and the cold fluid/wall interface. This boundary condition assumes that there is one-dimensional heat flow in the y-direction in the wall and that there is a constant heat transfer coefficient on the hot side. An overall heat transfer coefficient, U_o, is used in the boundary condition. This includes the contribution to the resistance to heat flow from the heat source and the wall.

The other two boundary conditions are those used by previous investigators and show that the temperature of the cold fluid falls to the ambient temperature at the boundary layer, and also, the temperature gradient at this point is zero.

$$\begin{aligned} -k_f \frac{\partial T_f}{\partial y} &= U_o (T_1 - T_f) \quad : \quad y=0;\ 0 < x < \infty \\ T_f &= T_\infty \quad : \quad y=\delta;\ 0 < x < \infty \\ \frac{\partial T_f}{\partial y} &= 0 \quad : \quad y=\delta;\ 0 < x < \infty \end{aligned} \tag{3.5}$$

where $\frac{1}{U_o} = \frac{1}{h_{hot}} + \frac{WT}{k_w}$

The boundary conditions for the velocity profile are again those used by previous investigators and state the no slip condition at the wall, and that the velocity and velocity gradient are zero at the edge of the boundary layer. As there are four unknowns in the expression for the velocity profile and only three boundary conditions, the final profile contains an unknown value Γ. It is this term which will be found, along with the boundary layer thickness, when the final equations are solved, rather than the velocity itself. However, a simple substitution at the end of the calculations will provide the velocity profile.

$$\begin{aligned} u &= 0 \quad : \quad y = 0;\ 0 < x < \infty \\ u &= 0 \quad : \quad y = \delta;\ 0 < x < \infty \\ \frac{\partial u}{\partial y} &= 0 \quad : \quad y = \delta;\ 0 < x < \infty \end{aligned} \tag{3.6}$$

Substituting the temperature boundary conditions (3.5) into the temperature profile and the velocity boundary conditions (3.6) into the velocity profile results in the following relationships:

Temperature profile:

$$\frac{T_f - T_\infty}{T_1 - T_\infty} = \frac{(y-\delta)^2}{\frac{2k_f}{u_o} + \delta} \tag{3.7}$$

Velocity profile:

$$u = \Gamma \frac{y}{\delta} \left(1 - \frac{y}{\delta}\right)^2 \tag{3.8}$$

The condition that has changed in the current study as compared with previous work, is the first boundary condition for the temperature

profile (equation 3.5). This introduces the term $2k_f/U_o$ in the expression for the temperature profile. It compares the resistance to heat flow presented by the fluid to that of the wall and heat source with the constant heat transfer coefficient.

If the term $2k_f/U_o << \delta$ then equations (3.1) and (3.2) reduce to those given by Squire [21], which is the solution of an isothermal wall at the same temperature as the heat source. When $2k_f/U_o >> \delta$ then the equations can be solved analytically as the problem becomes that of a plane wall only, as the resistance to heat flow on the fluid side is negligible. However, the expression for the boundary layer thickness changes and cannot be given by an analysis which does not consider the conjugate nature of the problem. The expression for the boundary layer thickness is found to be:

$$\delta = \left[\frac{180\alpha\ (28\alpha + 35\nu)}{\lambda}\right]^{1/5} \quad x^{1/5} \qquad \text{(A1.12)}$$

$$\text{where} \quad \lambda = \frac{35g\ \beta\ (T_1 - T_\infty)}{2k_f/U_o}$$

The means by which this is found is given in Appendix 1.

If a problem is considered in which either limit will give a satisfactory approximation then the more complicated analysis will not be required. It is therefore necessary to determine the likely values of the pertinent parameters.

For air the boundary layer thickness is typically of order 10^{-2} metres, and for water 10^{-3} metres. If the heat source is considered to be condensing steam, the heat transfer coefficient will be approximately 6000 W/m^2K. In this case, for air the value of $2k_f/U_o$ is found to be 9×10^{-6}, when using a steel wall, and 2×10^{-4} for water. Thus, for the air situation the resistance to

heat flow occurs mainly on the right hand side of the wall and a good approximation can be made by using the analysis for an isothermal wall. However, this is not the situation when water is being heated. If there is a low heat transfer coefficient on the hot side of the wall the isothermal assumption cannot be used even when air is being heated.

Therefore, it is necessary to consider the problem when the two terms in the denominator of the temperature profile are of comparable magnitude, as this situation will arise under many practical situations.

3.3 Possible Solution Techniques

By substituting the temperature and velocity profiles (equations 3.7 and 3.8) into the heat and momentum balance (equations 3.1 and 3.2) and carrying out the integrations the following expressions for the resultant heat and momentum balances are found:

$$\frac{1}{30} \frac{d}{dx} \left(\frac{\Gamma \delta^2}{2 \frac{k_f}{U_o} + \delta} \right) = \frac{2\kappa}{2 \frac{k_f}{U_o} + \delta} \qquad (3.9)$$

momentum balance;

$$\frac{1}{105} \frac{d}{dx} (\rho^2 \delta) = \frac{g \beta (T_1 - T_\infty) \delta^2}{2 \frac{k_f}{U_o} + \delta} - \nu \frac{\Gamma}{\delta} \qquad (3.10)$$

At this point Squire [21] and Eckert and Jackson [22] substituted in values for the boundary layer thickness, δ, and the velocity term, Γ, which were expressed in terms of the height up the wall,

to find the solution. However, if this were to be done with the current equations a solution could not be found due to the presence of the term $2\ k_f/U_o$ which appears in the denominator of both the heat and momentum balance.

To study the problem further the heat and momentum balances are reduced to two coupled ordinary differential equations. First, the following substitutions are made so that dimensionless variables can be used:

$$U^* = \Gamma \frac{2\ k_f/U_o}{\nu}$$

$$x^* = \frac{x}{2\ k_f/U_o} \qquad (3.11)$$

$$\delta^* = \frac{\delta}{2\ k_f/U_o}$$

Introducing the above variables into the heat and momentum balances (equations 3.9 and 3.10 respectively) and then carrying out the differentiations two simultaneous equations are obtained. These can then be reduced to the following two coupled non-linear ordinary differential equations.

$$\frac{d\delta^*}{dx^*} = \frac{(1+\delta^*)(105Pr + 120)}{\delta^* U^* (3+\delta^*)} - \frac{105\ Gr\delta^{*2}}{U^{*2}(3+\delta^*)} \qquad (3.12)$$

$$\frac{dU^*}{dx^*} = \frac{105\ Gr\delta^*(2+\delta^*)}{U^*(3+\delta^*)(1+\delta^*)} - \frac{105Pr(2+\delta^*)+60(1+\delta^*)}{\delta^{*2}\ (3+\delta^*)} \qquad (3.13)$$

These equations cannot be solved analytically due to the non-linearities which are inherent in the problem. However, there

UNIVERSITY LIBRARY LEEDS

are several possible methods by which these equations can be solved. The one chosen for the current problem is a Runge Kutta 4 method with the error checking procedure of Merson. This results in equations correct to the fourth differential in the Taylor expansion. This method is accurate to order (h^5) and also reduces the step length at any point where the required accuracy is not reached. This latter property is particularly useful in the current problem as a singularity occurs at the point x=0, and many steps are required to obtain an accurate solution near this position.

On solving the two differential equations the temperature and velocity profiles can be found using equations (3.7) and (3.8) respectively.

The heat flux is defined using the temperature gradient at the solid/fluid interface (on the right hand side of the wall):

$$\dot{q} = -k_{fo} \left(\frac{\partial T_f}{\partial y}\right)_{y=0} \tag{3.14}$$

Using equation (3.7) the heat flux can be written as:

$$\dot{q} = \frac{2\ k_{fo}\ \Delta T}{\frac{2\ k_f}{U_o} + \delta} \tag{3.15}$$

Again the term $2\ k_f/U_o$ occurs showing the importance of the conjugate nature of the problem. The expression for the heat flux obtained from the current analysis can be compared with the heat rate found by Squire [21]:

$$\dot{Q} = \frac{2\ k_f\ \Delta T}{3.93\ Pr^{-1/2}\ (0.952+Pr)^{1/4}\ \left(\frac{g\beta\Delta T}{\nu^2}\right)^{1/4}}\ \frac{4}{3}\ \left[x^{3/4}\right]_x^{x_{end}} \tag{3.16}$$

In [21] the boundary layer thickness, δ, is obtained explicitly in terms of the Prandtl and the Grashof numbers, whilst in the current analysis the value for the boundary layer thickness is only found after carrying out the numerical analysis.

In previous solutions, where it is assumed that the physical properties are constant, it must be stated at what temperature the value for the properties is calculated. The first solution methods used an average bulk temperature, and later research investigated the possible alternatives in a more rigorous manner, as discussed in the review of literature. However, by using any fixed temperature at which to evaluate the physical properties of the fluid under investigation, errors will be introduced. If the variation of properties is introduced directly into the solution procedure no approximation will take place. The variation of physical properties can be incorporated directly into the governing equations (3.1) and (3.2). To do this the change of all properties with temperature are represented using polynomials in temperature. Actual values of the properties are taken and a least squares fit is used for each parameter so that the three coefficients can be found for each of the quadratic expressions:

$$\begin{aligned} \rho &= a_o + a_1 T + a_2 T^2 \\ Cp &= b_o + b_1 T + b_2 T^2 \\ k_f &= c_o + c_1 T + c_2 T^2 \\ \mu &= d_o + d_1 T + d_2 T^2 \end{aligned} \qquad (3.17)$$

Substituting (3.17) into equations (3.1) and (3.2) new energy and momentum balances can be obtained in which the leading terms

comprise the first constants in the polynomials and the smaller subsequent terms are the products of all three terms for density and heat capacity.

The resulting equations are somewhat cumbersome but the treatment of them follows exactly the same procedure as that for the constant physical property case, once appropriate substitutions have been made. For that reason their analysis is only produced in Appendix 2, but the results are shown along with the results for the constant physical property situation, so that a comparison can be made to see if the introduction of variable physical properties is justified.

3.4 Solution Procedure

To solve the coupled ordinary differential equations (3.12, 3.13) the Runge Kutta Merson 4 method is used, which is a "marching" procedure. For such a method a starting solution is required at the base of the wall. However, at the base of the wall, where $x^*=0$, then $\delta^*=0$ also. Studying the two coupled equations to be solved, (3.12, 3.13) a singularity at $x^*=0$ is noticed. The solution procedure therefore needs to be started a small distance away from the singularity and a starting solution needs to be found at this new position. Equations (3.9) and (3.10) on eliminating the terms which are negligible near $x^*=0$ and introducing the dimensionless variables, become:

$$\frac{d}{dx^*}\ (U^{*2}\delta^*) = 105\ Gr\delta^{*2} - 105\ Pr\ \frac{U^*}{\delta^*} \qquad (3.18)$$

$$\frac{d}{dx^*}\ (U^*\ \delta^{*2}) = 6 \qquad (3.19)$$

The method adopted by Squire [21] was used to find expressions for the boundary layer thickness term and the velocity term in order to start the solution procedure. For this a profile for the boundary layer thickness and the velocity are assumed such that:

$$\delta^* = a_o \, x^{*a_1}$$
$$U^* = b_o \, x^{*b_1} \tag{3.20}$$

These profiles are substituted into the equations (3.18) and (3.19), and the exponents and coefficients of x^* are equated. This gives the values for a_o, b_o, a_1 and b_1:

$$\delta^* = \left[\left(\frac{48+60Pr}{Gr}\right) x^*\right]^{1/5} \tag{3.21}$$

$$U^* = 60 \left(\frac{48+60Pr}{Gr}\right)^{-2/5} x^{*3/5} \tag{3.22}$$

It should be noted that the above profiles are the same as those obtained in the case for a constant heat flux wall [70]. This is due to the assumption that $\delta^* << 1$ near the base of the wall, which results in a decoupling of the problem, such that the heat flow is nc. longer dependent on the growing boundary layer thickness and thus there is a constant heat flux at the wall/fluid interface.

To find the heat flux through the system, numerical integration using Simpson's method is used. The number of nodes required to calculate the heat flux is found by increasing the number used until a given increase does not alter the calculated heat flux by more than a specified tolerance.

The solution procedure when using variable physical properties is more complicated as iterations need to be carried out to ensure that the physical properties are evaluated at the correct temperature. To do this iterations are carried out at each position up the wall, where the viscosity and the thermal conductivity of the fluid are evaluated. This is done by calculating the boundary layer thickness using an initial guess for the wall temperature. Then, using equation (3.7) with y set to zero, the new wall temperature is found. If this is within $0.1^{o}C$ of the previous temperature then the procedure steps up to the next position on the wall. If, however, the new temperature differs by more than $0.1^{o}C$ new physical properties are calculated and the procedure repeated.

To check the current solution procedure the paper by Miyamoto and his co-workers [66] is used. In their study two dimensional effects were studied, as well as the one dimensional case, but the temperature (or the heat flux) on one side of the wall was specified a priori. By restricting their analysis to the one dimensional situation and the current method to a constant heat flux condition, or isothermal wall condition, then the two methods can be compared. The details of this can be found in Appendix 3. The results for the temperature at the wall/fluid interface are given in Figures 3.2 and 3.3. From these figures it can be seen that the current solution technique shows the same trends when calculating the temperature profiles for a one dimensional heat flow through a wall with a predefined temperature or heat flux on one side.

3.5 Results

This investigation looks at the laminar regime, so the maximum

height for any particular system (i.e. fluid being used, heat transfer coefficient on the heat source side, thickness of wall etc.) must be determined in every case. The limit of the laminar region will vary if the temperature at which the physical properties of the fluid are evaluated is varied. As the limit for the laminar region occurs at the top of the wall the temperature at this point is used to evaluate the physical properties of the fluid, rather than using an average bulk temperature. After each step up the wall the condition for the product of the Grashof and Prandtl number is checked for such that $GrPr<10^9$. This value has been determined by experimental work, such that after this point laminar flow breaks down and some turbulence occurs. Although the values used for the Grashof number and the Prandtl number are normally determined using a bulk temperature, which does not apply here, some end point must be used and this procedure is as valid as any other. When a value of Gr Pr is greater than 10^9 transition flow occurs and the governing equations used here are no longer valid so the calculation stops.

The following two effects are investigated:

(a) the type of fluid being heated;

(b) the overall heat transfer coefficient.

The overall heat transfer coefficient can be changed by either altering the heat transfer coefficient on the heat source side or by changing the thermal resistance of the wall.

To compare the results for the current method with the usual way in which the heat flux through the same system would be calculated, a sample calculation is given in Appendix 4.

Table 3.1 shows the heat flows obtained when water is being heated by steam through a wall, which gives an overall heat transfer coefficient of 2574 W/m^2K. The physical properties for all numerical

calculations are evaluated at the same average bulk temperature as found when using the procedure outlined in Appendix 4. This is done so that the effect of solving the problem as a conjugate one is shown without the additional complication of using variable physical properties. The per cent differences are given with respect to the sum of resistance method, as this is the method that would normally be used when estimating heat flows.

ht (m)	Ra (10^6)	heat flux (W/m^2)		% diff.
		numerical	sum of resistance	
0.01	1.64	83370	76600	-8.84
0.02	14.39	74780	69370	-7.80
0.04	125.40	67360	62450	-7.86
0.06	443.24	63010	58550	-7.62
0.08	1043.17	59600	55990	-6.45

Table 3.1 Heat flux to water by steam through a wall with an overall heat transfer coefficient of 2574 W/m^2K

The decrease in the difference between the two methods for the higher walls is to be expected due to the assumptions made for the sum of resistance method. Near the leading edge the temperature profile deviates markedly from the isothermal condition. This is because the temperature of the wall at the leading edge is the same as the ambient temperature of the fluid, as the boundary layer thickness is zero at this point. This means that assuming the temperature of the wall/fluid interface is constant is incorrect, especially near the leading edge. This is shown in Figure 3.4 where the temperature for both methods used in Table 3.1 are presented for different systems.

The generally accepted lower limit for the validity of the boundary layer theory approximations is taken as $Ra=10^4$ [63]. However, it has been suggested that the boundary layer approximations apply as low as Ra=10 [71]. Using the higher of these two limits the maximum deviation for the heat flux results for the two methods so far used can be found. This can be carried out for different fluids and for systems with different overall heat transfer coefficients. The results are given in Table 3.2.

Fluid	U_o (W/m^2K)	Height (m)	Ra (10^4)	Heat flux W/m^2		% diff
				S.R.	Numerical	
Air	2574	0.0120	0.995	1026	1064	-3.67
Air	499	0.0121	1.003	1034	1054	-3.09
Air	2.9	0.0165	0.999	181.9	181.1	+0.52
Water	2574	0.0085	0.986	78340	86680	-10.7
Water	499	0.0030	1.033	29620	30330	-2.41
Water	2.9	0.0117	0.996	243.8	237.4	+2.65

Table 3.2 Heat flux of different systems at a Rayleigh number of 10^4

For air the calculated heat flux is essentially the same for the two methods. However, when water is being heated a difference of over 10% occurs for the highest value of the overall heat transfer considered.

The results presented in Table 3.2 are found by evaluating the physical properties at an average bulk temperature. If this reference temperature is changed the results can vary greatly. This is best demonstrated by taking the extremes of temperature that exist across the system. Whilst it is obvious that neither

temperature would be the correct one to take in this situation the choice of reference temperature may not always be clear, and the extremes used here are intended to highlight the possible errors which might arise. Also, for comparison, the reference temperature proposed by Sparrow and Gregg [70] is employed. This temperature is found by the following relationship:

$$T_{ref} = T_w - 0.38^* (T_w - T_\infty)$$

The calculated heat fluxes when using these different temperatures for evaluating the physical properties are shown in Table 3.3.

Fluid	U_o (W/m^2K)	Heat flux (W/m^2)				
		S & G	source temp.	sink temp.	bulk	numerical
Air	2574	393.8	382.1	406.7	395.2	409.4
Air	499	390.1	378.5	402.6	391.4	404.7
Air	2.9	129.0	126.6	129.6	129.0	130.1
Water	2574	56534	70016	41255	55963	59604
Water	499	22861	26835	20382	22971	23514
Water	2.9	218.7	221.0	219.1	219.2	217.4

Table 3.3 Heat flux for different systems calculated using different reference temperatures

These results show that, for the same system, the heat flux can vary by as much as 51% with respect to the heat flux found using the average bulk temperature as the reference temperature to evaluate physical properties. This difference is between the extremes of temperature which exists across the system, so the error is greater than might be expected. However, this does highlight the importance of the temperature at which properties are evaluated. It would be best if the need to guess a temperature at which to evaluate all the system's physical properties is avoided. This

47

can be done if variable physical properties are used in the heat and momentum balances (equations 3.1 and 3.2).

Tables 3.4 and 3.5 show the growth of the boundary layer thickness for a steam/air system and a steam/water system, with a heat transfer coefficient of 2574 W/m^2K up to the wall fluid interface, respectively. There are two values for the boundary layer. One is the value calculated by the current numerical procedure and the other is that obtained using the technique proposed by Pohlhausen [11].

height (m)	δnumerical (m)	δPohlhausen (m)	ΔT at wall (^oC)
$2*10^{-5}$	$4.94*10^{-5}$	$3.77*10^{-5}$	15.94
0.056	$0.85*10^{-2}$	$0.95*10^{-2}$	84.22
0.111	$1.02*10^{-2}$	$1.01*10^{-2}$	84.28
0.167	$1.12*10^{-2}$	$1.12*10^{-2}$	84.29
0.222	$1.21*10^{-2}$	$1.21*10^{-2}$	84.30
0.278	$1.28*10^{-2}$	$1.28*10^{-2}$	84.31
0.332	$1.34*10^{-2}$	$1.33*10^{-2}$	84.32
0.390	$1.39*10^{-2}$	$1.39*10^{-2}$	84.33
0.445	$1.44*10^{-2}$	$1.43*10^{-2}$	84.33
0.500	$1.48*10^{-2}$	$1.48*10^{-2}$	84.33
0.555	$1.52*10^{-2}$	$1.52*10^{-2}$	84.33

Table 3.4 Boundary layer thicknesses for a steam/air system with U_o = 2574 W/m^2K and constant physical properties

height (m)	δnumerical (m)	δPohlhausen (m)	ΔT at wall (^oC)
$5*10^{-14}$	$4.09*10^{-5}$	$1.33*10^{-5}$	0.67
0.0058	$0.84*10^{-3}$	$0.77*10^{-3}$	52.56
0.0116	$0.98*10^{-3}$	$0.92*10^{-3}$	55.72
0.0174	$1.08*10^{-3}$	$1.02*10^{-3}$	57.50
0.0235	$1.16*10^{-3}$	$1.09*10^{-3}$	58.72
0.0293	$1.22*10^{-3}$	$1.16*10^{-3}$	59.67
0.0351	$1.27*10^{-3}$	$1.21*10^{-3}$	60.39
0.0408	$1.32*10^{-3}$	$1.26*10^{-3}$	61.00
0.0466	$1.36*10^{-3}$	$1.30*10^{-3}$	61.56
0.0524	$1.40*10^{-3}$	$1.34*10^{-3}$	62.00
0.0582	$1.44*10^{-3}$	$1.38*10^{-3}$	62.44

Table 3.5 Boundary layer thickness for a steam/water system

Figures 3.5 to 3.7 show the boundary layer thickness, calculated using the current numerical method, the velocity profile and the heat flows found using the sum of resistance method, with the expression found by Squire [21] to evaluate the heat transfer coefficient on the heat sink side, and the method using the current analysis. Figure 3.5 gives the results for the steam/air system when the heat transfer coefficient up to the heat sink is 2574 W/m^2K. This shows that the current analytical method does indeed predict the same boundary layer thickness as the isothermal wall case when parameters are chosen such that the temperature profile of the wall approaches an isothermal situation.

Figure 3.6 gives the results for the same system, except that the heat transfer coefficient is now only 2.89 W/m^2K. In this case the parameters chosen do not give an isothermal wall condition and the calculated boundary layer thicknesses do deviate noticeably from the isothermal wall case. Figure 3.7 is for a steam/water system when the heat transfer coefficient is again 2574 W/m^2K.

Table 3.6 presents the heat fluxes found using constant and variable physical properties. This provides a direct comparison between the two methods and shows the effect of allowing the physical properties to vary up the surface of the wall.

System	height	heatflux (W/m^2) constant properties	heatflux (W/m^2) variable properties	% differences
Water	0.030	$7.47*10^4$	$8.45*10^4$	13.3%
Water	0.046	$7.01*10^4$	$7.82*10^4$	11.7%
Water	0.055	$6.81*10^4$	$7.57*10^4$	11.2%
Air	0.152	558	526	7.8%
Air	0.305	470	444	5.5%
Air	0.457	424	403	5.0%

Table 3.6 Heat fluxes for different systems using constant and variable physical properties

Table 3.6 shows that the heatflux found when using variable physical properties as compared with constant physical properties varies significantly when water is being heated. In this situation the constant physical property analysis underestimates the heat flow. However, when air is being heated the heat flows found are much closer, and now the constant physical property analysis is overestimating the heat flows. This means that it is impossible to predict beforehand the error which is introduced in using the constant physical property approximation.

To compare the effect of using variable physical properties on the boundary layer thickness the same systems have been investigated as those that gave the results in Tables 3.4 and 3.5. When the heat sink is air the results for the boundary layer thickness are given in Table 3.7, whilst the results for the water situation are given in Table 3.8.

height (m)	δ variable (m)	ΔT at wall (^{o}C)
$1*10^{-5}$	$1.06*10^{-5}$	37.50
0.031	$0.87*10^{-2}$	84.33
0.061	$1.03*10^{-2}$	84.33
0.092	$1.14*10^{-2}$	84.33
.	.	.
.	.	.
0.491	$1.73*10^{-2}$	84.39
0.521	$1.76*10^{-2}$	84.39
0.552	$1.78*10^{-2}$	84.39

Table 3.7 Boundary layer thickness for a steam/air system with U_o = 2574 W/m^2K and variable physical properties

height (m)	δ variable (m)	ΔT at wall (^{o}C)
$3*10^{-14}$	$1.20*10^{-5}$	3.50
0.0029	$0.80*10^{-3}$	61.39
.	.	.
.	.	.
0.0579	$1.54*10^{-3}$	70.94
0.0607	$1.56*10^{-3}$	71.06
0.0664	$1.59*10^{-3}$	71.28
0.0695	$1.61*10^{-3}$	71.39

Table 3.8 Boundary layer thickness for a steam/water system with U_o = 2574 W/m^2K and variable physical properties

Comparing Tables 3.4 and 3.5 with Tables 3.7 and 3.8 respectively, it can be seen that in both cases the calculated values for the boundary layer thicknesses change for the entire length of the wall. However, the temperature of the wall surface does not change significantly when air is being heated (Table 3.4 and 3.7) as the interfacial temperature is approaching that of the heat source temperature. When water is being heated (Table 3.5 and 3.8) the effect on the interfacial temperature is much more noticeable with a difference of almost $10^{o}C$ occurring at the top of the wall.

Sparrow [60] looked at the constant heat flux situation using an integral analysis. In a later paper with Gregg [70] the following result for the Nusselt number was determined:

$$Nu = \frac{2}{360^{1/5}} \left(\frac{Pr}{4/5+Pr}\right)^{1/5} Ra_y^{1/5} \qquad (3.23)$$

Comparing this with the starting solution for the boundary layer thickness (equation 3.21) it appears as if the fluid being heated sees the wall as a constant heat source near to the leading edge.

However, the one fifth power no longer holds as we move away from the leading edge. By fitting the results obtained from Table 3.1 a similar relationship to that above can be found:

$$Nu = 0.563\ Ra^{1/3.95} \qquad (3.24)$$

This relationship is for water being heated by a system with an overall heat transfer coefficient of 2574 W/m^2K, in the range $10^4<Ra<10^9$. For Rayleigh numbers lower than this the results correlate with a coefficient of 0.559, but the exponent remains the same. When the overall heat transfer coefficient is changed to 2.89 W/m^2 K the correlation for the Nusselt number becomes:

$$Nu = 0.541\ Ra^{1/4} \qquad (3.25)$$

As would be expected, by looking at Table 3.2 and figure 3.2, the exponent is now 1/4, as the wall approaches the isothermal condition. Using the isothermal wall correlation [21]:

$$\frac{Nu}{4\sqrt{Gr/4}} = \frac{0.676\ Pr^{\frac{1}{2}}}{(0.861+Pr)^{1/4}} \qquad (3.26)$$

which for a Prandtl number of 8.46, the value used to find (3.25) becomes:

$$Nu = 0.496\ Ra^{1/4} \qquad (3.27)$$

Comparing the coefficients in equations (3.25) and (3.27) a difference of 9% in the coefficients of the Rayleigh number is found. This is because, at the same height, the Rayleigh number

for the isothermal wall case is different to that for the non-isothermal wall. This can be illustrated by looking at Figure 3.4. This shows the temperature profile and the isothermal wall temperature for different systems. When air is being heated the difference between the two temperatures is not very large. However, when water is being heated the temperature at any height predicted by the current method as compared with the isothermal wall temperature shows a significant difference at most heights. This means that the temperature used to find the Rayleigh number will be different when using the two different techniques. This difference shows itself in the different values for the coefficient in equations (3.25) and (3.27). This is best illustrated by looking at the water system with the overall heat transfer coefficient of 499.1 W/m^2K and the air system with a heat transfer coefficient of 2.89 W/m^2K. Even though the temperature profiles predicted by the method given here are almost identical the isothermal wall temperatures found using the sum of resistance method differ by 0.15 on the dimensionless scale. This is a difference of over 55% with respect to the water temperature of 0.27. Looking at Figure 3.4 the isothermal wall temperature for the air system approximates an average temperature for the appropriate temperature profile much more closely than is the case for the water system. Thus, the Rayleigh numbers for the air case are a better approximation than for the water situation.

The plots for air when there is an overall heat transfer coefficient of 2574 W/m^2K are not given in Figure 3.4 as they are indistinguishable from the line x=0.0.

3.6 Conclusions

The system investigated presents a distributed resistance to the heat flow from the heat source side (steam side) to the heat sink (water or air). Calculations in the past have used correlations to find the heat transfer coefficient on the heat sink side and then a sum of resistance method to determine the heat flow.

Two methods have been used in this chapter which solve the problem as a complete system rather than decoupling the system to find a heat transfer coefficient. The first method uses constant physical properties in the governing heat and momentum equations whilst the second introduces variable physical properties into the equations.

The effects of changing:

(1) the fluid being heated;

(2) the heat transfer coefficient on the heat source side;

(3) the thickness of the wall,

are shown. All three of these change the magnitude of the parameter $2k_f/U_o$ with respect to the boundary layer thickness, δ. Item (3) contributes little resistance to the flow of heat, except in the case of thick insulating materials. However, as the model used only considers one-dimensional heat flow, the present solution method would not be a valid one for this particular situation.

Changing the fluid from air to water has an analogous effect on the heat flow calculated by the numerical method, as to that found by the integral method, as reducing the heat transfer coefficient on the steam side. This is because, in both cases, the resistance to the heat flow on the steam side is becoming increasingly more important. This is demonstrated in Figures 3.5 to 3.7. Figure 3.5

shows a steam/air system with a high heat transfer coefficient on the steam side. As can be seen from the heat flows the change from the isothermal wall result to the numerical result is small. However, if the heat transfer coefficient on the steam side is reduced (Figure 3.6), or the fluid is changed to water (Figure 3.7) the difference in the heat flows become very pronounced. This is the expected result as the term $2k_f/U_o$ has a value comparable to that with the boundary layer thickness, δ. In such a situation, as was noted in the statement of the problem, section 2.3 this means that the governing equations cannot be approximated by the equations derived for an isothermal wall, and so a different result would be expected.

The effect on the heat flow when changing from constant physical properties to variable physical properties has different results when considering either air or water as the fluid on the heat sink side of the wall. When comparing Tables 3.4 and 3.7 is it noted that the temperature of the wall is not altered significantly when using variable physical properties rather than constant physical properties. This is because the wall temperature in this particular instance is already very high when compared with the heat source temperature. However, when the temperature of the wall is appreciably lower than the heat source temperature, as is the case when water is being heated, the effect of using variable physical properties in the calculations causes a marked increase in the wall temperature (shown by studying Tables 3.5 and 3.8).

Looking at the heat flows of the two systems (air or water), the heat flow in the air case decreases, and becomes very close to that found for the isothermal wall (in fact, at 0.457m, the two calculated values are the same). For water, the heat flow increases with respect to the constant physical property case, and the difference

between the heat flow calculated using the isothermal wall situation and the numerical, non-isothermal, problem varies by 22.7%. This occurs because, even though the boundary layer thickness increases in both water and air systems, the large increase in the temperature of the wall for the water system overcomes this increased resistance to give a larger heat flow.

Therefore, the isothermal wall approximation to the conjugate heat transfer problem can, in certain situations, be used to find the heat flow. This occurs when using a system with air on the heat sink side and a high heat transfer coefficient on the heat source side. The effect of ignoring the variable wall temperature and the variation of physical properties fortunately causes equal but opposite errors in the calculation of the heat flow. However, for the water system, the errors in the two approximations are cumulative and using an isothermal wall model with constant physical properties does not represent the actual system satisfactorily.

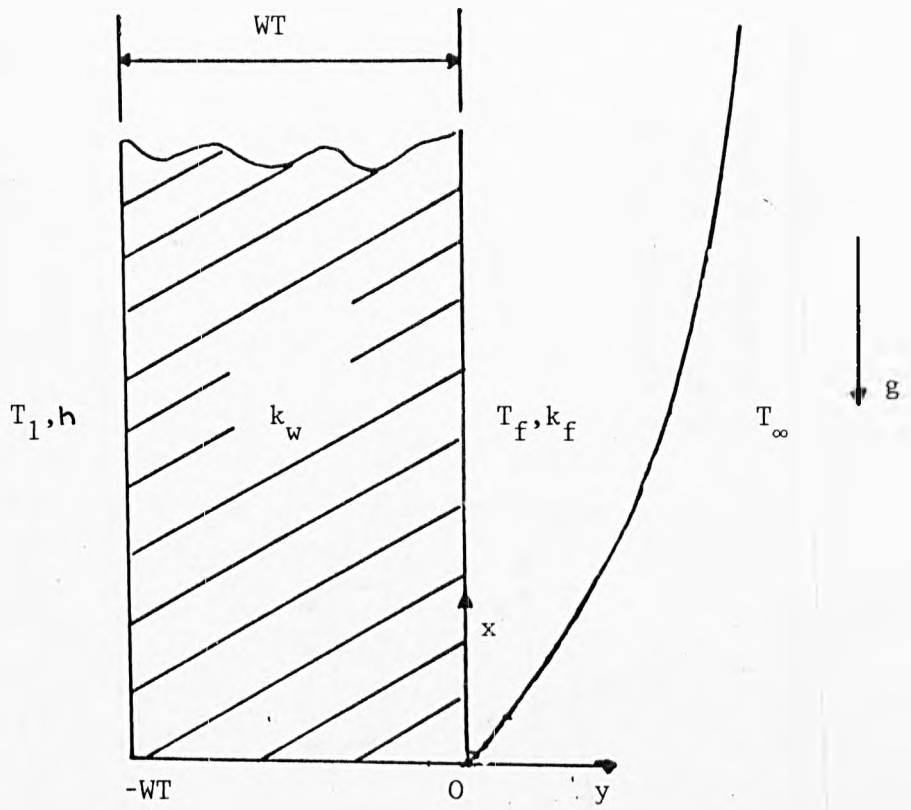

Fig. 3.1 Schematic Diagram of the Plane Wall System

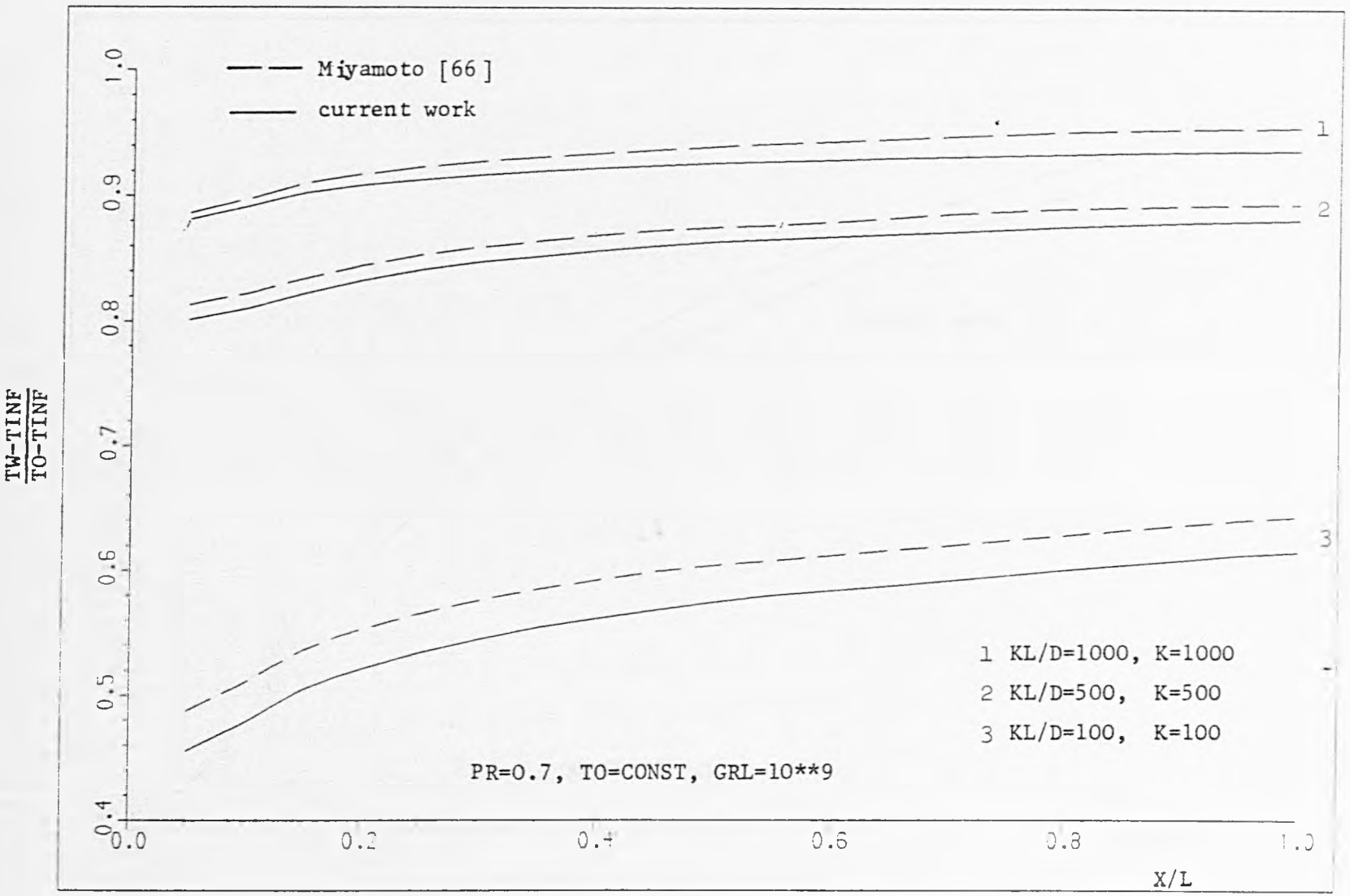

Fig. 3.2 Effect of Parameter KL/D on Wall Temperature

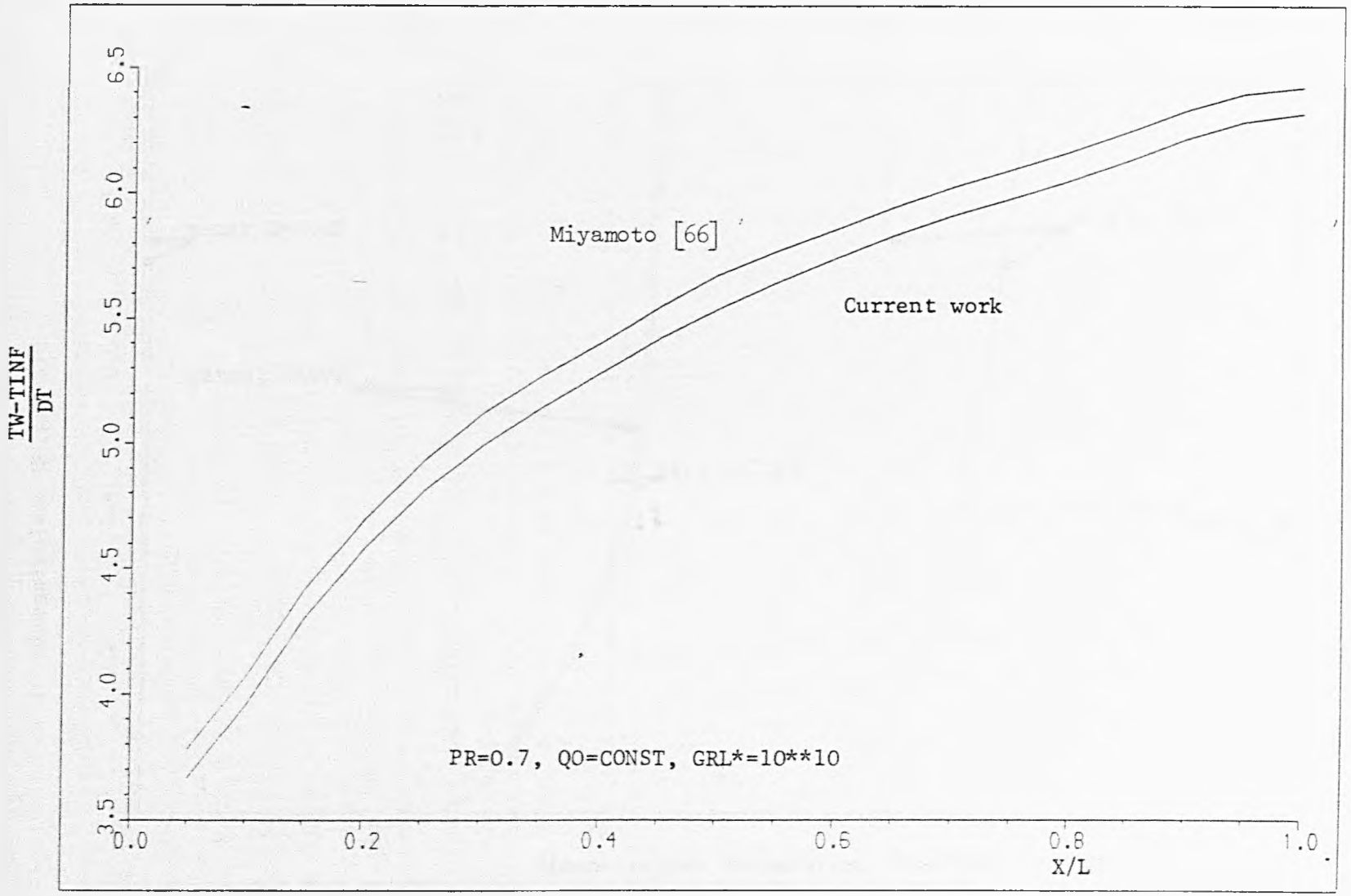

Fig. 3.3 Constant Heat Flow - Interfacial Temperature

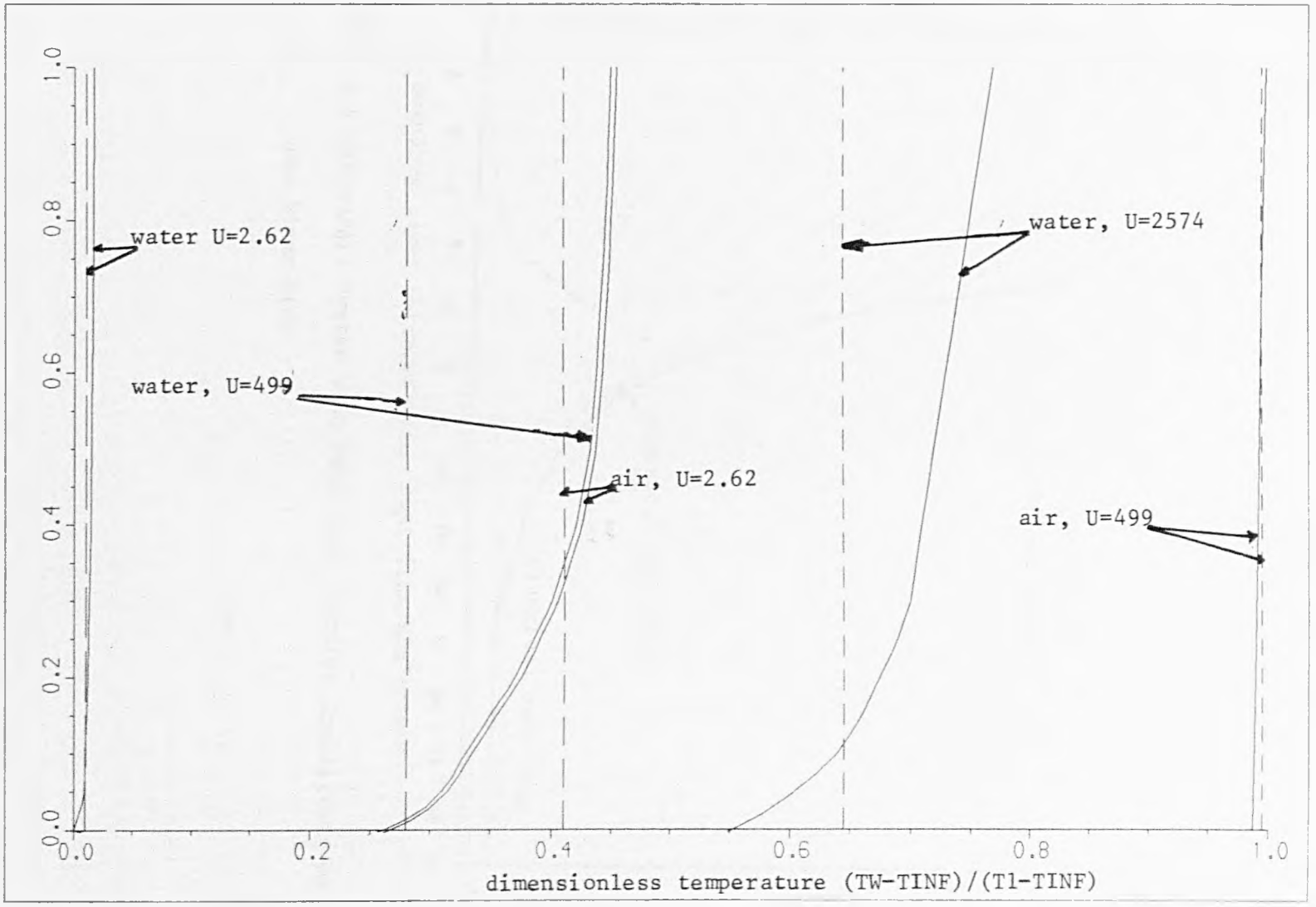

Fig. 3.4 Temperature Profiles at Wall

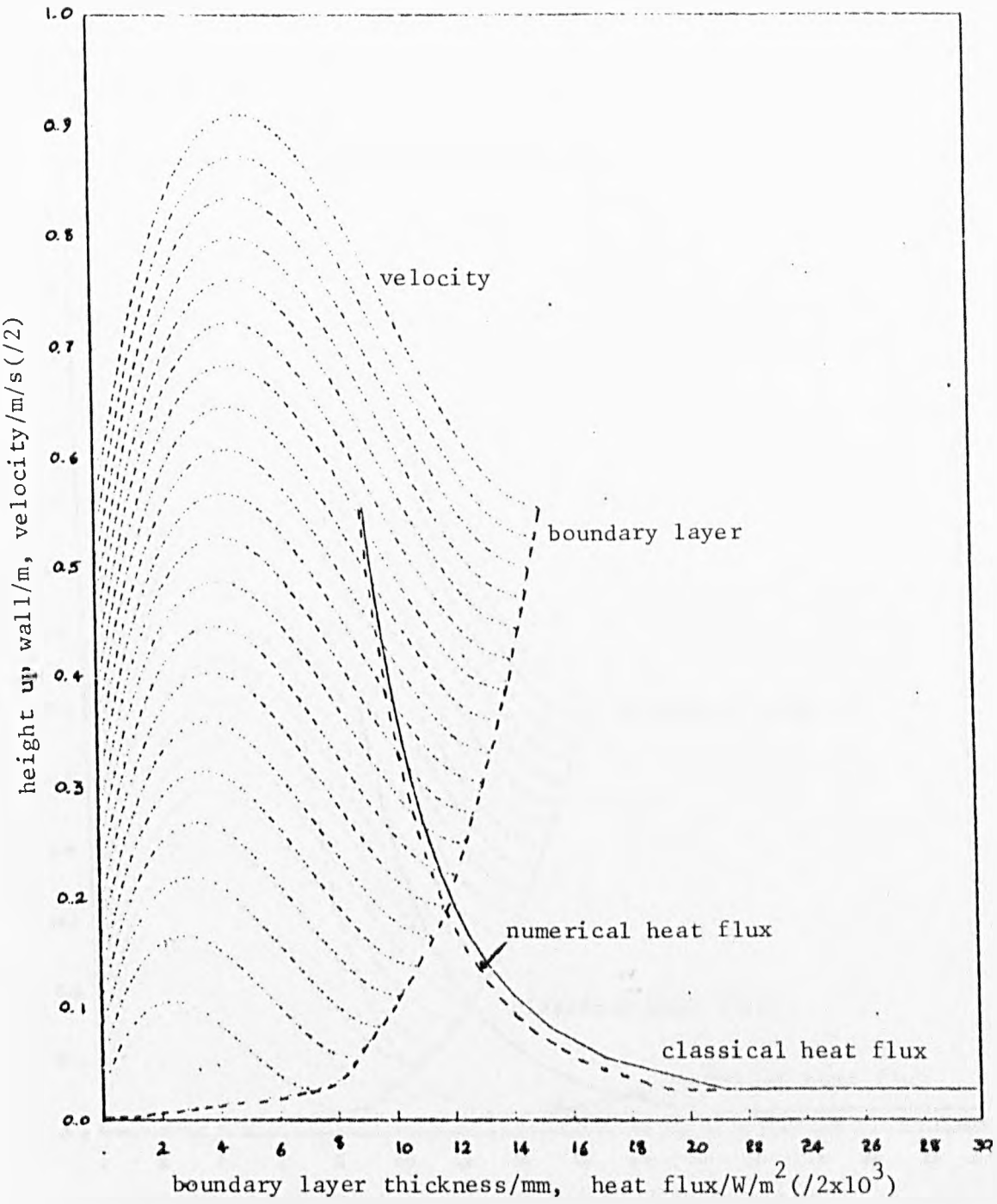

Fig. 3.5 Steam/Air System with High Heat Transfer Coefficient on the Steam Side

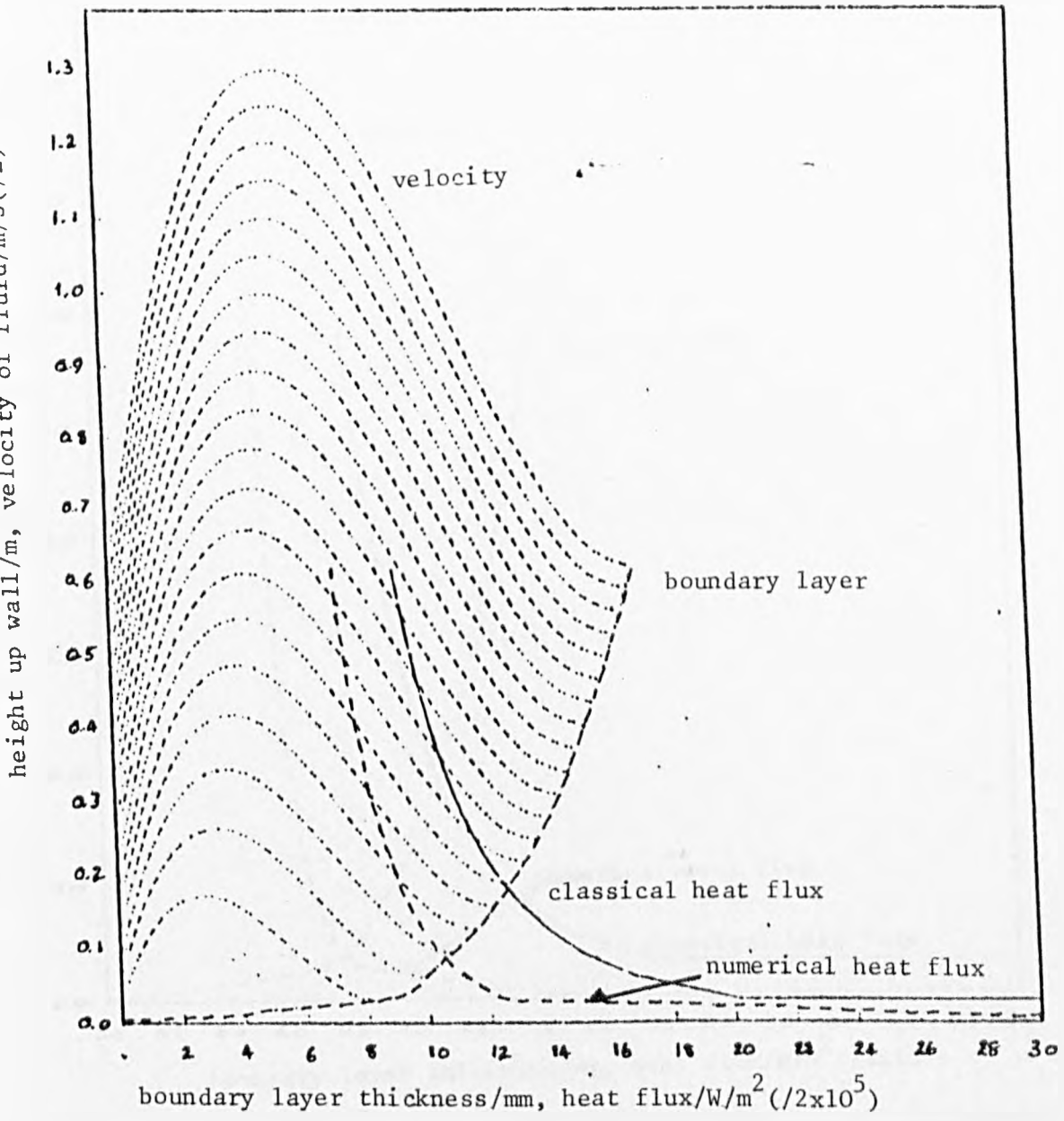

Fig. 3.6 Steam/Air System with Low Heat Transfer Coefficient on The Steam Side

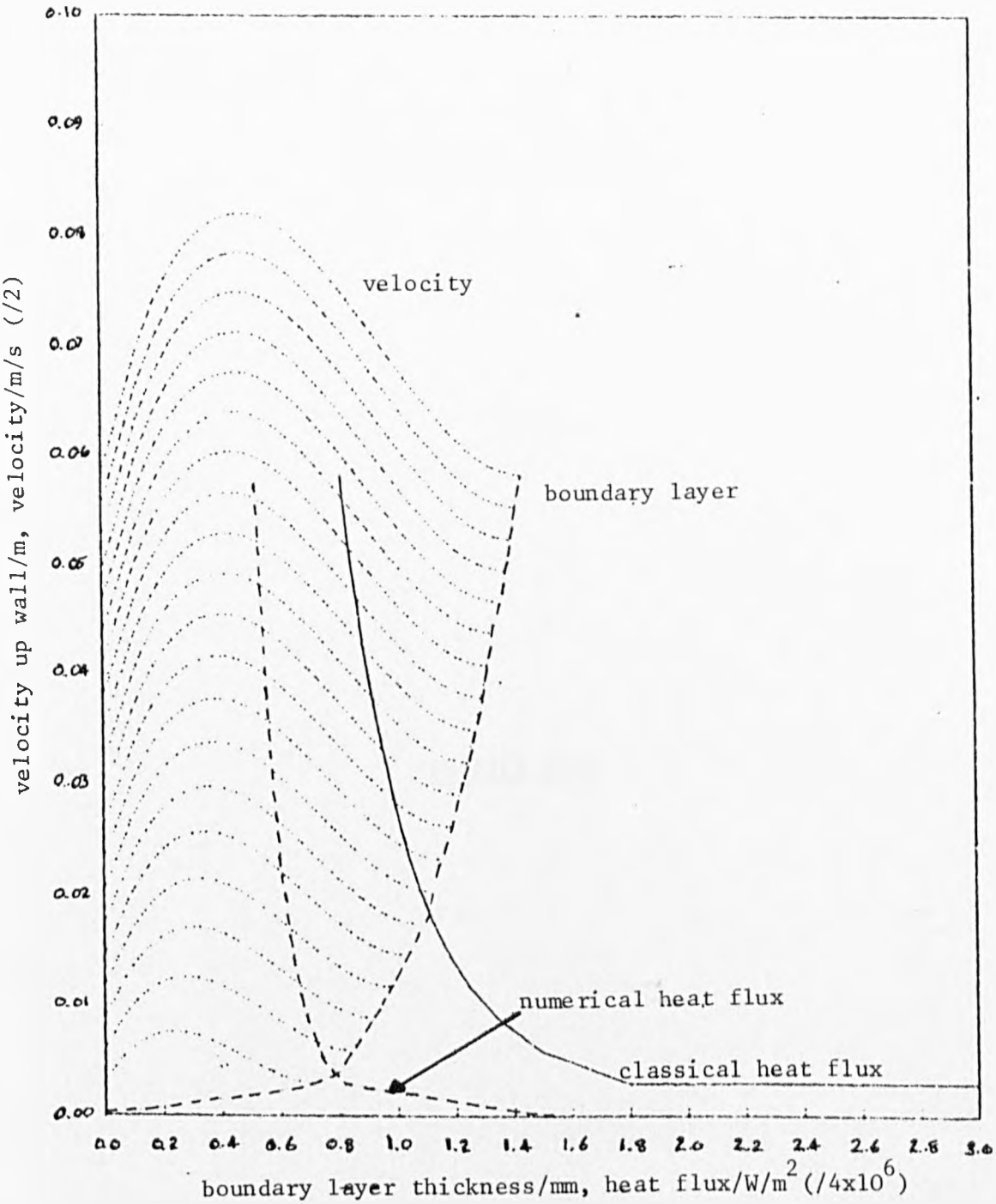

Fig. 3.7 Steam/Water System with High Heat Transfer Coefficient on the Steam Side

CHAPTER FOUR

4. Natural Convection Heat Transfer From a Downward Projecting Fin Immersed in a Free Fluid with 1-D Conduction

4.1 Introduction

The area of heat transfer from finned surfaces has many practical applications, including heat exchangers and waste heat removal systems. The shapes of these extended surfaces can take many forms ranging from circular pins to spiralled transverse fins. Each particular geometry has its own advantages and disadvantages.

The simplest geometry is that of a longitudinal fin of uniform thickness. This geometrically shaped fin was studied by Murray [72] when deriving the fin efficiency, which is defined as the total heat flow from the finned surface divided by the heat flow that would exist if the entire surface were at the same temperature as the primary surface. In deriving the characteristics of the fin efficiency, Murray [72] and later Gardner [4] used the following assumptions:

1) The heat flow and temperature distribution throughout the fin is independent of time;
2) The fin material is homogeneous and isotropic;
3) There is no heat source in the fin itself;
4) The heat flow to or from the fin surface at any point is directly proportional to the temperature difference between the surface at that point and the surrounding fluid;
5) The thermal conductivity of the fin is constant;
6) The heat transfer coefficient is the same over the entire surface of the fin;
7) The temperature of the fluid surrounding the fin is uniform;

8) The temperature of the base of the fin is uniform;

9) The fin thickness is small enough compared with the fin height to ignore temperature gradients across the width of the fin;

10) The heat transferred through the outermost edge of the fin is negligible compared with that passing into, or out of, the fin through its sides;

11) The joint between the fin and the primary surface is assumed to offer no bond resistance.

Using these assumptions, Gardner [4] was able to calculate the fin efficiencies for a wide range of fins with different geometrical profiles. Due to the assumptions made an analytical solution was obtained, which involved a term for the cross-sectional area. By the substitution of the appropriate relationship for the change in area with height complete solutions were obtained.

In the early experimental studies by Harahap and McManus [73] and Jones and Smith [74] the above assumptions were made even more stringent by considering only isothermal fin arrays, in order to find the total heat transfer rates. At the same time as this, both theoretical and experimental methods were being employed to determine the nature of the boundary layer about a single downward projecting fin [35]. The theoretical approach relaxed the assumption of a constant heat transfer coefficient about the fin. However, the temperature profile of the fin was prescribed in the following way:

$$\theta_f = \theta_b \left(\frac{x}{L}\right)^n \qquad (4.1)$$

The problem was then treated by using boundary layer theory. As the temperature profile had been described in the form given in equation 4.1 a similarity solution technique could be used. Previous studies to this had also relaxed the assumption of a constant heat transfer coefficient but only by substituting the constant value for a heat transfer coefficient that was known to vary in a given way. Two analyses used this particular method, one by Han and Lefkowitz [16] and the other by Chen and Zyskowski [17]. In [16] the heat transfer coefficient was defined such that its value fell to zero at the fin tip, whereas in [17] a non-zero value could be obtained at the tip of the fin.

The above three methods [35], [16], [17] all relax assumption 6, but replaced it with another assumption regarding either the temperature profile of the fin or the way in which the heat transfer coefficient varied. Ideally, it is required for the constant heat transfer coefficient assumption to be relaxed and not to introduce another assumption in its place.

The use of infinitely long fins in the analyses by Kwon and Kuehn [36] and then by Tolpadi and Kuehn [37] with boundary layer equations in the fluid allowed the true conjugate nature of a fin immersed in a free fluid to be studied. In [36] a successive under relaxation hybrid scheme is used to solve for the vorticity, stream function, and temperature. In [32] the complete Navier Stokes equations are solved using a vorticity vector potential approach. The drawback with these methods is that the fin is assumed to be infinitely long, so that it can be assumed that the fin tip temperature is at the same temperature as the ambient fluid. This overcomes the problems of the singularity that occurs at the fin tip. However, with most practical applications the fin tip is not at the same temperature as the ambient fluid, as fins are usually short, and so it is not possible to solve

such a problem in the ways suggested in [36] or [37].

In this chapter a method is proposed that solves the integrated boundary layer equations, such that a non-zero fin tip temperature is found. If the heat loss from the fin is by mixed convection then an alternative method can be used to find the temperature profile in the fin, as is shown in chapter 5. When the fin is surrounded by a saturated porous medium then both the mixed and natural convection situations can be analysed using a numerical method similar to that used in chapter 5. These problems are discussed and solved in chapter 6.

4.2 Statement of the Problem

The shape of the fin can take many forms, but the current analysis will be restricted to two, namely a rectangular fin and a tapered fin. These are shown in figures 4.1a and 4.1b along with the co-ordinate system to be used.

To derive the relationship for the heat flow in the fin a heat balance is carried out across an element in the fin, between the heat flowing down the fin and the heat flow into the surrounding fluid. The fin is assumed to have a variable cross-sectional area, and the heat flow into the fluid is not represented by a heat transfer coefficient but by using the temperature gradient of the fluid at the fin-fluid interface. If radiation effects are ignored the resulting heat balance is:

$$\frac{Ad^2\theta_f}{dx^2}\,dx + \frac{dA}{dx}\,\frac{d\theta_f}{dx} + k_{f\ell_o}\,\frac{\partial\theta_{f1}}{\partial n}\,\frac{1}{k_f}\,\Delta A_f = 0 \qquad (4.2)$$

where n is the direction normal to the surface of the fin.

Once the temperature gradient at the surface is known, equation 4.2 becomes a second order differential equation which requires two boundary conditions for the temperature. The first boundary condition given by equation 4.3 states that the temperature at the base of the fin is fixed at a constant, and in this case, known value. The second boundary condition cannot be expressed in the current analysis other than by saying that the fin tip temperature is greater than the ambient fluid temperature and finite.

$$\begin{aligned} &x = \llcorner,\ -WT < y < 0 \\ &\qquad \theta_f = \theta_b \\ &x = 0,\ -WT < y < 0 \\ &\qquad \theta_f > 0 \end{aligned} \tag{4.3}$$

The second boundary condition is a 'floating' condition as it allows the temperature of the fin tip to vary as the calculation of the problem proceeds. To specify the second boundary condition further an investigation of the fluid flow must be carried out. This will also allow the determination of the temperature gradient at the fin fluid interface ($\partial\theta_{fl}/\partial n$), which is needed to solve the conduction heat balance in the fin (equation 4.2), but which is as yet unknown.

Previous investigations [14] have shown that the temperature profile in a fluid, which is in the laminar region, can be approximated by a quadratic polynomial:

$$T_{fl} - T_\infty = a + by + cy^2 \tag{4.4}$$

where T_{fl} is the temperature of the fluid and y is the ordinate normal

to the plane of the heated surface.

The boundary conditions in the current problem show that there is continuity in the temperature between the fin and the fluid, and between the fluid in the boundary layer and the ambient bulk fluid. Also, at the edge of the boundary layer the temperature gradient of the fluid decreases to zero.

$$y = 0,\ 0 < x < L\ (0 < x < L/\cos\phi - \text{tapered fin})$$

$$T_{fl} = T_f$$

$$y = \delta,\ 0 < x < L\ (0 < x < L\cos\phi - \text{tapered fin})$$

$$T_{fl} = T_\infty$$

$$\frac{\partial T_{fl}}{\partial y} = 0 \qquad (4.5)$$

Substituting the boundary conditions (equation 4.5) into the expression for the temperature (equation 4.4), and defining a temperature excess, θ, as the temperature over the ambient bulk fluid temperature, the following relationships can be found for the temperature and the temperature gradient at the fin fluid interface respectively:

$$\frac{\theta_{fl}}{\theta_f} = \left(1 - \frac{y}{\delta}\right)^2 \qquad (4.6)$$

$$\frac{\partial \theta_{fl}}{\partial y} = \frac{-2\theta_f}{\delta} \qquad (4.7)$$

Equation 4.7 can now be substituted into the general fin equation, 4.2, to obtain the following relationship (with n=y):

$$\frac{Ad^2\theta_f dx}{dx^2} + \frac{dA}{dx}\frac{d\theta_f}{dx} + \frac{2k_{flo}}{k_f\delta}\Delta A_f\theta_f = 0 \qquad (4.8)$$

For the tapered fin: $A = 2x\tan\phi$; $\Delta A_f = 2dx/\cos\phi$

where ϕ is the fin half angle.

For the rectangular fin: $A = WT$; $\Delta A_f = 2dx$

Equation 4.8 can be solved numerically if the value of the boundary layer thickness, δ, is known.

To find the value of the boundary layer thickness the partial differential equations which represent the fluid flow have to be solved or an approximate integral analysis, similar to that proposed by Squire [21], can be used. A similarity solution cannot be used as the value of the temperature along the fin surface is not known a priori, and even if the profile is known it must take one of the forms which allow a similarity solution to be used (see [29]). The solution of the partial differential equations provides the most accurate solution but requires a grid to be imposed on the entire solution domain. This therefore leads to long solution times for the numerical procedure.

The underlying assumption in the integral analysis, which sets the thermal boundary layer thickness equal to the momentum boundary layer thickness, means that the analysis should only be carried out for fluids with a Prandtl number close to unity. In the current investigation the fluids being studied are air and water, which means that the integral analysis is a valid solution technique. This method is obviously much easier to use than having to carry out a numerical solution which obtains the full temperature and velocity

profile at every point in the fluid at every iterative step.

4.3 Integral Analysis

In chapter three the equations found by carrying out a momentum and energy balance across an elemental height at a height x across the boundary layer were presented. These equations (3.1 and 3.2) can again be used:

momentum balance:

$$\frac{d}{dx}\int_0^{\delta} \rho u^2\, dy = -\mu_o \left(\frac{du}{dy}\right)_o + g\left(\delta\rho_\infty - \int_0^{\delta} \rho\, dy\right) \qquad (4.9)$$

heat balance:

$$k_{flo}\left(\frac{dT_{fl}}{dy}\right)_o = \frac{d}{dx}\int_0^{\delta} \rho C_p u\,(T_\infty - T_{fl})\, dy \qquad (4.10)$$

When studying the tapered fin the co-ordinates are changed to $\bar{x}$ and $\bar{y}$ inclined at an angle ϕ from the original co-ordinates, and the acceleration due to gravity is modified to take into account the slope of the fin surface. Except for these two slight modifications the analysis for the tapered fin proceeds in an identical way as that for the rectangular fin.

To solve equations 4.9 and 4.10 the temperature and velocity profiles in the fluid need to be specified. As in Chapter three a quadratic polynomial is assumed for the temperature profile and a cubic expression used for the velocity profile. The temperature profile has already been determined, and given by equation 4.6. The velocity profile is that given in chapter 3 (equation 3.8) and

is also given here

$$V = y\ \Gamma\ (1 - \frac{y}{\delta})^2 \tag{4.11}$$

4.4 Solution of Heat and Momentum Balance

The physical properties incorporated in the integrals on the heat and momentum balances can either be allowed to vary across the boundary layer or remain constant. If variable properties are used a convenient representation is given by describing the variation using quadratic polynomials in temperature:

$$\begin{aligned} \rho &= a_o + a_1 T + a_2 T^2 \\ Cp &= b_o + b_1 T + b_2 T^2 \\ \mu &= c_o + c_1 T + c_2 T^2 \\ k_f &= d_o + d_1 T + d_2 T^2 \\ \beta &= e_o + e_1 T + e_2 T^2 \end{aligned} \tag{4.12}$$

The following analysis assumes that all physical properties are constant. (The resultant equations for variable physical properties can be found in the second section of Appendix 2, which also deals with the variable property equations for the plane wall problem). However, the effect of temperature must be taken into account for the density if there is to be a driving force for the fluid flow. This is done by using the coefficient of expansion in the momentum balance.

Carrying out the integrations given in equations 4.9 and 4.10 two ordinary differential equations can be found.

momentum balance:

$$\frac{1}{105}\ \frac{d}{dx}\ (\Gamma^2\delta) = \frac{g\delta\beta(T_f-T_\infty)}{3} - \nu_o\ \frac{\Gamma}{\delta} \tag{4.13}$$

heat balance:

$$\frac{1}{30}\ \frac{d}{dx}\ (\Gamma\delta\theta_f) = \frac{2\alpha\theta_f}{\delta} \tag{4.14}$$

Equations 4.13 and 4.14 can be expanded by carrying out the differentiations, and the resultant equations are given by:

momentum balance:

$$\frac{2\Gamma\delta}{105}\ \frac{d\Gamma}{dx} + \frac{\Gamma^2}{105}\ \frac{d\delta}{dx} = \frac{g\beta\theta_f\delta}{3} - \nu_o\ \frac{\Gamma}{\delta} \tag{4.15}$$

heat balance:

$$\frac{1}{30}\ \{\Gamma\delta\ \frac{d\theta_f}{dx} + \delta\theta_f\ \frac{d\Gamma}{dx} + \Gamma\theta_f\ \frac{d\delta}{dx}\} = \frac{2\alpha\theta_f}{\delta} \tag{4.16}$$

The heat balance in the fin and the heat and momentum balances in the fluid (equations 4.8, 4.15, and 4.16 respectively) form a non-linear boundary value problem which can be solved in a number of different ways. All methods will, however, require iterations to be carried out because:

(i) the problem as stated is non-linear

(ii) the nature of the problem requires iterations to be carried out if the system is decoupled.

Usually a temperature profile would be assumed along the interface and, using this, the heat flow would be calculated and the velocity of the fluid found. However, in this analysis, no temperatures are known at the interface, so neither is the velocity

73

profile. Therefore, an initial guess must be made to work out the heat flow. This calculated heat flow is then used to update the temperature profile, which in turn redefines the velocity profile. This procedure is repeated until consecutive temperature profiles agree to within a specified tolerance.

4.4.1 Solution Using Matrices

The first method looks at the possibility of solving the problem as a whole, i.e. the values of boundary layer thickness, velocity in the fluid and the temperature in the fin. To do this equations 4.8, 4.15 and 4.16 are approximated by central differences. Equation 4.8 is used to express the temperature in the wall, equation 4.15 the boundary layer thickness, and equation 4.16 the velocity term in the fluid. The matrix formed by the resultant equation is given in matrix 4.1.

From this matrix it can be seen that for i mesh points up the wall a matrix of size 3i by 3i is needed. To find the values of θ_f,δ and Γ the matrix needs to be inverted. As mentioned before iterations will still be needed as the original equations are non-linear and so the matrix elements themselves depend on the final solution. Thus, the number of points used up the fin will be limited as the matrix would quickly become too large for inversion to take place. The problem of the size of the matrix can be overcome by either assuming the system to be an initial value problem and iterating on the other boundary condition, or decouple the problem. In either case 4.15 and 4.16 can be solved by a Runge Kutta technique, and it is only the solution of equation 4.8 that differs from one approach to the other. In the first instance a shooting method is used, but the solution of the parameters of δ and Γ are found in one step, whereas in the second approach two stages are required to

$$
\begin{bmatrix}
0 & 0 & \frac{\Gamma-(i)^2\delta(i)}{710\ \Delta x} & 0 & \nu & \Gamma(i)\delta(i)\ \frac{\Gamma(i+1)-\Gamma(i-1)}{105\ \Delta x} - \frac{g\beta\theta_f(i)\ (i)}{3} & 0 & 0 & \frac{\Gamma(i)^2\delta(i)}{210\ \Delta x} \\
0 & \frac{-\delta(i)^2\theta_f(i)}{60\ \Delta x} & 0 & -2\alpha & \frac{\delta(i)^2\theta_f(i+1)-\theta_f(i-1)}{60\ \Delta x} + \frac{\theta_f(i)\delta(i)(\delta i+1)-\delta(i-1)}{60\ \Delta x} & 0 & 0 & \frac{\delta(i)^2\theta_f(i)}{60\ \Delta x} & 0 \\
(\frac{Adx}{\Delta x^2} - \frac{dA}{dx}\ \frac{1}{2\Delta x} & 0 & 0 & \frac{-k_{fo}\ \Delta A_f}{k_w\ \delta(i)} - \frac{-2Adx}{\Delta x^2} & 0 & 0 & \frac{Adx}{\Delta x^2} + \frac{dA}{dx}\ \frac{1}{2\Delta x} & 0 & 0
\end{bmatrix}
\begin{bmatrix}
\theta_{f(i-1)} \\ \Gamma(i-1) \\ \delta(i-1) \\ \vdots \\ \theta_f(i) \\ \Gamma(i) \\ \delta(i) \\ \vdots \\ \theta_f(i+1) \\ \Gamma(i+1) \\ \delta(i+1)
\end{bmatrix}
=
\begin{bmatrix}
0 \\ 0 \\ 0 \\ \vdots \\ 0 \\ 0 \\ 0 \\ \vdots \\ 0 \\ 0 \\ 0
\end{bmatrix}
$$

Matrix 4.1 Central Difference Representation of Equations 4.8, 4.15 and 4.16

find all the parameters.

4.4.2 Shooting Technique

The Runge Kutta solution method can solve sets of simultaneous ordinary differential equations. Looking at the momentum and heat balances in the fluid (equations 4.15 and 4.16 respectively) and the heat balance in the fin (equation 4.8) it can be seen that these equations, in their current form, are not suitable to be used in a Runge Kutta analysis. Firstly, the second order fin heat balance needs to be reduced to two first order equations. This is done by letting a variable, u, represent the first differential of the fin temperature. In the case of the square fin this gives:

$$u = \frac{d\theta_f}{dx} \tag{4.17}$$

$$\frac{du}{dx} = \frac{4\ k_{fo}}{WT\ k_s}\ \frac{\theta_f}{\delta} \tag{4.18}$$

Using equation 4.17 in equation 4.16 and eliminating either $d\delta/dx$ or $d\Gamma/dx$ from 4.15 and 4.16 the following first order differential equations are found:

$$\frac{d\delta}{dx} = \frac{105\nu}{\delta\Gamma} + \frac{120\alpha}{\delta\Gamma} - \frac{35g\beta\theta_f\delta}{\Gamma} - \frac{2\delta u}{\theta_f} \tag{4.19}$$

$$\frac{d\Gamma}{dx} = \frac{35g\beta\theta_f}{\Gamma} + \frac{\Gamma u}{\theta_f} - \frac{105\nu}{\delta^2} - \frac{60}{\delta^2} \tag{4.20}$$

The analysis for the tapered fin is a simple extension of the rectangular fin case and is presented in Appendix 5.

Equations 4.17 to 4.20 present the full coupled equations for a downward projecting rectangular fin in a free fluid. However, to solve these equations a starting solution is required near the leading edge. The profiles of the boundary layer thickness and velocity term are assumed to be similar to those found by previous workers (e.g. [11], [21]) and the temperature profile of the fin is assumed to be akin to that proposed by Lock and Gunn [35]. This gives the relationships for the three terms as:

$$\begin{aligned} \delta &= a_o \times a_1 \\ \Gamma &= b_o \times b_1 \\ \theta_f &= c_o + d_o \times d_1 \end{aligned} \tag{4.21}$$

By substituting 4.21 into equations 4.17 to 4.20 and equating exponents values then a_1, b_1 and d_1 are found to be 1/2, 1/4 and 7/4 respectively. The values of a_o, b_o, c_o and d_o cannot be defined uniquely as there are only three relationships for the four unknowns. Thus, three of the variables can be defined in terms of the other one, which much be evaluated in some other way. Letting a_o be the unknown to be found later, b_o, c_o and d_o are given by:

$$\begin{aligned} b_o &= \frac{60\alpha\ (1+\text{const})}{\frac{3}{2} a_0^2\ (\text{const}) + \frac{g\beta a_o}{3}\ (\text{const})} \\ c_o &= b_0^2\ A\ (\frac{421}{420}) + \nu \frac{b_o}{a_o} \\ d_o &= c_o\ (\text{const}) \\ \text{const} &= \frac{\frac{4\ k_{ft_o}}{WT\ k_s}\ x^{7/4}}{\frac{21}{16}\alpha_o - \frac{4k_{fo}}{WT\ k_s}\ x^{7/4}} \end{aligned} \tag{4.22}$$

The value of a_o is fixed by employing the boundary condition at the top of the fin (equation 4.3). This is done by setting a_o to a certain value, and then "shooting" up the fin using equations 4.17 to 4.20. Then, the predicted value of θ_b is compared with the boundary condition, which fixes the value of the fin base temperature, and the value of a_o is altered accordingly for the next calculation. Having done this the procedure is repeated until the calculated value of the fin base temperature agrees with the value given by the boundary condition.

The heat flow from the fin can be found very easily, as the solution provides the temperature gradient at all points. Thus, using the temperature gradient found at the base of the fin, the heat flow into the fin is known. By satisfying the heat balance, this must also be the heat flow out. If the temperature gradient at the fin base is multiplied by the area and the thermal conductivity of the base, and then divided by the surface area of the fin, the heat flow per unit area can be calculated.

The difficulty with this solution technique is the computer time required to find the solution. As the main purpose of this work is to investigate the effect on the fin efficiency results when considering a conjugate problem rather than imposing a heat transfer coefficient, or similar restraint, on the fin, comprehensive data sets are required. If the Runge Kutta method were used to find all the data required to draw up fin efficiency charts the time used would be very large and the program would have to be run interactively at first for all new input data to ascertain how the value of the base temperature changes with changes in a_o. Therefore, if a method can be found which decreases the calculation time and does not require the programmer to operate interactively with the computer, this would be very advantageous.

However, the accuracy of any new approach must be checked with the results found using the Runge Kutta method to ensure that any approximations which are introduced do not produce excessively large errors.

4.4.3 Two Stage Solution

The first two methods presented in sections 4.4.1 and 4.4.2 will give solutions for θ_f, δ, and Γ in one step and subsequent iterations by using the heat and momentum balance in the fluid at the same time as the conduction heat balance in the fin. However, both methods present problems in either computer storage or computer time. The initial step in overcoming these problems at first appears to be contradicting the motives of solving the current model (i.e. of looking at a conjugate problem without making any prior assumptions regarding a heat transfer coefficient or temperature profile). The suggestion of solving the fin immersed in a free fluid has been treated primarily as a conduction problem, with boundary conditions imposed by the surrounding fluid, as used by previous investigators, [16], [17] yet the method now proposed introduces variations into the technique which provides a much more realistic model.

The problem is approached by initially decoupling the model by assuming that a temperature profile on the fin surface is known. The boundary layer problem in the fluid is then approached using this fact. The system is subsequently conjugated by solving the heat conduction problem in the fin with the boundary layer solution already calculated. Although this is an iterative procedure it is found that the calculation is more rapid than the Runge Kutta method, with the factor by which the speeds differ dependent on the initial estimate of a_o, and the solution can be produced without any interaction from the

programmer. The formulation of the problem by this two stage method is given below.

Once it is suggested that the temperature profile on the surface of the fin is known the solution of the momentum and heat balances in the fluid (equations 4.15 and 4.16) can proceed much the same way as the integral analysis for the isothermal wall. To do this, the differential term for the temperature on the surface of the fin is approximated by a central difference and it is assumed that the boundary layer thickness and velocity term are given by:

$$\begin{aligned} \delta &= a_o x^{a_1} \\ \Gamma &= b_o x^{b_1} \end{aligned} \tag{4.23}$$

The substitution of these parameters into the momentum and heat balances allows the coefficients and the powers of x to be found. These substitutions are only strictly true when a_o and b_o are independent of x, which in this case is not true as the temperature term introduces variations in the x direction. It is this fact that introduces the approximations which make the solution to this problem different to that from the Runge Kutta solution discussed in the previous section. It is, therefore, necessary to determine the effect that the substitution given by equation 4.23 has on the resultant fin efficiencies. The expressions for the boundary layer thickness and the velocity term are:

$$\delta = \left(\frac{105\nu + 120\alpha}{1/4\ b_o + \frac{35g\beta\theta_f}{b_o} + b_o \frac{d\theta_f}{dx} \frac{x}{\theta_f}}\right)^{1/2} x^{1/4} \tag{4.24}$$

$$\Gamma = \left(\frac{20\alpha g\beta\theta_f}{\frac{3}{4}\nu + \frac{5}{7}\alpha + \frac{\nu x}{2\theta_f}\frac{d\theta_f}{dx}}\right)^{\frac{1}{2}} x^{\frac{1}{2}} \qquad (4.25)$$

This procedure decouples the problem of finding the heat flow from a downward projecting fin in the same way that previous workers did (e.g. by assuming a temperature profile on the surface of the fin [35]). To couple the fluid boundary layer problem to the heat transfer from the fin the solution of the conduction heat balance in the fin is solved using the value of the boundary layer thickness found from solving the fluid side problem.

To show that the boundary layer can be represented by equation 4.24 a problem can be solved, which has an analytical solution, and the results of the numerical method and the analytical method compared. This will be done in the results section after the solution procedure has been established.

4.4.3.1 Solution Procedure Using Explicit Relationship

Now that the boundary layer thickness, δ, is known the solution to the conduction heat balance over the fin can be obtained. The following solution procedure is for a rectangular fin. The procedure for the triangular fin is similar, but the heat balance includes an extra differential term due to the change in fin thickness with the distance from the fin tip. Also, the term for the acceleration due to gravity is reduced to $g\cos\phi$ where ϕ is the fin half angle.

Equation 4.2, with the boundary layer thickness term included instead of the expression for the temperature gradient normal to the fin surface, is given by:

$$\frac{d^2\theta_f}{dx^2} - \frac{4\,k_{flo}}{k_f}\,\frac{\theta_f}{\delta WT} = 0 \qquad (4.26)$$

To solve this equation for the temperature in the fin a central finite difference substitution can be used which results in a tri-diagonal matrix. This can be solved by a special Gaussian elimination and back substitution, which takes into account the tri-diagonal nature of the matrix. This needs a minimum of computer storage. However, before the matrix can be formed, two boundary conditions are required to resolve the problem at the fin tip and fin base. The boundary conditions have already been given by equation 4.3. However, the condition at the fin tip, which only provides a 'floating' boundary condition, does not provide enough information to solve the above equation. Therefore, the boundary condition at the fin tip must be investigated further.

The explicit expression for the boundary layer thickness, as given by equation 4.24 shows that at the fin tip, where x=0, then the boundary layer thickness must also be zero. This is equivalent to letting the heat transfer coefficient become infinite, and so the temperature of the fin tip becomes that of the surrounding ambient fluid. This can be shown by looking at the heat conduction equation and setting x and δ equal to zero:

$$-4k_{fl}\theta_f = 0$$

Thus $\theta_f = 0$ at the fin tip.

This boundary condition is valid if only long fins are considered, as was done by previously by Lock and Gunn [35] when finding similarity solutions. To find a solution by using similarity

a temperature profile is imposed over the fin surface:

$$\theta_f = \theta_b \left(\frac{x}{L}\right)^n \tag{4.1}$$

This equation shows that at the fin tip where x is set to zero the temperature of the fin is equal to the ambient fluid, $\theta_f = 0$.

However, when the fin is short, equation 4.1 forces the temperature of the fin tip to the temperature of the ambient fluid even though this would not be the actual temperature found in practice. For long fins the approximation that the fin tip temperature is equal to the ambient temperature can be used. Also, this approximation can be used when comparing the current method with previous results. Using the boundary condition for the fin base which gives the temperature at this position (equation 4.3) and setting the fin tip temperature equal to zero a matrix can be formed which uses the finite difference representation of the fin conduction heat balance (equation 4.26). The matrix is given overleaf.

As can be seen from matrix 4.2 the problem has been posed such that a tri-diagonal coefficient matrix must be solved, and this is diagonally dominant. The boundary layer thickness, δ, is expressed in terms of the wall temperature excess, θ_f, as shown in equation 4.26. Iterations must be carried out between the solution for θ_f obtained from the matrix inversion, and the solution of the boundary layer thickness, found using the explicit relationship 4.24.

$$\begin{bmatrix} \frac{-2WT}{(H/N-1)^2} - \frac{4k_{fo}}{k_s\delta(2)} & \frac{WT}{(H/N-1)^2} & 0 & 0 & 0 \\ \frac{WT}{(H/N-1)^2} & \frac{-2WT}{(H.N-1)^2} - \frac{4k_{flo}}{k_s\delta(3)} & \frac{WT}{(H/N-1)^2} & 0 & 0 \\ 0 & 0 & \frac{WT}{(H/N-1)^2} & \frac{-2WT}{(H/N-1)^2} - \frac{4k_{flo}}{k_f\ (N-2)} & \frac{WT}{(H/N-1)^2} \\ 0 & 0 & 0 & -1 & \frac{2k_{flo}(H/N-1)^2}{\delta(N-1)\ WT\ k_f} \end{bmatrix} \begin{bmatrix} \theta_f(2) \\ \theta_f(3) \\ \theta_f(N-2) \\ \theta_f(N-1) \end{bmatrix} = \begin{bmatrix} 0 \\ 0 \\ 0 \\ \theta_b \end{bmatrix}$$

Matrix 4.2 Central difference representation of equation 4.26.

It has already been noted that the above solution is not valid for short fins as the temperature of the fin tip will not be equal to the ambient fluid temperature. To solve the problem with a non-zero fin tip temperature, the heat flow about the tip must be investigated more closely. Recent studies [75], [76] have been carried out to find effective boundary layers about a downward facing heated plate. This can only be an effective boundary layer thickness as a true boundary layer only exists for an upward facing heated plate [77 corrected by 78]. However, this approach is still not fully acceptable as the plates investigated are of infinite extent and are therefore not applicable to the current geometry. To overcome the problem of using a rectangular fin with a zero boundary layer thickness at the fin tip, a heat balance can be carried out over the first element.

Previously [35], the heat balance at the fin tip was not required as the boundary condition required was given by setting the temperature excess equal to zero. If the temperature condition at the fin tip is allowed to vary a heat balance (or some other way of determining a boundary condition) must be carried out. The heat balance is illustrated in figure 4.2a and is given below:

$$k_f WT \left.\frac{d\theta_f}{dx}\right| - \frac{4}{\Delta x} \int_{x=0}^{x=\Delta x} \frac{k_{flo}}{\delta} \Delta x \, \Theta_f \, dx = 0 \qquad (4.27)$$

Because equation 4.24 gives an explicit relationship for the boundary layer thickness the integration can be carried out very easily to find the effective heat transfer coefficient about the fin tip. However, the boundary layer thickness about the downward facing surface is not known so it is assumed, for simplicity, that the fin base is adiabatic. As no other statement about the fin tip can

be stated with any confidence, it is assumed that the fin is long and thin for this condition to be true. This is ensured within the calculation procedure by giving a fin length and then setting the fin thickness to 1% of that value. The matrix to be solved can now be written as matrix 4.3 shown overleaf.

This matrix now contains elements incorporating the temperature at the fin tip, i.e. $\theta_f(1)$. The solution procedure is the same as that used before except the integral term must be evaluated at every iteration.

The only problem with the above analysis is that the assumption of an adiabatic fin tip limits the extent of the possible fin dimensions available for the calculation procedure. This assumption can be dropped if a triangular fin is considered instead of the rectangular fin. If a triangular fin is investigated the boundary condition at the fin tip will change and also the limits of the numerical procedure and the acceleration due to gravity. The condition at the fin tip can again be determined by either allowing the boundary layer to decrease to zero at the tip, and so forcing the temperature of the tip to that of the ambient fluid, or by calculating an average heat transfer coefficient over the first interval. In both cases the matrix formed by the respective boundary conditions are similar to those found for the rectangular fin. For the zero boundary layer at the tip the matrix is shown as matrix 4.4.

$$\begin{bmatrix} \frac{-2k_f WT}{(H/N-1)^2} - I & \frac{2k_f WT}{(H/N-1)^2} & 0 & 0 & 0 \\ \frac{k_f WT\delta(n)}{(H/N-1)^2} & \frac{-2k_f WT\delta(n)}{(H/N-1)^2} - 4k_{flo} & \frac{k_f WT\delta(n)}{(H/N-1)^2} & & \\ & 1 & \frac{-2-4k_{flo}}{\frac{k_s WT\delta(N-1)}{(H/N-1)^2}} & & \end{bmatrix} \begin{bmatrix} \theta_f(1) \\ \theta_f(n) \\ \theta_f(N-1) \end{bmatrix} = \begin{bmatrix} 0 \\ 0 \\ -\theta_b \end{bmatrix}$$

where $I = \frac{4}{\Delta x} \int_{x=0}^{x=\Delta x} \frac{k_{flo}}{\delta} \, dx$

Matrix 4.3 Central Difference Representation of Equation 4.27

$$
\begin{bmatrix}
\frac{-2k_f\cos\phi(N-1)}{H} - \frac{2k_{flo}}{\sin\phi\delta(2)} & \frac{(N-1)\cos\phi k_f}{H}\left((n-1)+\frac{1}{2}\right) & 0 & 0 & 0 \\
\frac{(N-1)\cos\phi k_f}{H}\,(n-1)-\frac{1}{2} & \frac{-2k_f(n-1)\cos\phi(N-1)}{H} - \frac{2k_{flo}}{\sin\phi\delta(n)} & \frac{(N-1)\cos\phi k_f}{H}\,(n-1)+\frac{1}{2} & 0 & \\
 & & & & \\
 & \frac{(n-1)-\frac{1}{2}}{(n-1)+\frac{1}{2}} & \frac{\frac{-2k_f(n-1)\cos\phi(N-1)}{H} - \frac{2k_{flo}}{\sin\phi\delta(N)}}{\frac{(N-1)\cos\phi k_f}{H}\left((n-1)+\frac{1}{2}\right)} &
\end{bmatrix}
\begin{bmatrix} \theta_f(2) \\ \theta_f(n) \\ \\ \theta_f(N) \end{bmatrix}
=
\begin{bmatrix} 0 \\ 0 \\ \\ -\theta_b \end{bmatrix}
$$

Matrix 4.4 Central Difference Representation of Heat Flow From a Tapered Fin.

The heat flow at the fin tip for the triangular fin is illustrated in figure 4.2b. Looking at this figure and using an integral term to express the heat flow from the fin tip the heat balance is given by:

$$\frac{d\theta_f}{dx} - \frac{2\,\theta_f}{k_f \sin\phi WT} \int_{x=0}^{x=\Delta x} \frac{k_{flo}}{\Delta x \delta}\, dx = 0 \qquad (4.29)$$

As with the rectangular fin the average heat transfer coefficient can be found by integrating the term $2k_{flo}/\delta$ between the fin tip and the second node.

Using a forward difference scheme equation 4.29 can be re-written in terms of the temperature at node 1 and node 2.

$$\theta_f(1)\left(\frac{-k_f\cos\phi}{\Delta x} - \frac{2\int_0^{\Delta x} k_{flo}/\delta\, dx}{\sin\phi\, x}\right) + \frac{\theta_{f(2)} k_f \cos\phi}{\Delta x} = 0 \qquad (4.30)$$

This will result in the required matrix containing elements down to the fin tip temperature. However, the numerical procedure for the rest of the fin uses central differencing which has truncation errors only of the second order of the step size (i.e. $O(h)^2$), whereas at the fin tip the forward difference scheme is only first order accurate. To overcome this, a matrix similar to that given before, matrix 4.4, for the triangular fin can be used. The temperature at the fin tip is related to the temperature at the second node by assuming that the analytical solution for the triangular fin with a constant heat transfer coefficient can be used. This will be valid in this case, as the integral term found in the heat balance at the fin tip could be represented by an average, and constant, heat transfer coefficient.

At node two the central difference representation of the conduction heat balance is:

$$\theta_f(3)\ \left[\frac{(N-1)}{H}\cos\phi\ ((n-1)+\tfrac{1}{2})\right] + \theta_f(2)\ \frac{-2(n-1)(N-1)\cos\phi}{H} - \frac{\frac{2}{\Delta x}\int_0^{\Delta x}\frac{k_{flo}}{\delta}\,dx}{k_f \sin\phi}$$

$$+\ \theta_f(1)\ [(N-1)\cos\phi((n-1)-\tfrac{1}{2}) = 0$$

The analytical solution for the surface temperature for a fin with a constant heat transfer coefficient is [79]

$$\theta_f(x) = \theta_f(0)\ \frac{I_o(2\sqrt{\beta'}x)}{I_o(2\sqrt{\beta'}L)} \qquad (4.32)$$

Which, between the first and second node, results in the following relationship between the temperature at the fin tip and the temperature at the second node:

$$\theta_f(1) = \frac{\theta_f(2)}{I_o(2\sqrt{\beta'}\Delta x)} \qquad (4.33)$$

By using this relationship with the finite difference relationship found for node 2 (equation 4.31) a heat balance is obtained that only involves the temperatures at nodes two and three. This results in a matrix similar to that of matrix 4.4 which only involves temperatures down to and including the temperature at node two. However, now the fin tip temperature can be found by using equation 4.33 again, which relates the fin tip temperature to the temperature at node two which is now known. Whereas this method does not use a first order approximation at the fin tip the solution procedure is rather more involved than the solution technique which does make

use of a forward difference scheme. Also, the forward difference scheme provides a solution for all the fin surface temperatures in one step, whereas the approach which uses the Bessel functions has to use two steps to find the complete set of fin temperatures. Therefore, if it is found that the forward difference scheme does not cause a significant difference in the calculated surface temperatures from those found using the analytical method at the fin tip, then matrix 4.5 can be used to find the temperature profile down the fin.

4.4.3.2 Fin Efficiency

By solving the fin conduction problem as given by the matrices 4.2 to 4.5 along with the boundary layer problem, as given by equation 4.24 the temperature profiles of the fins under investigation can be found. All that is needed beforehand is the temperature of the fin base, the temperature of the ambient fluid and the physical properties of the fin and the surrounding fluid. Looking at any interval up the fin the heat flow is given by:

$$\dot{\Delta Q} = -2k_{flo}\,\Delta x\,\left.\frac{d\theta_{fl}}{dy}\right|_{y=0} \qquad (4.34)$$

To find the total heat output this heat flow over an interval needs to be integrated over the whole surface of the fin. Firstly, the differential term is replaced by the relationship given by equation 4.7 for the temperature gradient in the fluid. Thus the heat flow is now given by:

$$\dot{\Delta Q} = 4k_{flo}\Delta x\,\frac{\theta_f}{\delta} \qquad (4.35)$$

$$\begin{bmatrix} \frac{-k_f\cos\phi(N-1)}{H} - \frac{2}{\Delta x\sin\phi}\int_0^{\Delta x}\frac{k_{flo}}{\delta}\,dx & \frac{k_f\cos\phi(N-1)}{H} & 0 & 0 & 0 \\ \frac{(N-1)\cos\phi k_f(n-1)-\frac{1}{2}}{H} & \frac{-2k_f(n-1)\cos\phi(N-1)}{H} & \frac{-2k_{flo}}{\sin\phi\delta(n)} & \frac{(N-1)\cos\phi k_f((n-1)+\frac{1}{2})}{H} & \\ & \frac{(n-1)-\frac{1}{2}}{(n-1)+\frac{1}{2}} & \frac{-2k_f(n-1)\cos\phi(N-1)}{(N-1)\frac{\cos\phi}{H}k_f(n-1)+\frac{1}{2}} & \frac{-2k_{flo}}{\sin\phi\delta(N)} & \end{bmatrix} \begin{bmatrix} \theta_f(1) \\ \theta_f(n) \\ \theta_f(N-1) \end{bmatrix} = \begin{bmatrix} 0 \\ 0 \\ -\theta_b \end{bmatrix}$$

Matrix 4.5 Central Difference Representation of Heat Flow from Tapered Fin with a Forward Difference Scheme at the Fin Tip

This can be integrated numerically as the surface temperatures and the boundary layer thicknesses are known at every point. The two methods of integration investigated are trapezoidal integration and Simpson's method. Trapezoidal integration is the simplest method to use as it can be used for any number of points, and the programming of the method simply adds all the values of the function to be integrated together. However, this method brings in an error of integration of the order of the stepsize used. Thus, if the number of nodes required to reach sufficient accuracy is large it would be better to use Simpson's method of integration as the errors introduced by this method are only of the order $(\Delta x)^2$, where Δx is the stepsize.

Once the heat flow through the fin has been found the fin efficiency can then be evaluated. A value of the fin efficiency itself is no more useful for calculation purposes than just stating the heat flow for any particular fin. However, charts of fin efficiency plotted against a correlating fin characteristic can be produced to cover the whole range of fin geometries. It then only remains for the designer of heat exchange equipment to work out the heat flow from an isothermal fin (which is a simple equation resulting from a similarity solution) and then multiply this value by the fin efficiency found by consulting the graph. For this reason the heat flows found by using the current technique are compared with the heat flows found using an isothermal fin which is at the same temperature as the base of the actual fin.

Harper and Brown [3] and Gardner [4] established a definition for fin efficiency which is used today. The fin efficiency is given by:

$$\eta_{eff} = \frac{\text{actual heat transferred by fin}}{\text{heat which would have been transferred if the entire fin were at the base temperature}}$$

Therefore, to find the fin efficiency the expression for the denominator needs to be stated. Pohlhausen [11] with Schmidt and Beckmann [21] studied a vertical isothermal plate and correlated their data with:

$$\frac{Nu_x}{4\sqrt{Gr_x}/4} = \frac{0.676\ Pr^{\frac{1}{2}}}{(0.861+Pr)^{\frac{1}{4}}} \tag{4.36}$$

Using a similarity solution the following relationship for the Nusselt number is found [80]:

$$Nu_x = 0.507\ Ra^{\frac{1}{4}} \tag{4.37}$$

Equations 4.36 and 4.37 are only true for a vertical flat plate so when a tapered fin is being investigated the effect of inclination must be considered. Rich [81] carried out a series of experiments from which he concluded that there is no qualitative difference in the heat transfer coefficient when a plate is inclined between 0° and 40° from the vertical. Hassan and Mohamed [34] found a relationship which correlates experimental data to within 10%. In [34] the overall Nusselt number is given by:

$$Nu_x = 0.507\ (Ra\cos\phi)^{\frac{1}{4}} \tag{4.38}$$

for $Ra\cos\phi < 2.2\times10^9$

and $-60^\circ < \phi < 15^\circ$

Even though there is some discrepancy between results, the actual correlation used to determine the value of the denominator for the definition of the fin efficiency is insignificant provided that it is stated which correlation is used in deriving the final fin efficiency charts. The expression used in determining the charts to be presented in the results section are based on the correlation as given by Hassan and Mohamed [34]. Once the fin efficiencies for the different geometry of fin considered are found an expression to correlate the data onto one graph needs to be found. Analytical solutions to find fin efficiencies (which use constant heat transfer coefficients for the entire length of the fin, for example [79]) are correlated using the term:

$$L_c^{3/2} \, (\bar{h}/k_s A_m)^{\frac{1}{2}} \text{ along the x-axis where} \qquad (4.39)$$

$L_c = L + WT/2$ for rectangular fin

$= L$ for triangular fin

$A_m = WT.L$ for rectangular fin

$= \frac{WT}{2}.L$ for triangular fin

$\bar{h}$ = average heat transfer coefficient = fn $(L^{-\frac{1}{4}})$ $(\cos \phi)^{\frac{1}{2}}$

If the parameters for the triangular fin are taken and substituted into the expression 4.39 the abscissa becomes;

$$\frac{L^{7/4}}{WT} \; fn'(\cos\phi, k_f) \qquad (4.40)$$

The function involving $\cos\phi$ and k_f results from the Nusselt number which, in the current expressions, does not appear explicitly, but in a more complex form. Therefore, the term $L^{7/4}/WT$ could be used initially to see if it correlates the fin efficiencies found in the

current study, or if terms for the effect of inclination need to be included.

A slight modification to the expression 4.40 may prove useful for plotting the data for different fluids, so that results for different fluids could be easily shown on the same figure. The change suggested means that equation 4.40 is multiplied by k_{fl}/k_f where k_{fl} is the thermal conductivity of the fluid, and k_f the thermal conductivity of the fin. Also, for the triangular fin, the thickness of the base of the fin can be expressed as L tan ϕ, which may be a more appropriate factor when dealing with the triangular fin, rather than the thickness of the fin at the base.

4.5 Results

4.5.1 Check on Solution Procedure

In the following comparisons only constant physical properties are used, as the analytical solutions available cannot consider variation of physical properties. All properties are determined at the average bulk temperature (i.e. $(T_b-T_\infty)/2+T_\infty$).

Firstly, the numerical procedure itself should be checked. To do this a fin with a constant heat transfer coefficient is investigated. This means that the term $2k_{flo}/\delta$ must be replaced by the constant value, h. This can be done with either the rectangular or triangular fin. Using a rectangular fin (and hence the matrix 4.5 in the solution procedure) a temperature profile can be found for the fin surface by the current numerical technique and from this the heat flow from the fin.

For a rectangular fin with a constant heat transfer coefficient and a diabatic fin tip the temperature profile is given by [79]:

$$\frac{T_f - T_\infty}{T_b - T_\infty} = \frac{\cosh(n(L-x)) + (\bar{h}_L/mk_s)\sinh(m(L-x))}{\cosh(mL) + (h_L/mk_s)\sinh(mL)} \tag{4.41}$$

and the heat flow rate from the fin is:

$$\dot{Q} = \frac{\bar{P}\bar{h}Ak_s(T_b - T_\infty)\sinh(mL) + (\bar{h}_L/mk_s)\cosh(mL)}{\cosh(mL) + (h_L/mk_s)\sinh(mL)} \tag{4.42}$$

The temperature profile for the tapered fin with a constant heat transfer coefficient is given by:

$$\theta_f = \theta_b \frac{I_o(2\sqrt{\beta'}x)}{I_o(2\sqrt{\beta'}L)} \tag{4.43}$$

The matrix 4.5 which uses a heat transfer coefficient at the fin tip can be modified very easily by using h instead of the integral term for the heat flow out at the fin tip in the boundary condition. The solution procedure itself is checked by using a very coarse grid up the fin (only 11 nodes used) and the temperature profiles compared between the analytical and numerical results. The comparison is made using the results for a tapered fin. This is done as the approximation introduced by the current analysis is in the boundary layer thickness, which will be the same for both the tapered and rectangular fin. However, the analysis of the tapered fin would be expected to cause more problems, as the matrix formed for the tapered fin will not be as diagonally dominant as for the rectangular fin. This is due to the introduction of terms at the off-diagonal positions by the central differencing of the first differential of the area which occurs in the

fin conduction equation (4.2).

The results are given in table 4.1 for a tapered fin with a half angle of 0.1 radians, with a thermal conductivity of 17 W/m K. The heat transfer coefficient is 10 W/m^2K and the fin is 0.1m high. The base temperature of the fin is 100^oC and the ambient fluid temperature is 20^oC. Method number one is that corresponding to the Bessel function approximation for the temperature at the fin tip, whilst method two finds the fin tip temperature using the heat balance between the first two nodes.

node	method 1	method 2	analytical
11 (base)	80.000	80.000	80.000
10	79.543	79.543	79.543
9	79.087	79.087	79.087
8	78.637	78.637	78.637
7	78.174	78.174	78.174
6	77.276	77.276	77.276
5	76.827	76.827	76.827
4	76.378	76.378	78.378
3	75.931	75.931	75.931
2	75.486	75.486	75.486
1 (tip)	75.012	75.012	75.012

Table 4.1 Comparison of Surface Temperature for a Tapered Fin Using Three Different Calculation Methods

The number of nodes needed to find these identical results is small, because the matrix elements in the numerical procedure are independent of the final solution, and also the temperature profile is very smooth because of the constant heat transfer coefficient.

From table 4.1 it can be seen that the numerical procedure itself is correct. However, it still needs to be verified that the solution of more rigorous systems will give results that converge

when calculating temperature profiles using the numerical procedure. The results given in the following tables show the effect of changing the dimensions of the fin and the fluid in which it is immersed. Constant physical properties are used in all the following comparisons.

Initially, eleven nodes were used on the fin but this was found to be insufficient for calculating values of the heat flow from the fin. However, the temperature profiles and the boundary layer thicknesses do not change significantly between the solution found using 11 nodes and the solution found using 961 nodes. The number of nodes used to find the following results is excessive if the temperature profiles only are needed. However, as was mentioned earlier the heat flow needs to be calculated, and as will be shown later, it is this factor which requires a large number of data points for its accurate calculation.

In the section on the solution procedure two methods for calculating the temperature profile, using the two step method were proposed, (one using a forward difference approach to find the fin tip temperature, the other using the analytical result for a tapered fin). The former will be called method one whilst the latter method two for ease of reference. To test the two methods thoroughly the following set of parameters are used for the situation of a tapered fin surrounded by a fluid with a constant and known heat transfer coefficient. The parameters used are:

Table	h.t.c.	height	k_s	nodes	θ_b
4.3	5.0	0.01	17.0	961	80
4.4	1,000	0.01	17.0	961	80
4.5	10,000	0.01	17.0	961	80
4.6	0.01	0.01	17.0	961	80
4.7	5.0	1.0	17.0	961	80
4.8	5.0	0.0001	17.0	961	80
4.9	5.0	0.1	0.1	961	80
4.10	5.0	0.1	100.0	961	80
4.11	5.0	0.1	17.0	101	80
4.12	5.0	0.1	17.0	961	5
4.13	5.0	0.1	17.0	51	80

Table 4.2 Parameters Used in Testing the Numerical Procedure

Node	Method 1	Method 2	Analytical
961	80.000	80.000	80.000
951	79.957	79.957	79.957
941	79.909	79.909	79.909
931	79.862	79.862	79.862
.			
.			
.			
31	75.625	75.626	75.631
21	75.579	75.979	75.584
11	75.533	75.533	75.538
1 (fin tip)	75.486	75.486	75.492

Table 4.3 Comparison of Surface Temperatures for Three Different Calculation Procedures Using Parameter Set One

Node	Method 1	Method 2	Analytical
961	80.000	80.000	80.000
951	77.649	77.649	77.650
941	75.106	75.106	75.109
931	72.634	72.634	72.639
.			
.			
.			
31	0.754	0.754	0.763
21	0.678	0.678	0.685
11	0.605	0.606	0.612
1	0.537	0.538	0.543

Table 4.4 Comparison of Surface Temperatures for three Different Calculation Procedures Using Parameter Set Two

Node	Method 1	Method 2	Analytical
961	80.000	80.000	80.000
951	72.406	72.406	72.411
941	64.776	64.776	64.785
931	57.917	57.917	57.929
.			
.			
.			
31	3.41×10^{-6}	3.41×10^{-6}	3.45×10^{-6}
21	1.89×10^{-6}	1.89×10^{-6}	1.92×10^{-6}
11	9.21×10^{-7}	9.22×10^{-7}	9.39×10^{-7}
1	3.48×10^{-7}	3.51×10^{-7}	3.53×10^{-7}

Table 4.5 Comparison of Surface Temperatures for Three Different Calculation Procedures Using Parameter Set Three

Node	Method 1	Method 2	Analytical
961	80.000	80.000	80.000
951	80.000	80.000	80.000
941	80.000	80.000	80.000
931	80.000	80.000	80.000
.			
.			
.			
31	79.991	79.991	79.991
21	79.991	79.991	79.991
11	79.991	79.991	79.991
1	79.991	79.991	79.991

Table 4.6 Comparison of Surface Temperatures for Three Different Calculation Procedures Using Parameter Set Four

Node	Method 1	Method 2	Analytical
961	80.000	80.000	80.000
951	78.391	78.391	78.393
941	76.634	76.634	76.637
931	74.909	74.909	74.913
.			
.			
.			
31	3.988	3.988	4.028
21	3.767	3.767	3.804
11	3.552	3.552	3.587
1	3.343	3.343	3.377

Table 4.7 Comparison of Surface Temperatures for Three Different Calculation Procedures Using Parameter Set Five

Node	Method 1	Method 2	Analytical
961	80.000	80.000	80.000
951	80.000	80.000	80.000
941	79.999	79.999	79.999
931	79.999	79.999	79.999
.			
.			
.			
31	79.954	79.954	79.954
21	79.954	79.954	79.954
11	79.953	79.953	79.953
1	79.953	79.953	79.953

Table 4.8 Comparison of Surface Temperatures for Three Different Calculation Procedures Using Parameter Set Six

Node	Method 1	Method 2	Analytical
961	80.000	80.000	80.000
951	72.986	72.986	72.990
941	65.879	65.879	65.887
931	59.432	59.432	59.443
.			
.			
.			
31	1.380×10^{-5}	1.380×10^{-5}	1.404×10^{-5}
21	8.079×10^{-6}	8.080×10^{-6}	8.228×10^{-6}
11	4.251×10^{-6}	4.254×10^{-6}	4.329×10^{-6}
1	1.816×10^{-6}	1.830×10^{-6}	1.843×10^{-6}

Table 4.9 Comparison of Surface Temperatures for Three Different Calculation Procedures Using Parameter Set Seven

Node	Method 1	Method 2	Analytical
961	80.000	80.000	80.000
951	79.928	79.928	79.928
941	79.849	79.849	79.849
931	79.769	79.769	79.770
.			
.			
.			
31	72.776	72.776	72.784
21	72.702	72.702	72.709
11	72.625	72.625	72.633
1	72.549	72.549	72.558

Table 4.10 Comparison of Surface Temperatures for Three Different Calculation Procedures Using Parameter Set Eight

Node	Method 1	Method 2	Analytical
101	80.000	80.000	80.000
91	76.665	76.665	76.669
81	73.055	73.055	73.062
71	69.544	69.544	69.554
.			
.			
.			
31	56.445	56.446	56.465
21	53.398	53.400	53.421
11	50.439	50.441	50.464
1	47.566	47.572	47.593

Table 4.11 Comparison of Surface Temperatures for Three Different Calculation Procedures Using Parameter Set Nine

Node	Method 1	Method 2	Analytical
961	5.000	5.000	5.000
951	4.978	4.978	4.978
941	4.954	4.954	4.954
931	4.930	4.930	4.930
.			
.			
.			
31	3.028	3.028	3.030
21	3.010	3.010	3.011
11	2.991	2.991	2.993
1	2.973	2.973	2.975

Table 4.12 Comparison of Surface Temperatures for Three Different Calculation Procedures Using Parameter Set Ten

Node	Method 1	Method 2	Analytical
51	80.000	80.000	80.000
41	73.346	73.347	73.353
31	66.335	66.337	66.378
21	59.711	59.714	59.729
11	53.460	53.466	53.482
1	47.569	47.584	47.593

Table 4.13 Comparison of Surface Temperatures for Three Different Calculation Procedures Using Parameter Set Eleven

From the above tables (4.3 to 4.12) it can be observed that both methods one and two provide excellent approximations of the temperature profile derived from the analytical solution in all cases. Therefore, due to the fact that method one can be programmed more easily it is this method that is used for all future calculations.

In the last table (4.13) the results are shown for the temperature profiles when only 50 nodes are used in the fin. The maximum error occurs at the fin tip, as would be expected as this is the 'floating' boundary condition. However, even at this point the error is only 0.05% for method one and 0.02% for method two. This indicates that the number of nodes required to obtain an accurate solution is much less than is currently being used. This is true if the temperature profile alone were being found when it is known that the resistance to heat flow on the fluid side, i.e. the heat transfer coefficient, is constant. In the situations considered so far this is true as the analytical case was being studied at the same time to check the solution procedure. In the current, more realistic situation, when the boundary layer thickness, and hence the heat transfer coefficient, is changing up the fin the constant boundary conditions are not applied to the fin. This means that the number of nodes will be greater if an accurate solution is desired. Also, the fin efficiency of the fins is required, so the heat flow must be calculated. As was discussed in the solution procedure the heat flow from the fin is found by using numerical integration. This integration needs the point values of the temperature at the fin surface. Thus, the error in the heat flow will be greater than the error in the values of the temperature, as the calculation of the former depends on the values of the latter. It

is therefore necessary to find the number of nodes needed to calculate an accurate value of the heat flow.

Looking at one particular case when the pertinent parameters are:

$$H = 0.01m; \qquad \phi = 0.05 \text{ rads};$$
$$h = 5.0 \text{ W/m}^2\text{K}; \qquad k_f = 17.0 \text{ W/mK} \tag{4.44}$$

The fin efficiency for a tapered fin when there is a constant heat transfer coefficient is given by:

$$\eta_{eff} = \frac{1}{\sqrt{\beta' L}} \quad \frac{I_1(2\sqrt{\beta' L})}{I_o(2\sqrt{\beta' L})} \tag{4.45}$$

where $\beta' = (h/k_f \sin\phi)$

Using the parameters given in equation 4.44 in equation 4.45 the fin efficiency is 0.9717. Using the same parameters but solving the problem numerically with different numbers of nodes a set of results are found to show how the calculated fin efficiency changes when more nodes are used in the solution. The results given below are found using Simpson's method for numerical integration when the temperature profile is calculated using method one:

no. nodes	fin efficiency	analytical solution	% diff.
240	0.9677	0.9717	0.41
480	0.9697	0.9717	0.21
960	0.9707	0.9717	0.10

Table 4.14 Comparison of Fin Efficiency Using Different Numbers of Nodes

As the number of nodes chosen is such that the step size in the numerical procedure decreases by a factor of two each time, a simplified form of Richardson's extrapolation will yield the converged solution to the problem, as well as the order of the error in the procedure adopted. As could be found by inspection of the second column of table 4.14 the error is of the order of the mesh size, and the extrapolated solution is found to be the same as the analytical solution, namely 0.9717. This provides extra evidence to show that the current solution method is a valid one.

With the constant heat transfer coefficient the number of nodes needed does not have to be as large as 960 to find an accurate solution for the fin efficiency. However, by stating that there is a constant heat transfer coefficient implies that there is also a constant value for the boundary layer thickness. From the results given here the change in the boundary layer thickness is significant, and cannot be ignored. The only possible situation which may yield a constant heat transfer coefficient is for very long fins, where the rapidly changing boundary layer thickness at the fin tip does not significantly contribute to the overall heat flow. However, in such a case the assumption of laminar flow may be violated. In the conjugate problem now considered the boundary layer is permitted to change up the fin. This case needs to be studied separately to ensure that the number of nodes to be used in the calculation procedure provides converged solutions.

Given below (table 4.15) are the results for fin efficiency when air is being heated using a fin of height 0.1m with a base temperature of $100^{o}C$. The ambient fluid temperature is $20^{o}C$ and the fin has a thermal conductivity of 17.0W/mK. The physical properties of the air are assumed constant throughout (except that

the variation of density is taken into account by using the coefficient of expansion).

No. Nodes	Fin Efficiency
60	0.4704
120	0.4705
240	0.4705
480	0.4706
960	0.4706

Table 4.15 Change in the Calculated Fin Efficiency with Increasing Number of Nodes

These results show that the fin efficiency can be found very accurately and quickly with relatively few nodes up the fin. This result cannot be compared with an analytical result as a solution is not possible in this situation. However, the above result is obtained using the two step method, so it is desirable to check this solution with that obtained by the one step shooting technique (see section 4.4.2). The result for the temperature profile up the fin does not vary with the number of nodes required, as the Merson procedure divides down the actual elements into smaller elements where required. The method of finding the heat flow in this situation is different than for the two step method as the temperature gradient at all points is found, including the base of the fin, so that the heat flow per unit area is easily found, as discussed in the section on the solution procedure. Thus, only one calculation is required to find theheat flow, from which the fin efficiency can be calculated. The fin efficiency found using the one step method is 0.4624. Thus it can be seen that the fin efficiencies found from the two different methods used give results that are in good agreement, in this case the

difference between the two solutions is less than 2%.

The fin efficiencies for a complete range of fins can now be calculated by either the two step or one step method. As already mentioned the solution for the one step method is severely hindered by having to carry out a shooting procedure to find the value of the independent constant. Once experience has been gained, and the programmer can approximate the initial value of A (the independent constant), then an interactive procedure will not be necessary. However, it has been found that the Runge Kutta Merson technique, used in the one step method, is sensitive to the initial guess for A, and consequently the procedure fails if this initial guess is not sufficiently accurate. In some cases this is not the case and no matter what the starting value for A is, within reason, the procedure will find a final solution for A, and hence the fin efficiency and temperature profile. This anomalous behaviour is one of the reasons why the two step method is preferred to the one step method for finding the majority of fin efficiency results. Another reason for using the two step method is that the calculation of fin efficiencies when using variable physical properties is a simple extension of the method, and is very similar to the procedure used for the plane wall case discussed in chapter three.

The calculation of fin efficiencies is carried out for rectangular and tapered fins surrounded by either water or air. Figure 4.3 presents the results for a rectangular fin. As well as giving the results obtained by the two methods already described, the results found from a standard text [79] are also given. Figure 4.4 gives the same results as in Figure 4.3 except that a tapered fin is considered when obtaining these results. In [79] the scale on the

abscissa is given by $L^{7/4}\ (h/kA_m)$, so the results given normally cannot be plotted directly onto figures 4.3 and 4.4. Some value for the constant heat transfer coefficient term must be defined and used in transforming the standard fin efficiencies (i.e. those given in [79]) to values that can be used for comparison with the current results. Fortunately a correlation has already been proposed in the solution procedure which can also be used here. The correlation is that proposed by Hassan and Mohamed [34] and was given by:

$$Nu = 0.507\ (Ra.\cos\phi)^{\frac{1}{4}} \qquad (4.38)$$

$$Ra.\cos\phi < 2.2 \times 10^9$$

$$-60^\circ < \phi < 15^\circ$$

This relationship is now used to find a constant value for the heat transfer coefficient to be used in calculating the fin efficiencies. The results of Gardner [4] are used in calculating the fin efficiencies, which are then plotted on figures 4.3 and 4.4.

The results plotted using the present two step numerical method and the one step procedure are found using constant physical properties when the base temperature of the fin is $100^\circ C$ and the ambient temperature is $20^\circ C$.

Perhaps the first result that is apparent from looking at figure 4.3 and 4.4 is that for the short fins, or very thick fins, when the correlating parameter is small, the fin efficiencies obtained are greater than unity. This at first appears to be impossible until it is remembered how the fin efficiencies calculated here are derived. The heat flow from the fin is first calculated using one of the two numerical methods. This value is then divided by the heat flow

found using a correlation obtained by consideration of an isothermal fin immersed in the same fluid (equation 4.39). The latter value is found by assuming a constant heat transfer coefficient which is determined by a similarity solution. The fact that the subsequent fin efficiency is found to be greater than unity is in direct consequence of the evaluated average thickness of the boundary layer being less than that in the similarity solution. This means that the average heat transfer coefficient is therefore greater than predicted by the similarity solution, and therefore the calculated heat flow is greater when considering the conjugate problem than if the fin alone were considered. The fin efficiency charts may be used in exactly the same way as those already in current use, provided that the denominator in the definition of the fin efficiency is clearly defined.

For the longer fins (i.e. as we move further to the right hand side of the plots) the values of the fin efficiencies tend towards each other. In fact, between values of the abscissa of 0.65 and 0.35, the values for the fin efficiency of a rectangular fin immersed in air are the same for the standard fin efficiencies [79] and those calculated by the current method. The trends for both the tapered fin and rectangular fin are similar as the parameter $L^{7/4}k_L/WTk_f$ is increased. For very large values of this parameter (at which point the laminar region of flow about the fin is changing to the transition region), the values of the fin efficiency as calculated by the numerical methods and the analytical method are once again tending towards the same value. Although this may be theoretically gratifying this result is of little practical use in simplifying the solution procedure. Even though the analytical solution can be used for very long fins without

introducing a large error, it is very unlikely that fins of such dimensions would have any practical use, as for these long fins the fin efficiency has fallen to 0.1, or below, and the addition of fins would not make good economic sense.

Looking at the two different ways in which the numerical analysis calculates the fin efficiency, very good agreement can be seen between the two methods for all values of the correlating parameter. All trends in one are also shown in the other and the actual values themselves give excellent agreement. The greatest deviation between the two methods is shown for the rectangular fin when immersed in air. However, even here the difference between the two methods is less than 3%.

The temperature profile along the fin and boundary layer thickness about the fin are now investigated. From the investigation it is hoped that some insight might be obtained as to why the fin efficiencies found are greater than unity. Looking at a rectangular fin of height 0.1m with a base temperature of 100^{o}C when the ambient water temperature is 20^{o}C, table 4.16 shows the temperature of the fin surface and the boundary layer thickness up the fin. The two step method is used with 96 nodes on the fin.

node	$\delta(n)$/m	$\theta(n)/^{o}C$
961 (base)	0.0016	80.000
921	0.0022	26.982
881	0.0027	10.075
841	0.0034	4.169
801	0.0041	1.875
.		
.		
.		
161	0.0195	$5.34*10^{-2}$
81	0.0190	$3.96*10^{-2}$
41	0.0169	$3.13*10^{-2}$
1 (tip)	0.0000	$2.81*10^{-2}$

Table 4.16 Temperature Profile and Boundary Layer Thickness for a

For the same system, but when the fin is only of height 0.001m, the boundary layer thickness and temperature are found to be:

node	$\delta(n)/m*10^{-4}$	$\theta(n)/^{o}C$
961 (base)	5.28	80.000
921	5.49	65.067
881	5.72	52.858
.		
.		
.		
281	8.53	3.411
241	8.53	2.921
201	8.45	2.521
161	8.27	2.200
121	7.93	1.950
81	7.35	1.766
41	6.29	1.645
1 (tip)	0.00	1.597

Table 4.17 Temperature Profile and Boundary Layer Thickness for a Rectangular Fin of 0.001m Immersed in Water

The previous two tables show interesting results for the value of the boundary layer thickness with an increase in distance from the leading edge. Near the fin tip the boundary layer grows, as one would expect. However, as the distance from the leading edge increases the boundary layer thickness shrinks. The initial increase in the boundary layer thickness is due to the increase in distance from the leading edge, as represented by the $x^{\frac{1}{4}}$ term which occurs in the analytical solutions (see, for example, [21]). The decrease in the boundary layer thickness at greater distances from the leading edge is due to the fact that the temperature profile is having an opposite effect on the growth of the boundary layer, and at a certain

critical point, dominates the distance term. This is best shown by looking at a simplified representation of the expression giving the boundary layer thickness. The equation for the boundary layer thickness (equation 4.24) can be simplified to give:

$$\delta = \text{constant } (\frac{x}{\theta_f})^{\frac{1}{4}} \tag{4.46}$$

The temperature profile found for the situations given by tables 4.16 and 4.17 are such that at the critical point from the leading edge (i.e. the fin tip), the term x/θ_f starts to decrease with x (as while x is increasing so is θ_f). This result can be compared with an analysis carried out by Sparrow and Gregg [63].

Although the increase in boundary layer thickness found in the present study is not a unique result it has not previously been noted specifically. This seems strange as this result will effect how closely fins can be spaced together in a fin array. In a standard text [82] it is stated that fins should be placed at such a distance so that boundary layers of neighbouring fins do not interfere with each other. They then proceed to state that by considering boundary layer theory a certain value is found, but that this distance can be reduced without affecting the efficiency of the array. This suggests that the boundary layer thickness found is the incorrect one. Such a situation will arise if the boundary layer is calculated using an isothermal fin, or a fin with a temperature profile that is not the correct one. In either of these cases the value of the boundary layer will be found to increase monotonically for the complete height of the fin. If the conjugate situation is considered, as here, then the correct boundary layer thickness can be calculated and so an accurate placement of fins in an array may be obtained.

At this point the present results will be compared with those available by looking at the similarity solution obtained by Sparrow and Gregg [63]. (However, as pointed out by Gebhart and Mollendorf [83] this solution is, in fact, an asymptotic solution for $x_L=\infty$, or for a vertical plate starting from $x=-\infty$. The analysis by Kao, Domoto and Elrod [65], shows that for a semi-infinite vertical plate the solution is non-similar).

Assuming that the temperature profile as given in table 4.17 can be fitted using the assumed temperature profile as given in [63]

$$(T_f-T_\infty) = (T_b-T_\infty)e^{-(m(1-x))} \qquad (4.47)$$

A least squares fit can be carried out to find a value for m. This profile is chosen as it is the one used in [63] not because it will necessarily give a good fit. By carrying out a least squares fit the value of -14.38 is found for m. Also, the standard deviation is found to be high as compared with the actual values of the temperatures, which indicates that the fit is not a very good one. However, the trend in the temperature profile is what is required at this point, and not an accurate fit. This value of m can now be used with the results found by Sparrow and Gregg to find the boundary layer thickness about a plate with such a temperature profile.

In [63] the edge of the boundary layer can be found using the plot of velocity against $y/x(Gr_x/x)^{\frac{1}{4}}mx^{\frac{1}{4}}$, which is the abscissa. By estimating the point at which the velocity decreases to zero the value of y, the boundary layer thickness, can be found.

At $y/x(Gr_x/4)^{\frac{1}{4}}mx^{\frac{1}{4}}=10$, the velocity of the heated fluid about the plate is very small. From this, the boundary layer thickness for various values of x, the distance from the fin tip, can be found by

using:

$$y.const.e^{-14.38/4\ (0.1-x)} = 10 \qquad (4.48)$$

At the average bulk temperature, which is 60°C, the value of the constant is 11,100. This gives rise to the following set of results for the boundary layer thickness:

height	δ/m
0.01	0.00125
0.02	0.00120
.	.
0.10	0.00090

Table 4.18 Sample Boundary Layer Thicknesses Calculated from [63]

From these results, it can be seen that for this particular temperature profile the boundary layer thickness decreases with distance from the leading edge.

Although the results using this temperature profile do not show good agreement with the boundary layer thickness results as given in table 4.17 the trend of decreasing boundary layer thickness with height is reproduced. The discrepancy is not surprising as the temperature profile found to fit the similarity solution is only a rough guide to indicate the trend of the manner in which the temperature changes up the fin. However, the important result of the decreasing boundary layer thickness is highlighted. This shows that the current results are in line with the similarity solutions. The comment referring to the fact that the decreasing boundary layer thickness found by the numerical analysis is not a unique solution results from carrying out the above comparison.

The only reason for this decrease in boundary layer thickness not being noted before is because the correct temperature profiles for a fin were not known. This serves to reinforce the fact that the conjugate nature of a fin immersed in a quiescent fluid should be studied without imposing a temperature profile or a heat flux at the fin surface. These two parameters cannot be predicted with enough accuracy before calculations are carried out on the fin.

So far the case of a rectangular fin in water has been considered. Looking now at a rectangular fin immersed in air the boundary layer thickness and temperature profiles can be obtained for a completely different system. Table 4.19 gives the results for a fin of height 1.0m whilst table 4.20 gives the results for a fin of height 0.01m. The fin heights are larger than for the water case as the laminar region extends much further in this case.

node	$\delta(n)/m$	$\theta_f(n)/^oC$
961 (base)	0.0179	80.000
921	0.0189	64.548
881	0.0198	51.118
841	0.0207	40.691
.		
.		
.		
281	0.0316	2.485
241	0.0818	2.094
201	0.0316	1.780
161	0.0310	1.531
121	0.0299	1.339
81	0.0277	1.120
41	0.0230	1.110
1	0.000	1.076

Table 4.19 Boundary Layer Thickness and Temperature Profile for a Rectangular Fin 1.0m Long Immersed in Air

node	$\delta(n)/m$	$\theta s(N)/^{o}C$
961 (base)	0.00571	80.000
921	0.00570	77.263
881	0.00569	74.371
841	0.00568	71.629
.		
.		
.		
201	0.00464	45.115
161	0.00445	44.445
121	0.00423	43.897
81	0.00357	43.477
41	0.00301	43.198
1 (tip)	0.00000	43.091

Table 4.20 Boundary Layer Thickness and Temperature Profile for a Rectangular Fin 0.01m Long Immersed in Air

In Table 4.19 the increase and subsequent decrease in the boundary layer thickness can be seen. However, in table 4.20, which is for the much shorter fin, the boundary layer thickness increases for the complete length of the fin, but it would be expected that for a slightly longer fin the boundary layer thickness will decrease with increasing height. From these results for the rectangular fin, it is seen that it is impossible to pre-define a heat transfer coefficient, and even allowing the heat transfer coefficient to increase or decrease along the fin will not predict the correct nature of the problem, unless the conjugate nature of the fin is studied along with boundary layer analysis.

The results for the tapered fin are given below in tables 4.21 to 4.24. The first two are for the case when water is being heated, and third and fourth tables are when air is being heated. The heights considered are 0.1m, 0.001m, 1.0m and 0.1m. The fin half angle in all situations is 0.01 rads.

node	$\delta(n)/mx10^{-3}$	$\theta s(n)/^{o}C$
961 (base)	1.67	80.000
921	1.80	56.056
881	1.95	39.188
841	2.11	27.566
.		
.		
.		
201	5.83	0.112
161	6.12	0.074
121	6.38	0.047
81	6.56	0.028
41	6.46	0.015
1 (tip)	0.00	$5.03x10^{-3}$

Table 4.21 Boundary Layer Thickness and Temperature Profile for a Tapered Fin 0.1m Long Immersed in Water

node	$\delta(n)/mx10^{-3}$	$\theta s(n)/^{o}C$
961 (base)	5.27	80.000
921	5.30	75.500
881	5.32	71.081
841	5.34	66.851
.		
.		
.		
201	5.08	19.362
161	4.94	17.312
121	4.74	15.312
81	4.44	13.333
41	3.89	11.307
1 (tip)	0.00	8.794

Table 4.22 Boundary Layer Thickness and Temperature Profile for a Tapered Fin 0.001m Long Immersed in Water

node	$\delta(n)/m$	$\theta s(n)/^{o}C$
961 (base)	0.0181	80.000
921	0.0182	75.252
881	0.0183	70.235
841	0.0184	65.479
.		
.		
.		
201	0.0183	15.971
161	0.0178	14.058
121	0.0172	12.219
81	0.0162	10.429
41	0.0142	8.633
1 (tip)	0.0000	6.523

Table 4.23 Boundary Layer Thickness and Temperature Profile For a Tapered Fin 1.0m Long Immersed in Air.

node	$\delta(n)/m$	$\theta s(n)/^{o}C$
961 (base)	0.00571	80.000
921	0.00566	79.585
881	0.00561	79.122
841	0.00555	78.635
.		
.		
.		
201	0.00399	70.316
161	0.00378	69.680
121	0.00353	69.006
81	0.00320	68.280
41	0.00269	67.460
1 (tip)	0.00000	66.345

Table 4.24 Boundary Layer Thickness and Temperature Profile for a Tapered Fin 0.01m Long Immersed in Air

With the tapered fin similar results are obtained compared with the rectangular fin, except that the position at which the boundary layer starts to decrease is changed. Some typical results are presented graphically in figures 4.5 to 4.8. In these the temperature gradient in the fin is given, as well as the results for the boundary layer thickness and the temperature. The first two figures are for the same system parameters, except that the fin half angle in figure 4.6 is 0.25 rads, whilst the angle for all the other situations is 0.01 rads. The decrease in the boundary layer thickness is shown most dramatically in figures 4.7 and 4.8 where the fin is 1.0m and 10.0m respectively.

The values for the temperature gradient and temperature have been suitably scaled so that their values can be read directly from the x-ordinate. An interesting result which is apparent from these figures is the change in the temperature gradient with height up the fin. For the short fins, most heat is transferred from the bottom of the fin where the boundary layer thickness is smallest, but there is a significant temperature difference between the fin tip and the ambient fluid. For the long fins there is little transfer of heat at the fin tip as the driving force for heat flow, which is the temperature drop from the fin surface to the ambient fluid, is negligible for a great extent of the fin. This effect is reinforced by the fact that for the long fins the boundary layer thickness is greatest at the fin tip, which gives a large resistance to any heat flow that does take place.

The effects of variable physical properties are best noted by returning to fin efficiency charts which plot values of fin efficiency

for the same situations, but when the theoretical analysis is carried out using either the constant or variable physical property equations. The consideration of variable physical properties is usually considered as a fine tuning exercise, and yet little evidence is given to back this up. Investigations have been carried out into the heat flow into gases at high temperatures but only using analyses which do not consider conjugate effects. The figures 4.9 and 4.10 show how fin efficiency changes when the effect of variable physical properties is considered over the boundary layer. Tapered fins are considered when calculating the curves for both figures. In figure 4.9 water is the ambient fluid and figure 4.10 gives analogous results for the case when air is being heated.

In figure 4.9 is can be seen that the results for all but the situation when the base temperature of the fin is $10^{o}C$ and the ambient fluid temperature $5^{o}C$, give very similar results. However, when the low temperature situation is considered the variation in fin efficiency is very noticeable. The fact that the fin efficiency for the constant physical property case is higher is not unexpected, as at these temperatures the properties of water change very significantly with temperature. However, the fact that the calculated fin efficiency is very much higher when variable properties is used shows that for this situation the use of variable properties is anything but a fine tuning exercise. Even though the values of fin efficiency follow the same trend with the length of fin for both the constant and variable physical property case the difference is very great. For example, for a value of the x-coordinate of $5*10^{-3}$ the fin efficiency as calculated using constant properties is 0.67, whilst that found when using variable properties is 0.8. When changed into heat flows

through a fin this results in a difference of 20%. In the case when the base temperature is 100°C and the ambient fluid is 5°C the effect of the low temperatures is negligible, as the majority of the fin will be at a significantly higher temperature.

In figure 4.10 it is interesting to note how there are two results for the fin efficiency for the longer fins (i.e. larger values of the x-ordinate). For the cases when the fin base temperature and ambient fluid temperature are close together, the fin efficiency is higher than when the two temperatures are very different. However, for the shorter fins this effect does not occur. For the situation when the temperatures of the fin base and ambient fluid are very different there is no significant effect in the fin efficiency when using variable or constant physical properties. When the temperatures are close there is a noticeable difference between the two calculated values. In one case, when the base temperature is 10°C, the variable property result is lower than the constant property result. When the fin base temperature is 250°C this trend is reversed, so that variable property calculations give higher values for the fin efficiency. Thus, it is shown that for accurate calculations, variable physical properties should be used in many cases as no trend emerges between the constant and variable physical property results.

4.6 Conclusions

The two numerical methods proposed in this chapter can be used to find the heat flow and hence the fin efficiency from a downward projecting fin. All that is required to be known beforehand are the physical properties of the fluid to be heated and the fin material, the temperature of the base of the fin and the ambient temperature of

the bulk fluid. This is in marked contrast to previous methods that have either assumed a heat transfer coefficient or some temperature profile on the fin surface. To find the heat flow a boundary layer problem is solved as an intermediate stage. This analysis yields the thickness of the boundary layer and the temperature profile up the fin. The boundary layer thickness values give an indication of the heat transfer coefficient.

From the results found for the boundary layer thickness, it is shown that the expected result of an increasing boundary layer as we move away from the leading edge is not always realised. However, it is not possible beforehand to predict the way in which the boundary layer will grow. It is therefore invalid to pre-define a heat transfer coefficient along the fin, even if the heat transfer coefficient is allowed to vary.

For short fins, the exact size depending on the conditions (but generally speaking for water $L < 0.0001m$ and for air $L < 0.01m$) the boundary layer thickness does increase monotonically as the distance from the leading edge is increased. However, as the fin becomes longer a critical point is reached where the boundary layer begins to decrease with increasing distance from the leading edge. Again, the position of the critical point depends on the conditions and the geometry of the fin, and its position cannot be predicted accurately beforehand.

For the shorter fins, immersed in air or water, fin efficiencies are greater than unity and this is due to the definition of the fin efficiency. This shows that using a conjugate heat transfer analysis to calculate the heat flow gives an overall heat transfer coefficient larger than would be expected. However, as the fins under consideration

become longer the predicted value of the fin efficiency as given by the current study becomes comparable to that predicted by standard texts [79] (see figures 4.3 and 4.4). In fact in the case of air, the fin efficiency found numerically drops below that found analytically. This overestimate would, however, be correct when designing a piece of equipment by the addition of safety factors to ensure that it would operate under the required conditions. This overestimation only occurs for long fins where the fin efficiency is below approximately 0.4, in which case it would not normally be economically viable to attach fins to a heat exchange surface. Fortunately, for fins which would be of much more practical use, i.e. their fin efficiencies are high, the standard figures for predicting fin efficiencies underestimate the actual fin efficiency that would be obtained. This does not cause any problems for the operation of equipment designed this way, but it does mean that any heat exchanger would be grossly over sized, and hence more expensive than is necessary for the required specification.

When calculating fin efficiencies using variable physical properties it can be seen from figure 4.9, and to a certain extent 4.10, that it is important to determine the temperature range that the fin will be operating in. In the case of water, figure 4.9, for most lengths of fin the fin efficiency is the same for all values of the fin base temperature and the ambient fluid temperature except when the base temperature is $10^{o}C$ and the ambient fluid temperature is $5^{o}C$. Operating across this temperature range has a significant effect on the fin efficiency due to the change in properties across the boundary layer. This only occurs for water at this temperature, as in this temperature range the physical properties of water change very dramatically. Therefore, once again, an effect is noticed which distinguishes the current study from previous solutions presented.

It is demonstrated that it is not possible to accurately predict the behaviour of a fin immersed in a free fluid. This means that no assumptions can be made a priori regarding the heat transfer coefficient or the temperature profiles, so that analytical solutions to the fin problem can be produced.

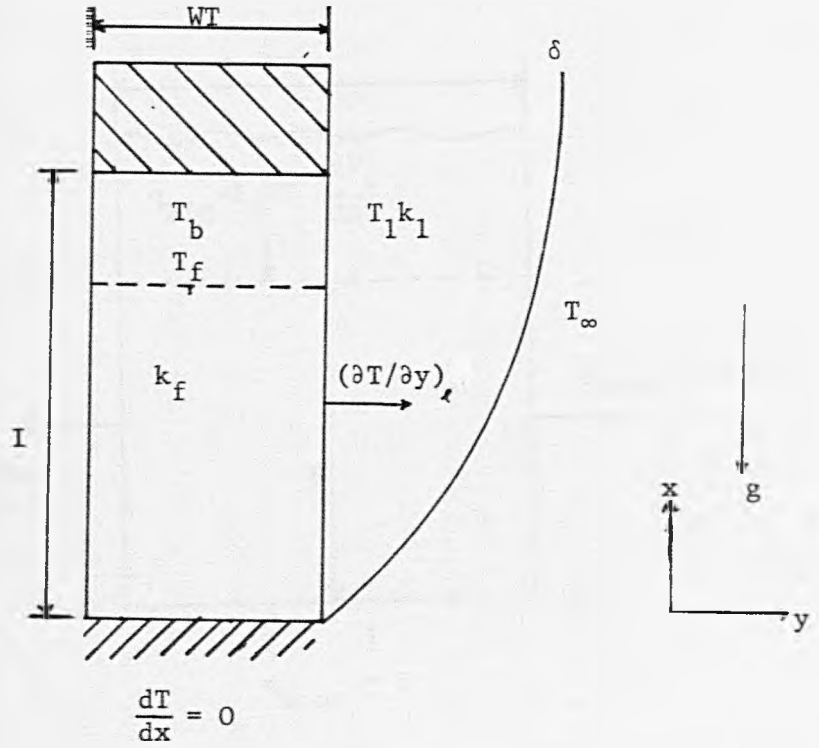

Fig. 4.1a Diagram of system and coordinates of a downward projecting rectangular fin in a free fluid

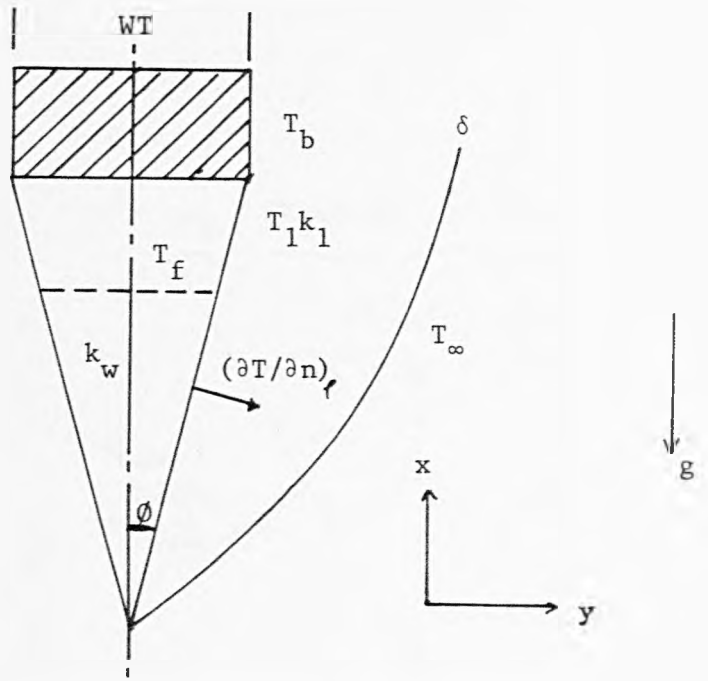

Fig. 4.1b Diagram of system and coordinates of a downward projecting tapered fin in a free fluid

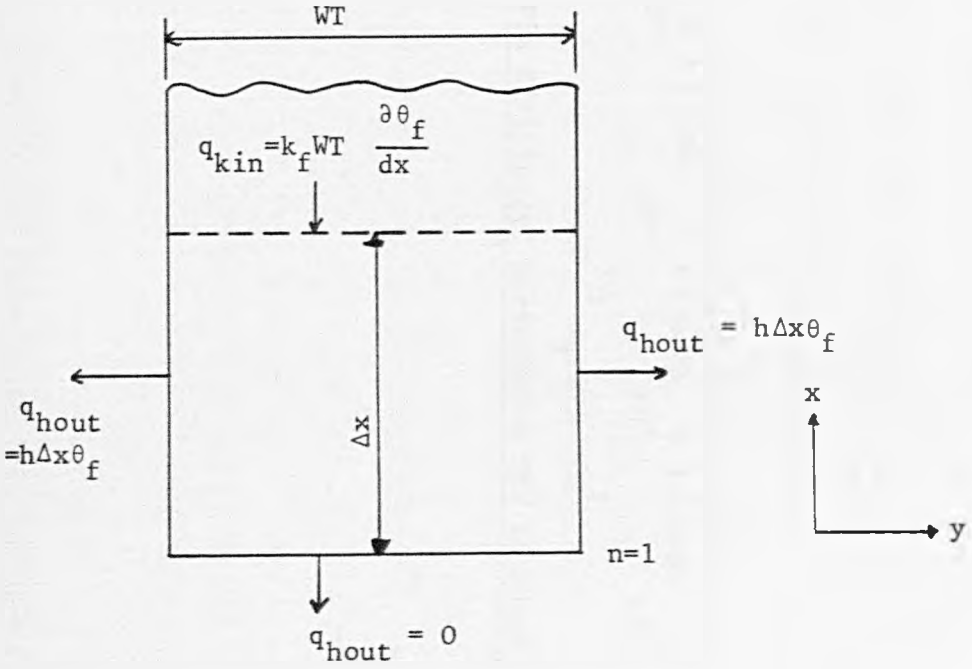

Fig. 4.2a Heat flow from fin tip of a rectangular fin

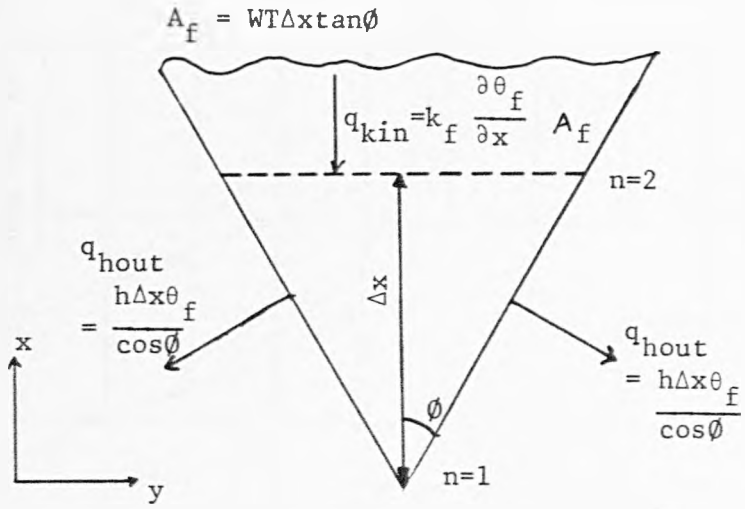

Fig. 4.2b Heat flow from fin tip of a tapered fin

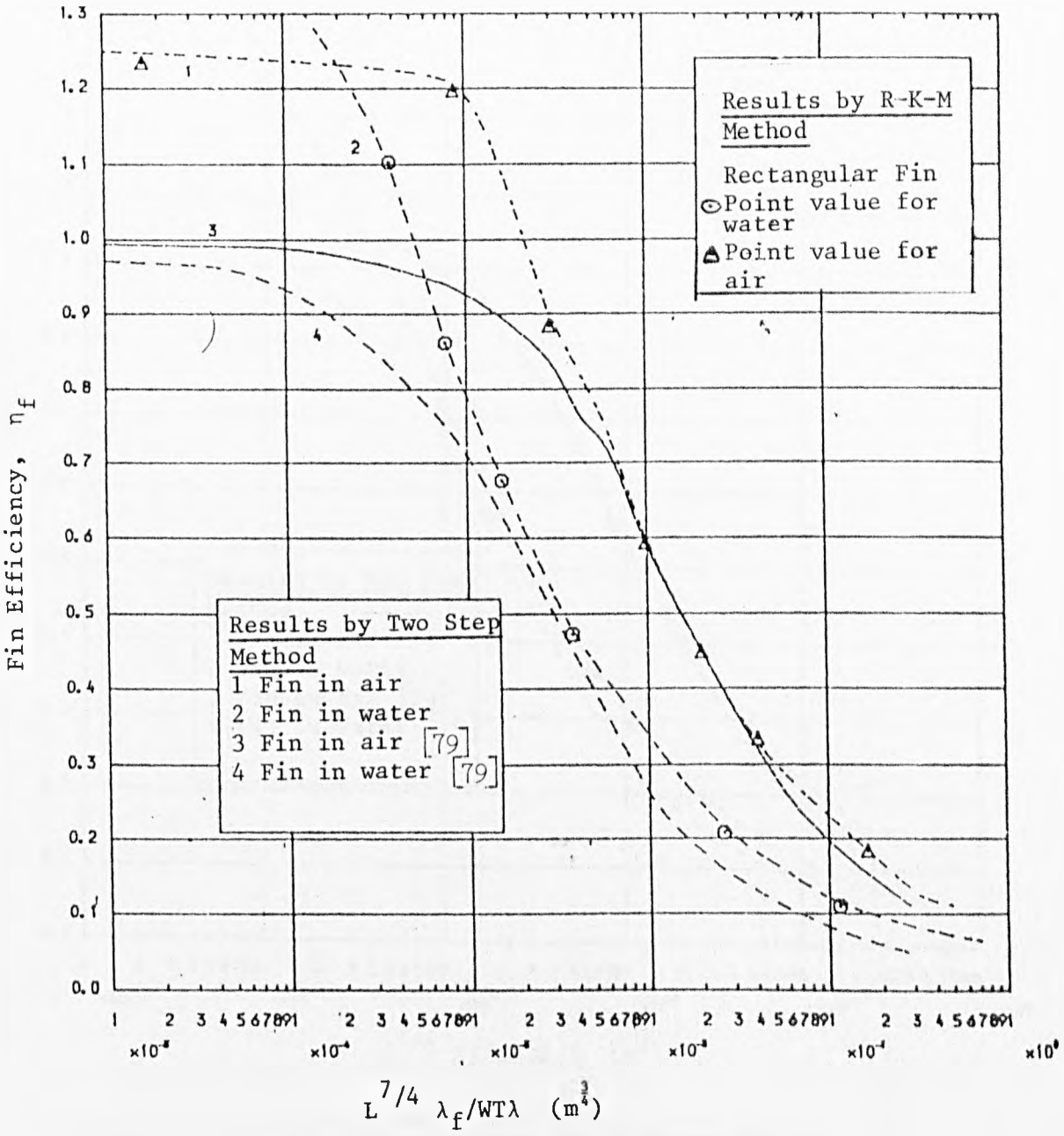

Fig. 4.3 Fin Efficiency, Rectangular Fin in Water or Air

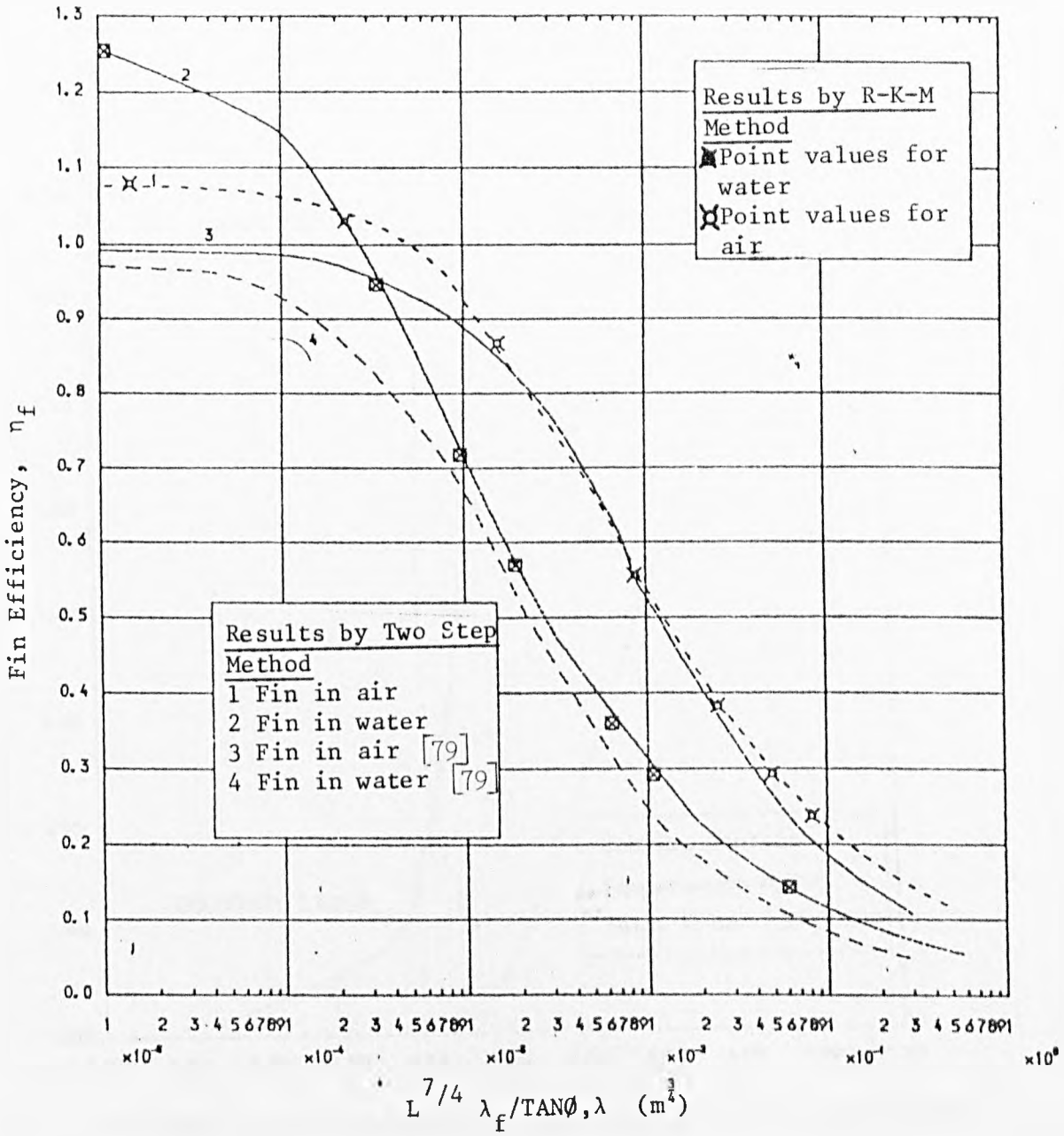

Fig. 4.4 Fin Efficiency, Tapered Fin in Water or Air

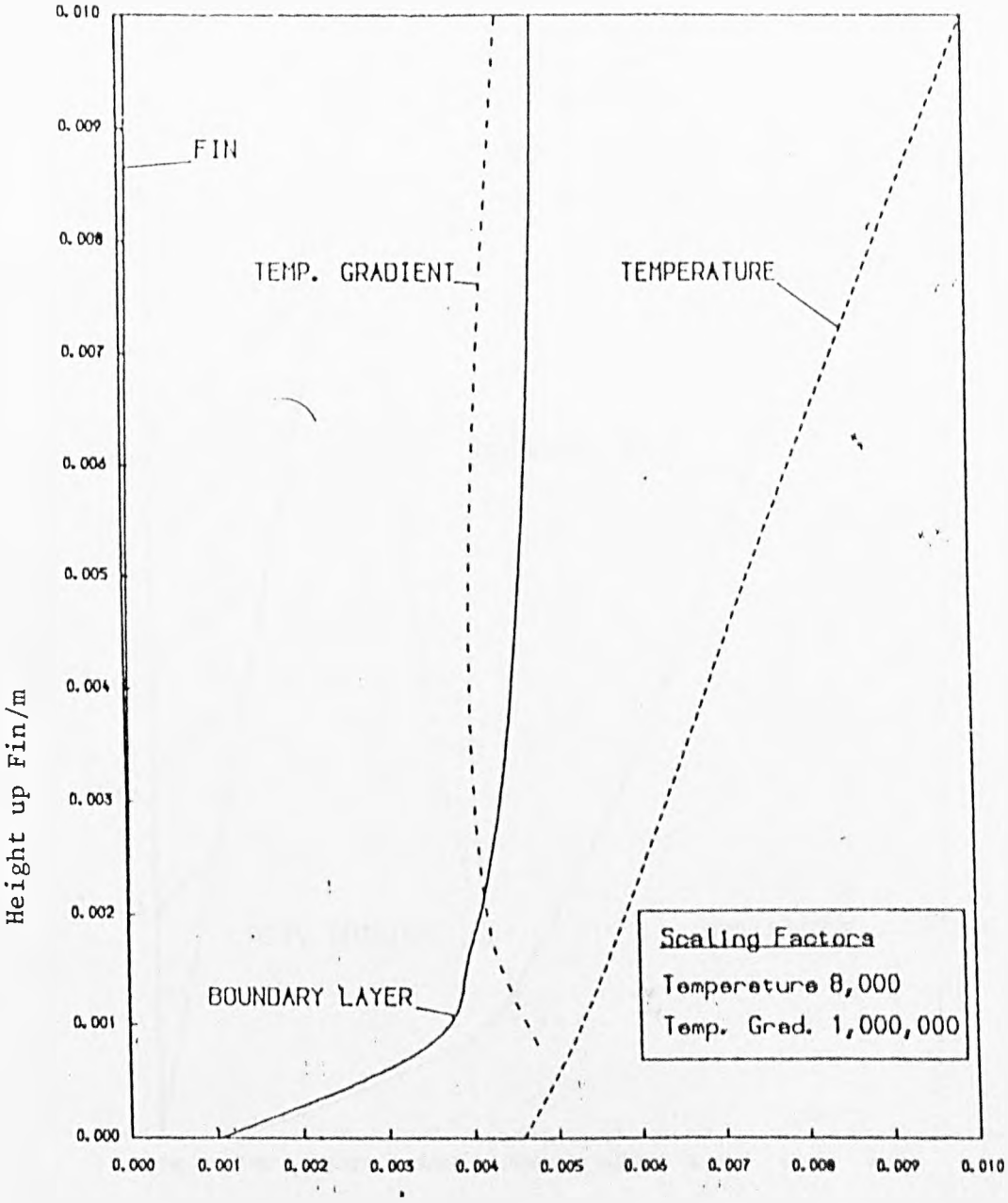

Boundary layer thickness/ m, temp. grad/k/m, fin temperature difference/^{o}C

Fig. 4.5 Tapered Fin of Height 0.01m In Air

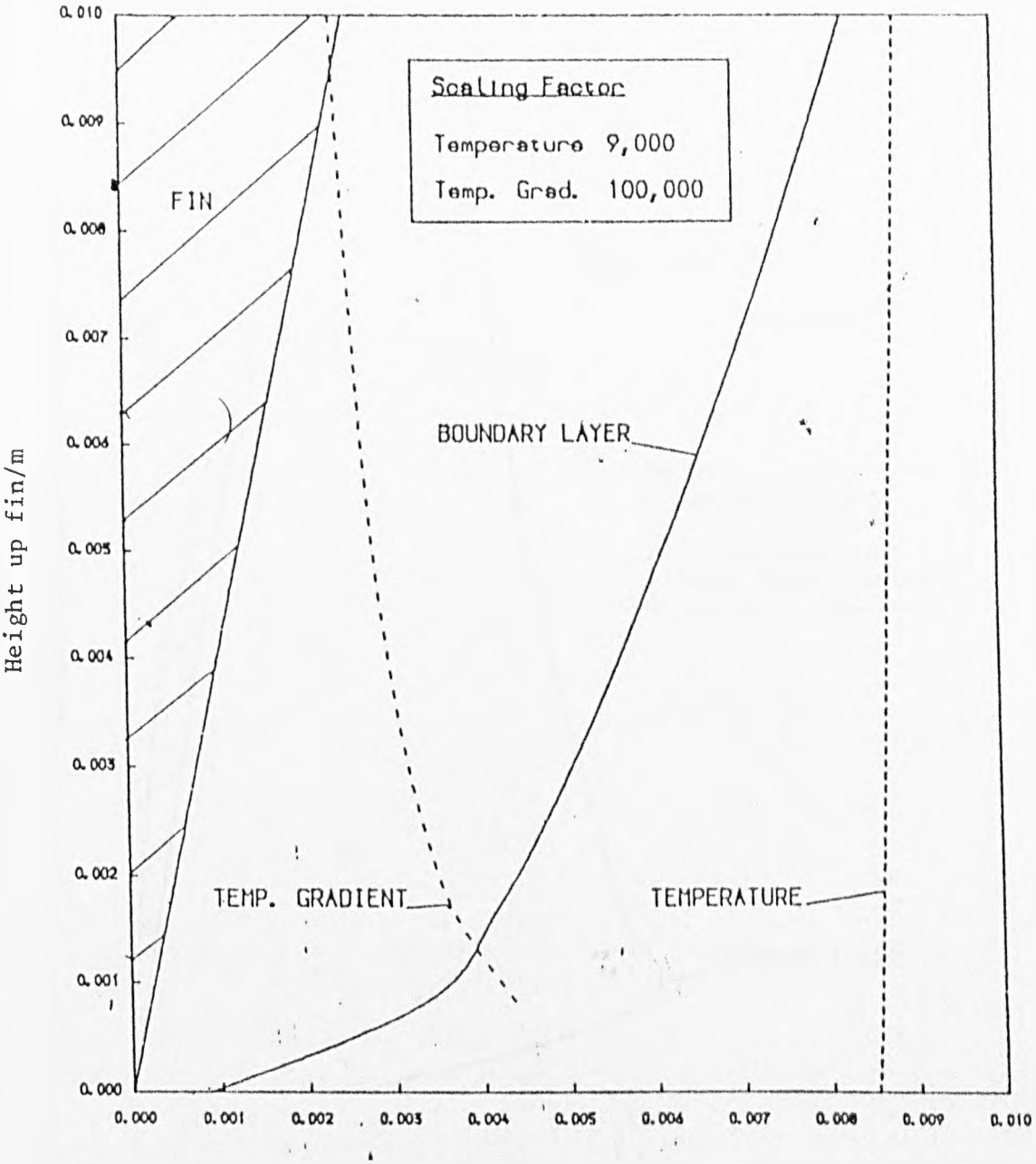

Fig. 4.6 Tapered Fin of Height 0.01m in Air

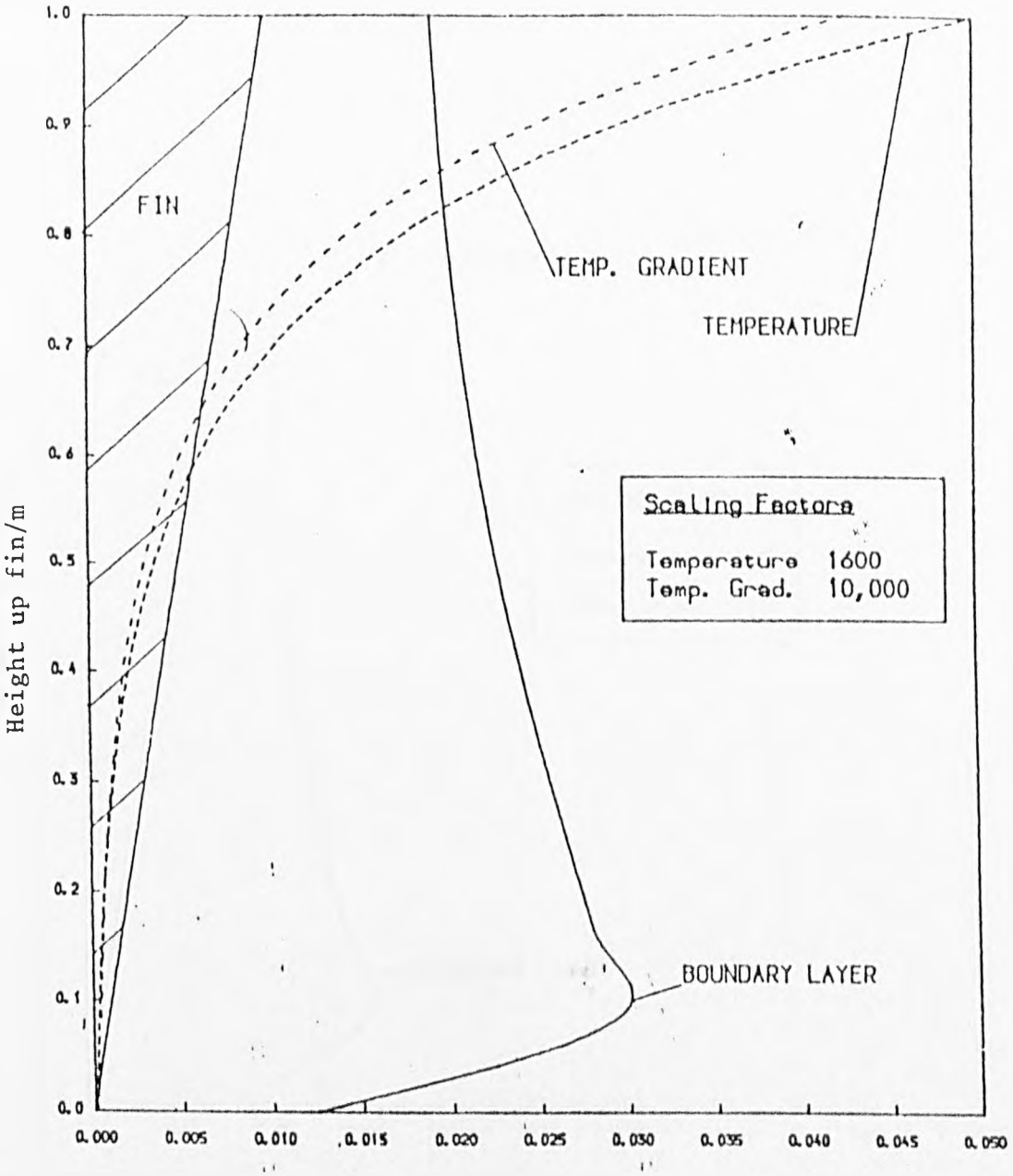

Boundary layer thickness/m, temp. grad/k/m, fin temperature difference/^{o}C

Fig. 4.7 Tapered Fin of Height 1.0m in Air

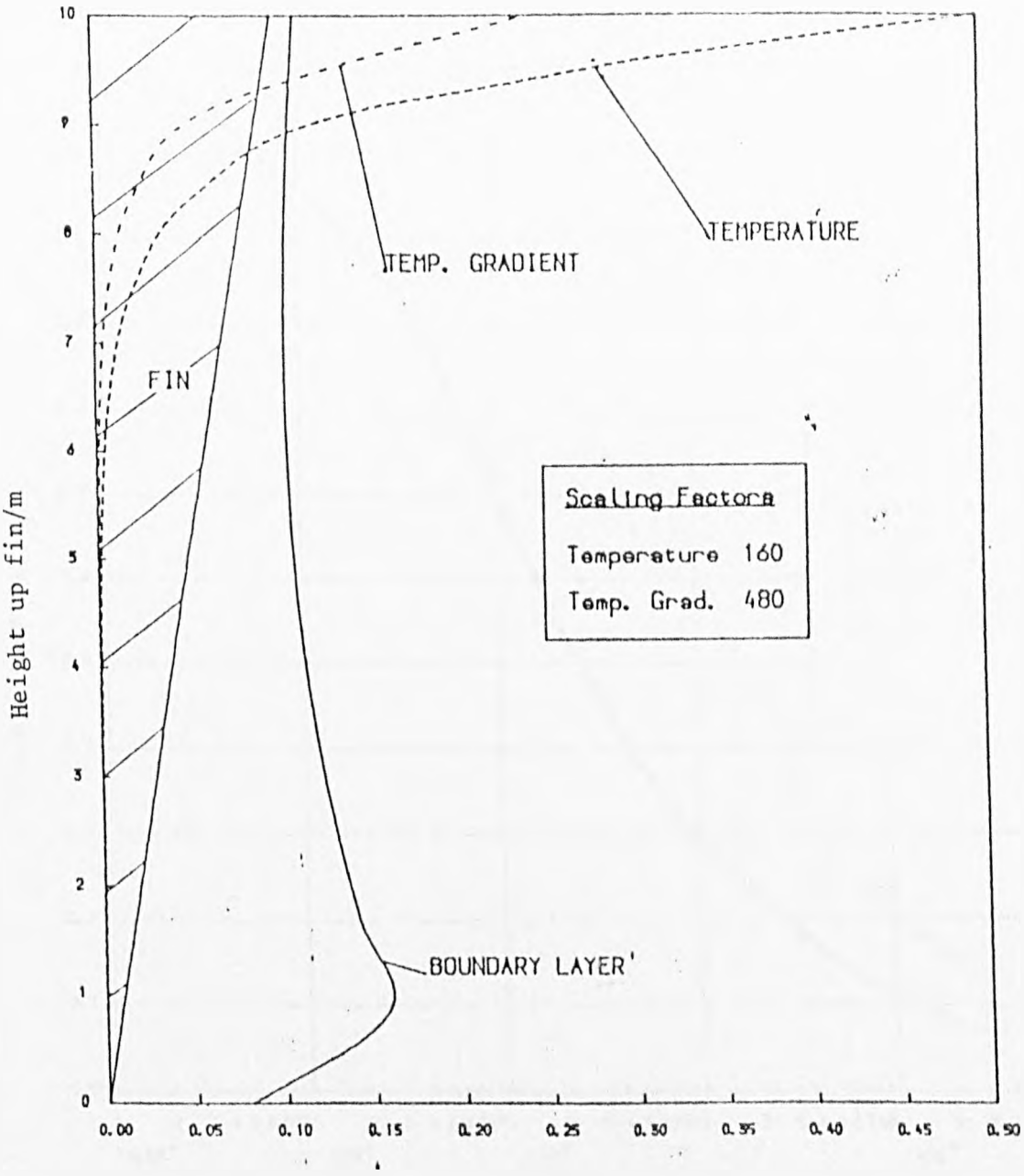

Boundary layer thickness/m, temp. grad/k/m, fin temperature difference/^{o}C

Fig. 4.8 Tapered Fin of Height 10.0m in Air

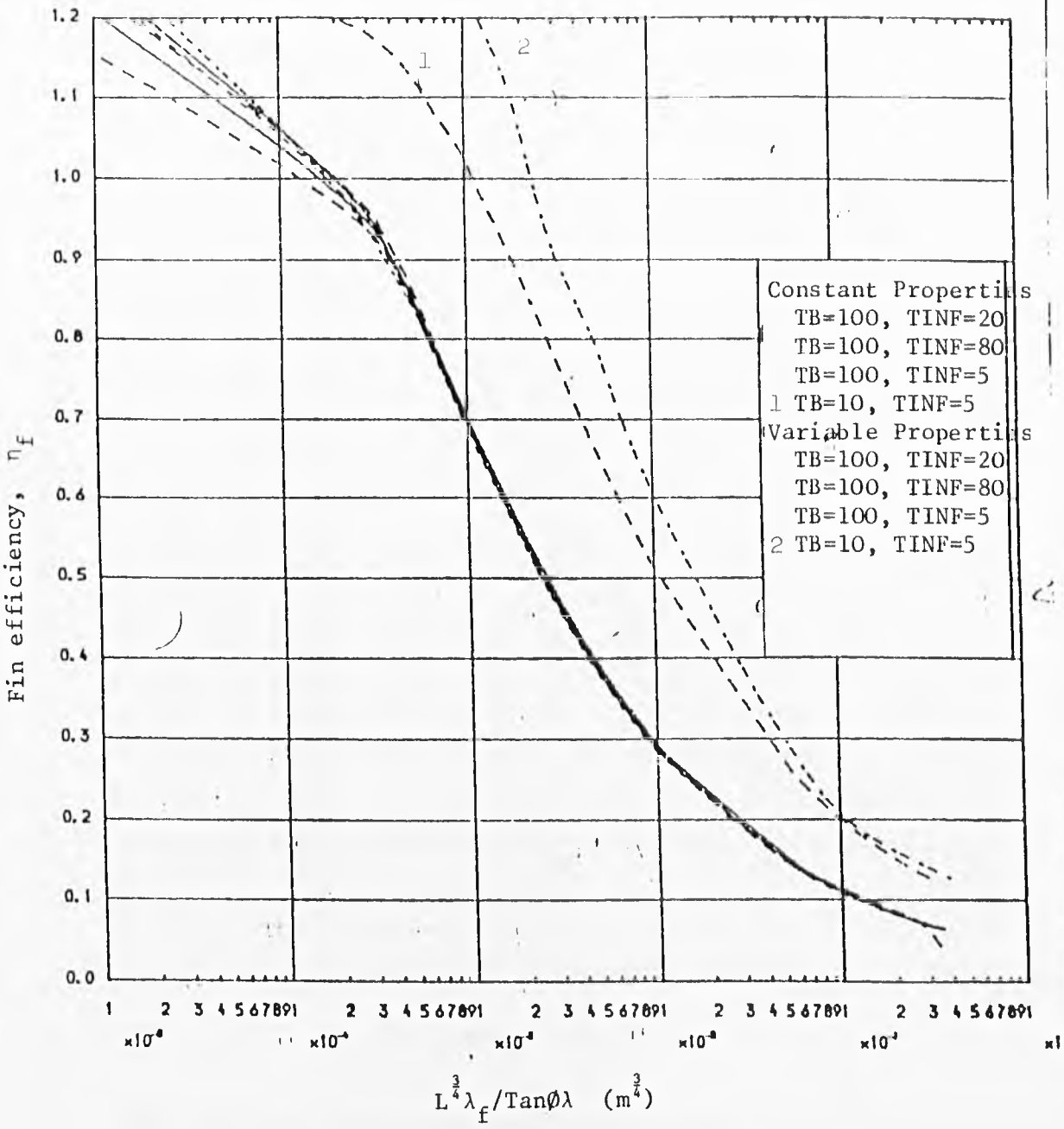

Fig. 4.9 Effects of Variable Physical Properties for Water

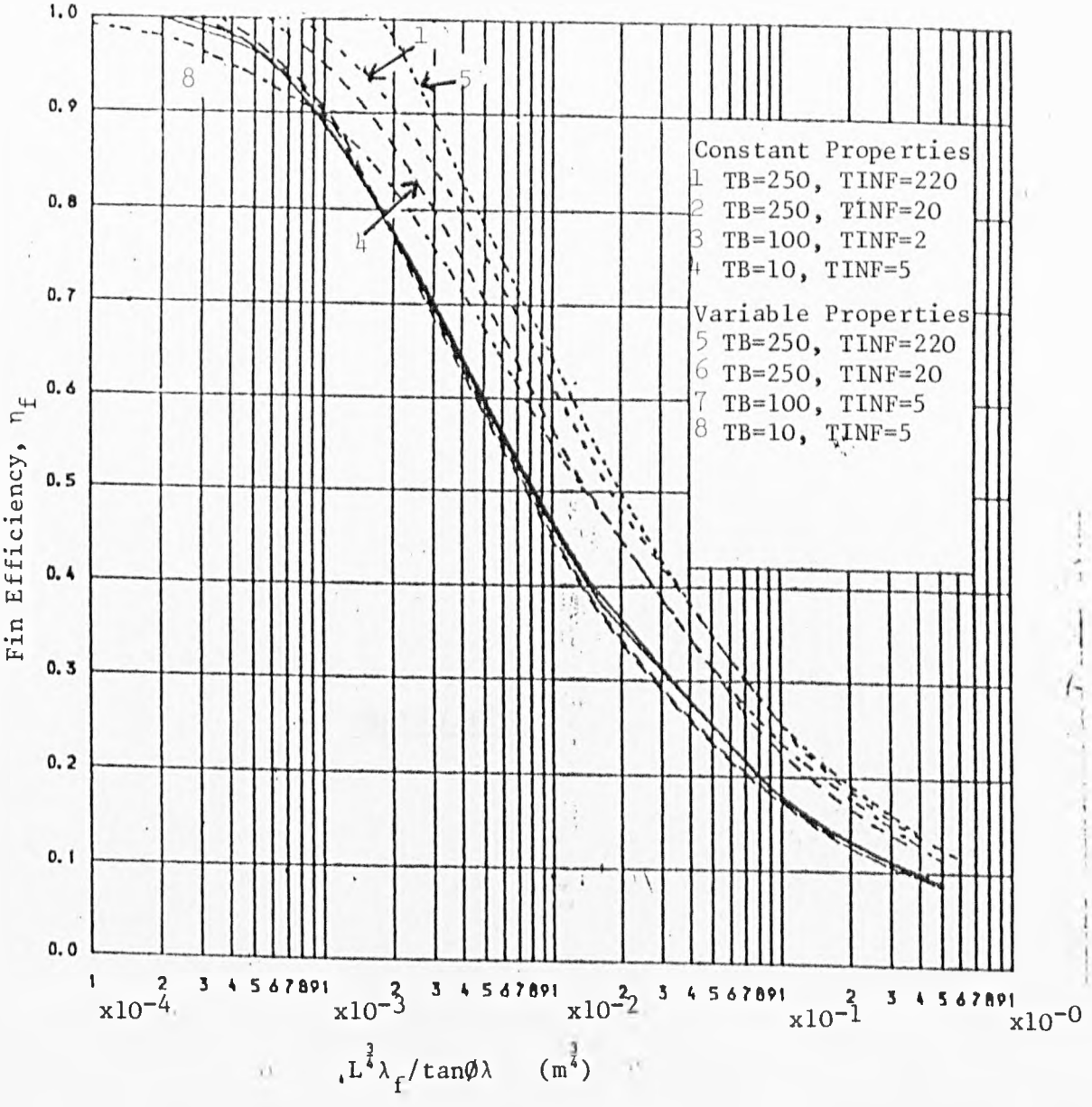

Fig. 4.10 Fin Efficiency, Tapered Fin in Air

CHAPTER FIVE

5. Mixed Convection Heat Transfer From a Downward Projecting Fin in a Free Fluid with 1-D Conduction

5.1 Introduction

This section of the current study addresses the problem of finding a numerical solution to mixed convection from a fin. Although this area has been investigated before [84] and [85] the numerical solution was not entirely satisfactory. Also, the numerical analysis presented here is to be used in the solution of a fin immersed in a porous medium.

Mixed convection occurs when a flat plate is placed in a moving fluid, and the fluid and plate are at different temperatures. Mixed convection is made up from the forced convection component, due to the fluid being pumped over the plate, and the natural convection component, due to the density change of the fluid as it is heated or cooled. Even though heat flow can never take place by forced convection alone, as there will always be some contribution from natural convection, the effect of the forced component will quickly dominate the natural convection effects.

The flat plate can represent many situations, but the one of interest is that of a plate fin protruding from a heat exchanger surface. If the temperature at the base of the fin is known, and is greater than that of the flowing fluid, and the fin is placed vertically, such that gravity acts parallel to the surface, the system to be investigated is that given in Figure 5.1. This figure shows the situation when both natural and forced convection act in the same direction, and also the situation when they act in opposite directions, called the adverse case. In the adverse situation there will be a set of conditions, for the fin and the flow about the fin, for which

flow separation will occur. This will take place when the natural convection component and the forced convection component of flow are approximately equal. In such a case, when the forced convection provides a constant flow of fluid, flow will initially be in that direction at the fin tip. As the velocity of the fluid changes, due to the natural convection flow, the fluid velocity will decrease up the fin, until a critical point is reached where the flow will stop. The fluid will then flow back down the fin, in the same direction as the natural convection component of flow. The only way this reversal of flow can occur is by separation of the fluid from the plate. The critical point for this flow reversal will be when the flow just stops at the fin base, where the velocity component due to natural convection is at its greatest. Beyond this critical value of the forced flow, the surrounding fluid about the plate, will pass over in just one direction.

As in the natural convection case, there are many ways of studying the model of mixed convection heat transfer. Following on from the previous chapter an integral analysis type method could be used to find skin friction and heat transfer properties. However, the situation has become more complicated than the natural convection case, as the two boundary layers, momentum and thermal, cannot be assumed to be equal in thickness due to the introduction of the forced convection flow. Also, as was true previously, the temperature of the fin cannot be assumed to be isothermal, nor can the temperature profile be assumed. If numerical methods are used to solve the governing equations directly, then these equations should be stated in such a way as to allow for their representation suitable for programming

on a computer. Recently, an approach has been proposed and carried out for calculating the flow and heat transfer properties about a flat plate fin [84] and [85]. These works, however, produced many problems in the solution procedure, by the way in which the equations were posed and subsequently represented in finite difference form.

In this chapter the same problem as that studied by Sunden [84] and [85] is investigated, that is mixed convection about a plate fin with a constant base temperature. The problems posed by the method given in [84] and [85] are addressed and resolved. This leads to an accurate and efficient solution technique to the problem.

The conditions about the fin assume that the temperature of the bulk fluid is constant, and that the forced flow velocity is constant across the whole fluid. Apart from these boundary conditions, nothing else is assumed about the flow or temperature of the fluid, or the temperature profile of the fin. Posing the problem in such a way distinguishes the current work very significantly from the early works of Pohlhausen, Schmidt and Beckman [11] and [26], which assumed that the plate under investigation was isothermal.

5.2 Statement of the Problem

The fin is considered to be sufficiently long with respect to the thickness for there to be only one-dimensional heat flow in the fin, and for the fin tip to be considered adiabatic. Whilst this will not always be the case, the solution technique is sufficiently general to be applicable to most fins. Also, the solution technique developed in this chapter can be modified to solve the situation of a fin immersed in a porous medium. Heat pipes used in solar collectors are a typical use of fins immersed in a porous medium. Fins used in

this way are much longer than those found in heat exchangers installed on chemical plants, where size of fins is an important restrictive factor. Using the one-dimensional heat flow assumption, and the adiabatic fin tip assumption, a heat balance can be found for the fin:

$$\frac{d^2T_f}{dx^2} = -2\,\frac{k_l}{k_f b}\,\left(\frac{\partial T_l}{\partial y}\right)_f \qquad (5.1)$$

In the fluid the usual mixed convection equations can be written for the flow field and the convective heat transfer into the fluid.

flow field

$$u\,\frac{\partial u}{\partial x} + v\,\frac{\partial u}{\partial y} = -1/\rho\,\frac{\partial P}{\partial x} + \nu\,\frac{\partial^2 u}{\partial y^2} + g\beta\,(T_l - T_\infty) \qquad (5.2)$$

$$\frac{\partial u}{\partial x} + \frac{\partial v}{\partial y} = 0 \qquad (5.3)$$

convective heat transfer

$$u\,\frac{\partial T_l}{\partial x} + v\,\frac{\partial T_l}{\partial y} = \frac{\partial^2 T_l}{\partial y^2} \qquad (5.4)$$

For mixed convection along a vertical fin the boundary conditions for the velocity perpendicular to the fin must show that the fin is impermeable. Also, there is no flow in the y-direction at the fin tip. The boundary conditions for the velocity in the y-direction can be stated as:

$$v = 0 \qquad y = 0\ ;\ 0 < x < L \qquad (5.5)$$

$$v = 0 \qquad x = 0\ ;\ 0 < y < \infty \qquad (5.6)$$

For the velocity parallel to the fin (denoted by u - which is the velocity in the x-direction) the boundary conditions must show that there is zero velocity at the fin surface (the no-slip boundary condition), and the velocity approaches that of the bulk fluid at an infinite distance from the fin surface. Boundary conditions which are valid at the edge of the boundary layer must be stated such that there is no possibility of forcing the solution to the boundary condition values too close to the surface of the fin. In theory this is done by making the boundary condition true at an infinite distance away from the fin surface. Obviously, this cannot be carried out in practice, so a value of y (the distance from the fin surface) must be given at which to apply the boundary conditions. The details of how this is achieved are given in detail in the section on the solution procedure. At the fin tip the velocity in the x-direction must be equal to the bulk fluid velocity. Thus the boundary conditions are stated as:

$$u = 0 \qquad y = 0 \; ; \; 0 < x < L \tag{5.7}$$

$$u \to u_\infty \qquad y \to \infty \; ; \; 0 < x < L \tag{5.8}$$

$$u = u_\infty \qquad x = 0 \; ; \; 0 < y < \infty \tag{5.9}$$

The boundary conditions for the temperature of the fluid show that the fluid temperature is equal to the fin temperature at the fin/fluid interface (i.e. there must be continuity of temperature over an interface), and approaches that of the bulk fluid at long distances from the fin. These conditions are given by:

$$T_1 = T_f \qquad y = 0 \; ; \; 0 < x < L \tag{5.10}$$

$$T_1 \to T_\infty \qquad y \to \infty \; ; \; 0 < x < L \tag{5.11}$$

In the fin the condition of the adiabatic fin tip is used to provide the boundary condition at one end of the fin. At the fin base the temperature is specified at the beginning of a problem, and is kept constant. These two statements provide the final two boundary conditions to the problem:

$$\frac{dT_f}{dx} = 0 \quad x = 0 \; ; \; -b < y < 0 \tag{5.12}$$

$$T_f = T_b \quad x = H \; ; \; -b < y < 0 \tag{5.13}$$

Due to the fact that the boundary layer thickness grows with increasing height, the solution domain in the fluid should also ideally change with height to provide an efficient numerical analysis technique. This is particularly important in this problem, as opposed to that already investigated in chapter four, as the entire boundary layer domain investigated, and velocities and temperatures calculated at all points across the region. The importance of changing the solution domain with height is graphically illustrated by figure 5.2a. This shows the change of boundary layer thickness with height in the normal x- and y-coordinates, and the effect this has on the number of nodes available for the calculations in the boundary layer. If a grid is superimposed over the boundary layer, then to cover the whole region toward the base of the fin where the boundary layer is largest, the grid will have to be large. However, looking at the fin tip region, the area of interest is very narrow, and if a coarse grid mesh is used then there may be only one, or possibly no nodal points, lying within the boundary layer. If the mesh is fine, so that a sufficient number of nodes within the boundary layer are obtained, then there will be a large number of redundant nodal points lying outside the

boundary layer. To overcome this problem, the solution domain must be transformed, so that the edge of the domain follows more closely the edge of the boundary layer. This is achieved by the introduction of the similarity variables used in the solution of the forced convection problem.

$$\text{Let } u = \frac{\partial \psi}{\partial y} \quad ; \quad v = -\frac{\partial \psi}{\partial x} \tag{5.14}$$

where ψ is defined by

$$\psi = \sqrt{\nu x \, v_\infty} \quad f(\eta, x)$$

and $f(\eta)$ represents a function perpendicular to the fin in the new ordinate, η. The equations are made dimensionless if the x coordinate is replaced by the term ξ, and the temperature excess at any point on the fin, or in the fluid, is divided by the maximum temperature drop in the system, i.e. $T_b - T_\infty$, and the y coordinate is replaced by the term η. This gives rise to the following substitutions:

$$\xi = \frac{x}{L}$$

$$\theta_{f,1} = \frac{T_{f,1} - T_\infty}{T_b - T_\infty} \tag{5.16}$$

$$\eta_m = y \sqrt{\frac{U_\infty}{\nu x}}$$

Substituting equations given in 5.16 into the heat flow equation for the fin (equation 5.1) and the fluid flow and convective heat transfer equations, 5.2 and 5.4, the following relationships are obtained:

$$\frac{\partial^2\theta_f}{\partial\xi^2} = -\frac{2\,k_l\,L}{k_f\,b\sqrt{\xi}}\,\sqrt{Re}\,\frac{\partial\theta_l}{\partial\eta_m} \tag{5.17}$$

$$\xi\,F\,\frac{\partial F}{\partial\xi} = F\,\xi\,\frac{\partial f}{\partial\xi} - \tfrac{1}{2}\,f\,F' - F'' = \frac{Gr}{Re^2}\,\theta_f\xi \tag{5.18}$$

$$\frac{1}{Pr}\,\frac{\partial^2\theta_l}{\partial\eta_m^2} + \tfrac{1}{2}\,f\,\frac{\partial\theta_l}{\partial\eta_m} + \xi\,\frac{\partial f}{\partial\xi}\,\frac{\partial\theta_l}{\partial\eta_m} - \xi F\,\frac{\partial\theta_l}{\partial\xi} = 0 \tag{5.19}$$

where $F = f'$ (5.20)

The primes denote differentiation with respect to η_m.

The equation for heat flow in the fin (equation 5.17) only contains the $\partial^2\theta_f/\partial\xi^2$ term, and no terms involving $\partial\theta_f/\partial\eta_m^2$, as one-dimensional heat flow was assumed at the start of the solution. If this had not been done then equation 5.17 would have included terms for the temperature gradient in the η_m direction.

The boundary conditions are also transformed using equation 5.16. Thus, the complete description of the downward projecting fin, which loses heat by mixed convection, is given by equations 5.17 to 5.20 and the following boundary conditions:

$$f = f' = 0\ ;\ \theta_l = f(\xi) \qquad \eta_m = 0\ ;\ 0 < \xi < 1$$

$$\theta_l \to 0\ ;\ F \to 1 \qquad \eta_m \to \infty\ ;\ 0 < \xi < 1$$

$$\frac{\partial\theta_f}{\partial\xi} = 0\ ;\ \theta_l = 0\ ;\ F = 1\ ;\ f = 0 \qquad \xi = 0\ ;\ 0 < \eta_m < \infty$$

$$\theta_f = 1 \qquad \xi = 1\ ;\ 0 < \eta_m < \infty \tag{5.21}$$

Solving these equations (5.17 to 5.21) as opposed to the equations derived using the cartesian coordinates (5.1 to 5.5) allows more nodes to be used in the solution domain near the fin tip, without having to use a very fine grid, as was discussed before.

5.3 Solution Procedure

Equation 5.18 is parabolic and it is proposed to solve this equation, as well as the other associated equations (5.19 and 5.20) using a marching technique. Equation 5.17 is solved using a special Gaussian elimination which takes advantage of the sparse nature of the matrix formed.

As a marching procedure is used, it is necessary to provide an initial profile at the fin tip (where $\xi=0$). Following the work of Sunden [84], it is found that if starting profiles are near the leading edge, with the direct application of the boundary conditions, the results produced are very dependent on the mesh size, and a converged solution (with increasing nodes) is not found. Therefore, to overcome this problem, an initial profile is produced at an intermediate point between the fin tip and the next node up the fin. A convenient point at which to find the starting profile is at $\Delta\xi/2$ where $\Delta\xi$ represents the mesh size in the ξ direction. Once this is done, the calculation procedure for the next node up the fin must be changed to accommodate for the different step lengths.

5.3.1 Initial Profile

If local similarity in the fluid can be assumed near the fin tip, this means that all differentials with respect to ξ (the ordinate parallel to the fin surface) can be assumed to be zero. This is done as all terms, in the region considered must be constant in the ξ-direction. Thus, the equations representing the flow of fluid

(equations 5.18, 5.19 and 5.20) can be re-written as:

$$F'' + \tfrac{1}{2} f F' = - \frac{Gr}{Re^2} \theta_1 \xi \qquad (5.22)$$

$$\frac{1}{Pr} \frac{\partial^2 \theta_1}{\partial \eta_m^2} + \tfrac{1}{2} f \frac{\partial \theta_1}{\partial \eta_m} = 0 \qquad (5.23)$$

$$F = f' \qquad (5.20)$$

The boundary conditions for the initial profile must also be stated separately from those of the rest of the problem, because the solution is calculated at $\Delta\xi/2$. The change which occurs in the boundary conditions, is for the temperature at the fin tip, and the temperature of the wall at the third node. The boundary conditions are:

$$f = F = 0 \; ; \quad \theta_1 = \theta_f (\Delta\xi/2) = (\theta_f(0) + \theta_f (\Delta\xi))/2 \qquad \eta_m = 0 \; ; \; \xi = \frac{\Delta\xi}{2}$$

$$F \to 1 \; ; \quad \theta_1 \to 0 \qquad \eta_m \to \infty \; ; \; \xi = \frac{\Delta\xi}{2}$$

(5.24)

The fluid flow equations (equations 5.20, 5.22, and 5.23) can be solved subject to the boundary conditions given in equation 5.24, by using numerical integration. The method used here employs a finite difference method. This is done because the procedure for the remainder of the problem is best solved using finite differencing. There is, therefore, no problem in passing the results from the initial profile calculations over to the main part of the program, to form the input data to calculate the flow in the remainder of the fluid.

After representing equations 5.20, 5.22 and 5.23 by their appropriate central difference equations, an iterative procedure can be employed to find the values of f, F and θ_1 subject to the boundary conditions (equation 5.24). To start this iterative procedure an initial guess is needed for the starting values of θ_1 and F. The boundary conditions for θ_1 and F are known at the surface of the fin, and in the bulk fluid. It is also known that f is the integral of F, so that the starting values of f can be found directly. For an initial estimate, it is assumed that the values of θ_1 and F decrease exponentially. This leads to the following guesses to the starting values of θ_1, f and F.

$$\theta_1 = e^{-\eta_m}$$

$$F = 1-e^{-\eta_m} \qquad (5.25)$$

$$f = \int F \, d\eta_m = \eta_m + e^{-\eta_m}$$

Now the equations for fluid flow (equations 5.20, 5.22 and 5.23) can be expressed in finite difference form. Using central differencing at all points the resultant equations are:

$$\frac{F(i+1)-2F(i)+F(i-1)}{\Delta\eta_m^{\,2}} + \tfrac{1}{2} f(i) \left(\frac{F(i+1)-F(i-1)}{2\,\Delta\eta_m}\right) = -\frac{Gr}{Re^2}\,\theta_1(i)\,\xi \qquad (5.26)$$

$$\frac{\theta_1(i+1)-2\theta_1(i)+\theta_1(i-1)}{\Delta\eta_m^{\,2}} + \frac{Pr}{2}\, f(i) \left(\frac{\theta_1(i+1)-\theta_1(i-1)}{2\Delta\eta_m}\right) = 0 \qquad (5.27)$$

$$F(i) = \frac{f(i+1)-f(i-1)}{2\Delta\eta_m} \qquad (5.28)$$

Using equations 5.26 to 5.28, new solutions for $\theta_1(i)$, f(i), and F(i) can be found. Firstly, the above equations need to be re-written to obtain relationships for the new values of the parameters in terms of the old values. Equation 5.26 is used to find new values of F, equation 5.27 is used for values of θ_i while equation 5.28 can be manipulated to given an updated value for f:

$$F(i)^{n+1} = \frac{F(i+1)^n \left(\frac{1}{\Delta\eta_m^2} + \frac{f(i)^n}{4\Delta\eta_m}\right) + F(i-1)^{n+1}\left(\frac{1}{\Delta\eta_m^2} - \frac{f(i)^n}{4\Delta\eta_m}\right) + \frac{Gr}{Re^2}\,\frac{\theta_1(i)^n}{2\Delta\xi}}{2/\Delta\eta_m^2} \tag{5.29}$$

$$\theta_1(i)^{n+1} = \frac{\theta_1(i+1)^n \left(\frac{1}{\Delta\eta_m^2} + \frac{Prf(i)^n}{4\Delta\eta_m}\right) + \theta_1(i-1)^{n+1}\left(\frac{1}{\Delta\eta_m^2} - \frac{Prf(i)^n}{4\Delta\eta_m}\right)}{2/\Delta\eta_m^2} \tag{5.30}$$

$$f(i)^{n+1} = 2F(i-1)^{n+1}\,\Delta\eta_m + f(i-2)^{n+1} \tag{5.31}$$

Equations 5.29 to 5.31 can be used successively, until new values of the three parameters are all within a given tolerance of theprevious values. These final values are then passed on to the rest of the program as the initial profile near the fin tip, and the fluid flow can be calculated in the rest of the fluid by the fin.

It is possible to split the problem of finding the solution for the parameters in the fluid into three distinct parts, in the same fashion as has been done for the initial profile. This is now discussed in the following section.

5.3.2 Solution of the Flow Field and Convective Heat Transfer Equation

So far a second order accurate method has been used in the solution procedure. If, at any point a first order accurate scheme is employed, then this will negate the effects of the second order scheme already utilised. To use central differencing in the remainder of the fluid a fictitious node must be introduced into the calculations (see figure 5.3). Using this fictitious node the central difference representation of equations 5.18 to 5.20 must be treated by using average values (which are assumed to be the values of the parameters at the fictitious node). By using this imaginary node, there is no problem in representing the differentials of f, F and θ_1 by central differences. The fluid flow equations (5.18 to 5.20) are now written as:

$$\xi_{av} F_{av} \left(\frac{F(i,j+1)-F(i,j)}{\Delta\xi}\right) - \xi_{av} \left(\frac{f(i,j+1)-f(i,j)}{\Delta\xi}\right) \tfrac{1}{2} \left(\frac{F(i+1,j+1)-F(i-1,j+1)}{2\Delta\eta_m} + \frac{F(i+1,j)-F(i-1,j)}{2\Delta\eta_m}\right)$$

$$-\tfrac{1}{2} f_{av} \tfrac{1}{2}\left(\frac{F(i+1,j+1)-F(i-1,j+1)}{2\Delta\eta_m} + \frac{F(i+1,j)-F(i-1,j)}{2\Delta\eta_m}\right)$$

$$- \tfrac{1}{2} \left(\frac{F(i+1,j+1)-2F(i,j+1)+F(i-1,j+1}{\Delta\eta_m^2} + \frac{F(i+1,j)-2F(i,j)+F(i-1,j)}{\Delta\eta_m^2}\right)$$

$$= Gr/Re^2 \quad \theta_{1av} \quad \xi_{av} \qquad (5.32)$$

$$\frac{1}{Pr}\ \tfrac{1}{2}\ \left(\frac{\theta_1(i+1,j)-2\theta_1(i,j)+\theta_1(i-1,j)}{\Delta\eta_m^{\,2}}+\frac{\theta_1(i+1,j+1)-2\theta_1(i,j)+\theta_1(i-1,j+1)}{\Delta\eta_m^{\,2}}\right)$$

$$+\ \tfrac{1}{2}\ f_{av}\ \left(\frac{\theta_1(i+1,j)-\theta_1(i-1,j)}{2\Delta\eta_m}\right)+\xi_{av}\ \left(\frac{f(i,j+1)-f(i,j)}{\Delta\xi}\right)\ \left(\frac{\theta_1(i+1,j)-\theta_1(i-1,j)}{2\Delta\eta_m}\right)$$

$$-\ \xi_{av}\ F_{av}\ \left(\frac{1(i,j+1)-\ 1(i,j)}{\Delta\xi}\right)\ =\ 0 \qquad (5.33)$$

$$F(i,j)\ =\ \frac{f(i+1,j)-f(i-1,j)}{2\Delta\eta_m} \qquad (5.34)$$

The subscript (av) denotes an average value, which is given by using the values of the appropriate parameter at the j^{th} row and the $j+1^{th}$ row.

Equations 5.32 to 5.34 need to be re-arranged so that all parameters on the $j+1^{th}$ row are expressed in terms of known values (i.e. those on the j^{th} row).

5.3.2.1 Solution for F

Using equation 5.32, terms in F on the $j+1^{th}$ row can be collected together so that points on the $j+1^{th}$ row are expressed in terms of values on the j^{th} row.

$$a_1\ F(i-1,j+1) + b_1\ F(i,j+1) + c_1\ F(i+1,j+1) = d_1 \qquad (5.35)$$

where

$$a_1 = \frac{\xi_{av}}{4\Delta\eta_m}\ \frac{f(i,j+1)-f(i,j)}{\Delta\xi} + \frac{f_{av}}{8\Delta\eta_m} - \frac{1}{2\Delta\eta_m^{\,2}}$$

$$b_1 = \frac{\xi_{av} F_{av}}{\Delta\xi} + 1/\Delta\eta_m^{\,2}$$

$$c_1 = -\frac{\xi_{av}}{4\Delta\eta_m}\ \frac{f(i,j+1)-f(i,j)}{\Delta\xi} - \frac{f_{av}}{8\Delta\eta} - \frac{1}{2\Delta\eta_m^{\,2}}$$

$$d_1 = F(i-1,j)\ \left(\frac{1}{2\Delta\eta_m^{\,2}} - \frac{f_{av}}{8\Delta\eta_m} - \frac{\xi_{av}}{4\Delta\eta_m}\ \left(\frac{f(i,j+1)-f(i,j)}{\Delta\xi}\right)\right)$$

$$+ F(i,j)\ \left(\frac{\xi_{av} F_{av}}{\Delta\xi} - \frac{1}{\Delta\eta_m^{\,2}}\right)$$

$$+ F(i+1,j)\ \left(\frac{1}{2\Delta\eta_m^{\,2}} + \frac{f_{av}}{8\Delta\eta_m} + \frac{\xi_{av}}{4\Delta\eta_m}\ \left(\frac{f(i,j+1)-f(i,j)}{\Delta\xi}\right)\right)$$

$$+ \frac{Gr}{Re^2}\ \theta_{1av}\ \xi_{av}$$

Equation 5.35, when written in matrix form, gives a tri-diagonal matrix, which can be solved for F(i,j+1) by using Gaussian elimination. The elements a_1, b_1, c_1 are such that the matrix is diagonally dominant by the quantity $\xi_{av}\ F_{av}/\Delta\xi$.

5.3.2.2 Solution for θ

The solution for the temperature term proceeds in the same way as that for F, described above. Terms for the temperature on the $j+1^{th}$ row are collected together and expressed such that a tri-diagonal matrix is formed that is diagonally dominant.

$$a_2\ \theta_1(i-1,j+1)+b_2\theta_1(i,j+1)+c_2\ \theta_1(i+1,j+1) = d_2 \qquad (5.36)$$

where

$$a_2 = \frac{f_{av}}{8\Delta\eta_m} - \frac{1}{2\Delta\eta_m^2 Pr}$$

$$b_2 = \frac{\xi_{av} F_{av}}{\Delta\xi} + \frac{1}{\Delta\eta_m^2 Pr}$$

$$c_2 = -\frac{f_{av}}{8\Delta\eta_m} - \frac{1}{2\Delta\eta_m^2 Pr}$$

$$d_2 = \theta_1(i-1,j)\ \left(\frac{1}{2\Delta\eta_m^2 Pr} - \frac{f_{av}}{8\Delta\eta_m} - \frac{\xi_{av}}{2\Delta\eta_m}\left(\frac{f(i,j+1)-f(i,j)}{\Delta\xi}\right)\right.$$

$$+\ \theta_1(i,j)\ \left(\frac{F_{av} F_{av}}{\Delta\xi} - \frac{1}{2\Delta\eta_m^2 Pr}\right)$$

$$\left.+\ \theta_1(i+1,j)\ \left(\frac{1}{2\Delta\eta_m^2 Pr} + \frac{f_{av}}{8\Delta\eta_m} + \frac{\xi_{av}}{2\Delta\eta_m}\left(\frac{f(i,j+1)-f(i,j)}{\Delta\xi}\right)\right)\right.$$

Equation 5.36 can again be solved using Gaussian elimination and back substitution, to find the temperature profile along the $j+1^{th}$ row. Again, the terms a_2, b_2, and c_2 are such that the matrix is diagonally dominant by the term $\xi_{av}\ F_{av}/\Delta\xi$. This term occurs in b_2.

5.3.2.3 Solution for f

The solutionfor f appears to be the simplest when looking at equation 5.34. However, if a central difference method is to be used for all values of f then equation 5.34 cannot be used, as at position 2, the new value for f(2,j) will be given by:

$$f(2,j) = 2\Delta\eta_m F(i,j) + f(0,j) \tag{5.37}$$

where F = 0, as given by the boundary condition (5.21). Equation 5.37 cannot be used as the value of f(0,j) is not known. This problem can be easily overcome by using a backward difference scheme, but as already discussed this will introduce a first order accurate equation into an otherwise second order procedure. Therefore, if it is possible, it would be desirable to use a central difference representation. To do this, equation 5.20 (which is the simplest relationship between f and F) is not solved, but the equation is differentiated further. This does not change the relationship between the two parameters, but it does allow central differencing to be used and will give a solution for all values of f. The resulting equation and its finite difference representation are given by:

$$f'' = F' \tag{5.38}$$

$$\frac{f(i-1,j)-2f(1,j)+f(i+1,j)}{\Delta\eta_m^2} = \frac{F(i+1,j)-F(i-1,j)}{2\Delta\eta_m} \tag{5.39}$$

Equation 5.39 can now be solved using Gaussian elimination, like equations 5.35 and 5.36, as long as the solution for f on the $j+1^{th}$ row is carried out before. By using equations 5.35, 5.36 and 5.39

to find the solutions for F, θ_1 and f respectively, a second order accurate technique is employed on the entire fluid flow region.

Once the fluid flow region has been calculated, the fin conductivity equation (5.18) can be investigated.

5.3.3 Solution of the Fin Conduction Equation

In equation 5.17 the term for the temperature gradient at the fin fluid interface needs to be known. Once the fluid flow problem has been solved the value for $\partial\theta_1/\partial\eta_m$ is known for all nodes up the fin. It is now possible to express the fin conduction equation in finite difference form, but still using central differences at all points.

$$\frac{\theta_f(i,j-1)-2\theta_f(i,j)+\theta_f(i,j+1)}{\Delta\xi^2} = -\frac{2\,k_1 L}{k_f b\sqrt{\xi}}\ \mathrm{Re}\ \left(\frac{\partial\theta_1}{\partial\eta_m}\right)_j \qquad (5.40)$$

Equation 5.40 with the boundary conditions 5.12 and 5.13 can again be solved using Gaussian elimination and back substitution to find the values of θ_f from $\xi = \Delta\xi/2$ to $\xi = 1$. However, the boundary condition at the fin tip (5.13) needs to be specified more closely, as the condition, at the moment, only provides a 'floating' condition. The starting position is set at $\Delta\xi/2$ so that the initial profile can be found so that it is relatively independent of the mesh size. To find the fin tip temperature a separate heat balance is carried out (see figure 5.4). The relationship for the heat flow from the fin tip in cartesian coordinates is given by equation 5.41, whilst the heat balance found after the introduction of the transformation variables

(5.14) is given by equation 5.42.

$$k_f\, b\, \frac{\partial T_f}{\partial x} = -2\, k_1\, \frac{\Delta x}{2} \int_0^{\Delta\xi} \frac{\partial T_1}{\partial y}\, dx \qquad (5.41)$$

$$\frac{k_f b}{k_1 L}\, \frac{1}{\sqrt{Re}\ \Delta\xi}\, \frac{\partial \theta_f}{\partial \xi} = -\left(\frac{\partial \theta_1}{\partial \eta_m}\right)_{\eta_m=0} \int_0^{\Delta\xi/2} \frac{1}{\sqrt{\Delta\xi}}\, d\xi \qquad (5.42)$$

The expression for $(\partial\theta_1/\partial\eta_m)_{\eta_{m=0}}$ is taken outside the integral, as it is assumed that the value for the temperature gradient at $\eta_{m=0}$ is constant between the fin tip and the first node. This is consistent with the assumption of local similarity, which was used in the region when developing the relationship for the initial profile. Equation 5.42 can now be expressed in finite difference form, and the integral calculated to find a relationship for the fin tip temperature $\theta_f(1)$.

$$\theta_f(1) = \theta_f(3) - \frac{\frac{1}{2}\left(\frac{\partial \theta_1}{\partial \eta_m}\right)_{\eta_{m=0}}\, \sqrt[3]{\frac{\Delta\xi}{2}}}{\frac{k_f b}{k_1 L}\, \frac{1}{Re}}$$

5.3.4 Flow Diagram of the Solution Procedure

Due to the conjugate nature of the problem to be solved, the parameters in the calculations are interlinked. This results in an overall iterative solution which requires the calculation of individual parameters beforehand. The best way of presenting the procedure is by using a simplified flow diagram which shows the progression of the calculation generally, rather than detailing each subroutine. The flow diagram is given in figure 5.5.

From figure 5.5 it can be seen that the initial profile finds F, f and θ_f by an iterative procedure. This is because all three parameters need to be solved for simultaneously, but the solution of one parameter depends on the others. However, after the initial profile has been calculated, there are no other iterations required in the other subroutines. This is because, for each parameter calculated, it is assumed that all the other parameters are known. The only other iterative loop involved in the calculation procedure is that to find the temperature on the fin. As will be discussed in the results, the tolerance required for the solution to be accepted for both iterative loops must be specified with care if a correct solution is to be obtained.

5.3.5 Calculation of the Pertinent Parameters

The solution procedure solves equations 5.17 to 5.20 from which, by direct substitution, using equations 5.14 to 5.16 (the transformations), the velocity and temperature profiles in the fluid can be found, and also the temperature profile on the fin surface. However, other parameters are of importance, and are easily available from the already calculated values.

The temperature gradient at the fin surface needs to be known to solve the fin conduction equation (5.17). From the temperature gradient the local heat flux can be calculated very easily, and if it is required, a heat transfer coefficient can be found.

If the fluid flow properties are of importance, e.g. it is necessary to know the pressure drop across a fin surface, the total shear stress can be found by calculating the rate of change of velocity parallel to the surface of the fin (velocity u).

5.4 Results

To obtain accurate results the first thing that needs to be established is, at what point must the infinite boundary conditions be applied? If the condition is applied too close to the fin the solution of the fluid flow equations will be forced to the boundary condition values too quickly, and so produce erroneous results. If the infinite conditions are applied too far away unnecessary calculations are performed and accuracy lost. The only way to find the position at which to apply the infinite boundary conditions, is to move its position further away from the fin until it is found that the results do not change when conditions are applied slightly further away. A good estimate for its position can be found by looking at previous forced convection solutions in which the velocity and temperatures of the boundary layer fluid fall to the bulk fluid values in the region of η_m=8. Setting the infinite boundary conditions at this point is found to give satisfactory results.

The current investigation looks at the effect of changing the convection conduction parameter, and the ratio Gr/Re^2. In the results presented here, a convection conduction parameter for mixed convection (CCP_m) is used. This represents the ratio between the heat flow in the fin by conduction to the heat flow in the fluid from the fin. The results obtained are for values of CCP_m equal to 1.0, 5.0 and 10.0. For each of these values the value of Gr/Re^2 is set to either 2.0, or 0.0, the latter corresponding to pure forced convection. The Prandtl number is set at 0.7, which corresponds to the air being heated. Also the adverse case is investigated for the situation when the CCP_m

is 1.0. To find the limit of the adverse case a series of runs are carried out so that the value of Gr/Re^2 can be found for which flow separation just occurs.

The only way pure forced convection can be studied in practice is to set the temperature of the fin to the same temperature as the bulk fluid. This would obviously yield no results for the temperature profile down the fin, so a parameter in calculating the Grashof number must be set to a very small value. The parameters used for the calculations are given in table 5.1.

	$Gr/Re^2 = 0.0$			$Gr/Re^2 = 2.0$		
	CCP_m			CCP_m		
	1.0	5.0	10.0	1.0	5.0	10.0
b	0.01168	0.00234	0.001168	0.01168	0.00234	0.001168
β	3.22e-3	3.22e-3	3.22e-3	3.22e-10	3.22e-10	3.22e-10

All other parameters kept constant

H	0.1 m
ν	1.88e-5 m^2/s
T_b	90.0°C
T_∞	20.0°C
U_∞	0.3325 m/s
k_f	9.0 W/mK
k_l	0.025 W/mK

Table 5.1 Parameters used to obtain results

A set of calculated temperatures is stored in the program and subsequently compared with the next set of temperatures. The difference between the two values is then summed and this summed value is compared with a set tolerance. If this criterion for a converged solution is not met the stored array of temperatures is replaced by the

newest set of values. This series of calculations is repeated until the necessary tolerance is met. The tolerance used in all iterative procedures was varied, but it was found that a value of 0.001 was sufficiently small to obtain accurate results. However, it was found that on calculating the fin tip temperature using a heat balance at every sweep through the fin, the convergence of the numerical procedure was significantly impaired. For this reason the fin tip temperature was set to the same value as the temperature at the second node until the calculated deviation for every iterative step was less than 0.01. This, of course, causes the change for the next sweep through to be greater than 0.01, so once the fin tip temperature was calculated using the heat balance, the fin tip temperature was calculated by the heat balance for all subsequent steps.

In updating the solutions for temperature and velocity under relaxation was used. Unfortunately the same relaxation factor could not be used for all values of CCP_m and Gr/Re^2 if efficient calculations were to be carried out. This occurred because, if the first guess for the temperature profile was not satisfactory, the heat conduction equation for the fin would estimate a new temperature profile which allowed temperatures to be negative. This then caused the rest of the numerical procedure to enter an infinite loop. This effect is particularly noticeable for the temperature profiles which have low fin tip temperatures. A very small relaxation parameter, therefore had to be used when the value of the CCP_m was 10.0. If the same relaxation parameter is used for the better behaved conditions, long calculation times would be encountered. It was found that for the case when the CCP_m was 1.0 the relaxation parameter 0.8 should be used. When the CCP_m was 10.0 this was reduced to a value of 0.1.

From equations 5.35 to 5.39 the results obtained are for the dimensionless temperature and velocity parallel to the wall, and also the term 'f' which is used to find the velocity perpendicular to the wall, v. The velocity v is found by replacing the transformed variables with the original terms. These three terms are plotted in figure 5.6 to 5.8 by the use of isoprojections. These are used so that it can in fact be shown that the edge of the boundary layer is reached before the values of the parameters are forced to their infinite boundary conditions. The figures are for the case when the parameter $Gr/Re^2 = 2.0$, and the convection conduction parameter has a value of 1.0. The orientation between each of the figures changes, so that the variation of the parameter under investigation is shown to best effect. In figure 5.6 the temperature profile in the boundary layer is shown. The fin in this diagram can be imagined to by lying at the back of the figure, with the fin tip nearest to the bottom of the figure. This figure shows how the temperature of the fin surface varies with height. The coordinates for these plots are in the dimensionless variables ξ and η_m. Therefore, even though the temperature of the fluid next to the fin tip is given as greater than zero, in the normal cartesian coordinates the boundary layer thickness is zero, so this temperature variation would not be seen. Figure 5.7 has been rotated so that the fin is now lying towards the front of the figure. The fin tip is still at the bottom of the page and the boundary layer increases away from the viewer. This figure plots the dimensionless velocity parallel to the fin. Therefore, the velocity next to the fin surface is zero, showing the no slip boundary condition, while at the

edge of the boundary layer the velocity is unity (i.e. the same as the forced flow at the base of the fin). The final isoprojection shows the velocity perpendicular to the wall. The projection in this case is the same as that for the temperature, with the fin at the far side of the projection, and the fin tip at the bottom of the page. The velocity next to the fin is again zero, showing that the wall is impermeable, and further out the velocity term becomes increasingly more negative. This shows that the fluid is flowing towards the fin as the flow moves upwards.

The boundary layer thickness cannot be seen on the figure 5.6 to 5.8. To calculate the boundary layer thickness some criteria must be given to state at what point in the flow the fluid is at the bulk conditions. The criterion used is that the velocity of the fluid parallel to the fin must be 99% of the forced flow value. In dimensionless form, this means that the value of F must reach 0.99. Calculating the boundary layer using this criterion for the parameters used to find figures 5.6 to 5.8 gives a steadily increasing boundary layer, which at the base of the fin has a thickness of 9.46 cm. The phenomenon of the decreasing boundary layer is not likely to occur in the current problem as the fin is quite short when compared with the limit of the laminar region in air (which is an order of magnitude greater, as found from the work in chapters three and four).

The temperature profile along the fin surface can be seen from figure 5.6, but this is not the best way to show how its value changes with a change in parameters. The effect of a change in parameters on the temperature profile is shown in figure 5.9 and 5.10. In these figures the dimensionless temperature profile is plotted against

the dimensionless height for a given value of Gr/Re^2 with CCP_m as a parameter in the figure. Figure 5.9 shows the results when Gr/Re^2 has a value of 2.0, and figure 5.10 is for the situation when Gr/Re^2 is effectively zero. On the same figures the corresponding values for the temperature profiles are given as would be found using an analytical fin analysis, which assumes a constant heat transfer coefficient (which is calculated from the corresponding isothermal case).

As can be seen from the figures 5.9 and 5.10 the fin tip temperatures as calculated by the current numerical method and the conventional fin theory are significantly different, especially so for the case when $CCP_m = 1.0$. This difference decreases towards the fin base, as at the fin base the constant temperature boundary condition has been imposed. This decrease in the calculated temperature shows that there is more heat loss than would normally be expected if investigating an identical system, but using the conventional fin theory.

The total shear stress can be calculated from the results for the velocity parallel to the fin surface. The relationship between the shear stress at any point and the velocity is given by:

$$\tau_s = \mu \left(\frac{\partial u}{\partial y}\right)_{y=0}$$

As the velocity profile across the boundary layer has already been found the calculation of the shear stress at any point is fairly trivial. The total shear rate is found by numerical integration. This value is then non-dimensionalised by dividing the result by the total shear stress when $Gr/Re^2 = 0.0$. This value is used as it remains

constant with changing values of the parameter CCP_m. This is because the change in temperature profile with a change in CCP_m does not affect the velocity in the fluid, as there is no contribution from natural convection, which changes with the temperature of the fin. Fig. 5.11 shows how the total shear stress changes with CCP when Gr/Re^2 is equal to 2.0. As can be seen from this figure the shear stress is considerably increased by the effect of natural convection, especially at small values of CCP_m. It is, therefore, unwise to neglect the effects of natural convection when considering pressure drop or power requirements of pumps, thinking that its effect is not significant if forced convection is present.

The adverse case when the CCP_m has a value of 1.0 is found, such that flow separation occurs at the base of the fin. This is the limiting case in that any value of Gr/Re^2 which is less than the calculated value will give flow separation at some point along the fin. The value of Gr/Re^2 which represents this limiting value is hard to find as the solution of the flow field must be followed very closely. This is because the governing equations are parabolic, and so will not solve past the point where flow separation occurs. As this is the case the point must be found where the flow is just about to become negative at the base of the fin and no earlier. Provided the initial guess is such that the iterative procedure approaches this condition from the positive flow case the limiting case can be found after a number of trial and error runs. From the work by Lloyd and Sparrow [86] on free and forced convection flow about vertical surfaces, a figure showing how the Nusselt number changes

with the relationship $Re^{1/4}/Re^{1/2}\ Pr^{1/3}$ can be plotted (see figure 5.12). From this figure the point where free and forced convection have similar influences can be estimated. It is this point that indicates the condition for flow separation to occur.

The value for Gr/Re^2 that is found to limit flow separation is -0.261 for a Prandtl number of 0.7. This point is plotted on figure 5.12 to compare with the free and forced convection flow. The intersection of the free and forced convection lines occurs at a value of approximately 0.65, and the value of the Gr/Re^2 for the limit of flow separation gives a point of the line x = 0.74.

5.5 Conclusions

An efficient algorithm has been developed for finding the mixed convection heat transfer from a downward projecting fin immersed in a free fluid. The numerical procedure uses second order finite differences at all points in the fluid and the fin. The only boundary condition on the fin temperature requires the base temperature to be known and constant. Apart from this the temperature profile on the fin surface is left to find its own value and profile, only being influenced by the solution of the boundary layer flow about the fin. The variables used in the governing equations are found from similarity solutions for forced convection flow. The substitution of these "pseudo-similarity" variables into the governing equations results in a solution procedure that can impose a grid of nodes over the solution domain, such that roughly equal numbers of nodes fall within the boundary layer at the base and tip of the fin. This means that accuracy need not be lost at the tip, or that program running times are greater than necessary. As this work is an improvement on that by

Sunden [84] and [85] it is worth noting at this point the major differences between the two schemes.

	Sunden	Present
1)	Uses second order backward differencing to maintain errors of $O(h^2)$- does not allow for easy alteration of step size	Uses central differencing at all times to obtain errors of $O(h^2)$
2)	Needs to find the integral $\int_{y-\Delta y}^{y} (du/dx)dy$ Uses trapezium method for integration (only $O(h^2)$)	Eliminates integral by using similarity variables
3)	Solves close to leading edge where y is small-large number of nodes required	Use η coordinate near leading edge - can solve much nearer to fin tip

Using this numerical method provides results which are graphically indistinguishable from those given by Sunden in his two papers already mentioned. These results show that the fin temperature profile is not calculated accurately using the analytical fin theory. The fin tip temperature is markedly higher than that calculated using the current numerical method, indicating that the heat flow would be calculated at a lower value than is actually true.

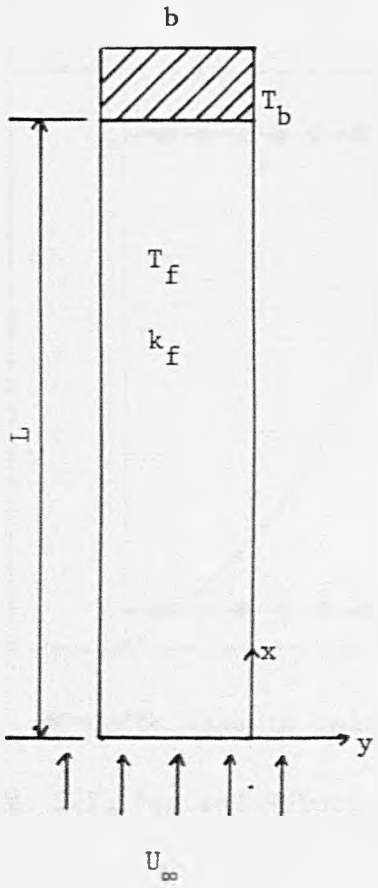

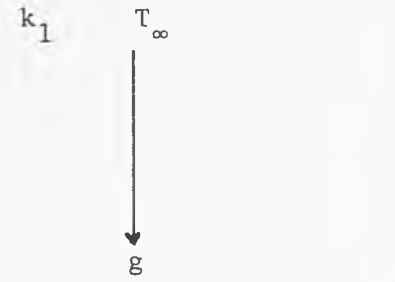

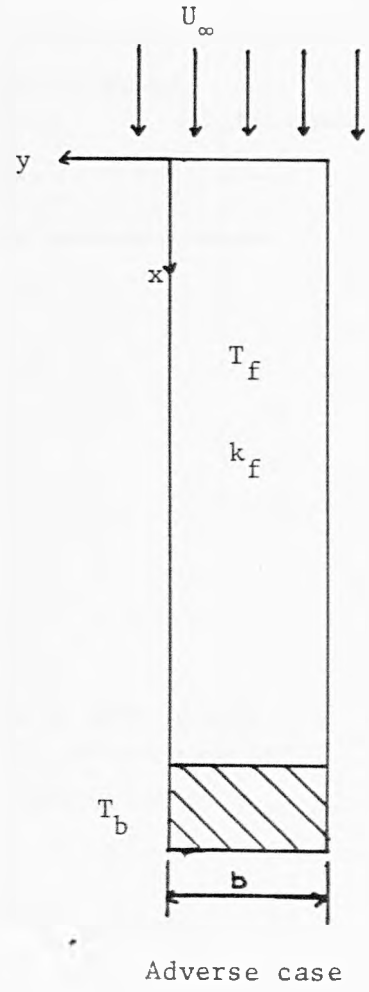

Fig. 5.1 Flow Model and Co-ordinate System for Mixed Convection in a Porous Medium / Free Fluid

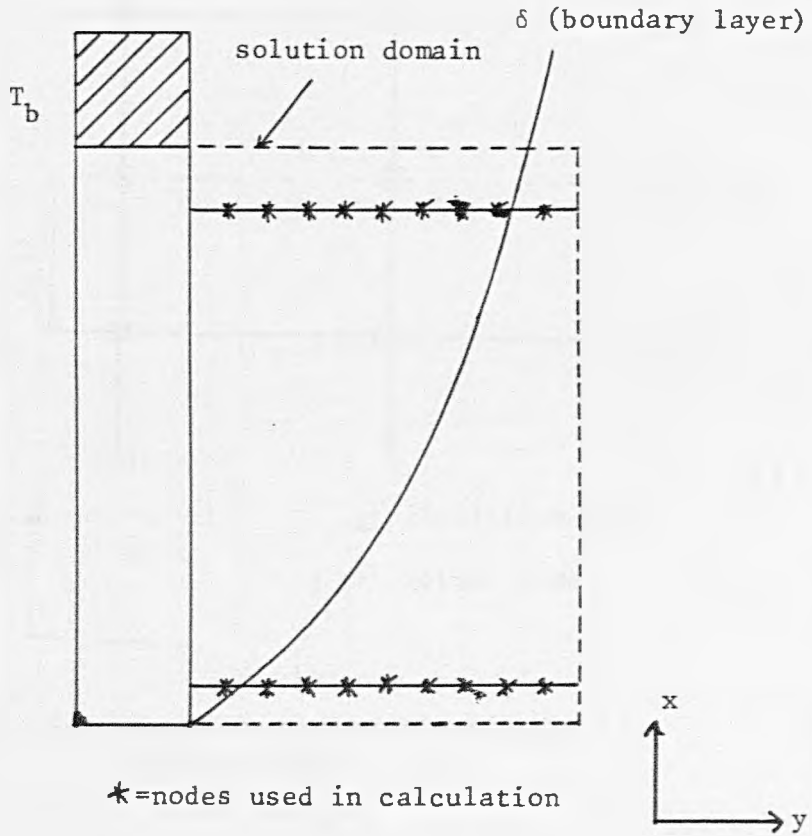

Fig. 5.2a Fin and Solution Domain in Cartesian Co-ordinates

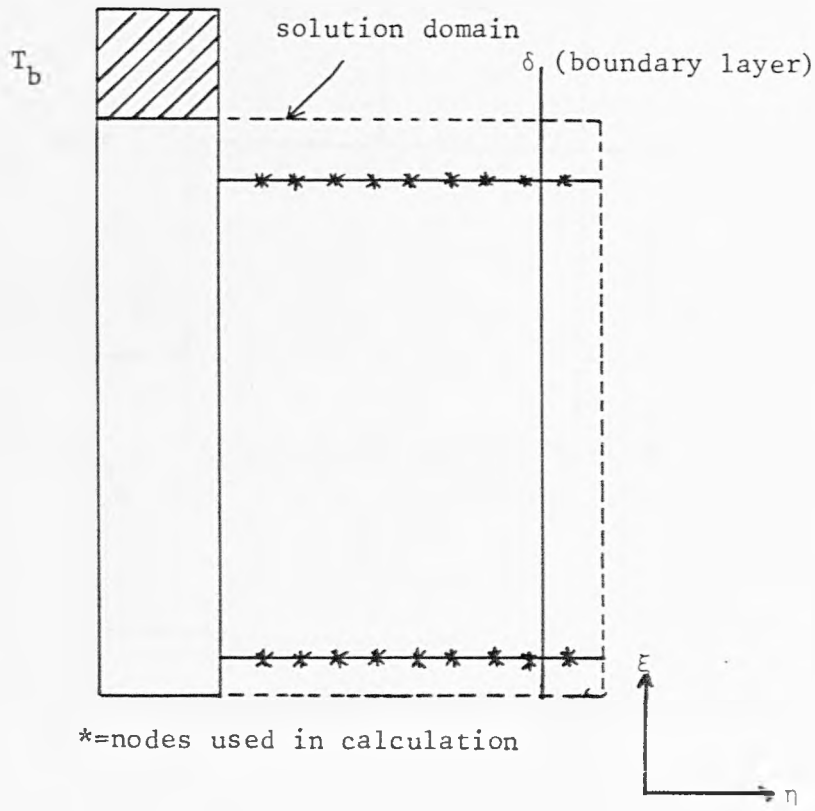

Fig. 5.2b Fin and Solution Domain in Transformed Co-ordinates

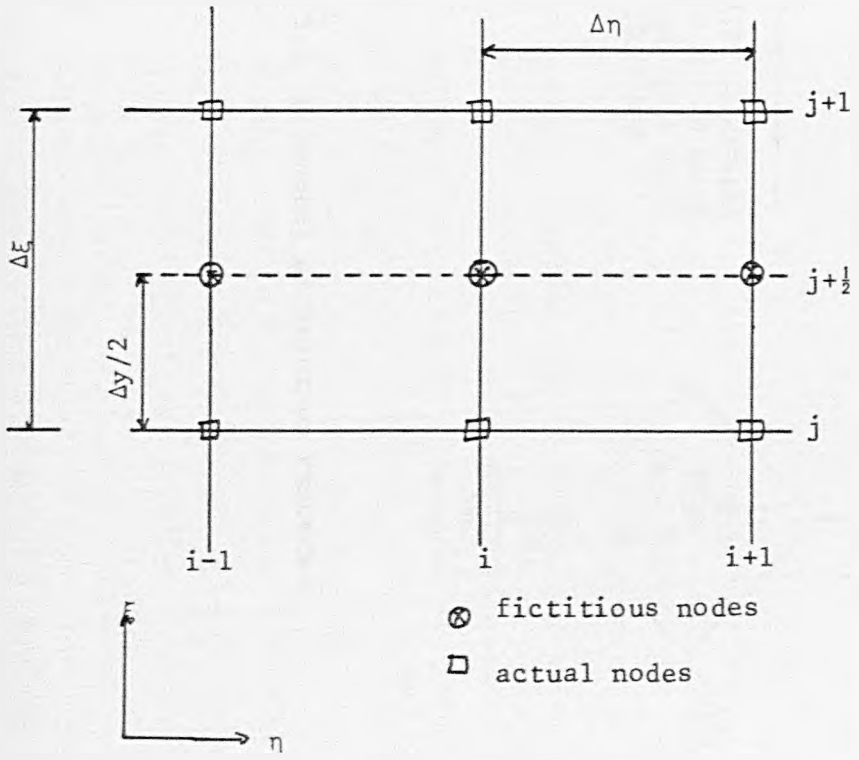

Fig. 5.3 Position of Fictitious Nodes in Boundary Layer

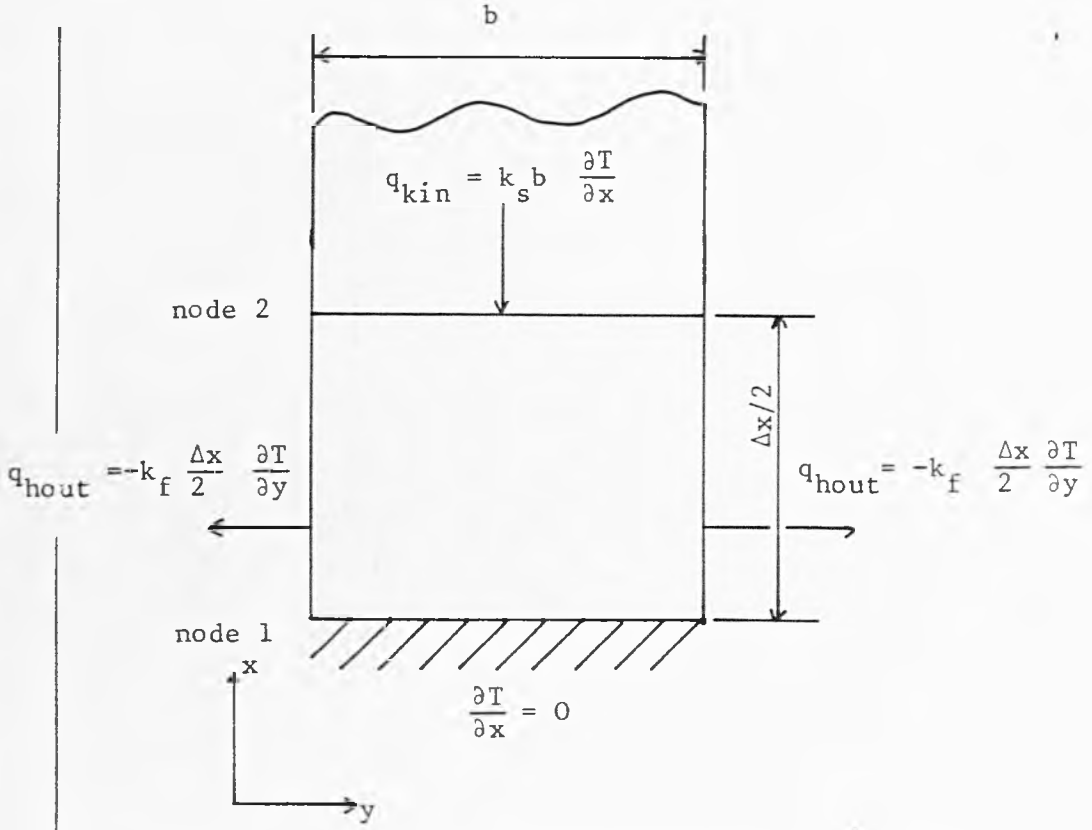

Fig. 5.4 Heat Balance Between Fin Tip and Second Node

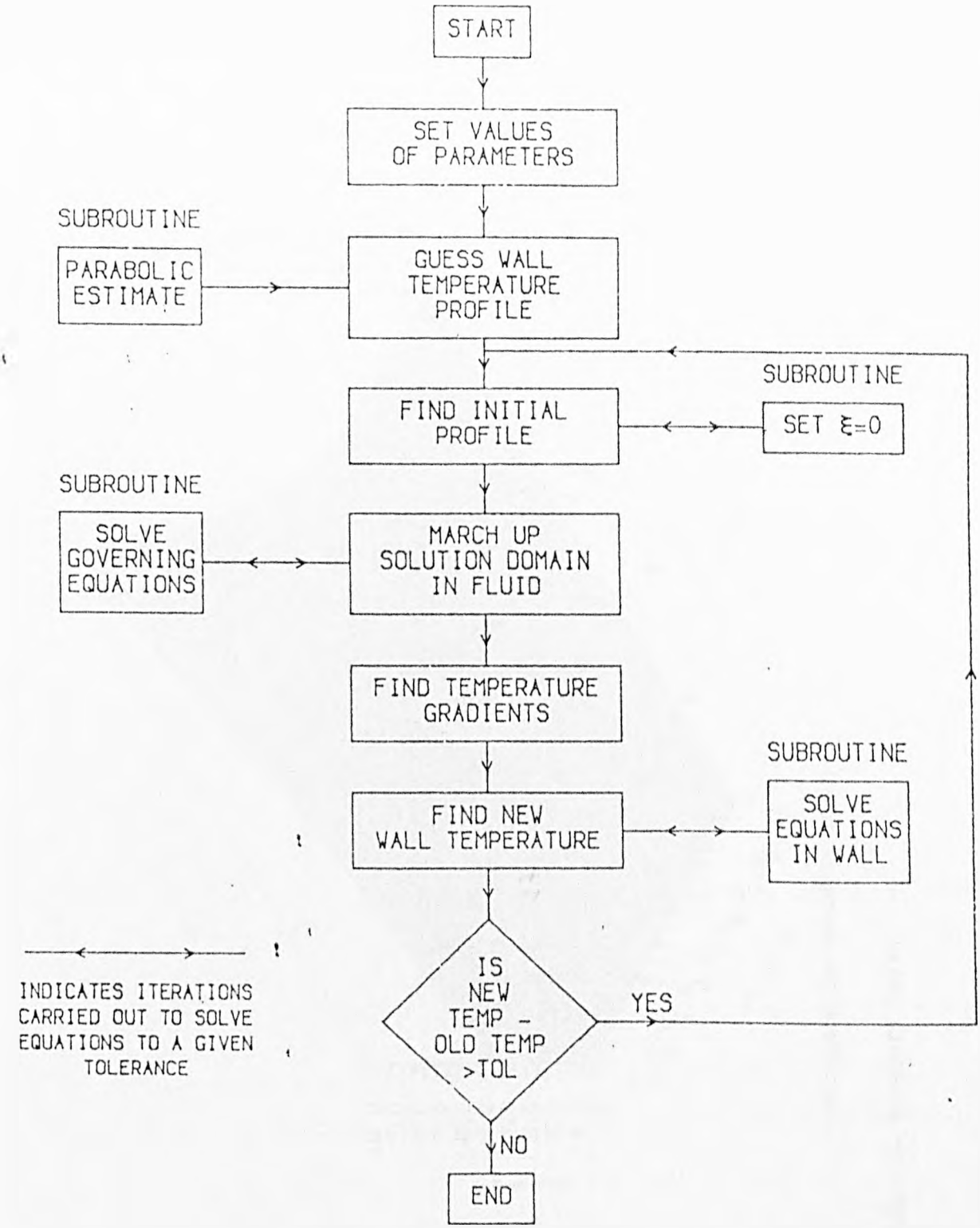

Fig. 5.5 Flowsheet of Solution Procedure

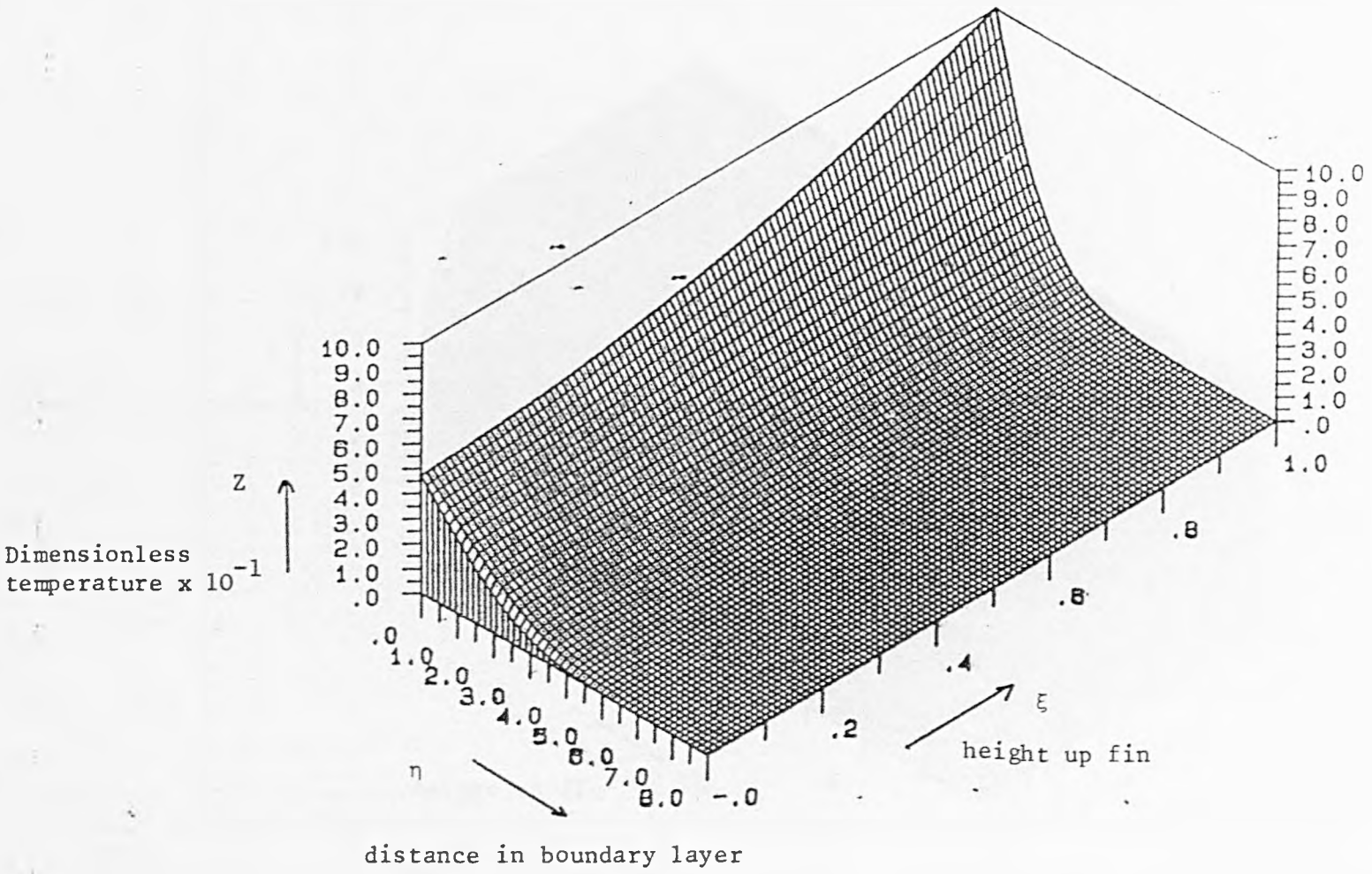

Fig. 5.6 Temperature in Boundary Layer

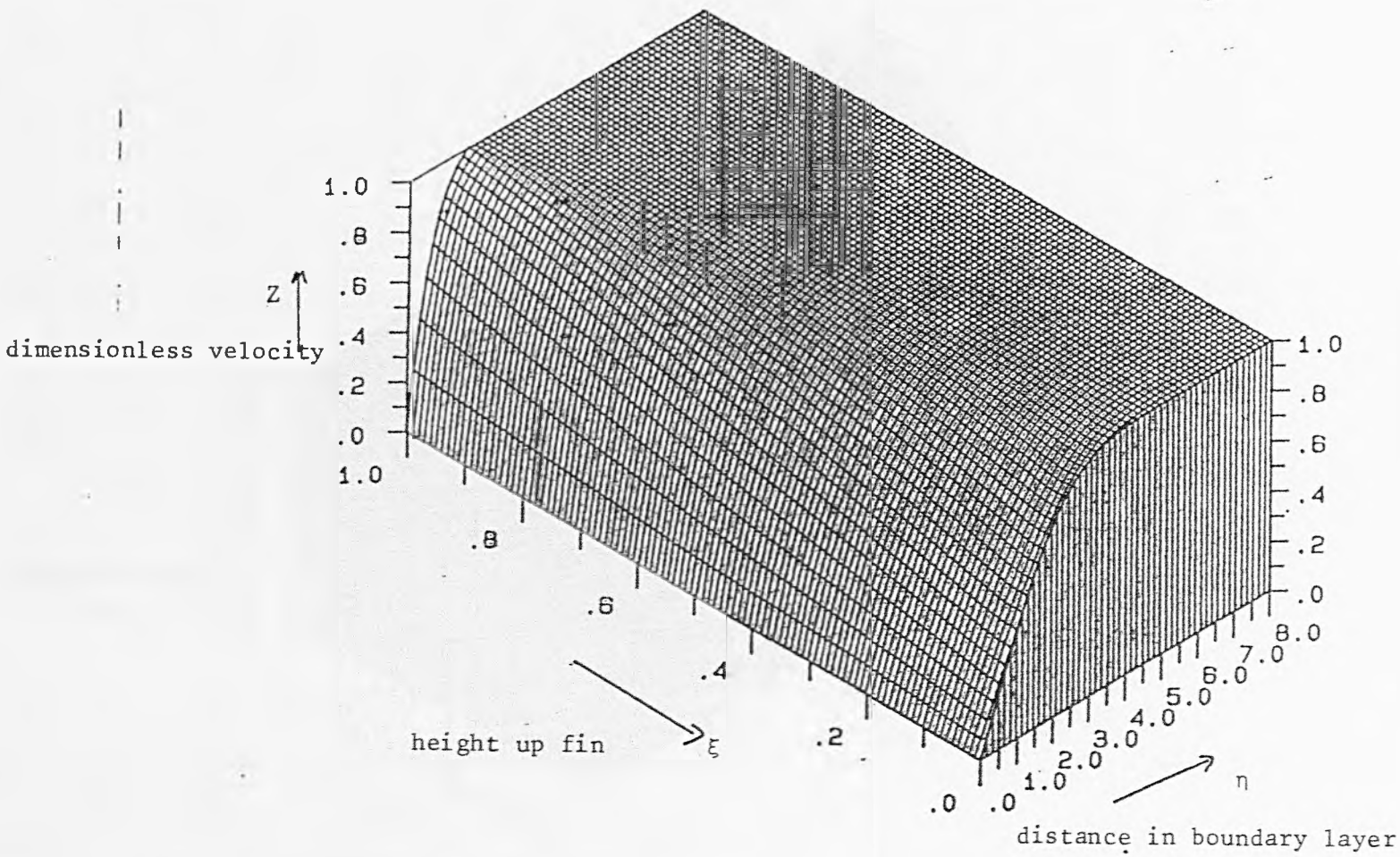

Fig. 5.7 Velocity in the Boundary Layer

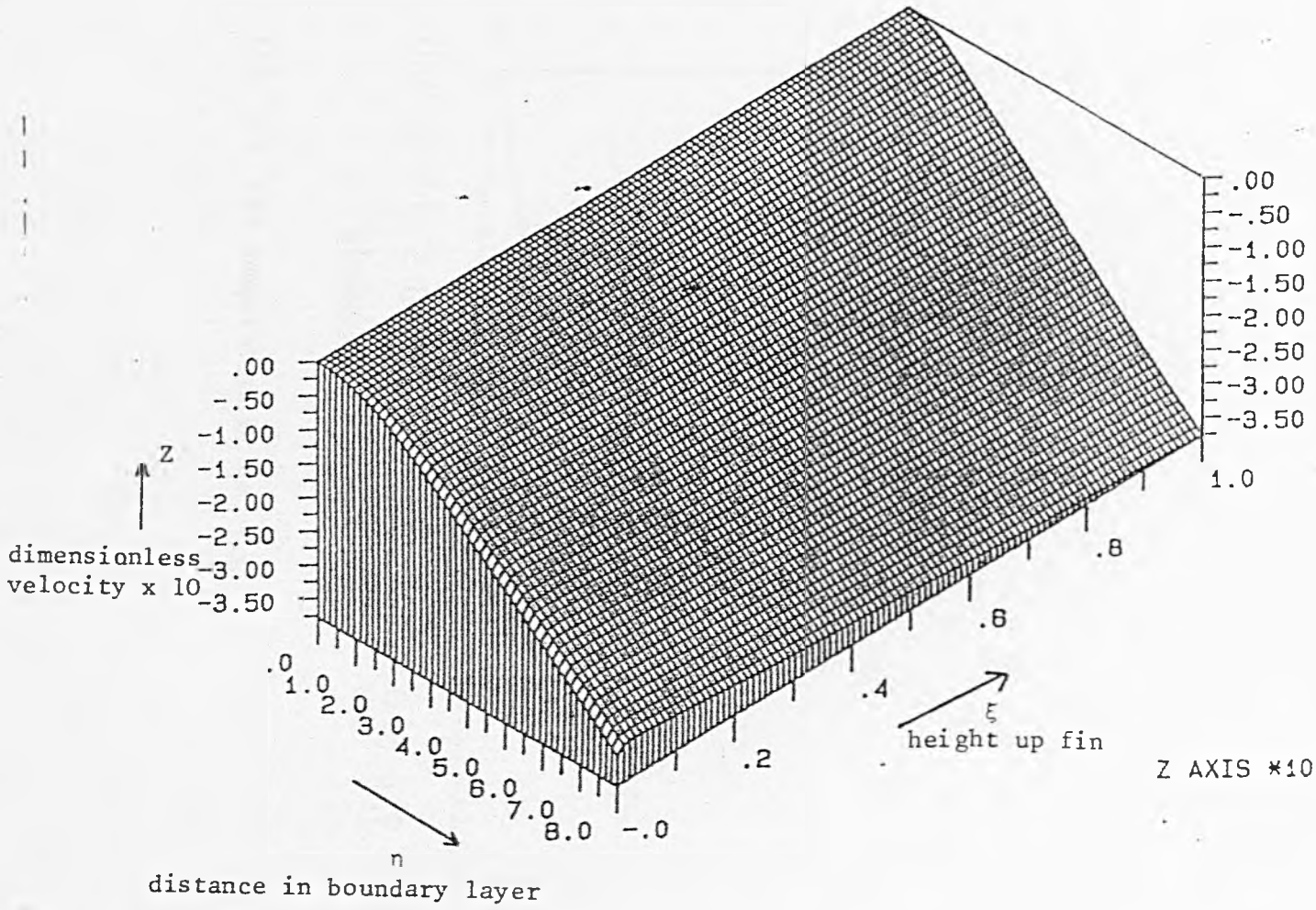

Fig. 5.8 Velocity v in Boundary Layer

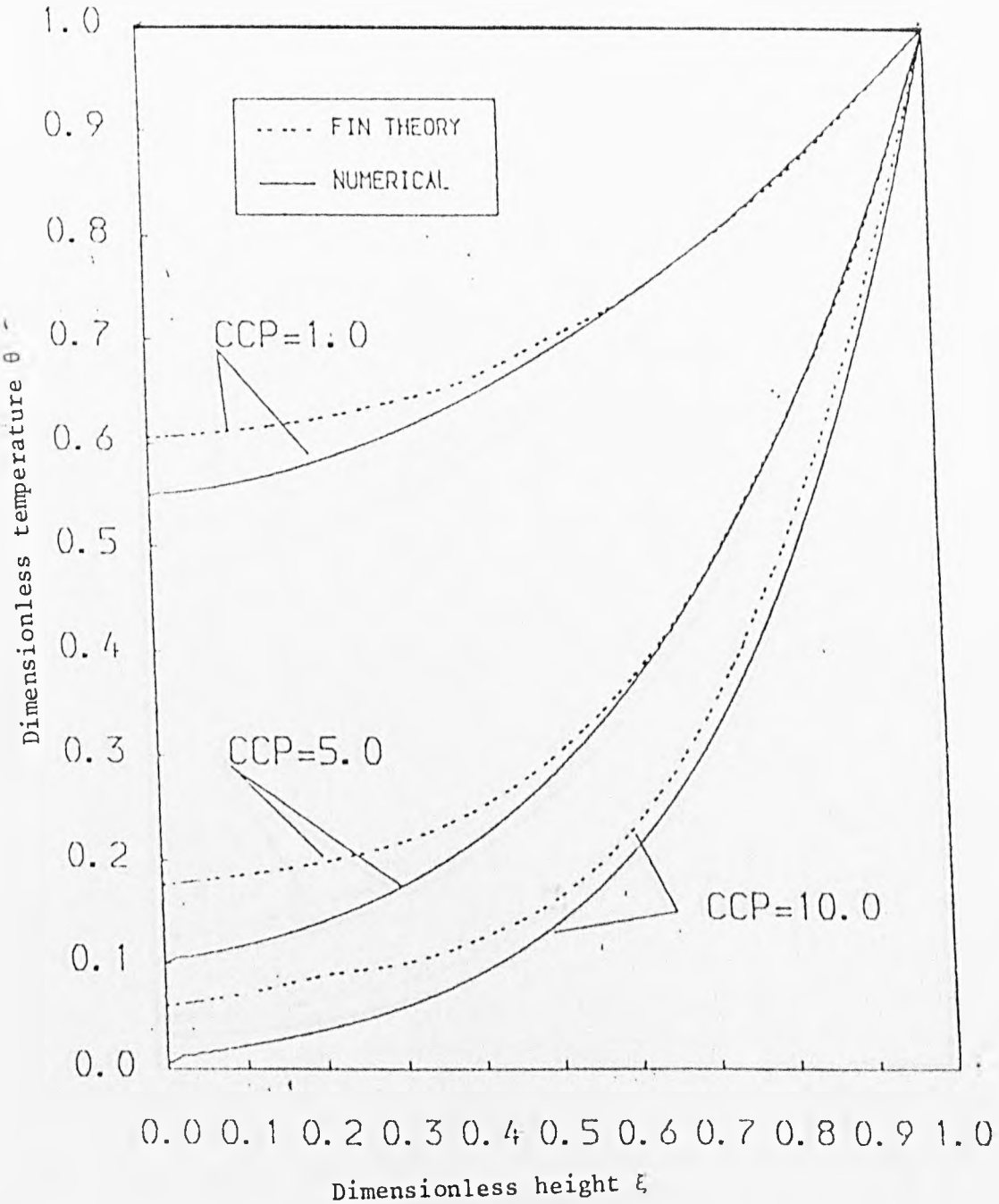

Fig. 5.9 Fin temperature $Gr/Re^2 = 2$

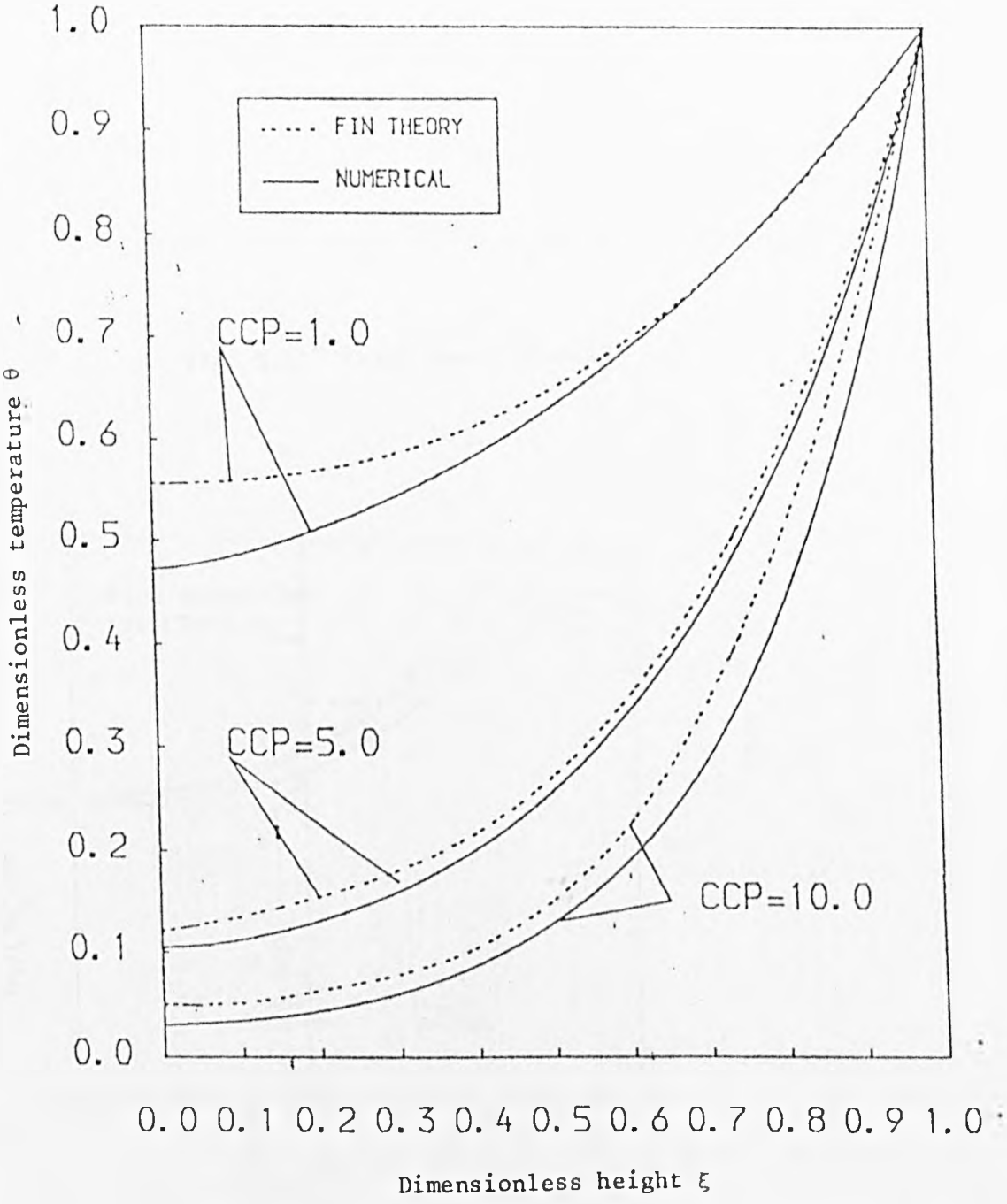

Fig. 5.10 Fin temperature $Gr/Re^2 = 0$

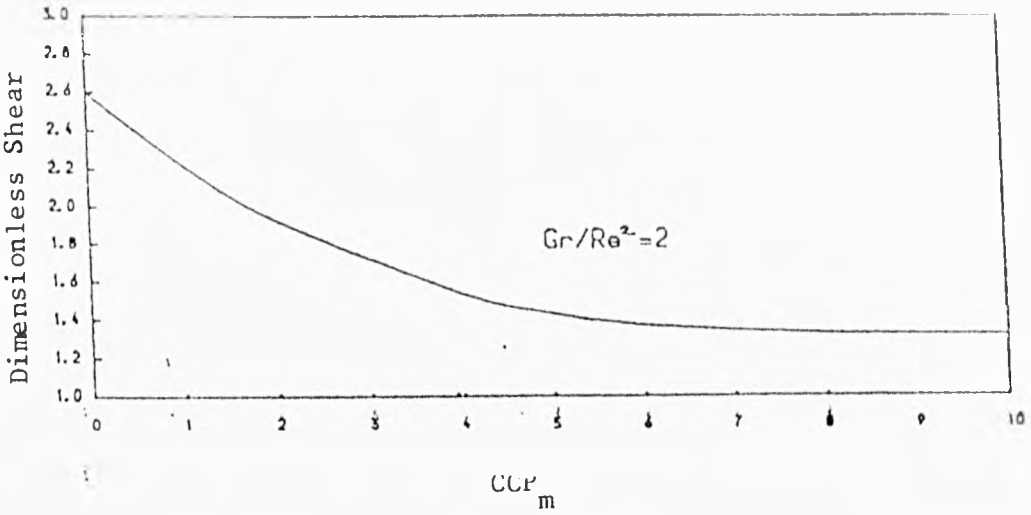

Fig. 5.11 Total Shear Stress

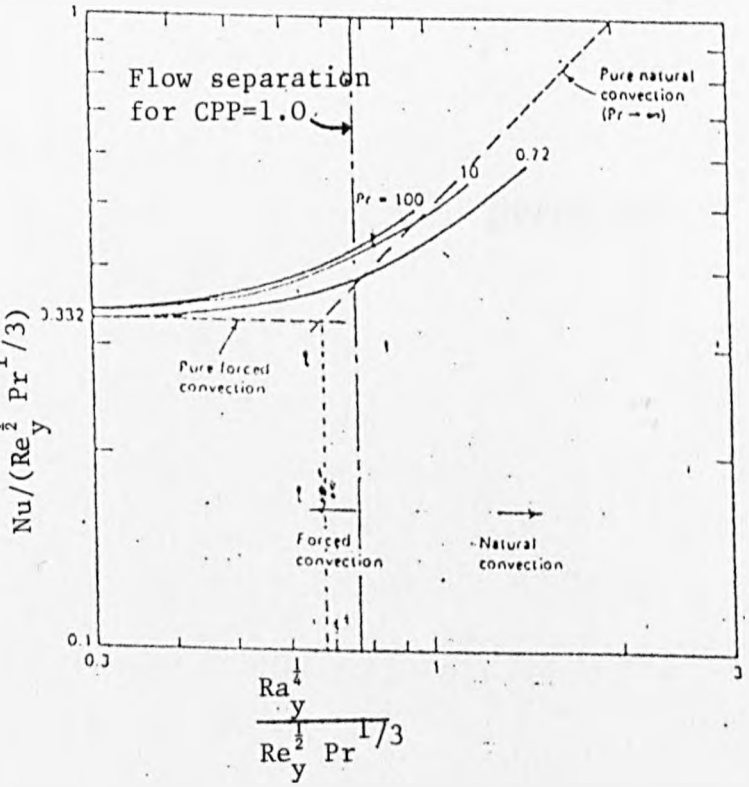

Fig. 5.12 Limit of Onset of Flow Separation

CHAPTER SIX

6. Mixed Convection Heat Transfer From a Downward Projecting Fin Immersed in a Saturated Porous Medium with 1-D Conduction

6.1 Introduction

There is a great variety of porous materials both in nature and in the industrial world. Water, petroleum and natural gas are some of the substances which are held within the pores of natural rocks. In fact, one of the main reasons which caused interest in the study of heat transfer in a porous medium was to study the possibility of extracting geo-thermal energy.

On the industrial side, porous materials can be found in many applications. For example, in adsorption processes substances such as silica gel and activated charcoal are used. Fixed and fluidised bed reactors also represent a porous medium problem. For the control of fixed and fluidised bed reactors, it is important to know the exact temperatures inside the bed. To find these temperatures it is sometimes necessary to place inserts, containing thermocouples, into the bed. For this reason an understanding of fin heat transfer in a porous medium is important. Solar energy collectors also require an understanding of fin heat transfer in a porous material, as one method of storing the heat is by heating water flowing in a porous medium.

Due to the large range of possible mediums it is obvious that there will be no single pore structure which defines every medium. Shapes of pores range from spherical, for example in concrete, to flat and slit shaped, as is found in mica. In between these two extremes, the shapes of pores can take on a completely irregular form, which cannot be defined by any standard shape. As well as the different shapes of pores, the way in which they are inter-connected can also vary greatly. There is little point, even if it were possible, in

177

trying to determine the exact structure of any material, as this structure would change from one specimen to the next. Therefore, the way in which a porous medium is defined, is to represent the bulk properties of the material, in a similar way to that of turbulent flow about a surface. However, the accurate analysis of pore structure provides an important link in that it provides the information required to formulate a bulk material model.

The application and theory of heat transfer by natural convection from finned bodies has now been studied for over half a century, see for example Harper and Brown [3]. However, the conjugate nature resulting from the conduction in the fin and the natural or mixed convection from the surface of the fin, has only been investigated more recently. In a porous medium Cheng and Minkowycz [41] studied the transfer of heat, by natural convection, from a vertical wall. However, no calculations have yet been published in which the effect of conjugate heat transfer from a downward projecting fin in a porous material has been considered. The present work fills this gap by using the improved method of Sunden's solution for solving conjugate heat transfer with mixed convection from a downward projecting fin [84] which was presented in chapter five.

Anderson and Bejan [64] and [87] have investigated the conjugate heat transfer through an impermeable wall in both the porous medium and free fluid problem. However, these solutions are only applicable to symmetrical problems in which the Oseen linearization technique can be used.

Cheng and Minkowycz [41] and Hsu and Cheng [88] consider the heat transfer from a semi-infinite vertical plate which is maintained at a temperature T_w, which is given by:

$$T_w = T_\infty + Ax^a$$

where x is the distance from the leading edge of the plate. Cheng and Minkowycz [41] consider the situation when the fluid flow may be approximated by the Darcy law, whilst in [88] the Brinkmann model is used.

In the present work the mixed and free convection heat flow from a rectangular fin is investigated. The fin extends from a plane wall which is maintained at a constant temperature. Since the temperature of the fin is not known a priori, it is necessary to solve the conjugate convection and conduction problem. It is this problem that was solved by Sunden and in the previous chapter, except that this work is for the case when the fin is in a porous medium. However, Sunden [84] discretises the governing partial differential equations when expressed in scaled cartesian co-ordinates. Since the boundary layer has zero thickness at the tip of the fin, then such a discretisation results in very few mesh points within the boundary layer near the tip of the fin. Hence, the solution in this vicinity will be inaccurate unless a great number of nodes are used at each station up the fin. Further, since the governing equations are parabolic, these inaccuracies are transmitted along the full length of the fin.

In the present work the natural convection similarity variables are used in order to transform the boundary layer equations into their natural co-ordinates η and ξ. This choice of variables then allows the solution of both the natural and mixed convection problems with the same basic formulation. This contrasts with the situation in the non-porous medium where this is not possible. As well as allowing a sufficient number of grid points near the leading edge the current formulation also allows a second order finite difference scheme to be imposed over the entire solution domain.

The problem of the fin in a porous material is solved for the case when the no slip boundary condition is relaxed. The criteria for such an assumption to be made is studied, and its validity is checked for each solution.

6.2 Solution Procedure

The geometry of fin considered here is the same as that used when investigating the fin in a free fluid (chapter five), except that the fluid around the fin is considered to be part of a saturated porous medium. Therefore, the figure 5.1 can be used again to give the schematic representation of the fin. The length of the fin is taken to be L, the thickness b and the temperature at the base of the fin T_b. The fluid in the medium is flowing at a constant velocity, U_∞, at a large distance from the fin. Both cases of assisting and opposing convection flows are considered so that the condition for flow reversal and separation can be found. Again, as when the free fluid situation was studied,the only change between the assisting and opposing flow regimes is that the sign for the gravity term is changed in the governing equations.

The height of the fin is considered to be much greater than the thickness of the fin, so one-dimensional heat flow in the fin can be assumed, as well as assuming that the fin tip is adiabatic. However, the height of the fin must be such that the entire flow about the fin is in the laminar regime. This does not cause much of a restriction for the current analysis, as the current work is aimed mainly at studying heat exchange equipment. In these conditions it is important to have short fins for efficient and economic use. Under the Boussinesq approximation and assuming there is negligible viscous dissipation the boundary layer equations become:

$$\frac{\partial u}{\partial x} + \frac{\partial v}{\partial y} = 0 \tag{6.1}$$

$$u = u_\infty + g\beta K(T_1 - T_\infty) \tag{6.2}$$

$$u \frac{\partial T_1}{\partial x} + v \frac{\partial T_1}{\partial y} = \alpha \frac{\partial^2 T_s}{\partial y^2} \tag{6.3}$$

For the fin an energy balance gives:

$$\frac{\partial^2 T_f}{\partial x^2} + \frac{k_1}{k_f b} \left(\frac{\partial T_1}{\partial y}\right)_{y=0} = 0 \tag{6.4}$$

The boundary conditions for the fluid flow equations (6.1 to 6.3) show that the fin surface is impermeable (i.e. no flow of fluid perpendicular to the fin), and that at the surface of the fin there is continuity in the temperature and heat flow.

$$\begin{aligned} v &= 0 \\ T_1 &= T_f \qquad\qquad y = 0 \quad x > 0 \\ -k_1 \frac{\partial T_1}{\partial y} &= k_f \frac{\partial^2 T_{fb}}{\partial x^2} \end{aligned} \tag{6.5}$$

The conditions for the fluid infinitely far from the surface of the fin show that the flow parallel to the wall reaches that of the forced flow component and the temperature of the fluid falls to a bulk value.

$$\begin{aligned} u &\to u_\infty \\ T_1 &\to T_\infty \end{aligned} \qquad y \to \infty \; ; \quad x < L \tag{6.6}$$

The last boundary conditions are used in solving the conduction convection balance for the fin. The first states that the temperature at the base of the fin is kept constant at the value T_b and the second shows that there is an adiabatic fin tip.

$$T_f = T_b \qquad x = L$$

$$\frac{dT_f}{dx} = 0 \qquad x = 0 \tag{6.7}$$

When the fin is surrounded by a free fluid the relationship between the boundary layer and the solution domain was such that when a grid is laid over the boundary layer very few mesh points lay within the boundary layer itself near the fin tip, most falling outside where the conditions of temperature and velocity are constant. This is also the case when the fin is immersed in a saturated porous medium, as the nature of the boundary layer is similar in both free fluid and porous media cases. To overcome this for the free fluid the similarity variables appropriate for forced convection were introduced. This allowed the study of mixed and forced convection, but not the pure natural convection situation. In this problem the similarity variables for natural convection can be introduced without any difficulties in the subsequent solution. If the forced convection variables are introduced the parameter Ra/Pe would be found, and this cannot be used in the pure natural convection case as Pe=0. At the same time as introducing the natural convection similarity variables, a dimensionless group for temperature can also be used. Therefore, the variables used in the present analysis are given by:

$$\eta = \frac{y}{x} Ra_x^{\frac{1}{2}} \quad , \quad \xi = x/L$$

$$\psi = \alpha \, Ra_x^{\frac{1}{2}} \, f(\eta, \xi)$$

$$\theta_{1 \text{ or } f} = \frac{T_{1 \text{ or } f} - T_\infty}{T_b - T_\infty} \tag{6.8}$$

$$u = \frac{\partial \psi}{\partial y} \quad , \quad v = - \frac{\partial \psi}{\partial y}$$

$$F = \frac{\partial f}{\partial \eta}$$

where f is a function of η and ξ.

On introducing these natural convection similarity variables (which in this case should really be called pseudo-similarity variables), equation 6.1 is identically satisfied. The remaining governing equations are then given by:

$$F = \frac{\partial f}{\partial \eta} \tag{6.9}$$

$$F = \frac{Pe}{Ra} + \theta_1 \tag{6.10}$$

$$\xi \frac{F \partial \theta_1}{\partial \xi} - \tfrac{1}{2} \frac{f \partial \theta_1}{\partial \eta} - \xi \frac{\partial \theta_1}{\partial \xi} \frac{\partial \theta_f}{\partial \eta} = \frac{\partial^2 \theta_1}{\partial \eta^2} \tag{6.11}$$

$$\frac{\partial^2 \theta_f}{\partial \xi^2} + \frac{CCP}{\xi^{\frac{1}{2}}} \frac{\partial \theta_1}{\partial \eta}_f = 0 \tag{6.12}$$

where CCP (the convection conduction parameter) is given by:

$$CCP = \frac{k_1 L Ra^{\frac{1}{2}}}{k_f b} \tag{6.13}$$

This parameter can take different forms, each depending on the particular transformations that are carried out on the governing equations.

The boundary conditions used to solve equations 6.9 to 6.11 are the transformed conditions given by 6.5 and 6.6. After introducing the variables given by 6.8 the boundary conditions for the fluid flow are:

$$f = 0, \quad \theta_f = \theta_1, \quad \left(\frac{\partial^2 \theta_f}{dy^2}\right) = - CCP \left(\frac{\partial \theta_1}{\partial \eta}\right)_f \quad \text{on} \quad \eta = 0 \tag{6.14}$$

$$F \to 1, \quad \theta_1 \to 0 \qquad \text{as} \quad \eta \to \infty \tag{6.15}$$

Similarly, the boundary conditions for the fin itself can be altered using the substitutions given by equation 6.8:

$$\begin{aligned} \theta_f &= 1 \qquad \text{on} \quad \xi = 1 \\ \frac{d\theta_f}{d\xi} &= 0 \qquad \text{on} \quad \xi = 0 \end{aligned} \tag{6.16}$$

As the fluid flow equations (6.9 to 6.11) are parabolic, an initial profile is required at the fin tip. This is found by setting ξ=0 in the governing equations, which then reduce to:

$$F = \frac{df}{d\eta} \tag{6.17}$$

$$F = \frac{Pe}{Ra} + \theta_1 \tag{6.18}$$

$$\frac{d^2\theta_f}{d\eta^2} + \tfrac{1}{2} f \frac{d\theta_1}{d\eta} = 0 \tag{6.19}$$

which are also subject to the boundary conditions 6.14 and 6.15.

When solving the fin conduction equation it is found that it is best not to start the initial profile at the fin tip itself, but at a certain distance away. A convenient value for the starting

position is $\xi = \Delta\xi/2$. The reasons for this are that if the initial profile is taken at the fin tip the solution is found to be very dependen on the step size taken up the fin. Thus, if the initial profile is taken away from the fin tip accurate solutions can be found much more easily. However, carrying out the solution procedure in this way means that the fin tip temperature must be found later, but this does not cause any problems.

To obtain an accurate solution in the fluid and the wall by numerical analysis a second order accurate technique is used throughout. This is achieved by carrying out central differencing about a fictitious point in the fluid. This is demonstrated in figure 6.1. The resultant central difference equations about the fictitious node are:

$$F(i,j) = \frac{f(i+1,j)-f(i-1,j)}{2\Delta\eta} \tag{6.20}$$

$$F(i,j) = \frac{Pe}{Ra} + \theta_{1(i,j)} \tag{6.21}$$

$$\xi_{av} F_{av} \left(\frac{\theta_{1(i,j+1)}-\theta_{1(1,j-1)}}{\Delta\xi}\right) - \tfrac{1}{2} f_{av} \tfrac{1}{2} \left(\frac{\theta_{f(i+1,j+1)}-\theta_{1(i-1,j+1)}}{2\Delta\eta} + \right.$$

$$\left.\frac{\theta_{1(i+1,j)}-\theta_{1(i-1)}}{2\Delta\eta} - \xi_{av} \left(\frac{f(i,j+1)-f(i,j)}{\Delta\xi}\right) \tfrac{1}{2} \left(\frac{\theta_{1(i+1,j+1)}-\theta_{1(i-1,j+1)}}{2} + \right.\right.$$

$$\left.\left.\frac{\theta_{1(i+1,j)}\ \theta_{1(i-1,j)}}{2\Delta\eta}\right) = \tfrac{1}{2} \left(\frac{\theta_{1(i+1,j+1)}-2\theta_{1(i,j+1)}+\theta_{1(i-1,j+1)}}{\Delta\eta^2} + \right.\right.$$

$$\left.\left.\frac{\theta_{1(i+1,j)}-2\theta_{1(i,j)}+\theta_{1(i-1,j)}}{\Delta\eta^2}\right) \right. \tag{6.22}$$

Equations 6.21 and 6.22 can be used as they stand to find values of F and θ_1 respectively. However, equation 6.20 cannot be used as it is to find f, as, when the problem is solved using Gaussian elimination and back substitution, the matrix formed will not be

diagonally dominant. Also, the value of f(2,j) could not be found as f(0,j) does not exist (and cannot be determined from any boundary conditions). To overcome this equation 6.17 is differentiated with respect to η and then expressed in finite difference form. The resulting equation is given by:

$$\frac{F(i+1,j)-F(i-1,j)}{2\Delta\eta} = \frac{f(i+1,j)-2f(i,j)+f(i-1,j)}{\Delta\eta^2} \tag{6.23}$$

Using equation 6.21 to 6.23 the solution for F, θ_1 and f can be found. As can be seen from these equations the solution of one variable is dependent of the values of the others. Equation 6.22 is used to find the value of θ_1, and as this equation involves both f and F, is solved last, after new values for f and F have been determined. The choice in the order of solving equations 6.21 and 6.23 is not quite as obvious. It is decided to solve equation 6.21 first as the value of θ_1 needs to be known, but as this is found last it does not matter in the solution of F whether it is calculated before or after f. However, the solution of f depends on the value of F, so if the updated value of F were used then this would be better when solving equation 6.23. Therefore the order of solution is equation 6.21 followed by 6.23 and finally equation 6.22.

Equation 6.21 can be used directly to find updated values of F. Equations 6.22 and 6.23 need to be rearranged to give tri-diagonal matrices, which are subsequently solved by Gaussian elimination and back substitution.

6.2.1 Solution of the Initial Profile

The solution of the initial profile is easier to calculate than the rest of the fluid flow as a fictitious point does not have to be introduced. A second order accurate scheme is again used. If this were not done then the effort in enforcing a second order accurate method in the rest of the fluid flow would be wasted. This is due to the fact that the governing equations are parabolic. In such a case, the information is taken from the initial profile and used to sweep up the boundary layer. If the information at the starting point is only first order accurate, there is no way in which the remainder of the problem can be solved to greater accuracy.

Equations 6.17 to 6.19 are to be solved for the initial profile. Again, as in the main flow problem, the expression relating F and f cannot be used as it stands to solve for the second node from the fin surface using a second order accurate equation. Therefore the equation 6.17 is differentiated with respect to η, and this is used to find f(2,2). Using equations 6.17, 6.18 and 6.19 to find f, F and θ_1 respectively the relationships are:

$$f(2,2) = \frac{f(3,2)}{2} + (F(1,2) - F(3,2)) \frac{\Delta\eta}{4} \qquad (6.24)$$

or

$$f(i,2) = 2F(i-1,2)\Delta\eta + f(i-2,2) \qquad (6.25)$$

$$F(i,2) = \frac{Pe}{Ra} + \theta_{1(i,2)} \qquad (6.26)$$

$$\theta_{1(i,2)} = \frac{\theta_{1(i+1,2)} \left(\frac{f(i,2)}{4\Delta\eta} + \frac{1}{\Delta\eta^2}\right) + \theta_{1(i-1,2)} \left(\frac{1}{\Delta\eta^2} - \frac{f(i,2)}{4\Delta\eta}\right)}{2\Delta\eta^2} \qquad (6.27)$$

187

6.2.2 Solution of Fin Conduction Equation

Once the fluid flow problem has been solved, the fin conduction equation (6.12) can be investigated, as all values of $\partial\theta_f \Delta\eta$ are known. Central differencing is used to obtain the following relationship:

$$\frac{\theta_{f(j+1)} - 2\theta_{f(j)} + \theta_{f(j-1)}}{\Delta\xi^2} + \frac{CCP}{\xi^{\frac{1}{2}}} \frac{\partial\theta_{1(j)}}{\partial\eta} = 0 \qquad (6.28)$$

This yields a tri-diagonal matrix which is solved using Gaussian elimination and back substitution to find values for $\theta_f(2)$ to $\theta_f(M)$, where M denotes the number of the node before the fin base. The temperature of the fin tip cannot be found using equation 6.28 as the temperature gradient into the fluid is only known at node 2 and above. The fin tip temperature can be found by carrying out a heat balance between the first and second nodes.

Figure 6.2 shows the heat flows into and out of the fin tip in the normal x and y co-ordinates. Transforming the co-ordinates into η and ξ and carrying out the integration involved in finding the heat flow out, the following relationship is found between the temperature at the fin tip and the temperature at the third node up the fin:

$$\theta_f(1) = \theta_f(3) + 2 \frac{\partial\theta_1}{\partial\eta} \Delta\xi^{3/2} CCP \qquad (6.29)$$

The value for $\partial\theta_1/\partial\eta$ is that found when solving the initial profile, as it is assumed that there is local similarity over the first interval. This means that the temperature gradient is assumed to be constant, which is what allows the integral involved in the heat flow out to be solved. Using equation 6.29 along with the results from 6.28 provides a complete solution for the fin temperature.

6.3 Numerical Procedure

Within the fin, the governing equation (6.12) is discretised using M intervals, so that the grid size is $\Delta\xi = 1/M$ and the calculations performed with M=100, 200 and 400. Within the boundary layer a rectangular grid is used with $\Delta\xi = 1/M$ and $\Delta\xi = \eta_\infty/N$. All results presented here correspond to N=80. The value of η_∞ is varied until an increase in its value does not produce different results from those found for a slightly smaller value.

The solution procedure may be summarised as follows:

1) The parameters k_f, k_1, L, b, Ra and Pe are specified.
2) The variation of the wall temperature is guessed. It is found that a parabolic variation produces a reasonable first approximation.
3) The initial profiles at $\xi=0$ are obtained by solving the ordinary differential equations 6.17 to 6.19 subject to the boundary conditions $f(0)=0$, $\theta_1(0)=\theta_f$, $\theta_1(\infty) = 0$.
4) Since equations 6.9 to 6.11 are parabolic, a marching procedure, which is similar to the Crank-Nicholson scheme is employed.
5) The temperature gradient $(\partial\theta_1/\partial\eta)$ at $\eta=0$ is evaluated using a second order approximation.
6) Using equation 6.12 a new temperature profile along the fin wall is obtained. It is observed that equation 6.12 cannot be used at $\xi=0$ due to the term $\xi^{-\frac{1}{2}}$ which occurs in that equation. Thus, in the first element at the fin tip a heat balance is carried out. In order to find the heat flow from the first element an integration is carried out.

7) The new temperature variation of the wall is now compared with the previous variation. If the sum of the absolute values of the differences in temperature at corresponding nodes is within a prescribed tolerance then the iteration procedure is complete, otherwise we return to step 3 and repeat the procedure.

In order to obtain very accurate results the Richardson extrapolation, or deferred approach to the limit, is used. This method requires three different solutions using different grid sizes. Here, the grid sizes used are in the ratio of 1:2:4 so that the extrapolation procedure is simplified as much as possible. Using these results then the extrapolated result u_e can be obtained from the expression $u=u_e+A(\Delta\xi)^a$ where A and a are unknown constants and u is the physical quantity required.

In setting the size of the solution domain it must be ensured that the infinite boundary condition is sufficiently far from the wall, i.e. the value of η_∞ must be sufficiently large. If this is not done then artificially high values of the velocity and temperature gradients will be calculated. This is because the velocity and temperature are forced to the ambient conditions too quickly, thus resulting in the rapid fall of their values near the wall.

In the case of adverse flow, when U_∞ is sufficiently small, such that neither free nor forced convection dominates, separation may occur. The range of values of Pe/Ra for which separation occurs can be found by using the numerical scheme as described above, but the negative values of Pe/Ra. Separation will first occur at the base of the fin when the upflow due to the natural convection is largest, since, at this point, the temperature difference, and hence the buoyancy force, is greatest.

The numerical procedure employed here is unable to solve the finite difference equations past the point where flow reverses as the governing equations are parabolic, and a marching procedure is used. The onset of separation indicates that information is travelling to the node under investigation from the fin tip. If flow reversal occurs along the surface of the fin, or within the fluid itself, information concerning the flow is coming from both directions, rather than from the fin tip alone. This means that the governing equations become singular parabolic partial differential equations, and the solution procedure fails.

6.4 Results

To compare the current results with those found for the free fluid in the previous chapter, the same parameters are used. However the term Pe/Ra is now the governing parameter rather than Gr/Re^2 which was appropriate in chapter 5. Figure 6.3 compares the temperature profile along the fin surface between the porous medium situation and the non-porous medium case, for a value of 550 for Pe/Ra (which corresponds to Gr/Re^2 equal to 2) when the convection conduction parameter is either 0.0359 or 0.1792)(which corresponds to CCP_m = 1 or 5 in the non-porous medium). Figure 6.4 looks at the same CCP values but Pe/Ra is set to either 275 or 0. A value of zero for Pe/Ra is equivalent to pure natural convection flow, the condition that could not be studied for the non-porous medium situation due to the position of the term U_∞ in the governing equations.

The values of the parameters used in obtaining the results is given in table 6.1 below.

	Pe/Ra = 550		Pe/Ra = 275		Pe/Ra = 0	
	CCP		CCP		CCP	
	0.0359	0.1792	0.0359	0.1792	0.0359	0.1792
b	0.0117	0.0023	0.0117	0.0023	0.0117	0.0023
U_∞	0.3325	0.3325	0.1663	0.1663	0.0000	0.0000

All other parameters kept constant

H 0.1m

β 3.22e-3/K

ν 1.88E-5 m^2/s

T_b 90.0°C

T_∞ 20.0°C

k_f 9.0 W/m K

k_l 0.025 W/m K

K(permeability) 5.19e-9 m^2

Table 6.1 Parameters used to obtain results for mixed convection flow in a porous medium

Using the physical quantities given in table 6.1 the characteristics of the flow and temperature about a fin are found.

Before any results are presented it must be established that the assumption of Darcian flow is not violated. In the experimental and theoretical study by Hsu and Cheng [88] a parameter was found that compared the thickness of the thermal boundary layer with that of the viscous sub-layer. The parameter is:

$$Pn_x = \sqrt{\frac{K^2 g \beta (T_s - T_\infty)}{\varepsilon \nu \alpha x}} \qquad (6.30)$$

For Darcy's law to hold the value of Pn_x must be much less than unity (i.e. the viscous sub-layer must form a very small part of the total boundary layer). Clearly, at the fin tip, where x=0 Darcy's law does not hold, as the value of Pn_x is infinite, but at this point the boundary layer approximations also break down. For the temperature differences of order $100^{o}C$ the value of Pn_x is found to be of order 10^{-3}. Therefore, the approximations used by assuming that Darcy's law holds are valid. However, Hsu and Cheng [88] found that even when the viscous sub-layer is significant the effect on the temperature profile across the boundary is not very significant.

As well as the above proviso on the calculations Cheng and Ali [89] have shown that Darcian flow can only be observed when the value of the non-Darcian Grashof number, $\hat{Gr}$, is less than about 0.3. Using typical values for the constants associated with the porous medium, i.e. the particle diameter, permeability and porosity, it is found that the system considered here has a value for $\hat{Gr}$ of approximately 0.002. This means that the flow is taking place well within the limits of the Darcian flow approximations.

The position of the infinite boundary conditions needs to be assessed so that in practice its position can be placed at an appropriate distance from the surface of the fin. The same procedure as was used for the non-porous medium is adopted so that this position may be found. After trying several values of η_∞, it was found that $\eta_\infty = 10$ was sufficiently large for all values of the parameter CCP. In fact it was observed that the velocity and temperature profiles had effectively reached their ambient values at $\eta = 7$.

The tolerance used in all the iterative procedures was varied but it was found that a value of 10^{-3} was sufficiently small in order to obtain accurate results. In all cases the tolerance was

obtained by evaluating the sum of the absolute differences at all mesh points between two iterations for all quantities being calculated. It is found that the solution procedure is very sensitive to the tolerance imposed on the iterative procedures and this is due to the fact that the partial differential equations are coupled. If the tolerance is set too low the solution procedure ends rapidly while the errors in the solution for f, F and θ_1 are still oscillating about a high tolerance level. As soon as the tolerance is decreased below this oscillating point errors reduce monotonically, and reducing the tolerance still further does not have a significant effect on the results, although it does on the computational time.

Figure 6.3 shows the temperature profile along the surface of the fin for two values of the convection conduction parameter and for Pe/Ra = 550. Also shown are the results as found in the previous chapter on the non-porous medium (which are also the results as obtained by Sunden [84] and [85]). The calculations are carried out for three different grid sizes and then extrapolated using a deferred approach to a limit. This is done in the current problem and not for the non-porous problem, as no results are available with which the current problem can be directly compared. The method of the deferred approach to the limit calculated the error caused by using finite difference techniques and then extrapolates to find a converged solution (the one that would be found if an infinite number of nodes are used) using two of the results. By carrying out this procedure it is ensured that very accurate results are obtained.

From figure 6.3 it can be seen that for the same forced flow rate the temperature of the fin in the porous medium is lower than that

found for the non-porous medium. This indicates that the heat flow from the fin immersed in a porous medium is greater than that for the fin immersed in the non-porous medium. This temperature difference is noticeable for most of the length of the fin. Obviously, as the fin base is approached the temperatures of the two fins converge, as the constant temperature boundary condition is imposed at the base of the fin.

Figure 6.4 shows the variation of the temperature along the fin as a function of distance for two different values of the ambient velocity, one of which is zero and so corresponds to natural convection. As would be expected, the temperature of the fin increases as the contribution to the flow from forced convection is reduced. In fact, for the natural convection situation for a value of CCP = 1 the fin is almost approaching the isothermal situation.

The adverse situation is studied by considering the trend of the flow parallel to the surface of the fin. When the value of this parameter becomes very small it indicates that the forced and natural convection flows are almost equal, but opposite. If the temperature of the wall is increased very slightly then flow reversal will occur. As this causes the solution procedure to fail, as the governing equations are parabolic, the numerical procedure must be stopped just before this happens and the position of the flow reversal examined. If flow reversal occurs at a significant distance away from the base of the fin, the forced flow component is increased. If the numerical procedure does not fail the ambient flow is decreased. After several runs the point at which flow reversal occurs just at the base of the fin can be found. For CCP = 0.03585 the range for flow reversal is found to be $0.0 < Pe/Ra < 0.98$.

6.5 Conclusions

The present numerical method gives general results for a fin which is embedded in a porous medium. The method of solution does not require a form for the temperature profile on the fin to be assumed a priori, unlike previous similarity solutions [41] and [88]. The variables employed are the similarity variables as used when solving the natural convection problem with the fin maintained at a constant temperature. This allows the mixed and free convection problems to be solved, and also the pure forced convection problem if the temperature of the fin is set equal to the ambient fluid.

It is found that surrounding the fin in a porous medium, as opposed to a free fluid, decreases the temperature of the fin. This shows that the heat transferred from a fin embedded in a saturated porous medium is greater than from an identical fin in a free fluid.

The temperature of the fin tip is significantly higher than the ambient fluid. Therefore, if one assumes that the fin tip temperature to be the same as that of the ambient fluid, inaccurate results will be obtained for all other parameters, for example, the heat flow or the flow patterns. Hence it is inappropriate to approximate the conjugate fin problem with any existing similarity solution, except for the most carefully chosen conditions where it is known that the fin tip temperature is close to the ambient temperature.

Flow separation occurs only when the value of Pe/Ra is small and negative. This range of values is found to lie between 0.0 and -0.98 when the CCP is 0.0359. Solutions to the problem can be found for a value of Pe/Ra with an absolute value greater than 0.98, as for these flow rates the forced flow dominates the natural convection flow, and so not allowing flow reversal to take place.

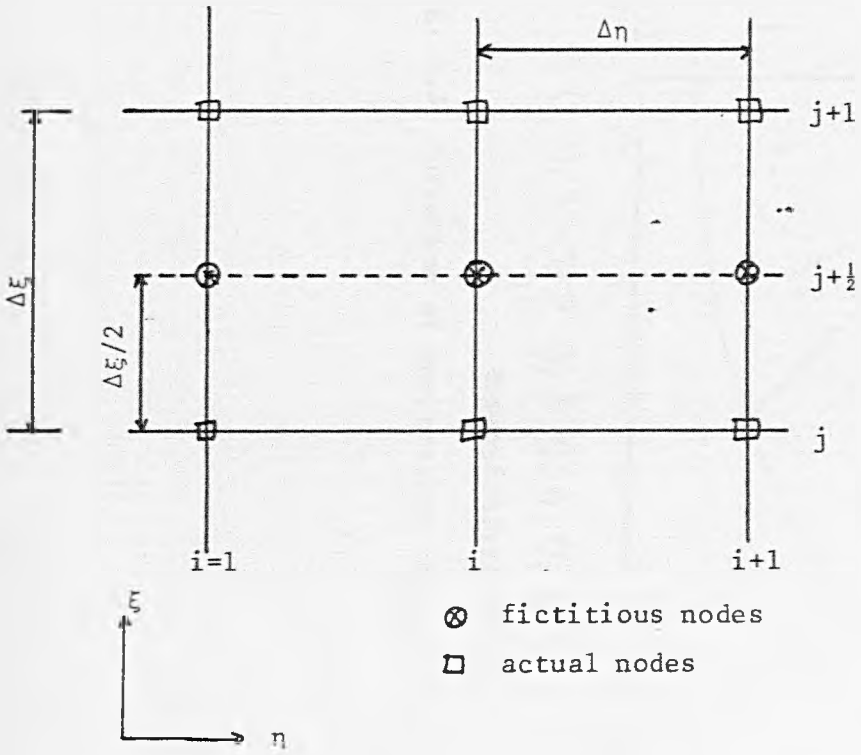

Fig. 6.1 Position of fictitious nodes in the boundary layer

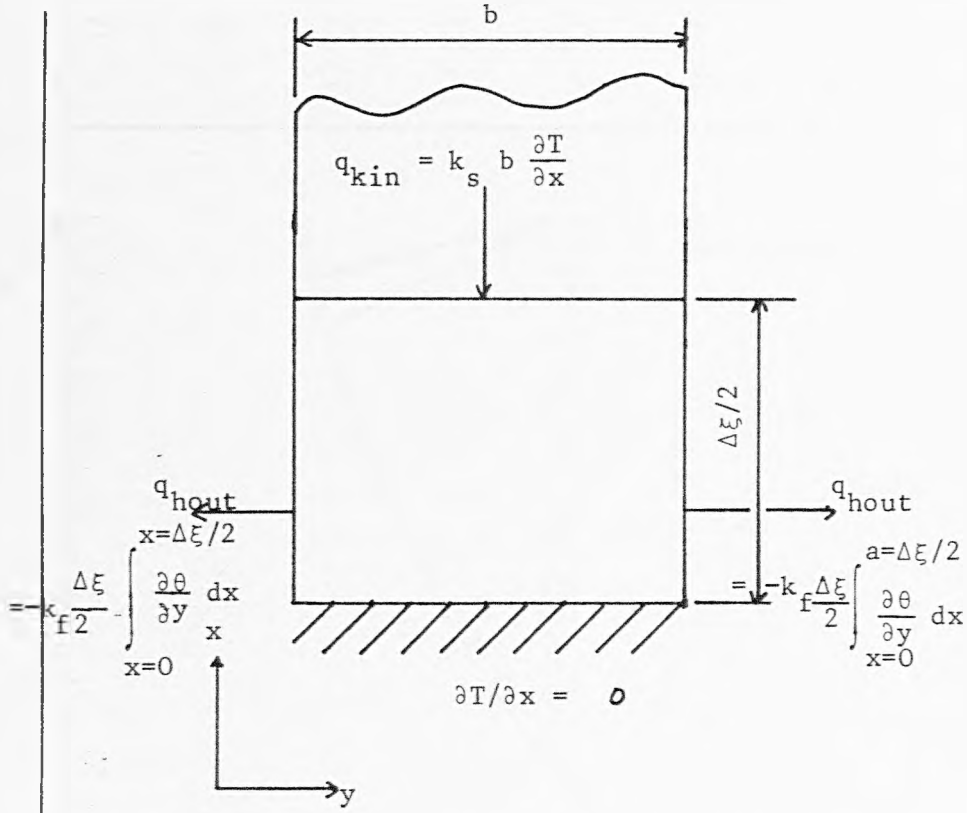

Fig. 6.2 Heat balance between fin tip and second node

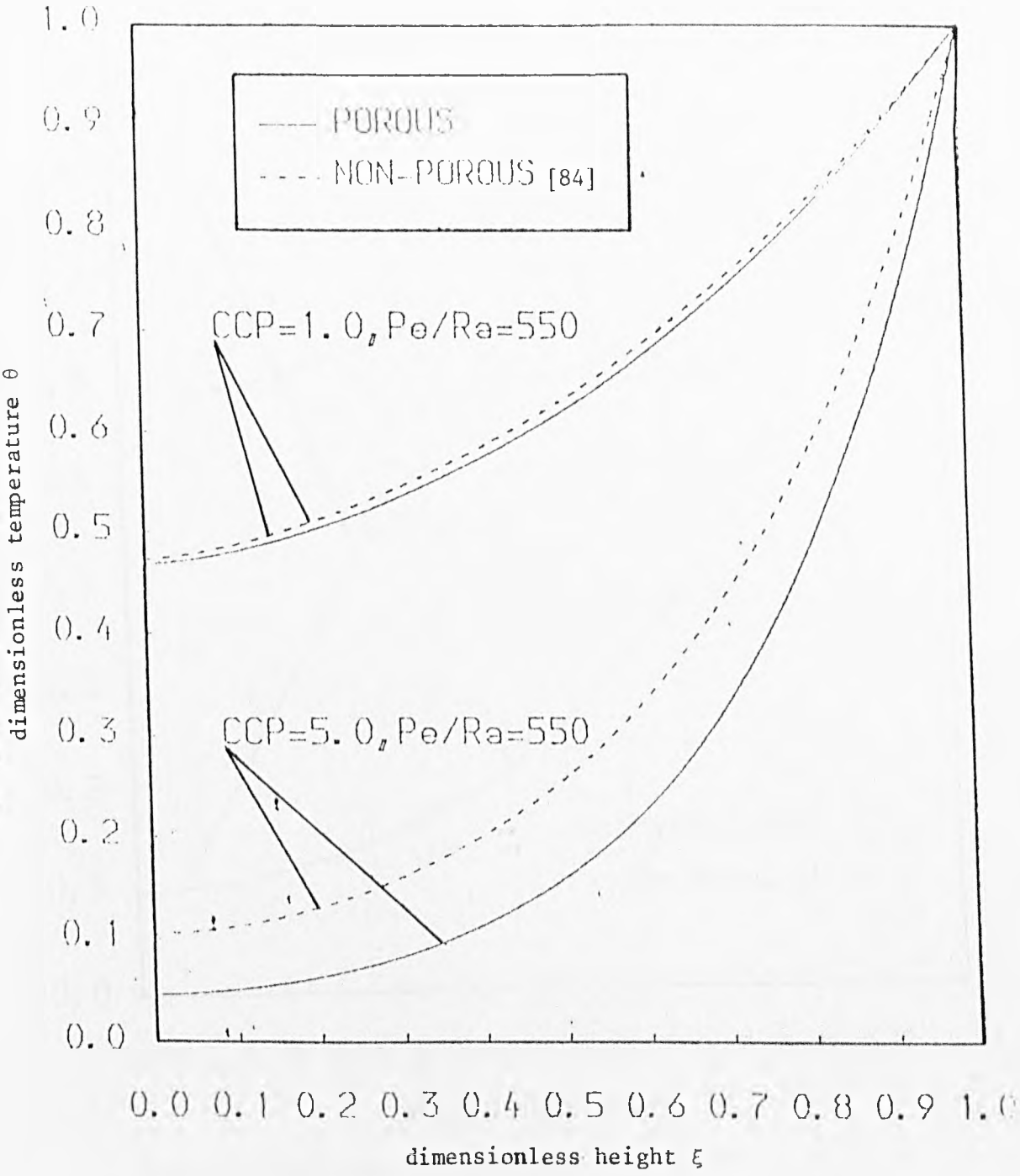

Fig. 6.3 Variation of temperature along fin

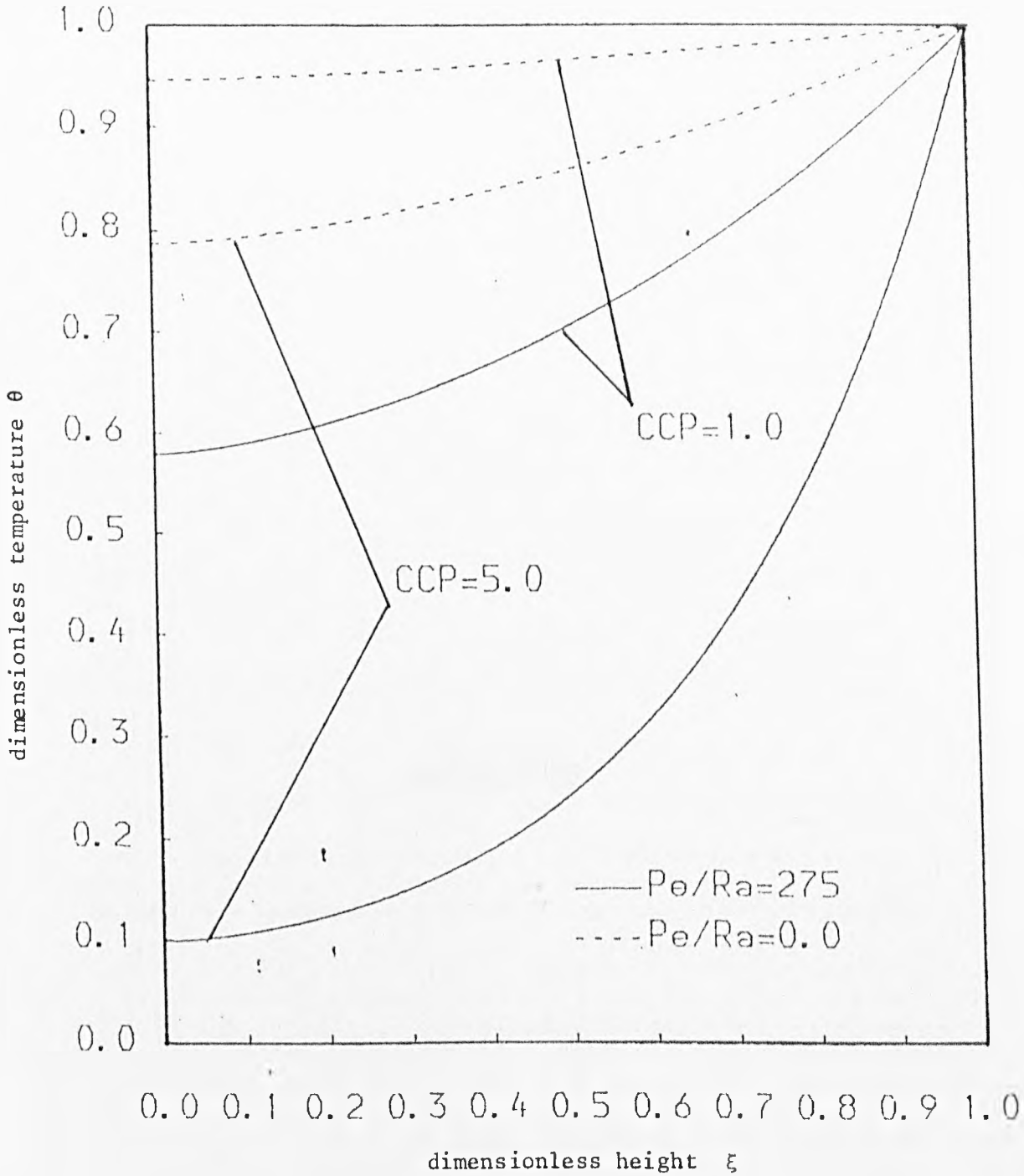

Fig. 6.4 Variation of temperature along fin

CHAPTER SEVEN

7. Natural Convection From a Plane Wall with 2-D Conduction

7.1 Introduction

So far the conduction in all the solid surfaces investigated has been assumed to be one-dimensional. This will be true if the aspect ratio of the solid is such that the object is long and thin, or if the thermal conductivity of the solid is very high. However, for aspect ratios close to unity, or if the solid is an insulating material, the one-dimensional assumption will not always be valid. It is the purpose of this section of work to determine the types of wall (geometry and material) for which it is necessary to use a two-dimensional heat conduction equation in the solid. Further, having found when a two-dimensional analysis is necessary, the effect of using such an analysis, as opposed to a one-dimensional model as used in chapter three, is investigated. This can be done by evaluating the heat flow through a material using either a one or two-dimensional model. This will then directly tell us the error introduced when simplifying from two to one-dimensional heat flow. The assessment of whether the additional complication introduced into the calculations is necessary can only be decided for an individual case and not generally.

As discussed in the introduction to chapter three, work has been carried out for the interaction between fluid flows only very recently. The first work was done by Lock and Ko [68] in 1973, when they looked at the heat transfer between two natural convection systems through a flat wall with a finite thickness. The effect of axial conduction in a solid with a prescribed heat flux or temperature profile on one side was investigated by Miyamoto and his

co-workers [66]. Later Anderson and Bejan [69] and Viskanta and Lankford [33] studied the same system as Lock and Ko but in greater detail. Anderson and Bejan [87] studied a similar problem later, except that a geothermal system was considered such that an open space and a porous medium were separated by a wall.

The conjugate nature of heat transfer between two forced convection flows was studied by Mori [90]. In this work a counter flow heat exchanger operating under laminar flow conditions was investigated. Sparrow and Faghri [91] looked at the forced convection inside a tube as it heated a fluid outside the tube by natural convection. In this latter case, the heat flow through the wall itself was not included in the model. As pointed out by Mori [92] the wall conduction will play an important role in the heat transfer process because of the poor heat transfer properties of natural convection flow. To study the conjugate nature, Mori and his co-workers extended their work on the plate heat exchanger [90] to look at a forced convection flow heating a plane wall which heats an external fluid by natural convection [92]. From this work they found that introducing two-dimensional heat flow in the intervening wall relaxes the thermal interaction between the two convective flows. Although their work covers similar ground to the proposed investigation, it is still felt that this area of research is worth further study. This is because several features of the work by Mori in [92] pose other problems, which will be addressed as the current solution procedure is given, as well as in the results found and the conclusions drawn from this work.

7.2 Statement of the Problem

The system to be investigated consists of a hot fluid with a constant temperature and a known heat transfer coefficient, as might occur when condensing steam is used as a heating medium. This heats a

plane wall of finite thickness which is thermally insulated at the top and bottom of the region of interest. The wall in turn, heats a fluid, such that heat transfer takes place by natural convection. This is illustrated in figure 7.1. Heat flow in the wall is assumed to be two-dimensional. The boundary layer flow in the cold fluid is calculated using an integral analysis, which has been used in chapter four, where it was shown to provide accurate results when compared with analytical solutions.

The problem is approached such that the Laplace equation for heat conduction is used in the wall subject to the boundary conditions given by the fluid flow on one side, and the constant heat transfer coefficient on the other. As the wall is insulated at the top and bottom then adiabatic conditions are used for the final two boundary conditions on the surface of the wall. Thus the governing equation for the wall is simply given by:

$$\frac{\partial^2 T_w}{\partial x^2} + \frac{\partial^2 T_w}{\partial y^2} = 0 \qquad (7.1)$$

The boundary conditions represent the way in which the heat flows into and out of the wall surfaces. The first two state that the ends of the wall are adiabatic (equations 7.2 and 7.3). Equation 7.4 equates the heat flow in the wall next to the heat source to the heat flow from the heat source itself. The final boundary condition (equation 7.5) states that there is continuity in the heat flow from the wall into the cold fluid.

$$x = H,\ 0 < y < WT$$

$$\frac{\partial T_w}{\partial x} = 0 \qquad (7.2)$$

$$x = 0,\ 0 < y < WT$$

$$\frac{\partial T_w}{\partial x} = 0 \tag{7.3}$$

$$0 < x < H,\ y = 0$$

$$h(T_1 - T_{w|y=0}) = -k_w \frac{\partial T_w}{\partial y} |_{y=0} \tag{7.4}$$

$$0 < x < H,\ y = WT$$

$$- k_w \frac{\partial T_w}{\partial y} |_{y=WT} = -k_1 \frac{\partial T_1}{\partial y} |_{y=WT} \tag{7.5}$$

The boundary conditions 7.2 to 7.4 can be introduced into the Laplace equation if an approximation to T_w is given. However, in equation 7.5 the temperature gradient in the fluid also needs to be known before the final boundary condition can be calculated. Therefore, this boundary condition will be investigated first.

There are several methods of determining the fluid flow when natural convection heat transfer is studied. Some problems can be solved analytically if a given heat flux or temperature profile is given along the hot surface (see for example [75], [28], or [63]). Unfortunately neither of the above two conditions hold in this case, as will be true in most practical situations. Therefore, a numerical method must be used. In [92] the natural convection flow was modelled using the fluid flow equations with the Boussinesq approximation. Also, a method was developed earlier, in chapter four, which found the temperature profile for a fluid under similar conditions to that used here. As this method is readily available, and directly applicable to the current problem, the fluid flow about

the heated wall will be calculated in a similar manner to that already discussed in chapter four.

A brief description is given below of the fluid flow calculations for ease of reference, but the reader is directed to chapter four for the complete analysis. The solution procedure uses an approach similar to the integral analysis first proposed by Squire [21]. By considering an element of thickness Δx across the boundary layer the momentum and heat balances can be written as:

momentum balance:

$$\frac{d}{dx}\int_0^{\delta} \rho u^2 dy = -\,{}_o\left(\frac{du}{dy}\right)_0 + g(\delta\rho_\infty - \int_0^{\delta} \rho dy) \tag{7.6}$$

heat balance:

$$k_{lo}\left(\frac{dT_f}{dy}\right)_0 = \frac{d}{dx}\int_0^{\delta} \rho Cpu\,(T_\infty - T_1)dy \tag{7.7}$$

To solve the momentum and heat balance, the temperature and velocity profiles across the boundary layer need to be known. For this a quadratic polynomial is assumed for the temperature profile while a cubic expression is used for the velocity profile:

$$T_1 = a_1 + b_1\bar{y} + c_1\bar{y}^2 \tag{7.8}$$

$$u = a_2 + b_2\bar{y} + c_2\bar{y}^2 + d_2\bar{y}^3 \tag{7.9}$$

Equations (7.8) and (7.9) are then solved by using the boundary conditions given in (7.10) and (7.11). The boundary conditions for the temperature profile state that the temperature of the fluid is the same as the temperature of the wall at the interface. At the edge of the boundary layer the temperature of the fluid falls to that of the ambient fluid, and the temperature gradient is zero:

$$\bar{y} = 0, \quad 0 < x < H$$

$$T_1 = T_w$$

$$\bar{y} = \delta, \quad 0 < x < H \tag{7.10}$$

$$T_1 = T_\infty$$

$$\frac{\partial T_1}{\partial y} = 0$$

There are only three boundary conditions for the velocity profile and these show that the wall is impermeable and that the velocity and velocity gradient fall to zero at the edge of the boundary layer:

$$\bar{y} = 0, \quad 0 < x < H$$

$$u = 0$$

$$\bar{y} = \delta, \quad 0 < x < H \tag{7.11}$$

$$u = 0$$

$$\frac{du}{d\bar{y}} = 0$$

Substituting the boundary conditions given by equation (7.10) into the expression for the temperature profile (7.8), and the boundary conditions for the velocity (7.11) into the velocity profile expression (7.9) the resultant equations are obtained:

temperature profile

$$\frac{T_1 - T_\infty}{T_w - T_\infty} = \left(1 - \frac{\bar{y}}{\delta}\right)^2 \tag{7.12}$$

velocity profile

$$u = \Gamma \frac{\bar{y}}{\delta}\left(1 - \frac{\bar{y}}{\delta}\right)^2 \tag{7.13}$$

The term Γ appears in the velocity profile (7.13) because only three boundary conditions are known for the four constants given in the cubic expression 7.9. However, when the final solution is obtained the term Γ is part of the solution, so that this can then be substituted back into the above equation and hence the actual velocities found.

Substituting the temperature and velocity profiles into the heat and momentum equations (7.11 and 7,13 into 7.6 and 7.7) and carrying out the integrations necessary, the following ordinary differential equations are found:

momentum balance:

$$\frac{1}{105}\frac{d}{dx}(\Gamma^2\delta) = \frac{g\beta(T_f - T_\infty)}{3} - \nu_o \frac{\Gamma}{\delta} \tag{7.14}$$

heat balance:

$$\frac{1}{30}\frac{d}{dx}(\Gamma\delta\theta_w) = \frac{2\alpha\theta_w}{\delta} \tag{7.15}$$

where $\theta_w = (T_w - T_\infty)$

Equations (7.14) and (7.15) can be solved in a number of ways, as was discussed in chapter four. The method used then assumed values for the boundary layer thickness and velocity term such that:

$$\delta = Ax^\alpha \tag{7.16}$$

$$\Gamma = Bx^\beta \tag{7.17}$$

which are then substituted into equations (7.14) and (7.15). Coefficients and powers of x are then equated to find the values of A, B, α and β. If the full boundary layer problem were to be solved excessive computer time would be required. It has already been shown in chapter four that the approximations as given in equations (7.16) and (7.17) provide an accurate solution, and the fact that explicit relationships can be found is of great importance. If highly accurate velocity and temperature profiles were needed throughout the entire flow regime then there would be little point in making the above substitutions, but as it is the heat flow which is of interest then the simplification in the calculations far outweighs any loss of accuracy. By carrying out the algebraic manipulations the boundary layer thickness and velocity term are given by:

$$\delta = \left(\frac{105\nu + 120\alpha}{\frac{3}{4} + \frac{35\ g\beta\theta_w}{B} + B\ \frac{d\theta_w}{dx}\ \frac{x}{\theta_w}}\right)^{\frac{1}{2}} x^{\frac{1}{4}} \tag{7.18}$$

$$\Gamma = Bx^{\frac{1}{2}} \tag{7.19}$$

$$\text{where } B = \left(\frac{20\ \alpha\ g\beta\theta_w}{\frac{3}{4}\nu + \frac{5}{7}\alpha + \frac{\nu x}{2\theta_w}\ \frac{d\theta_w}{dx}}\right)^{\frac{1}{2}} \tag{7.20}$$

Using the expression for the temperature profile (7.12), the temperature gradient at the surface of the wall can be calculated:

$$\frac{dT_1}{d\bar{y}}\Big|_{\bar{y}=0} = \frac{-2T_1}{\delta}\Big|_{y=0} \tag{7.21}$$

This expression gives an explicit relationship for the temperature gradient in the fluid in terms of the fluid at the surface of the wall and the boundary layer thickness. The boundary layer thickness is only dependent on the average bulk properties, temperatures and temperature gradients at the wall surface, and the height of the wall. Therefore in calculating boundary layer thicknesses complete solutions do not need to be found throughout the fluid.

Although the boundary conditions given by equations (7.2) to (7.5) appear as if they should specify the problem fully this is not true. The problem arises from the fact that at the leading edge of the wall, the boundary layer thickness is usually taken as zero. If this condition is used in the governing equations then the temperature gradient at the leading edge must become infinite (from equation 7.21). This means that the wall temperature must become equal to the ambient fluid temperature, which seems correct theoretically as the wall and ambient fluid will be in contact. However, in any practical situation this would not be true, except the condition might be approached in some exceptional circumstances. Again, this is a similar problem as that already encountered in chapter four when solving for a downward projecting fin. To determine the leading edge temperature a heat balance is carried out between the wall edge and the first internal node. Two solutions will be found, one for the zero temperature difference, and one for the heat balance boundary condition. The two solutions may then be compared to find the difference in the calculated heat flow, as the temperature profiles will obviously be completely different.

If the zero temperature difference condition is used the evaluation of the temperature at the leading edge is simple. When this point is reached in the solution procedure the wall temperature is automatically set to the ambient temperature without trying

to calculate boundary layer thicknesses. The calculation of the temperature of the remainder of the wall then proceeds using the equations already derived.

If the temperature of the leading edge of the wall is not to be taken as the same as the ambient fluid temperature then a heat balance must be carried out. This is done by considering the heat flow into the section of wall just before the wall/fluid interface and the heat flow from the wall into the fluid, thus:

$$- k_w \left.\frac{\partial T_w}{\partial y}\right|_{y=A} = -k_w \left.\frac{dT_w}{dy}\right|_{y=WT} \qquad (7.22)$$

where y=A is some position just inside the wall equivalent to the first internal nodes. Provided the temperature down the rest of the wall at the fluid interface is known, and the temperature within the wall is known, then the temperature at the leading edge can be calculated. The most accurate way this may be achieved depends on the solution procedure, and will therefore be discussed in detail after a solution procedure has been proposed.

As was noted earlier, if the temperature difference at the leading edge is taken to be zero there is obviously no problem in the determining the temperature at this point. However, this means that a singular point is introduced into the governing Laplace equation (7.1). This suggests that there may be problems in solving the equations near the leading edge. To forestall this, transformations may be introduced such that any nodes near the leading edge will be packed in very closely, whilst further out the grid of points becomes sparse. This is done by introducing the variables ξ and η, such that:

$$\xi = x^{c1} \qquad (7.23)$$

$$\eta = y^{c2} \qquad (7.24)$$

It is not known beforehand what values of c1 and c2 are the best for any problem, so the general relationship for equation (7.1) is given below.

$$c1^2 \; \xi^{(2-2/c1)} \; \frac{\partial^2 T_w}{\partial \xi^2} + (c1^2 - c1) \; \xi^{1-2/c1} \; \frac{\partial T_w}{\partial \xi}$$

$$+ c2^2 \; \eta^{(2-2/c2)} \; \frac{\partial^2 T_w}{\partial \eta^2} + (c2^2 - c2) \; \eta^{(1-2/c2)} \; \frac{\partial T_w}{\partial \eta} = 0 \qquad (7.25)$$

To use equation (7.25) such that the area about the leading edge is indeed magnified care must be taken as to the placement of the origin. To do this without producing negative ordinates (e.g. if the origin were simply transposed to the leading edge then the point y=0 given in figure 7.1 would become y=-WT) then the ordinates must be reflected. On figure 7.1 the new ordinate system is given by $\bar{x}$ and $\bar{y}$. Using these new co-ordinates the boundary condition for equation (7.25) are:

$$\bar{x} = H, \; 0 < \bar{y} < WT \quad (\xi = H^{c1}, \; 0 < \eta < WT^{c2})$$

$$c1 \; \xi^{1-1/c1} \; \frac{dT_w}{d\xi} \; H^{c1}, \eta) = 0 \qquad (7.26)$$

$$\bar{x} = 0, \; 0 < \bar{y} < WT \quad (\xi = 0, \; 0 < \eta < WT^{c2})$$

$$c1 \; \xi^{1-1/c1} \; \frac{dT_w}{d\xi} \; (0,\eta) = 0 \qquad (7.27)$$

$$\bar{y} = WT,\ 0 < \bar{x} < H\ (\eta = WT^{c2},\ 0 < \xi < H^{c1})$$

$$-(c2\eta^{(1-1/c2)})\ k_w \frac{dT_w}{d\eta}(\xi, WT^{x2}) = h(T_1 - T_w/\xi, WT^{c2}) \qquad (7.28)$$

$$\bar{y} = 0,\ 0 < \bar{x} < H\ (\eta = 0,\ 0 < \xi < H^{c1})$$

$$-(c_2\eta^{(1-1/c2)})\ k_w \frac{dT_w}{d\eta}(\xi,0) = -k_1 \frac{dT_1}{d}(\xi,0) \qquad (7.29)$$

Looking at equation (7.29) it can be seen that this equation cannot be used, as when $\eta = 0$ then the temperature gradient also must equal zero. This means that there is no heat loss from the wall into the ambient fluid. Also the boundary conditions at x=0 and x=H cause problems with the solution procedure to be used. A central difference finite difference technique will be employed to solve equation (7.1) or (7.25). This being the case, the boundary conditions at the top and bottom of the wall need to take into account the change in grid size that will occur when using the transformed ordinates. This can be best shown by looking at figure 7.2. This figure shows the nodal points about the top of the wall in the normal cartesian co-ordinates and the transformed co-ordinates. The analogous boundary conditions for the top of the wall are equations (7.2) and (7.26). Using a central difference representation for both equations yields:

$$T_w(i-1,j) = T_w(i+1,j) \qquad (7.30)$$

However, from figure (7.2) it can be seen that this cannot be true for the transformed co-ordinates. This results from the fact that the term $c_1\xi^{1-(1/c1)}$ is dropped from equation (7.26) and (7.27) which is the term accounting for the change in grid. For this reason the governing equation (7.25) is not solved throughout the entire solution domain, but is altered depending on whether a point at the edge of the wall is being calculated or not. At the top and bottom of

the wall the equation to be solved is:

$$\frac{\partial^2 T_w}{\partial x^2} + c_2^2 \eta^{2-2/c2} \frac{\partial^2 T_w}{\partial \eta^2} + c2(c2-1) \eta^{1-2/c2} \frac{\partial T_w}{\partial \eta} = 0 \tag{7.31}$$

whilst on the left and right of the wall the governing equation is:

$$c_1^2 \xi^{2-2/c1} \frac{\partial^2 T_w}{\partial \xi^2} + c1(c1-1)\xi^{2-2/c1} \frac{\partial T_w}{\partial \xi} + \frac{\partial^2 T_w}{\partial y^2} = 0 \tag{7.32}$$

At the corners of the wall the governing equation is the standard Laplace equation in cartesian co-ordinates (7.1). All internal points are calculated using the fully transformed equation (7.25). As the boundaries use the cartesian coordinates the boundary conditions to be used must also be in cartesian coordinates (ie. equations (7.2) to (7.5)).

7.3 Solution Procedure

The governing equations (7.1) or (7.25, 7.31 and 7.32) are expressed using central differences. First, the Laplace equation given in cartesian co-ordinates (7.1) is investigated fully and results derived in the solution of this are used to solve the transformed problem (7.25, 7.31 and 7.32). First a temperature difference is defined as:

$$\theta = T - T_\infty \tag{7.33}$$

This is substituted into equation (7.1) and the central difference representation is then used to represent the differential equation:

$$\frac{\theta_w(i+1,j)-2\theta_w(i,j)+\theta_w(i-1,j)}{\Delta x^2} + \frac{\theta_w(i,j+1)-2\theta_w(i,j)+\theta_w(i,j-1)}{\Delta y^2} = 0 \tag{7.34}$$

Although the direction of numbering the nodes on the grid placed over the solution domain does not matter in deriving the above equation (as it is symmetrical about the node at point (i,j)), it will be important when writing down the boundary conditions. The "reversed" numbering system is only necessary for the transformed equations, but will be used here for continuity.

From equation (7.34) it can be seen that at the boundaries (where i or j are equal to 1 or M or N, the latter two representing the total number of nodes in either the X or Y directions respectively), then a point will be introduced that lies outside the solution domain. These nodes are replaced by introducing the boundary conditions. Therefore, the boundary conditions (7.2) to (7.5) also need to be expressed in finite difference form. Again using central differences (to maintain a second order accurate solution) the equations are given by:

$$\underline{x = H,\ 0 < y < WT}$$

$$\frac{\theta_w(N+1,j)-\theta_w(N-1,j)}{2\Delta x} = 0 \tag{7.35}$$

$$\underline{x = 0,\ 0 < y < WT}$$

$$\frac{\theta_w(2,j)-\theta_w(0,j)}{2\Delta x} = 0 \tag{7.36}$$

$0 < x < H,\ y = 0$

$$h(\theta_l - \theta_w(i,1)) = -k_w \frac{\theta_w(i,2) - \theta_w(i,0)}{2\Delta y} \tag{7.37}$$

$0 < x < H,\ y = WT$

$$-k_w \frac{\theta_w(i,M+1) - \theta_w(i,M-1)}{2\Delta y} = -2\, k_l \frac{\theta_w}{\delta}(i,M) \tag{7.38}$$

Equations (7.35) to (7.38) are then rearranged to give explicit relationships for the nodes that fall outside the wall. At the corners of the wall two imaginary points will need to be found. Therefore, a total of nine separate equations will be needed, four at the corners, four along the edges of the wall, and one for the interior region of the wall. Once the terms have been collected together the nine resultant equations are:

For the interior region of the wall:

$$\theta_w(i+1,j)\left(\frac{1}{\Delta x^2}\right) + \theta_w(i,j)\left(\frac{-2}{\Delta x^2} - \frac{2}{\Delta y^2}\right) + \theta_w(i-1,j)\left(\frac{1}{\Delta x^2}\right)$$

$$+ \theta_w(i,j+1)\left(\frac{1}{\Delta y^2}\right) + \theta_w(i,j-1)\left(\frac{1}{\Delta y^2}\right) = 0 \tag{7.39}$$

Along the hot side of the wall (y=0):

$$\theta_w(i+1,1)\frac{1}{\Delta x^2} + \theta_w(i,1)\left(-\frac{2}{\Delta x^2} - \frac{2}{\Delta y^2} - \frac{2h}{\Delta y k_w}\right) + \theta_w(i-1,1)\frac{1}{\Delta x^2}$$

$$+ \theta_w(i,2)\frac{2}{\Delta y^2} + \frac{2h\theta_1}{\Delta y k_w} = 0 \tag{7.40}$$

Along the cold side of the wall (y=WT):

$$\theta_w(i+1,M)\ \frac{1}{\Delta x^2} + \theta_w(i,M)\ \left(-\frac{2}{\Delta x^2} - \frac{2}{\Delta y^2} - \frac{4k_1}{\Delta y k_w \delta}\right) + \theta_w(i-1,M)\ \frac{1}{\Delta x^2}$$

$$+ \theta_w(i,M-1)\ \frac{2}{\Delta y^2} = 0 \qquad (7.41)$$

Along the bottom of the wall (x=0):

$$\theta_w(2,j)\ \frac{2}{\Delta x^2} + \theta_w(1,j)\ \left(-\frac{2}{\Delta x^2} - \frac{2}{\Delta y^2}\right) + \theta_w(1,j+1)\ \frac{1}{\Delta y^2}$$

$$+ \theta_w(1,j-1)\ \frac{1}{\Delta y^2} = 0 \qquad (7.42)$$

Along the top of the wall (x=H):

$$\theta_w(N,j)\ \left(-\frac{2}{\Delta x^2} - \frac{2}{\Delta y^2}\right) + \theta_w(N-1,j)\ \frac{2}{\Delta x^2} + \theta_w(N,j+1)\ \frac{1}{\Delta y^2}$$

$$+ \theta_w(N,j-1)\ \frac{1}{\Delta y^2} = 0 \qquad (7.43)$$

Looking at the corners of the wall:

(y=0, x=0)

$$\theta_w(2,1)\ \frac{2}{\Delta x^2} + \theta_w(1,1)\ \left(-\frac{2}{\Delta x^2} - \frac{2}{\Delta y^2} - \frac{2h}{\Delta y k_w}\right) + \theta_w(1,2)\ \frac{2}{\Delta y^2}$$

$$+ \frac{2h}{\Delta y k_w}\ \frac{1}{} = 0 \qquad (7.44)$$

(y=0, x= H):

$$\theta_w(N,1)\ \left(-\frac{2}{\Delta x^2} - \frac{2}{\Delta y^2} - \frac{2h}{\Delta y k_w}\right) + \theta_w(N-1,1)\ \frac{2}{\Delta x^2} + \theta_w(N,2)\ \frac{2}{\Delta y} + \frac{2h}{\Delta y k_w}$$

$$= 0 \qquad (7.45)$$

y=WT, x=0

$$\theta_w(2,M)\ \frac{2}{\Delta x^2} + \theta_w(1,M)\ \left(-\frac{2}{\Delta x^2} - \frac{2}{\Delta y^2} - \frac{4k_1}{\Delta y k_w}\right) + \theta_w(1,M-1)\ \frac{2}{\Delta y^2} = 0 \qquad (7.46)$$

y=WT, x= H:

$$\theta_w(N,M)\ \left(-\frac{2}{\Delta x^2} - \frac{2}{\Delta y^2} - \frac{4k_1}{\Delta y k_w}\right) + \theta_w(N-1,M)\ \frac{2}{\Delta x^2} + \theta_w(N,M-1)\ \frac{2}{\Delta y^2} = 0 \qquad (7.47)$$

If the equations (7.39) to (7.47) are expressed in the form of a matrix then the resultant matrix will be diagonally dominant or contain elements such that the major diagonal is equal to the sum of the off diagonals. This indicates that successive iterations in the solution procedure will converge. The matrix formed is given by matrix 7.1.

The terms A, B and C which are used in matrix 7.1 are found by applying the appropriate equation from (7.39) to (7.47).

The main equation to be solved is the Laplace equation (7.1) which is a standard elliptic equation and can be solved in a number of ways. These can be split into two groups:

(a) direct methods;

(b) systematic iterative methods (i.e. indirect)

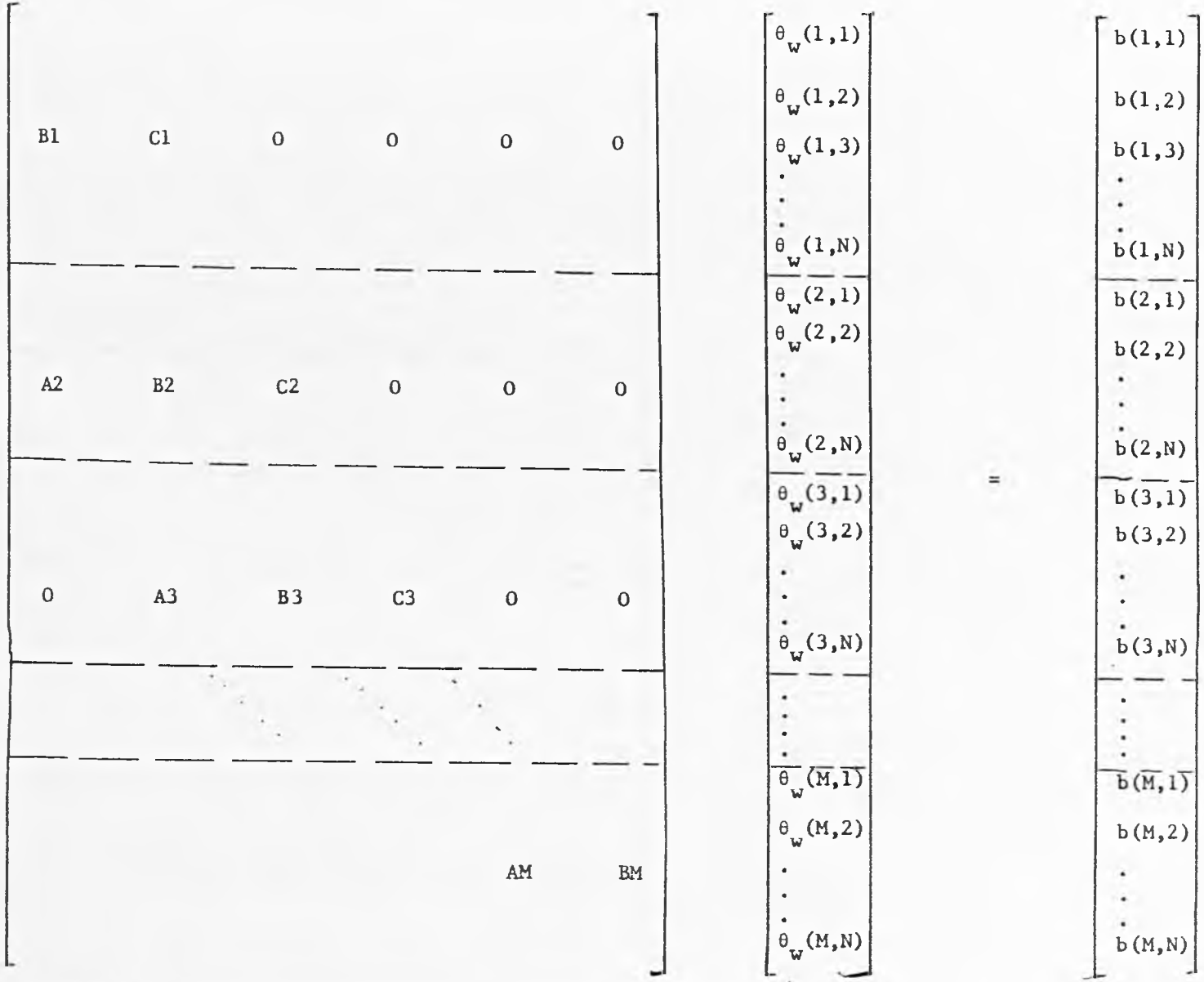

Matrix 7.1 Matrix representation of equations (7.39) to (7.47)

In general direct methods tend to be more efficient than iterative ones when:

(a) the matrix of coefficients is too complex for a rapid estimate of the optimum over-relaxation factor;

(b) the matrix is almost singular, so that small residuals do not imply small errors in the solution;

(c) there are several sets of equations with the same coefficients but different constants have to be solved, as in the deferred correction method.

An iterative procedure will be more efficient in this case as use is made of the sparse nature of a matrix when iterative procedures are employed.

Of the iterative methods available the Jacobi method is not used in practice. This is because the rate at which successive iterations converge to the exact solution of the equations is slower than for other methods. The Gauss-Seidel (or extrapolated Leibmann) method uses the latest iterative value as soon as it is available and scans the mesh points systematically from one direction to the other along successive rows. In the extrapolated Liebmann method the difference between the new calculated and the old value is multiplied by a relaxation factor (which is greater than unity) and then this quantity is added to the old value to give a new updated point. The Gauss-Seidel method is identical to the extrapolated Liebmann method if the relaxation factor were set to one. In well behaved problems (i.e. the solution procedure is stable, and accurate estimates are not necessary to produce a converging solution) the extrapolated Liebmann method will give a final solution more rapidly than the Gauss-Seidel method. Therefore, the extrapolated Liebmann method

will be used here. However, to use this method the equations (7.39) to (7.47) need to be re-arranged to provide an expression for the remainder of a point value (i.e. the difference between the n^{th} iteration and the $n+1^{th}$ iteration if no relaxation were used). The relationships to be used are given below with each equation corresponding to equation (7.39) to (7.47) respectively:

$$\theta_w(i,j)^{n+1} = \theta_w(i,j)^n + \frac{1}{\frac{2}{\Delta x^2} + \frac{2}{\Delta y^2}} \left(\frac{\theta_w(i+1,j)}{\Delta x^2} + \frac{\theta_w(i-1,j)}{\Delta x^2} + \frac{\theta_w(i,j+1)}{\Delta y^2}\right.$$

$$\left. = \frac{\theta_w(i,j-1)}{\Delta y^2} - \left(\frac{2}{\Delta x^2} + \frac{2}{\Delta y^2}\right) \theta_w(i,j)\right) \qquad (7.48)$$

$$\theta_w(i,1)^{n+1} = \theta_w(i,1)^n + \frac{1}{\frac{2}{\Delta x^2} + \frac{2}{\Delta y^2} + \frac{2h}{\Delta y k_w}} \left(\frac{\theta_w(i+1,1)}{\Delta x^2} + \frac{\theta_w(i-1,1)}{\Delta x^2}\right.$$

$$\left. + \frac{2\theta_w(i,2)}{\Delta x^2} + \frac{2h\theta_l}{\Delta y k_w} - \left(\frac{2}{\Delta x^2} + \frac{2}{\Delta y^2} + \frac{2h}{\Delta y k_w}\right) \theta_w(i,1)\right) \qquad (7.49)$$

$$\theta_w(i,M)^{n+1} = \theta_w(i,M)^n + \frac{1}{\frac{2}{\Delta x^2} + \frac{2}{\Delta y^2} + \frac{4k_f}{\Delta y k_w \delta}} \left(\frac{\theta_w(i+1,M)}{\Delta x^2} + \frac{\theta_w(i-1,M)}{\Delta x^2}\right.$$

$$\left. + \frac{2\theta_w(i,M-1)}{\Delta y^2} - \left(\frac{2}{\Delta x^2} + \frac{2}{\Delta y^2} + \frac{4k_f}{\Delta y k_w \delta}\right) \theta_w(i,M)\right) \qquad (7.50)$$

$$\theta_w(1,j)^{n+1} = \theta_w(1,j)^n + \frac{1}{\frac{2}{\Delta x^2} + \frac{2}{\Delta y^2}} \left(\frac{2\theta_w(2,j)}{\Delta x^2} + \frac{\theta_w(1,j+1)}{\Delta y^2}\right.$$

$$\left. + \frac{\theta_w(1,j-1)}{\Delta y^2} - \left(\frac{2}{\Delta x^2} + \frac{2}{\Delta y^2}\right) \theta_w(1,j)\right) \qquad (7.51)$$

$$\theta_w(N,j)^{n+1} = \theta_w(N,j)^n + \frac{1}{\frac{2}{\Delta x^2} + \frac{2}{\Delta y^2}} \left(\frac{2\theta_w(N-1,j)}{\Delta x^2} + \frac{\theta_w(N,j+1)}{\Delta y^2} \right.$$

$$\left. + \frac{\theta_w(N,j-1)}{\Delta y^2} - \left(\frac{2}{\Delta x^2} + \frac{2}{\Delta y^2}\right) \theta_w N,j) \right) \qquad (7.52)$$

$$\theta_w(1,1)^{n+1} = \theta_w(1,1)^n + \frac{1}{\frac{2}{\Delta x^2} + \frac{2}{\Delta y^2} + \frac{2h}{\Delta y k_w}} \left(\frac{2\theta_w(2,1)}{\Delta x^2} + \frac{2\theta_w(1,2)}{\Delta y^2} \right.$$

$$\left. + \frac{2h\theta_1}{\Delta y k_w} - \left(\frac{2}{\Delta x^2} + \frac{2}{\Delta y^2} + \frac{2h}{\Delta y k_w}\right) \theta_w(1,1) \right) \qquad (7.53)$$

$$\theta_w(N,1)^{n+1} = \theta_w(N,1)^n + \frac{1}{\frac{2}{\Delta x^2} + \frac{2}{\Delta y^2} + \frac{2h}{\Delta y k_w}} \left(\frac{2\theta_w(N-1,1)}{\Delta x^2} + \frac{2\theta_w(N,2)}{\Delta y^2} \right.$$

$$\left. + \frac{2h\theta_1}{\Delta y k_w} - \left(\frac{2}{\Delta x^2} + \frac{2}{\Delta y^2} + \frac{2h}{\Delta y k_w}\right) \theta_w(N,1) \right) \qquad (7.54)$$

$$\theta_w(1,M)^{n+1} = \theta_w(1,M)^n + \frac{1}{\frac{2}{\Delta x^2} + \frac{2}{\Delta y^2} + \frac{4k_1}{\Delta y k_w \sigma}} \left(\frac{2\theta_w(2,M)}{\Delta x^2} + \frac{2\theta_w(1,M-1)}{\Delta y^2} \right.$$

$$\left. - \left(\frac{2}{\Delta x^2} + \frac{2}{\Delta y^2} + \frac{4k_1}{\Delta y k_w \delta}\right) \theta_w(1,M) \right) \qquad (7.55)$$

$$\theta_w(N,M)^{n+1} = \theta_w(N,M)^n + \frac{1}{\frac{2}{\Delta x^2} + \frac{2}{\Delta y^2} + \frac{4k_1}{k_w \Delta y \delta}} \left(\frac{2\theta_w(N-1,M)}{\Delta x^2} \right.$$

$$\left. + \frac{2\theta_w(N,M-1)}{\Delta y^2} - \left(\frac{2}{\Delta x^2} + \frac{2}{\Delta y^2} + \frac{4k_1}{k_w \Delta y \delta} \right) \theta_w(N,M) \right) \qquad (7.56)$$

As the extrapolated Liebmann method is being used to speed up the rate of convergence it is necessary to find the optimum relaxation parameter, which is the term used to multiply the second term of the right hand side of the above equations.

It was stated before that a direct method would be more efficient if an optimum value for the over-relaxation parameter could not be found easily. In a paper by Frankel [93] it has been proven that the optimum value for the relaxation parameter is given by the smaller root of the quadratic equation:

$$\alpha^2 t^2 - 4\alpha + 1 = 0 \qquad (7.57)$$

where $t = \cos(\pi/p) + \cos(\pi/q)$ (7.58)

and p and q are the number of nodes in the x and y directions.

Also in the iterative procedure proposed, it is necessary to sweep from one side of the solution domain to the other. The direction of this sweep across the wall may be chosen in any way to achieve the best advantage in speed of solution (there being no other constraints on the numerical procedure). In the current problem the boundary condition on the hot side of the wall is given by a constant heat transfer coefficient and so would be expected to behave well. On the cold side of the wall, the boundary condition involves

the boundary layer thickness, and so changes with the solution of the temperature within the wall. For this reason, it is best to start the calculation on the cold side of the wall and step across the wall to the hot side. This means that the change in the boundary condition on the cold side will be transferred back across the wall in one sweep, rather than stepping back one column at a time.

In equations (7.48) to (7.56) the most recent value for any temperature is used as soon as it is available.

Now that a procedure has been developed for the majority of the wall, the problem concerning the temperature at the leading edge can be addressed. First, considering the case of the non-zero temperature difference, a heat balance must be carried out. This heat balance is made considerably simpler by the fact that no heat loss takes place from the top and bottom of the wall, because of the boundary conditions imposed. This means that any heat flow through an element of the wall must also flow through the cold side of the wall into the fluid. Equation (7.22) states this in terms of the temperature gradient. If all the temperatures are known down the cold side of the wall, except for the temperature at the leading edge, then the heat flow through this area can be found, but with the one unknown temperature. The heat flow through the rest of the wall can be evaluated across any section, as the heat flow should remain constant due to the assumption of adiabatic top and bottom edges. If the heat flow at the hot side of the wall is calculated and then equated to the heat flow out of the cold side, so that the unknown temperature can be determined, a heat balance across the whole system will be enforced. However, if this is done a check on the calculation procedure which uses the heat balance will be a trivial one and no

guarantee of correct programming. For this reason a heat balance is set up between the cold side of the wall and the adjacent section used in the numerical solution procedure, as indicated by equation (7.59) which is the integral of equation (7.22):

$$\int_0^L k_w \frac{\partial \theta_w}{\partial y} \, dx \Big|_{y=WT-\Delta y} = \int_0^L k_w \frac{\partial \theta_w}{\partial y} \, dx \Big|_{y=WT} \tag{7.59}$$

The temperature gradients are represented using a backward difference scheme and the trapezium method used to integrate from the bottom to the top of the wall. This gives the following expression for $\theta_w(1,M)$, which is the temperature at the leading edge.

$$\begin{aligned} \theta_w(1,M) &= \theta_w(1,M-1) + \theta_w(2,M-1) - \theta_w(2,M) \\ &+ \sum_{i=1}^{i=N-1} (\theta_w(i,M-1)-\theta_w(i,n-2)+\theta_w(i+1,M-1)-\theta_w(i+1,M-2)) \\ &- \sum_{i=2}^{i=N-1} (\theta_w(i,M)-\theta_w(i,M-1)+\theta_w(i+1,M)-\theta_w(i+1,M-1)) \end{aligned} \tag{7.60}$$

This new temperature is recalculated in every sweep through the wall and then used in the Laplace equation in the same way as all the other points.

As already mentioned, if the temperature at the leading edge is set equal to the ambient fluid temperature, then a singular point is introduced into the governing equations. Therefore, to move the mesh points either towards or away from the singularity, the transformed equations (7.25) or (7.31) and (7.32), and the standard Laplace

equation (7.1) will be used. The numerical procedure for these equations is exactly analogous to that already described for the solution of the Laplace equation (7.1). However, care must be taken when using the central difference scheme to ensure that the nodes are numbered in the correct way, as, when using the transformed equations, the spacing between nodes is not equal.

Having obtained the temperatures within the wall for a given mesh size, the number of nodes in both dimensions is doubled. The initial guess for the temperature within the wall for this new grid is found by interpolating between points of the previous solution. This procedure is repeated once more so that there are three solutions to the problem, but each of different accuracy. These solutions are then used with Richardson's extrapolation method to find a final solution, which, with well behaved governing equations, will give a solution equivalent to having solved the problem with an infinite number of grid points.

7.4 Results

The main difficulty in solving the Laplace equation (7.1) is knowing which boundary condition to impose at the leading edge. Also it has been found that imposing certain boundary conditions causes problems in the extrapolation procedure with the three grid sizes. Therefore, several steps have been used which introduce new conditions at each stage. The results of each step are compared with those of the previous step, where relevant, and an assessment made as to the reason why any problems arise.

The first problem considered is fairly trivial, but can be used to check the solution procedure itself and the difference between backward or central difference representations of the governing equation.

Step 1 - Fixed temperature on the hot side of the wall at a known value. Set the boundary layer thickness at a constant and finite value for the entire length of the fin. Using this value for the boundary layer thickness calculate the heat flow through the wall at all points on the cold side of the wall, including the leading edge, using the boundary condition as given by equation (7.5).

In this problem both first and second order finite difference representations are used for the boundary conditions. By using backward differencing a fictitious node lying outside the solution domain is not introduced, and so no assumption needs to be made about the temperature profile across the interface. However, the backward difference scheme is only first order accurate compared with the central difference scheme which is second order accurate. In this situation, due to the uniformity of heat flow, there is no difference in the results between the two schemes. Varying grid sizes are used such that the step size in both the x- and y-coordinates are halved. The number of nodes in each direction are 11, 21 and 41 for each new grid. This makes the extrapolation procedure easier. The thermal conductivity is that corresponding to stainless steel, and the fluid is assumed to be air. The temperature within the wall is found to be exactly the same for all three grid sizes, which means that the grid of 11 by 11 nodes is a converged solution. A contour map of the temperature is given in figure 7.4. This shows that the temperature along any section of the wall in the x-direction, i.e. parallel to the y-axis, is constant. This means that there is one-dimensional heat flow, as would be expected as the driving force and the resistance to heat flow is constant across the wall. The solution times for the different grid sizes are in the ratio 1:6:44,

with the shortest time being 13 seconds.

The solution procedure is very well behaved under these rather unreal conditions, so the behaviour of the technique must be tested more fully using slightly more realistic conditions.

Step 2 - Set the leading edge transformed temperature to zero, i.e. the same as the ambient fluid. Keep the remainder of the boundary conditions the same as in step 1.

Again first and second order representations are used for the boundary conditions. For the first order scheme each set of temperatures found using the different mesh sizes appear to give reasonable results. However, when the results are extrapolated the resultant temperatures are meaningless. The problem arises along the bottom of the wall where the temperatures are higher than those calculated at a position one nodal point further into the wall. This could result from either the problem itself being singular at the leading edge or from the extrapolation method itself. The method of deferred approach to the limit, suggested by Richardson, is known to be of dubious value when a specified function is not smooth. Therefore, it is to be expected that when a step change is introduced into a solution, in this case setting the leading edge temperature to zero, extrapolating the results will cause problems. However, by using a central difference representation of the boundary conditions, extrapolated results are found which may be correct. It is found that the final extrapolated results are much greater than those found for the corresponding temperatures in the final mesh near the leading edge. As the distance from the leading edge is increased the extrapolated results lie close to the fine mesh results. From this one can assume that the problem arises from the introduction of the step change.

The contour map for the results found used central differencing are given in figure 7.5, which shows how the temperature contours bend towards the leading edge. This means that the heat flow is two-dimensional. This effect is particularly noticeable closer to the leading edge as might be expected. Whereas in the first step the resistance to heat flow was constant for the entire length of the wall, this is no longer true. By setting the temperature at the leading edge to that of the ambient the boundary layer is effectively being set to zero. This means that at this point there is no resistance to heat flow from the wall into the fluid, and therefore heat will be 'drawn' from the rest of the wall to this corner, and this is shown very graphically by the bending of the temperature contours. It is difficult, though, for one to have great confidence in the results in this step due to the problem of extrapolation. It is worth noting at this point that if only one grid size were used there would be no suspicion of the problems brought to light here. Therefore, any calculation procedure which only uses one mesh size must be viewed with great care to make sure that the results found can genuinely be said to have converged.

From step 2 it can be seen that backward differencing at the boundaries cannot be used for there to be any confidence in the final results. Therefore central differencing will be used throughout the solution domain, including the boundary conditions.

Step 3 - Drop the assumption of a constant temperature on the hot side of the wall. This is replaced by the boundary condition used in the third chapter, that is a constant temperature heat source which has a constant heat transfer coefficient between it and the surface of the wall.

First of all the temperature on the left hand side of the wall, (see figure 7.1), is to be kept high, so that results can be compared with those found from step 2. Therefore, the heat transfer coefficient is taken as 1000 W/m^2K. The results of the extrapolation are very similar to those found in step 2 as would be expected. The contour map of the temperature in the wall is given in figure 7.6. The extrapolation procedure still shows the points near the leading edge as having been extrapolated over a large step. However, the results are consistent in that the temperature change throughout the wall is monotonic.

The conditions on the hot side of the wall are now made more stringent by reducing the heat transfer coefficient of the heat source.

Step 4 - Heat transfer coefficient is set to 10 W/m^2K, while all other boundary conditions remain the same.

By setting the heat transfer coefficient to this small value, the temperature on the hot side of the wall drops from a temperature over ambient of approximately 80^oC to 10^oC. Again, whilst each set of results obtained for different mesh sizes are consistent with the boundary conditions and appear to represent the temperature profile within the wall, the extrapolated results show anomalous behaviour about the leading edge. The contour map is given in figure 7.7, which shows this behaviour very graphically. The surface map is also given, figure 7.8. The leading edge is the point where the temperature excess drops to zero. From the surface map it can be seen that the temperatures about the leading edge shows an effect similar to an overshoot which may be found, for example, in control problems.

The temperature nearest to the leading edge is depressed while the next temperature value is greater than that expected. This then settles down to the expected value with distance away from the perturbation, i.e. the leading edge.

Looking at the results given by step 4, it seems as if the analysis using cartesian co-ordinates and an artificial zero temperature excess at the leading edge has been taken as far as it can. The results so far show the introduction of two-dimensional heat flow by setting a low resistance to heat flow near the leading edge. However, it must be said that these results can only be treated qualitatively, and to have confidence in the results a more sophisticated approach must be made. This can be done in two ways:
Step 5 - Firstly by transforming the co-ordinate system from cartesian co-ordinates to other variables that allow a finer mesh to be used near the leading edge, and
Step 6 - Secondly to find a better way of accounting for the temperature at the leading edge.

Looking first at the effect of transforming the co-ordinate system, an interesting effect is discovered that might not be expected. The equations for the transformed variables have already been developed and are given by equations 7.25, 7.31 and 7.32. These equations are formulated such that the grid size can be changed very easily. The procedure is checked by setting the transformation variables, ξ and η, to unity. The results obtained for these values are identical to those found when the problem was posed using cartesian co-ordinates. The values of c1 and c2 are now changed to 0.5 so that more points are packed in near the leading edge.

The same conditions are used as in step four, that is a low heat transfer coefficient of the hot side of the wall. As the points approach the leading edge the results found from carrying out the extrapolation change significantly from those found using a fine mesh. In fact, the results show an even more pronounced overshoot than was found using the cartesian co-ordinate system. Therefore, it is the setting of the leading edge temperature that is causing difficulties in solving the problem so a alternative method is now proposed to determine the leading edge temperature.

As mentioned in the statement of the problem an alternative, and physically more meaningful, boundary condition for the leading edge can be obtained from a heat balance. In the work by Mori [92] it is stated that the temperature at the leading edge should be the same as the ambient fluid temperature. However, from the results of the calculations carried out here the boundary condition at the leading edge seems to have little influence on the temperature of the rest of the wall. The problem as posed by Mori seems to be overspecified in that the temperature profile of the wall is given by:

$$\theta_{s2}(\bar{x}) = \zeta_o + \sum_{i=1}^{\infty} \zeta_i \bar{x}_i \qquad (7.61)$$

where $\theta_{s2}(\bar{x})$ is the temperature on the cold side of the wall. A cubic expression is used to approximate $\theta_{s2}(\bar{x})$ so in equation (7.61) terms up to i=3 are used. Calculations are performed until the error in the heat flow is minimised. However, even using this procedure errors are introduced which can be as high as 13%. Also, the authors, [92], note that under certain conditions results are obtained but

were "unreasonable from the viewpoint of physical meaning". Thus, it appears as if the introduction of a singularity in the solution domain presents insurmountable problems when using either the current analysis or that proposed in [92].

By using a heat balance to define the leading edge temperature and allowing the temperature to be greater than the ambient, the singular point is removed. This is similar to the procedure used when investigating the downward projecting fin.

Step 7 - The first step in this area is to ensure that for a long thin wall the two-dimensional analysis gives a heat flux through the wall equal to that of the one-dimensional analysis (as calculated in chapter three).

A high thermal conductivity of 100 W/mK is assumed for the wall which is 1m high and 1cm thick. The heat transfer coefficient on the hot side of the wall is set at 10 W/m^2K. The heat flow into and out of the wall is calculated using numerical integration. The effect of changing the number of nodes parallel to the heat flow is found and an extrapolated value calculated. The results for both one- and two-dimensional flow are given in table 7.1.

No. nodes in x-direction	heat flow out (1-d)	heat flow in (2-d)	heat flow out (2-d)
50	206.4	218.1	203.1
100	214.2	218.7	210.9
∞	216.8	218.9	213.5

Table 7.1 Heat Flow in and Out of Long Thin Wall (W/m^2)

The difference between the one- and two-dimensional analyses for the heat flow out of the wall is 1.5%. The discrepancy for the heat flow out and the heat flow into the wall when using the two-dimensional equations is 2.4%. Therefore it can be assumed that the two analyses give the same heat flow, and that this procedure can be used to determine when the added complication of a two-dimensional analysis is required.

The degree of suspected two-dimensional flow is altered by changing the thermal conductivity of the wall. For each new set of data, three sets of grids are used (11*11, 21*21 and 41*41), so that Richardson's extrapolation method can be used to find solutions that would be obtained when using an infinite number of nodes.
Step 8 - The heat transfer coefficient is set to 100 W/m^2K and the thermal conductivity of stainless steel is assumed. The wall section is square with sides of 10 cm.

The contour map is given in figure 7.9 for these conditions. From this it can be seen that the temperature contours only bend significantly near to the leading edge. The heat transferred through the wall for the 2-D flow is 169.3 W/m^2 whilst for the 1-D flow the total heat flow is 171.8 W/m^2. The difference between the heat flows through the wall as calculated by the two different methods only differ by 1.5%. This is not very significant if the heat flows only are considered. However, when looking at the temperatures on the cold side of the wall it can be seen that the distribution of the heat flow is quite different. Table 7.2 gives the temperatures along the wall as calculated by the one- and two-dimensional analyses.

1-D temp.	2-D temp.
51.661	51.053
51.624	51.006
51.534	50.907
51.409	50.758
51.236	50.565
51.033	50.327
50.745	50.044
49.206	49.716
47.409	49.354
44.292	48.899
5.740	45.098

Table 7.2 Comparison Between 1-D and 2-D Temperatures for Step 8 at the Cold Face of the Wall

As is obvious from the above table, the difference comes at the leading edge. The temperature given for the 1-D flow is in fact for a position near to the leading edge, which was used for starting the solution procedure off. It can be seen that introducing the 2-D procedure has had the effect of smoothing out the temperature profile, whilst making only a small difference in the actual heat flowing.

Step 9 - The heat transfer coefficient is dropped to 10 W/m^2K and the thermal conductivity of the slab is assumed to be 0.1 W/mK.

This step is trying to force the temperature profile into producing a significant effect at the leading edge, and thus testing the extent of this smoothing effect highlighted by the previous step. The final temperatures on the cold side of the wall are given in table 7.3.

1-D temp.	2-D temp.
18.870	18.953
18.551	18.681
18.198	18.323
17.805	17.922
17.360	17.465
16.844	16.933
16.229	16.291
15.463	15.477
14.433	14.359
12.904	12.620
0.694	9.785

Table 7.3 Temperature at the Wall Fluid Interface with a Low Thermal Conductivity Wall

The two-dimensional analysis has in fact smoothed the temperature profile out as compared with the one-dimensional analysis. The heat flow through the wall as calculated in the one-dimensional procedure is 629.1 W/m^2 whereas for the two-dimensional method is 628.2 W/m^2.

Step 10 - A slab 1cm by 1cm with a thermal conductivity of 17 W/m K (i.e. stainless steel) is heated by a constant temperature source which gives a heat transfer coefficient of 1000 W/m^2K.

Using these parameters the expected temperature profile within the wall would be isothermal. Again the two temperature profiles along the cold side of the wall can be compared, as in table 7.4.

1-D temp.	2-D temp.
78.750	78.401
78.723	78.399
78.686	78.393
78.642	78.384
78.590	78.372
78.525	78.358
78.442	78.340
78.329	78.320
78.155	78.298
77.817	78.271
44.231	78.064

Table 7.4 Temperature Profiles at the Wall Cold Fluid Interface for a Wall with a High Thermal Conductivity

Many more parameters can be used to investigate this interesting effect of temperature smoothing, but the procedure has now been established and no great benefit would arise in studying general conditions.

The boundary layer thickness can be calculated from the above results using the equation (7.18) which gives an explicit relationship for the boundary layer thickness in terms of the height up the wall and the temperature and temperature gradient along the wall at that point. This equation only requires the physical properties of the fluid, the temperature gradient, the actual temperature and the height up the wall to find the boundary layer thickness. Profiles for the boundary layer thickness are given in Figures 7.10 and 7.11. In Figure 7.10 the boundary layer thicknesses corresponding to steps 1, 2 and 3 are shown, whilst Figure 7.11 shows the boundary layer thicknesses for steps 4 and 8. Steps 1 to 3 are grouped together

because they all have the condition of a high heat transfer coefficient on the left hand side of the wall whereas, steps 4 and 8 use a low heat transfer coefficient. However, other conditions are changed between the steps as well and these are detailed in the main section of this chapter. The boundary layer thickness is found as part of the numerical procedure to obtain the temperature profile except that at the leading edge the zero boundary layer thickness is assumed and not used in calculating the temperature at this point. This is done because, from equation 7.21, the term for the thickness of the boundary layer appears in the denominator. Thus any calculations at this point would break down, and hence the need to either assume the temperature (as is done in steps 1 to 3) or to carry out a heat balance in the wall to find the temperature at the leading edge.

In all the cases considered air is being heated and average bulk properties are used in the boundary layer. The height of the wall is 0.1 metres, which falls into the laminar regime for air, and the wall is also 0.1 metres thick.

7.5 Conclusions

Two alternative solution procedures have been presented in this chapter to calculate the two-dimensional heat flow through a plane wall. The first specifies the leading edge temperature as that of the ambient fluid. This introduces a singularity into the problem which, in most cases, leads to erroneous results when an extrapolated profile is required.

The second procedure calculated the leading edge temperature by using a heat balance between the cold face of the wall and a section of the wall taken just inside the wall/fluid interface. This method

yields a more robust procedure which can be used over a wide range of boundary conditions and wall properties.

For the latter method a comparison is made with the results given in chapter three (a "one-dimensional" procedure) for the temperature at the wall/fluid interface. The results vary near the leading edge as the two-dimensional procedure used here allows the heat to flow more evenly across the wall, and thus eliminating the high heat flow found at the leading edge. However, the overall heat flow is found not to vary significantly between the two procedures, the maximum difference being only a few per cent for the parameters chosen. This is due, in part to the fact that the boundary condition on the hot side of the wall provides a very consistent condition.

In the case considered by Mori [92] the boundary condition on the hot side of the wall was given by a fluid flowing over the wall as in the Graetz problem. This gives rise to temperature profiles within the wall which do show a more two-dimensional nature than found here, but this is due entirely to the flowing fluid condition. Also in the work by Mori [92] the results of only one grid spacing are given when the temperature at the leading edge is set to that of the ambient. As was found in this work this must be viewed with some considerable scepticism, as a false singularity is introduced. Although one grid size may give seemingly meaningful results, when more than one mesh size is used and the results extrapolated the final temperature profile may be completely meaningless.

For the problem as investigated here it is found that, if the total heat flow is required, a good estimate can be found using the model as given in chapter three. This has the great advantage over the

current model that the computational time is less and the procedure more robust. However, if the temperature profile of the wall is required, and, or, the boundary layer thickness needs to be known very accurately, then the current procedure should be used, but great care taken in the way in which the results are handled.

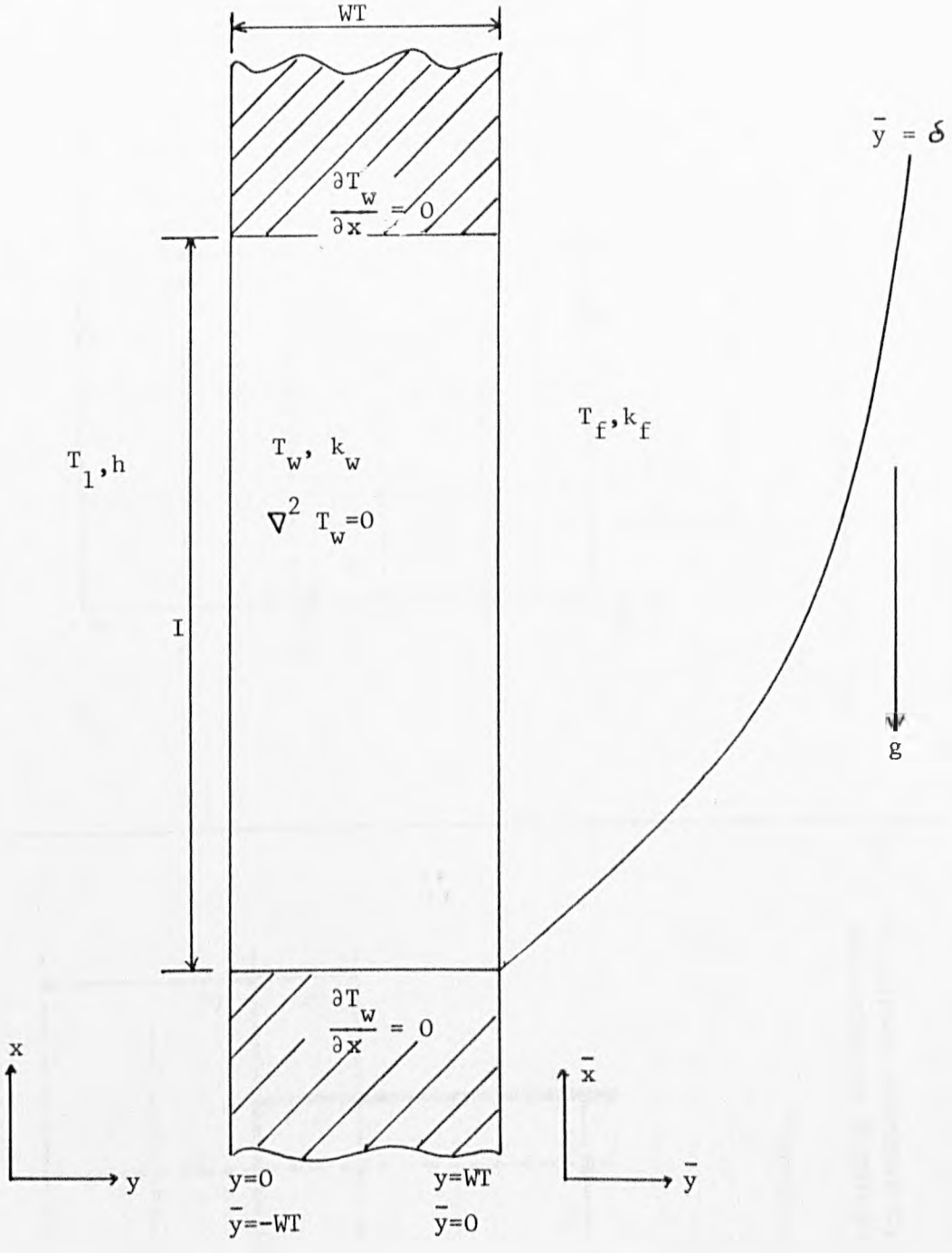

Fig. 7.1 Schematic diagram of system under investigation

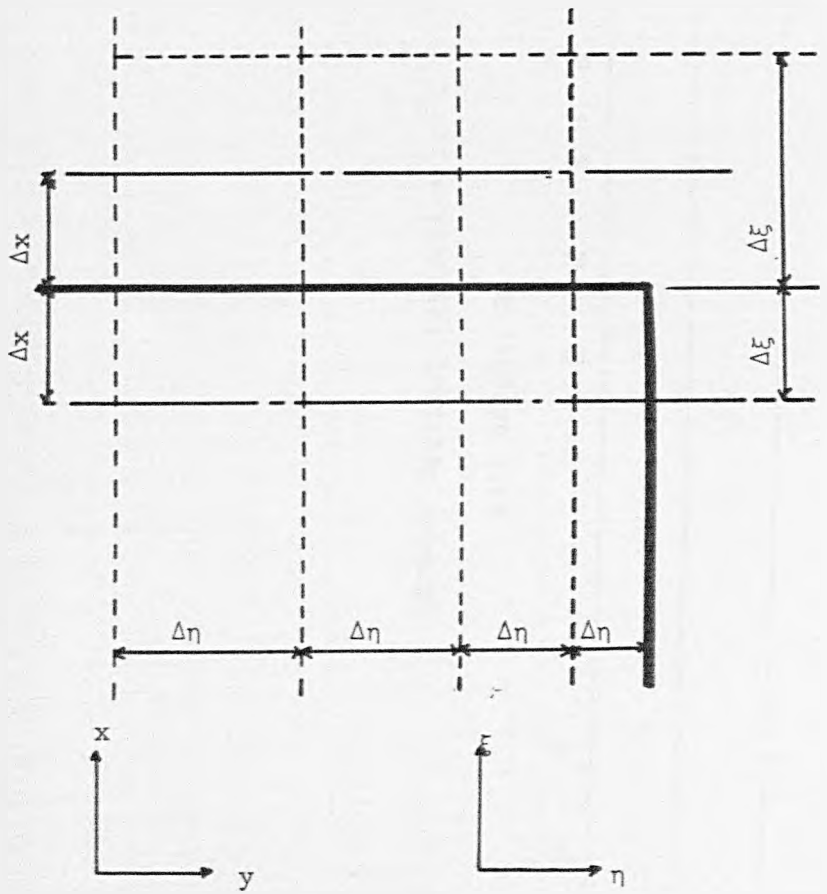

Fig. 7.2 Effect of transforming co-ordinates on nodes used in boundary conditions 7.26, 7.27

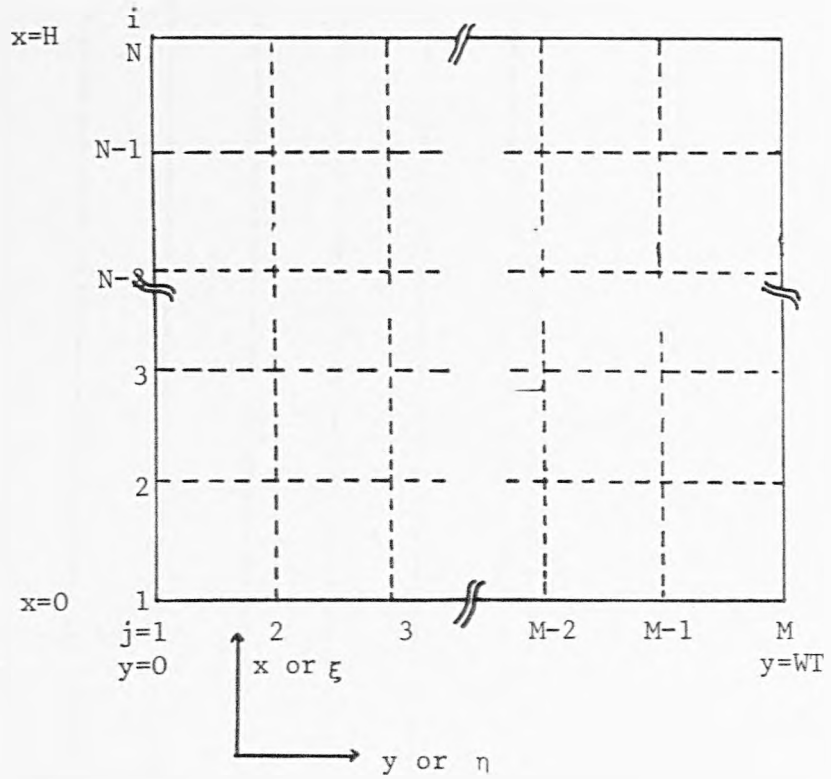

Fig. 7.3 Numbering of nodes in wall

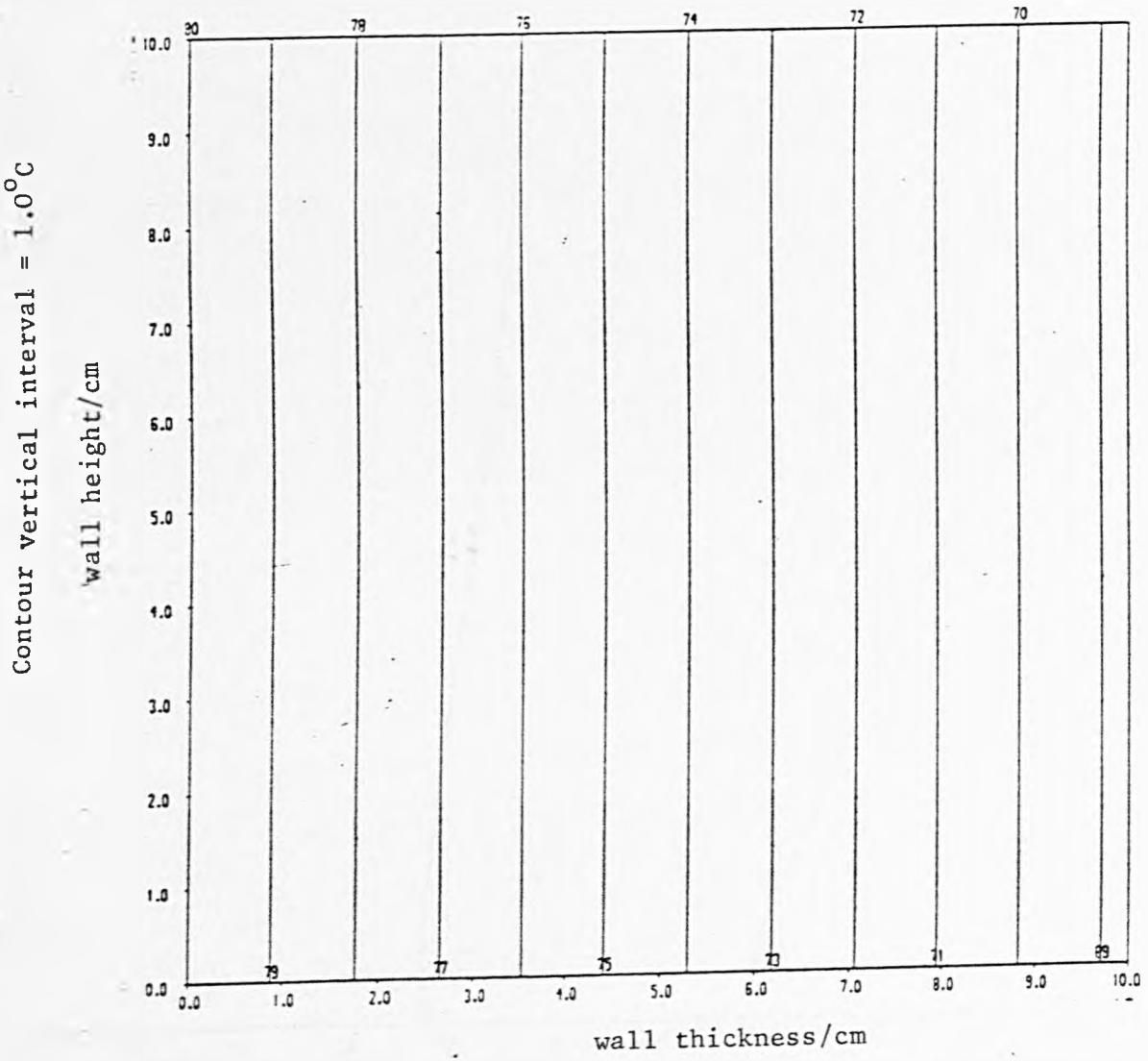

Figure 7.4 Temperature in wall for step 1

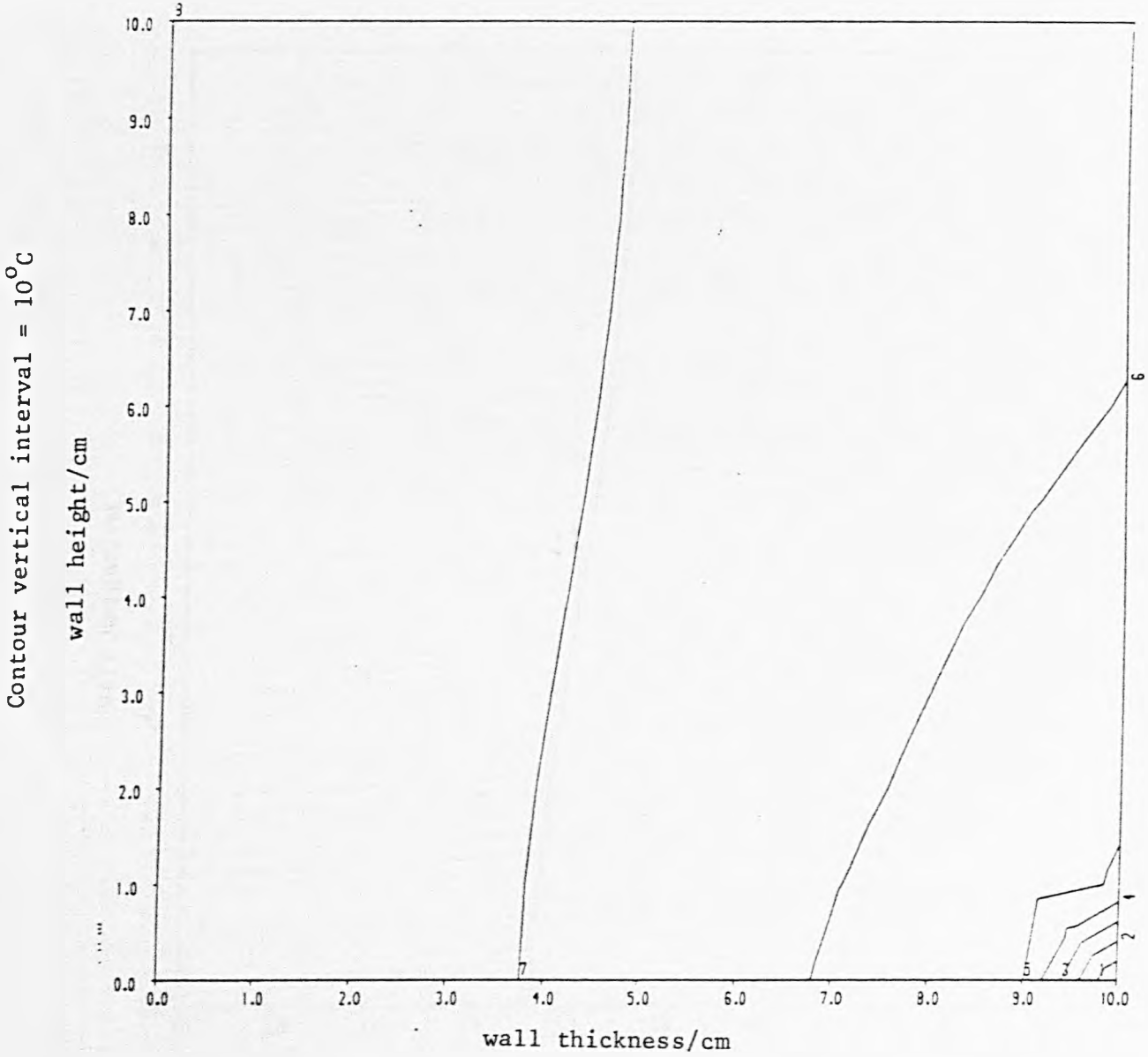

Figure 7.5 Temperature profile in wall for step 2

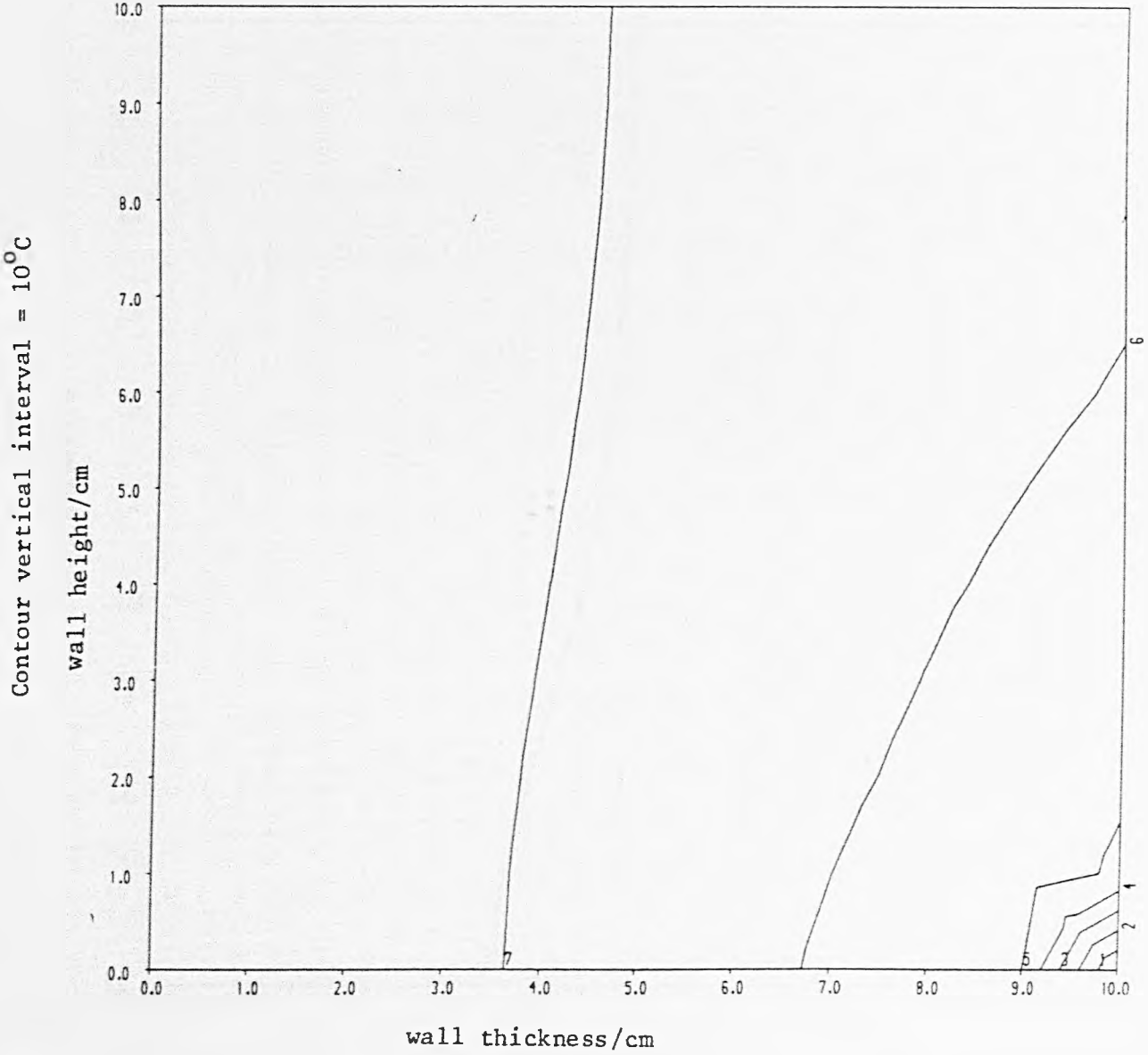

Figure 7.6 Temperature profile in wall for step 3

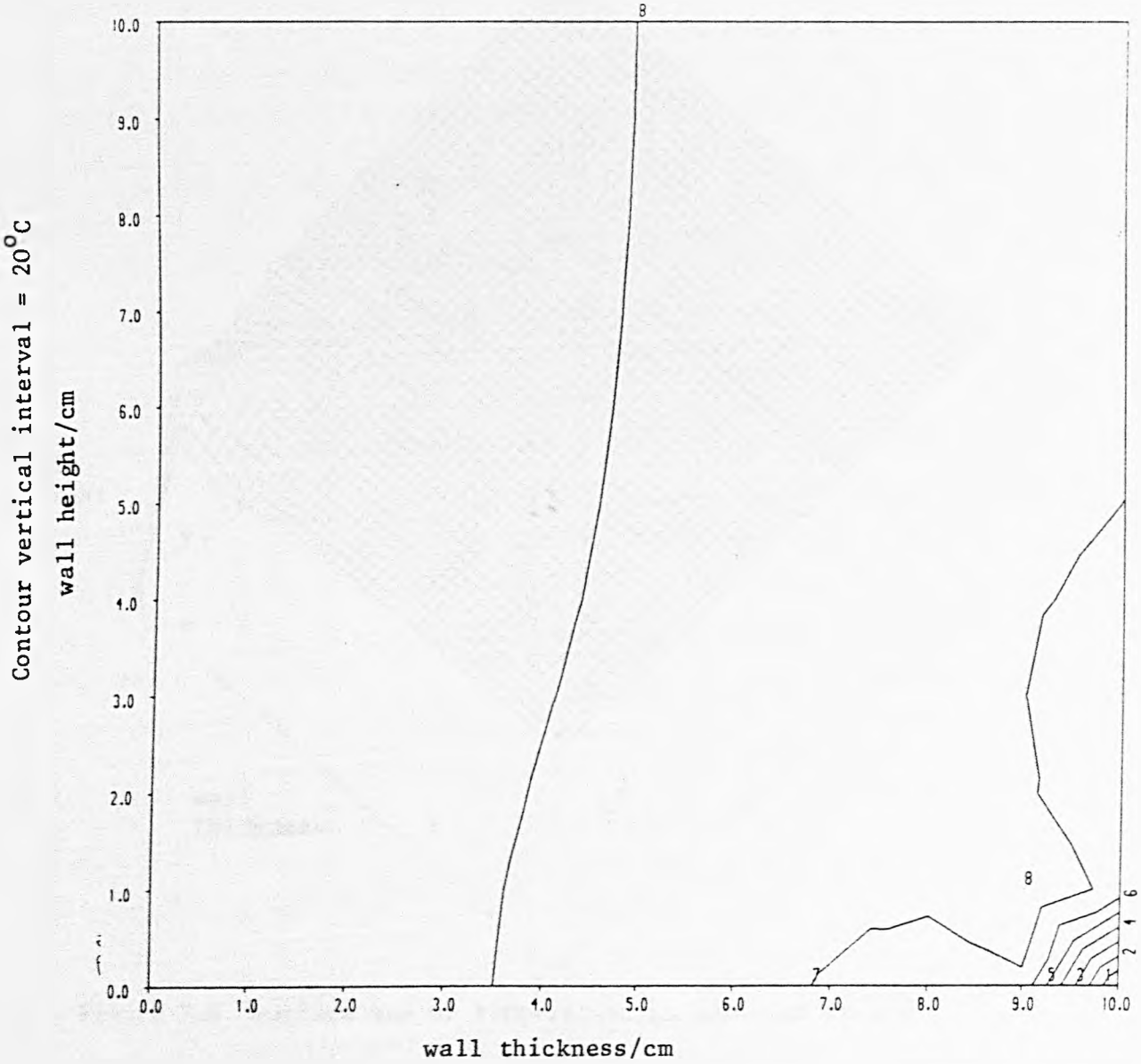

Figure 7.7 Temperature profile in wall for step 4

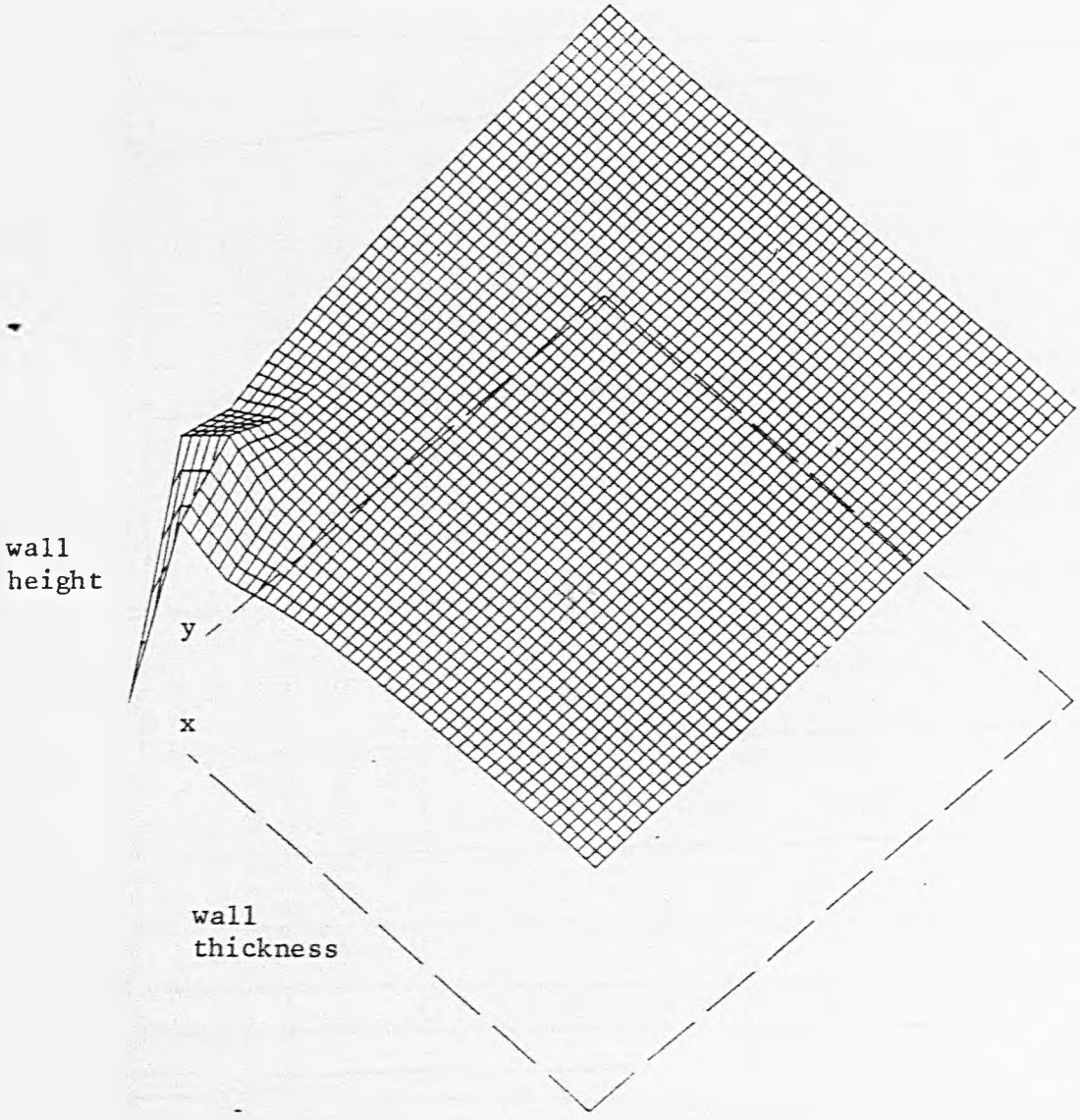

Figure 7.8 Surface map of temperature in wall for step 4

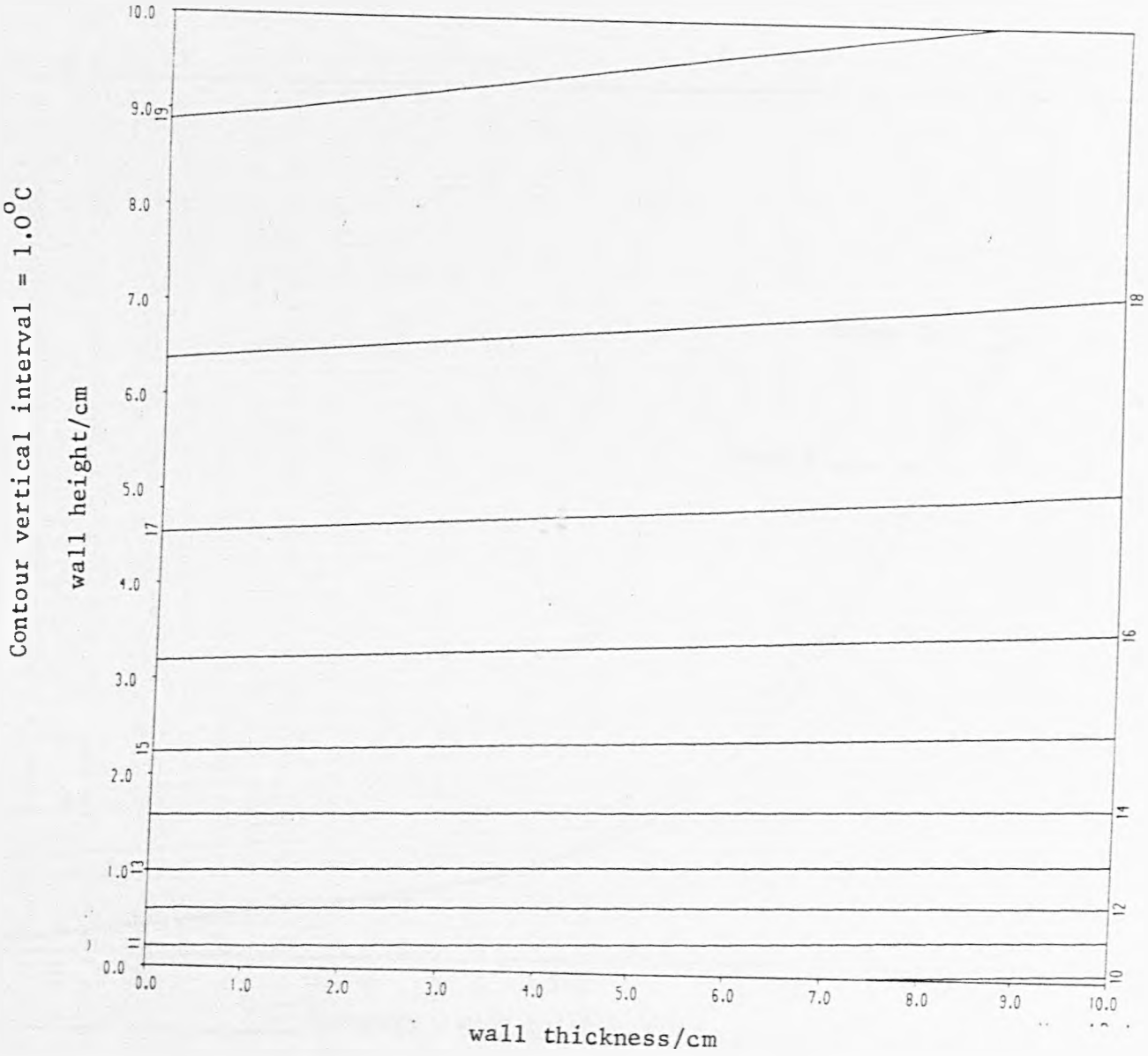

Figure 7.9 Temperature profile in wall for step 8

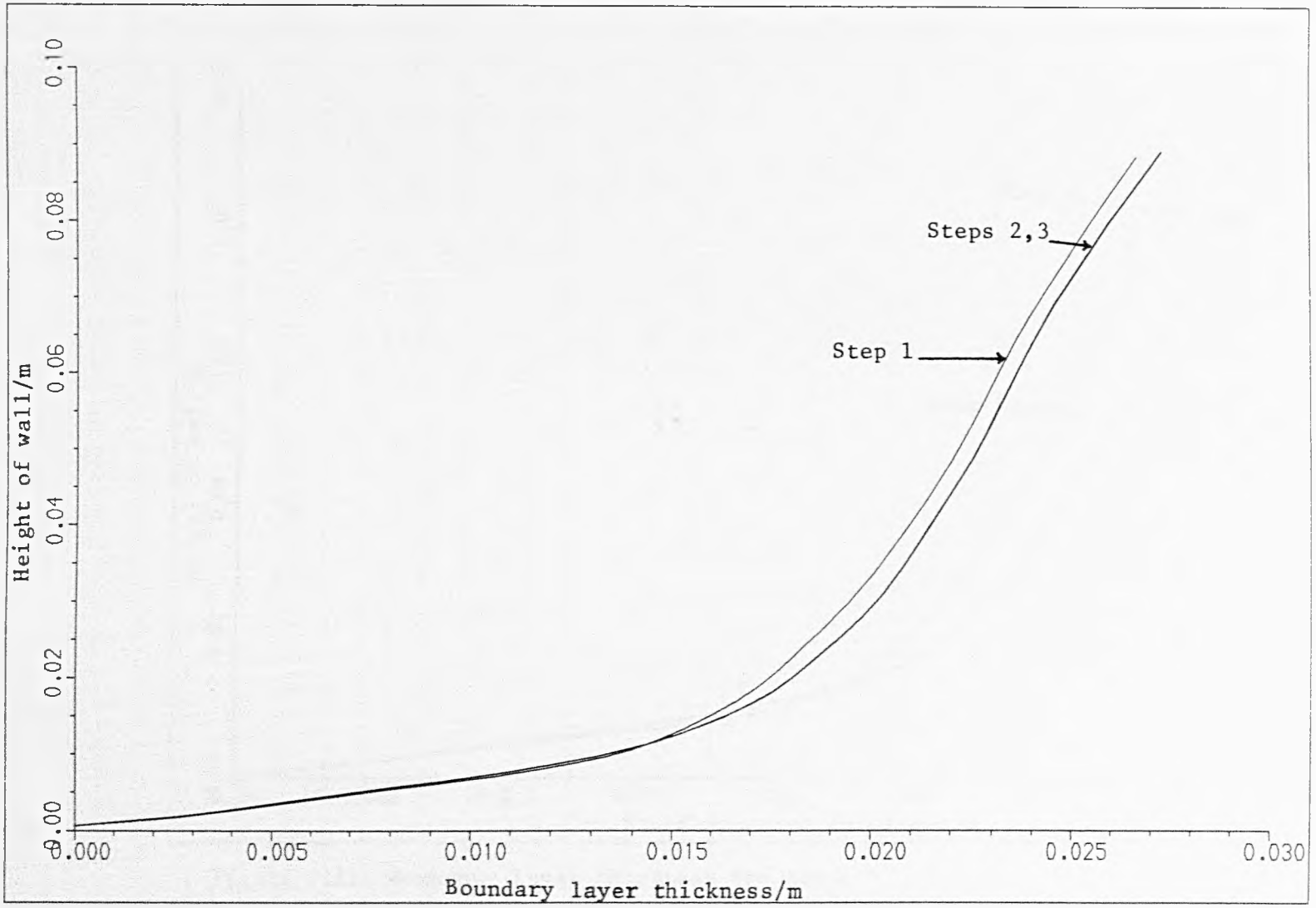

Figure 7.10 Boundary layer thickness for step 1, 2 and 3

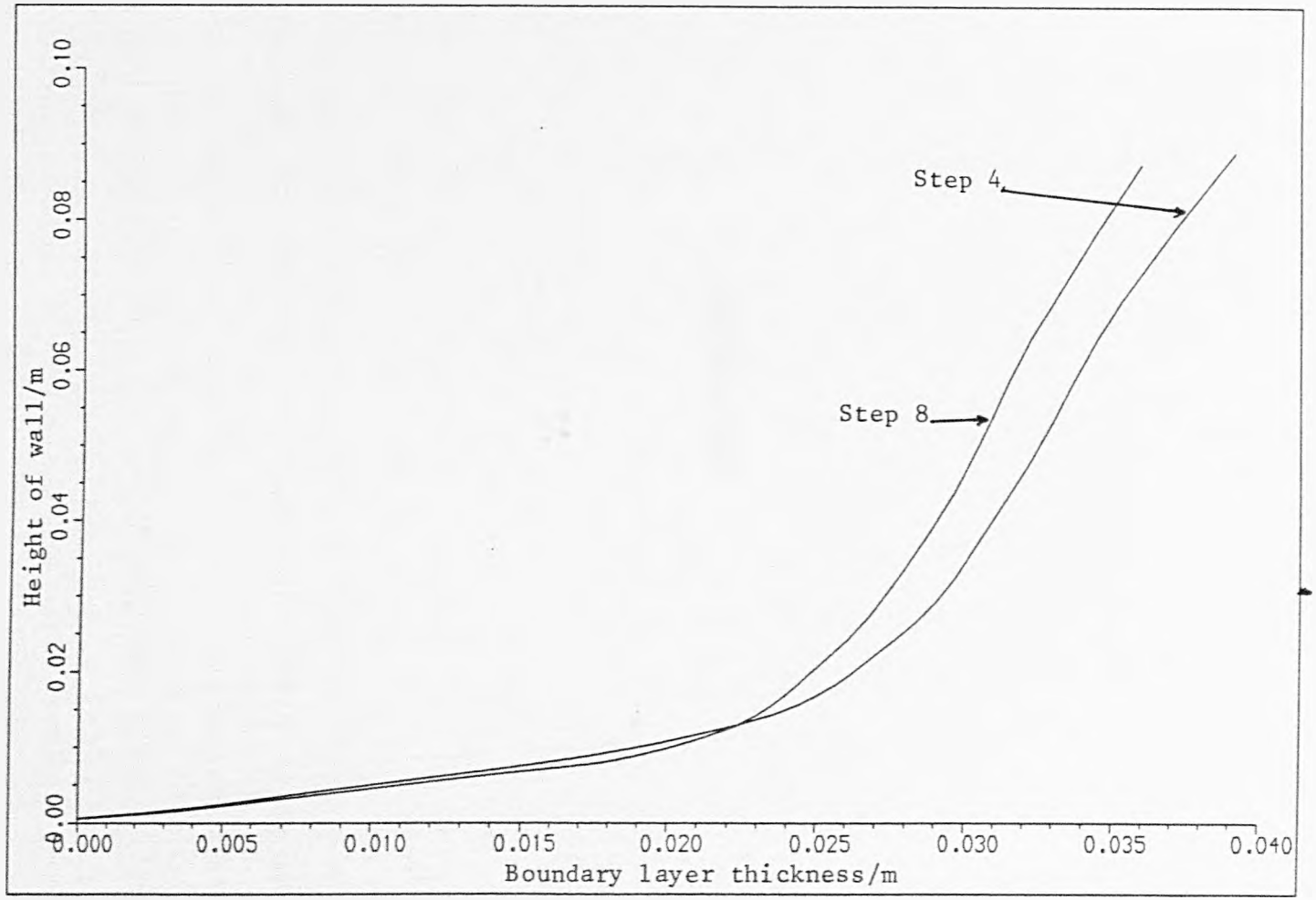

Figure 7.11 Boundary layer thickness for steps 4 and 8

CHAPTER EIGHT

8. Conclusions and Future Work

8.1 Conclusions

The conjugate heat transfer from a downward projecting fin and a plane surface has been studied using several different numerical methods. Both mixed and natural convection have been modelled, as well as the heat flow in a porous medium about a fin. The effect of using a two-dimensional analysis in a plane wall has been investigated in order to determine the limits for which a one-dimensional analysis is no longer valid.

The first problem studied looked at a plane wall with a constant temperature heat source on one side and a cold fluid on the other being heated by natural convection. The heat source was considered to have a constant heat transfer coefficient for the entire height of the wall, as may exist when a vapour is condensing. By modelling the problem in the fluid using an integral analysis two coupled ordinary differential equations are obtained. The solution to these equations is found using a Runge-Kutta-Merson numerical integration procedure. To check the solution procedure boundary conditions are imposed such that the resultant problem becomes one solved by previous workers. The agreement found between the proposed method and those already used is good. Computational times are very rapid and results for the temperature profile are obtained. The most important factor to note in the results is that the temperatures are not set beforehand nor is the heat flow. Both are allowed to vary and only depend on the driving force of the heat source as is true in real systems.

The second problem is that of a downward projecting fin immersed in a fluid reservoir. The temperature at the base of the fin and the temperature of the ambient fluid are fixed. Apart from these two temperatures and the physical properties of the fin and fluid, no other parameters are set before the calculation is initiated. Again an integral analysis in the fluid is used to model the natural convection flow. The solution procedure may proceed in several ways, two of which have been studied in detail. The first method uses a Runge-Kutta-Merson analysis, as with the plane wall problem. However, with the plane wall the boundary conditions were such as to provide an initial value problem, but with the fin a boundary value problem results. This means that initial guesses need to be made at the fin tip for the boundary layer thickness and the velocity of the fluid. Using these values the numerical procedure continues as before. A solution is then found at the base of the fin where the actual values are known. The solution is compared with these real values and, if the two do not agree, the initial guesses are changed appropriately. This is known as a "shooting" method because one is aiming for a solution which is known at some distance away from the starting position. This procedure is somewhat cumbersome and can take a long time for the final solution to be found. Under certain circumstances the procedure is extremely sensitive to the initial guesses and so may fail in finding a solution. An alternative procedure can be developed if it is assumed that at any point up the fin a temperature, T, exists which is given, but unknown before the solution is found. This then gives an explicit relationship for the boundary layer thickness which can be incorporated into the solution procedure. The result is a very robust and fast algorithm which gives results in good agreement with the slower, but

more mathematically rigorous, procedure. Fin efficiency results are calculated for both rectangular and tapered fins and compared with results found which use constant heat transfer coefficients for heat transfer from the fins to fluids. For very long fins the fin efficiencies as calculated by the constant heat transfer coefficient analytical method and the two numerical methods approach one another. However, for short fins there is a significant difference in the fin efficiencies, with the current methods showing much higher efficiencies. This arises because the analyses in the past have assumed temperature profiles or heat fluxes before calculating boundary layer thicknesses or heat transfer coefficients. If no assumptions are made beforehand concerning the temperature profiles thinner boundary layers are found than would normally be expected. Therefore, the heat flow from the fin will be higher than that normally predicted.

Boundary layer thicknesses are found by using several different methods of numerical analysis. In the case when a fin is heating a surrounding fluid it has been shown that under certain circumstances (e.g. long fins) the boundary layer thickness decreases with distance from the leading edge. This is in direct contrast to the assumed behaviour in which it is expected that the boundary layer increases in thickness monotonically with distance. This assumption arose from the fact that the systems considered initially, either plane walls or fins, were assumed to have isothermal surfaces. In such a situation the only factor which affects the boundary layer thickness is the distance away from the leading edge. In the current work the assumption of an isothermal surface is not made and so this extra term is introduced into the calculations. The change in temperature such that the leading edge is cold and the base hot (in the case of a downward projecting fin in a cold fluid) has an opposing effect

on the boundary layer thickness. At the base of the fin the distance moved from the leading edge dominates but, as this effect becomes less noticeable the changing fin temperature takes over, and hence the longer the fin the more noticeable the decrease in boundary layer thickness becomes. This fact means that an extended surface can have fins placed closer together than would be predicted from carrying out an analysis assuming isothermal surfaces.

For both the plane wall and the downward projecting fin, variable physical properties can be introduced very easily due to the use of an integral analysis. This has been done but the only significant effect of using variable physical properties occurs when water is being heated at temperatures near to its freezing point. This is because the physical properties change very rapidly between $0^{o}C$ and $10^{o}C$, and this cannot be modelled very successfully using average bulk properties.

The next system to be studied consisted of a downward projecting fin which loses heat to a fluid by mixed convection. The full boundary layer equations with the Boussinesq approximation were used to model the fluid flow. The solution procedure adopted used a finite difference representation for all the governing equations. However, if a cartesian coordinate system were used problems would be found in the solution near the leading edge. This arises because the boundary layer is too thin to contain many nodal points, and so accuracy is lost. To overcome this problem pseudo-similarity variables were introduced, which had the effect of opening up the boundary layer at the fin tip. The results obtained for the temperature profile of the fin and the total shear stress on the fin agreed extremely well with previous solutions. A similar procedure is used in calculating temperature profiles of fins embedded in a porous medium. The difference between

the free fluid and the porous medium solutions comes from the pseudo-similarity variables used for the substitutions. Before, the variables used were appropriate to pure forced convection flow. For the porous medium problem it is possible to substitute the variables used for a natural convection analysis. This gives the added advantage that the entire range of flows, from pure natural convection to substantially forced convection, can be investigated using the same set of governing equations. It is found that for identical fins, one embedded in a saturated porous medium and the other in a free fluid, the heat flow is greater from the fin in the porous medium and is shown by the temperature profiles found along the fins. This increase in heat flow is due to the breakdown of the boundary layer about the fin which is caused by the presence of the porous medium.

The adverse flow situation is studied for both conditions of free fluid and porous medium surroundings. The point where flow separation first occurs can be found but, after this, the solution procedure fails. This is because the governing equations are parabolic and therefore sweep information from the fin tip, the starting point of the calculations, to the fin base. When the boundary layer separates from the wall the flow direction reverses and information about the fluid is travelling in both directions, which mathematically means that the equations become singular and cannot be solved. The limiting value of the forced convection flow rate for flow separation to occur is found by investigating the flow pattern at the base of the fin. At this point the limiting condition for separation is met. This is because, at the base of the fin the highest temperature exists, and so the natural convection component of the flow is at its greatest. If the flow just stops at the base of the fin then any increase in the forced convection component will cause

separation to occur at some point along the fin until the other limit is reached. This other limit is the point at which the forced convection is so great it completely dominates any flow caused by natural convection. It is found that the value of these two limits, given in terms of the Peclet number, are very close together. In other words only a very small region of mixed convection flow cannot be solved using the method proposed, and this exists for slow flow.

The last problem considered investigates the two-dimensional heat flow in a wall separating the constant temperature heat source and the natural convection heat sink considered first. The problem is considered in a slightly different way from all the previous problems in that the main governing equations are those of the conduction within the wall and not the boundary layer equations in the fluid. By using the experience gained in solving the problem of a fin immersed in a free fluid losing heat by natural convection, the boundary condition on the cold side of the wall can be determined. The temperature at the leading edge is left to 'float', much as was done with all the fin problems, and found by carrying out a heat balance. By looking at a high thin wall the heat flow for the two-dimensional analysis is found to agree well with the one-dimensional case. The heat flow for other situations is studied, as well as the temperature profile within the wall, to study the effects of introducing a two-dimensional analysis and determining the parameters for which the more complicated two-dimensional analysis is required.

As can be seen from the above discussion a number of different geometries of heat exchange surfaces have been considered. In each case the possible solution techniques are considered and an appropriate one chosen. For any situation where assumptions need to be made to expedite the solution time on the computer, checks are made as to their validity. It is therefore shown that for any particular problem

the best technique is chosen to elucidate the underlying pertinent results without losing too much accuracy in the solution.

8.2 Suggestions for Future Work

From the work carried out to date several suggestions for future work can be made which use the principles already developed.

Following on from the work of two-dimensional heat transfer in the plane wall, a similar procedure can be set up to investigate the effect of two-dimensional heat flow in a fin. For the rectangular fin the only new boundary condition to be introduced would be that required to define a temperature at the base of the fin. The fin can be split in half with an adiabatic boundary condition imposed down the centre line. The boundary condition on the fluid side would be the same as for the plane wall. The tapered fin situation would be similar, except that the boundary condition used for the heat flow into the fluid would have to be dealt with more carefully. The boundary condition across the fin/fluid interface equates the heat flows by using the temperature gradients normal to the surface. If the fin half angle is 45° there is no problem as, by using an even grid spacing over the fin, the nodal points will give temperatures which are perpendicular to the surface. However, for any other fin half angle this will not necessarily be true. This can be overcome by resolving the heat flow from the fin into components parallel to the surface and parallel to the base of the fin. In other words, the temperature gradient normal to the surface can be found in terms of nodes which actually exist on the grid imposed over the fin.

The work on the plane wall has considered the conjugate heat transfer problem when the heat source side provides heat at a known temperature with a known heat transfer coefficient. This limitation

can be removed if another convection flow is considered as shown in figure 8.1. In such a problem there are four possible alternatives:

(a) natural to natural convection

(b) forced to natural convection

(c) natural to forced convection

(d) forced to forced convection

In each case, if the transient situation is ignored, there are four possible flow regimes:

(i) laminar to laminar

(ii) laminar to turbulent

(iii) turbulent to laminar

(iv) turbulent to turbulent

Considering (a) (i) a heat balance can be made across the system:

$$q = -k_h \left.\frac{\partial T_h}{\partial y}\right|_{y=-WT} = WT/k_w(T_h|_{y=-WT} - T_L|_{y=0}) = -k_c \left.\frac{\partial T_c}{\partial y}\right|_{y=0} \tag{8.1}$$

subject to the following boundary conditions:

$$y = -\delta_h - WT;\ 0 < x < H$$

$$T_h = T_{\infty h}$$

$$\frac{\partial T_h}{\partial y} = 0 \tag{8.2}$$

$$y = \delta_c;\ 0 < x < H$$

$$T_c = T_{\infty c}$$

$$\frac{\partial T_c}{\partial y} = 0 \qquad (8.3)$$

The temperature within either fluid will be given by:

$$T_1 - T_{\infty 1} = a + by + cy^2 \text{ where } 1 = c \text{ or } h$$

By carrying out an integral analysis in both the fluids, two coupled ordinary differential equations will be obtained. These two sets of equations will be coupled by matching the heat flow across the wall.

Returning to the case when only the heat sink side of the system exchanges heat by natural convection, the effect of radiation can be introduced. Radiation heat loss can be treated as a boundary condition for the temperature profile in the fluid. Thus the boundary conditions for the fluid temperature profile become:

$$y = \delta,\ 0 < x < H$$

$$T_1 = T_\infty$$

$$\frac{\partial T_1}{\partial y} = 0 \qquad (8.5)$$

$$\text{at } y = 0;\ 0 < x < H$$

$$U(T_1 - T_{1\ y=0}) = -k_1 \frac{\partial T1}{\partial y} + \sigma \mathcal{F}_{w-s} (T_w^4 - T_s^4) \qquad (8.6)$$

where U = overall heat transfer coefficient from heat source to wall/fluid interface

$\mathcal{F}_{w-s}$ = shape and emissivity factor between the wall and surroundings

Including equation 8.6 in the temperature profile for the fluid will prove very difficult and lead to highly non-linear terms. It may be better to change the boundary condition 8.6 to:

$$U\,(T_1 - T_{1|y=0}) = -k_s \frac{\partial T_1}{\partial y} + R \qquad (8.7)$$

where R is the heat lost by radiation. This may be assumed to be constant and an initial guess made as to its value at incremental points along the surface of the wall, using the results obtained in chapter three (with no radiation heat loss). New temperatures can be found for the surface of the wall and so new values for R, the radiation heat loss calculated. If these lie within a certain tolerance then the calculation can end. However, if the old and new values for the radiation heat loss are significantly different then the procedure can be repeated with the new values for radiation heat loss.

Moving on to the fin problem with one-dimensional heat flow the obvious boundary condition to change would be the constant base temperature. It is far more likely that the heat flow into the fin can be estimated by knowing a fluid temperature T_f, rather than the fin base temperature being known (see figure 8.2). If one-dimensional heat flow is assumed to exist in the fin then the fin base temperature will be constant, but unknown. The heat flow will be given by:

$$q_{in} = (T_1 - T_b)\, k_w / TT \qquad (8.8)$$

Iterations can be carried out using equation 8.8. The following

procedure is proposed for the iterations:

(1) Assume a value for T_b - calculate q_{out} in the usual way (chapter 4)

(2) Compare with value for q_{in}

(3) If the value is the same, then the solution is found

(4) If the value is different use:

$$q_{out} = q_{in} = (T_1 - T_b) \frac{k_w}{TT}$$

to find a new value of T_b and return to step (2)

The final suggestion for future work essentially follows on from the fact that it has been found that the boundary layer thickness actually decreases under certain circumstances. This means that the final thickness may not be as great as first expected and interference between neighbouring fins may not occur. It would, therefore, be worthwhile to study the interactions of two fins to see how close they could be placed without detrimentally affecting the overall heat flow. Looking at figure 8.3 it can be seen that the plane of symmetry in the fluid changes the infinite boundary conditions. A procedure similar to that used in chapter five can be used when conditions at a given distance η (distance from the fin surface) could be set. Before, the infinite boundary conditions would have been given by:

$$v = 0, \ \theta = 0 \text{ at } \eta = 10 \qquad (8.9)$$

Now, if the plane of symmetry occurs at, say, $\eta = 5$, the boundary condition will become:

$$b = 0, \ \frac{\partial \theta}{\partial \eta} = 0 \text{ at } \eta = 5 \qquad (8.10)$$

This then forces the solution in the fluid to give lower flowrates closer to the fin surface. Using this problem it would be possible to come up with an optimum spacing for fins so that the maximum heat flow can be obtained. If this is then used with an economic assessment of finned tubing a more cost-effective heat exchanger could be produced very quickly.

All the suggestions made above make use of at least one of the solution procedures already developed, and yet provide sufficient new ideas to give scope for new procedures and new results to be found.

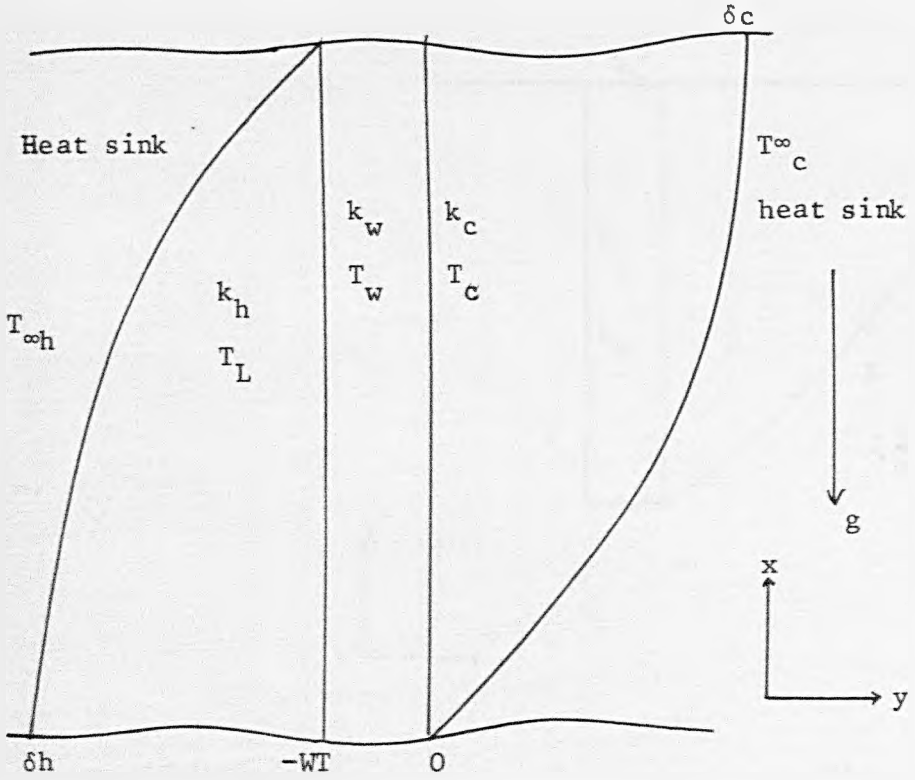

Fig. 8.1 Conjugate head transfer between two convective flow systems

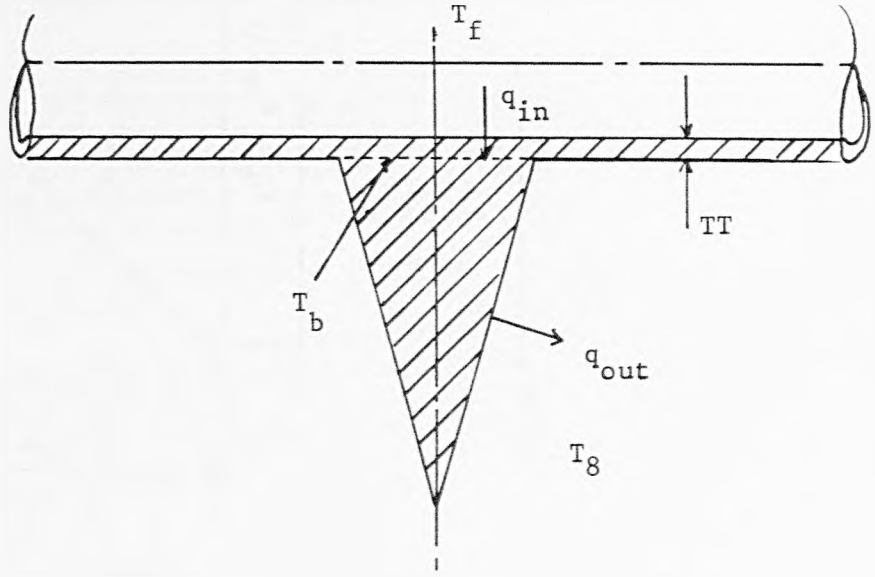

Fig. 8.2 Heat flow boundary condition for fin problem

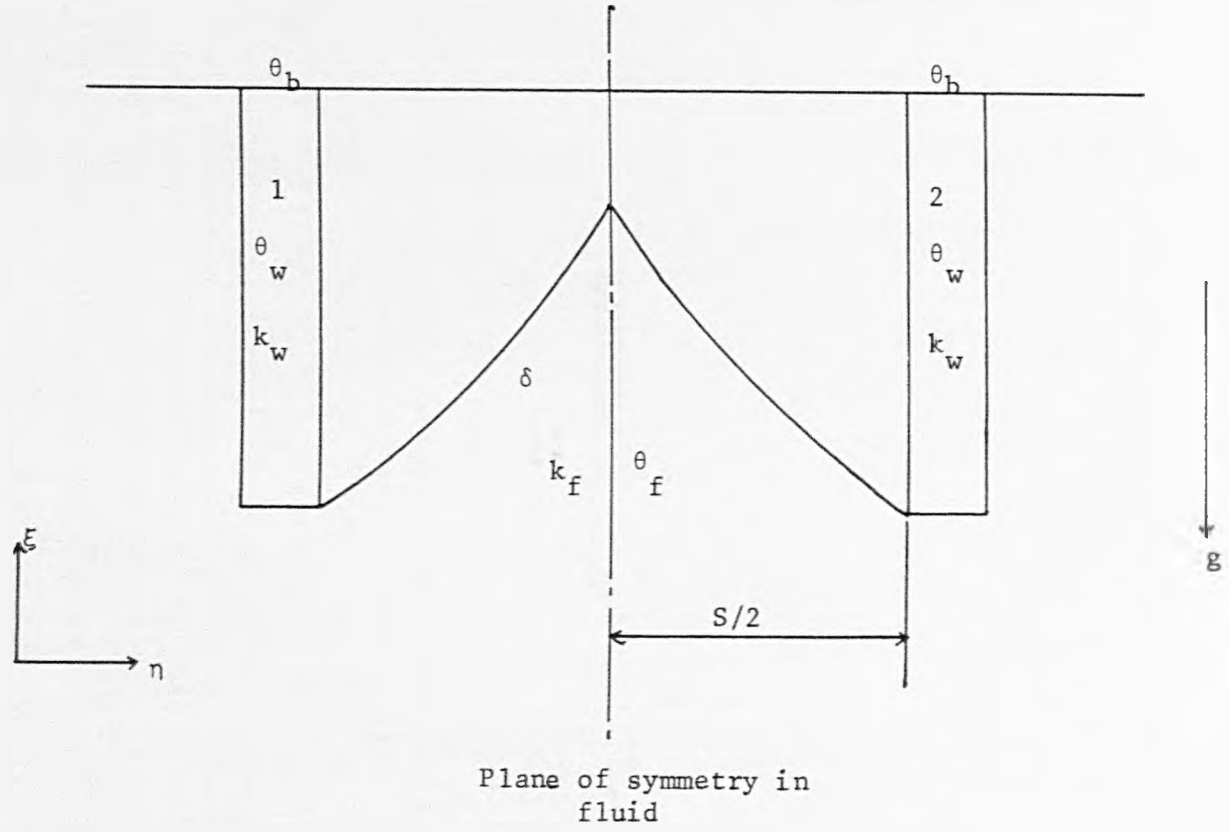

Fig. 8.3 Interaction between two fins and the effect on the boundary layers

APPENDICES

APPENDIX 1

Calculation of Boundary Layer Thickness for Plane Vertical Wall When $2 k_{fl}/U_o >> \delta$

From chapter three it is found that the momentum and energy balance found from the integral analysis are:

$$\frac{1}{105} \frac{d}{dx} (\Gamma^2 \delta) = \frac{g\beta (T_1 - T_\infty)\delta^2}{3(\frac{2 k_{fl}}{U_o} + \delta)} - \nu \frac{\Gamma}{\delta} \tag{A1.1}$$

$$\frac{1}{30} \frac{d}{dx} \left(\frac{\Gamma\delta^2}{\frac{2 k_{fl}}{U_o} + \delta}\right) = \frac{2\alpha}{\frac{2 k_{fl}}{U_o} + \delta} \tag{A1.2}$$

When $2 k_{fl}/U_o >> \delta$ equation (A1.1) and (A1.2) can be simplified to provide the following ordinary differential equations:

$$\frac{1}{105} \frac{d}{dx} (\Gamma^2 \delta) = \frac{g\beta (T_1 - T_\infty)\delta^2}{3 \frac{2 k_{fl}}{U_o}} - \nu \frac{\Gamma}{\delta} \tag{A1.3}$$

$$\frac{1}{30} \frac{d}{dx} (\Gamma\delta^2) = 2\alpha \tag{A1.4}$$

Equation (A1.4) is easily solved to give

$$\Gamma\delta^2 = 60\, \alpha x + C \tag{A1.5}$$

when $x=0$, $\Gamma\delta^2 = 0$ $\quad \therefore C = 0$

$$\Gamma\delta^2 = 60\alpha x \tag{A1.6}$$

This can be substituted into (A1.3) to give:

$$\frac{1}{105}\ \frac{d}{dx}\ (60\ \alpha x)^4\ \frac{1}{\delta^3}) \ = \ \frac{g\beta(T_1-T_\infty)\delta^2}{\frac{6\ k_{fl}}{U_o}} - \nu\ \frac{60\alpha x}{\delta^3} \qquad (A1.7)$$

$$\text{Let} \quad \lambda = \frac{35g\beta(T_1-T_\infty)}{\frac{2\ k_f}{U_o}}$$

$$\text{and } z = \frac{60\alpha x^2}{\delta^3} \qquad (A1.8)$$

Using (A1.8) in (A1.7) the resultant equation is:

$$\frac{dz}{dx} + \frac{105\nu}{60\alpha x}\ z = \ (60\alpha x)^{4/3}\ z^{-2/3} \qquad (A1.9)$$

Equation (A1.9) is a form of Bernoulli's equation.

To solve this equation one further substitution needs to be made:

$$P = z^{1-(-2/3)} = z^{5/3} \qquad (A1.10)$$

By substituting (A1.10) into equation (A1.9) and carrying out the required integrations the solution for P is found to be:

$$P \ = \ \frac{5\lambda(60\alpha)^{4/3}\ 4\alpha\ x^{7/3}}{2\delta\alpha + 35\nu} \qquad (A1.11)$$

Substituting back using (A1.8) and (A1.10) an explicit relationship for the boundary layer thickness is given:

$$\delta \ = \ [\frac{(180\ 128\ +35\ )}{\lambda}]^{1/5}\ \ x^{1/5} \qquad (A1.12)$$

This expression for the boundary layer thickness can be used to find the temperature at the wall surface by using the expression for the temperature profile in the fluid given by equation 3.7 when setting y = 0.

APPENDIX 2

Resultant Equations for Calculation of Boundary Layer Thickness with Variable Physical Properties When Integral Analysis is Used

Section One - Plane Wall

The variation of physical properties is found by fitting data between the temperatures of $0^{o}C$ to $400^{o}C$ for air, and $0^{o}C$ to $150^{o}C$ for water, to quadratic expressions in temperature. This is done for all properties used in the momentum and energy equations 3.1 and 3.2.

$$\begin{aligned}
\rho &= a_o + a_1 T + a_1 T^2 \\
Cp &= b_o + b_1 T + b_2 T^2 \\
k_1 &= c_o + c_1 T^2 + c_2 T^2 \\
\mu &= d_o + d_1 T + d_2 T^2 \\
\beta &= e_o + e_1 T + e_2 T^2
\end{aligned} \qquad \text{(A2.1)}$$

Substituting A2.1 into equations 3.1 and 3.2 the new heat and momentum balances are found. The leading terms are comprised of the first constants in the polynomials, and the smaller subsequent terms are the products of all three terms for density and heat capacity. To simplify the appearance of the resultant equations the following substitutions are made:

$$\begin{aligned}
M_1 &= a_o + a_1 \ T_\infty + a_2 \ T_\infty^{\ 2} \\
M_2 &= a_1 + 2a_2 \ T_\infty \\
H_1 &= a_o b_o + (a_1 b_o + a_o b_1) \ T_\infty + (a_2 b_o + a_1 b_1 + a_o b_2) T_\infty^{\ 2} \\
&\quad + (a_2 b_1 + a_1 b_2) \ T_\infty^{\ 3} + a_2 b_2 \ T_\infty^{\ 4} \\
H_2 &= a_1 b_o + a_o b_1 + 2(a_2 b_o + a_1 b_1 + a_o b_2) T_\infty + 3(a_2 b_1 + a_1 b_2) T_\infty^{\ 2} \\
&\quad + 4 a_2 b_2 \ T_\infty^{\ 2}
\end{aligned}$$

$$H_3 = a_2b_o + a_1b_1 + a_ob_2 + 3(a_2b_1 + a_1b_2)T_\infty + 6a_2b_2T_\infty^2$$
$$H_4 = a_2b_1 + a_1b_2 + 4a_2b_1T_\infty$$
$$H_5 = a_2b_2 \qquad \text{(A2.2)}$$

Using the dimensionless variables given in equation 3.11 and carrying out the differentiations in the heat and momentum balance two coupled ordinary differential equations are found similar to those given by equations 3.12 and 3.13:

$$MA\ \frac{dV^*}{dx^*} + MB\ \frac{d\delta^*}{dx^*} = \frac{-\mu_o a_o b_1 v^*}{k_{f1}\ \delta^*} \quad \frac{-g(a_o b_o^2)\kappa}{k_{flo}}\ (T_1 - T_\infty)$$
$$(\frac{M_2}{3}\ \frac{\delta^{*2}}{1+\delta^*} + \frac{a_2(T_1-T_\infty)}{5}\ \frac{\delta^{*3}}{(1+\delta^*)^2}) \qquad \text{(A2.3)}$$

$$HA\ \frac{dV^*}{dx^*} + HB\ \frac{d\delta^*}{dx^*} = \frac{2a_ob_o}{1+\delta^*} \qquad \text{(A2.4)}$$

where

$$MA = \frac{2V^*\delta^*M_1}{105} + \frac{(T_1-T_\infty)}{252}\ \frac{M_2\delta^{*2}V^*}{1+\delta^*} + \frac{a_2(T_1-T_\infty)}{495}\ \frac{2V^*\delta^{*3}}{(1+\delta^*)^2}$$

$$MB = \frac{V^{*2}M_1}{105} + \frac{(T_1-T_\infty)M_2}{252}\ \frac{V^{*2}\delta^*(2+\delta^*)}{(1+\delta^*)^2} + \frac{a_2(T_1-T_\infty)^2}{495}\ \frac{V^{*2}\delta^{*2}(3+\delta)}{(1+\delta^*)^3}$$

$$HA = \frac{H_1}{30}\ \frac{\delta^{*2}}{1+\delta^*} + \frac{(T_1-T_\infty)H_2\ ^{*3}}{(1+\delta^*)^2} + \frac{(T_1-T_\infty)^2}{90}\ \frac{H_3\delta^{*4}}{(1+\delta^*)^3} + \frac{(T_1-T_\infty)^3}{132}\ \frac{H_4\delta^{*5}}{(1+\delta^*)^4}$$
$$+ \frac{(T_1-T_\infty)^4}{182}\ \frac{H_5\delta^{*6}}{(1+\delta^*)^5}$$

$$HB = \frac{H_1}{30}\ \frac{V^*\delta^*(2+\delta^*)}{(1+\delta^*)^2} + \frac{(T_1-T_\infty)}{56}\ \frac{(H_2V^*\delta^{*2}(3+\delta^*)}{(1+\delta^*)^3} + \frac{(T_1-T_\infty)^2}{90}\ \frac{H_3V^*\delta^*(4+\delta^*)}{(1+\delta^*)^4}$$
$$+ \frac{(T_1-T_\infty)^3}{132}\ \frac{H_4V^*\delta^{*4}(5+\delta^*)}{(1+\delta^*)^5} + \frac{(T_1-T_\infty)^4}{182}\ \frac{H_5V^*\delta^{*5}(6+\delta^*)}{(1+\delta)^6}$$

As in chapter 3 the equations can be used to eliminate the $d\delta^*/dx^*$ term from one equation and the dv^*/dx^* from the other. The resulting coupled ordinary differential equations are:

$$\left(\frac{HB\ MA}{HA} - MB\right)\ \frac{d\delta^*}{dx^*} = \frac{2\ a_o b_o}{1+\delta^*}\ \frac{MA}{HA} + \frac{\mu_o a_o b_o}{k_{flo}}\ \frac{V^*}{\delta^*}$$

$$+ \frac{g(a_o b_o)^2\ \kappa^2\ (T_1-T_\infty)}{k_{flo}}\left(\frac{M_2}{3}\ \frac{\delta^{*2}}{1+\delta^*} + \frac{a_2(T_1-T_\infty)}{5}\ \frac{\delta^{*3}}{(1+\delta^*)^2}\right) \qquad (A2.5)$$

$$\left(\frac{MB\ HA}{HB} - MA\right)\ \frac{dV^*}{dx^*} = \frac{2a_o b_o}{1+\delta^*}\ \frac{MB}{HB} + \frac{\mu_o a_o b_o}{k_{flo}}\ \frac{V^*}{\delta^*}$$

$$+ \frac{g(a_o b_o)^2\ \kappa^3(T_1-T_\infty)}{k_{flo}}\left(\frac{M_2}{3}\ \frac{\delta^{*2}}{1+\delta^*} + \frac{a_2(T_1-T_\infty)}{5}\ \frac{\delta^{*3}}{(1+\delta^*)^2}\right) \qquad (A2.6)$$

These equations can be treated in the same way as those for the constant physical property case, as discussed in chapter 3. The fluid viscosity and the fluid thermal conductivity are evaluated at the temperature of the wall fluid interface, whilst the fluid density and heat capacity are evaluated across the boundary layer.

Equations A2.5 and A2.6 can be used in the constant physical property case by setting all the second and third terms, in the expressions for the variation of physical properties (equation A2.1), equal to zero, except for the density term. If the second and third coefficients for density are set to zero then no flow will occur as there is no change in density with temperature. Therefore, to calculate the boundary layer thickness with constant physical

properties using equations A2.5 and A2.6 the term M_2 must be replaced by the term for the coefficient of expansion. Having made this substitution the solution procedure may proceed as in the situation when constant physical properties are assumed at the outset of the problem.

Section Two - Downward Projecting Fin

In this section variable physical properties are introduced into the momentum and heat balance derived for a downward projecting fin. The momentum balance found by carrying out an integral analysis in the fluid about a downward projecting fin is identical to that found for the case of a plane wall. In the heat balance, however, an extra term is introduced to account for the temperature gradient on the surface of the fin.

Equations analogous to A2.3 and A2.4 can be found by applying a similar procedure to the heat and momentum balance as already discussed. The resultant equations are:

$$2MF1\ \beta\delta \frac{d\Gamma}{dx} + MF1\Gamma^2 \frac{d\delta}{dx} = -\mu_o \frac{\Gamma}{\delta} - \delta g_x MF2 \qquad (A2.7)$$

$$HF1\delta\theta_w \frac{d\Gamma}{dx} + HF1\theta_w\Gamma \frac{d\delta}{dx} + HF1\Gamma\delta \frac{d\theta_w}{dx} = \frac{2k_{flo}\theta_w}{\delta} \qquad (A2.8)$$

where $MF1 = \frac{1}{105}(a_o + a_1T_\infty + a_2T_\infty^2) + \frac{T_f-T_\infty}{252}(a_1+2a_2T_\infty) + \frac{(T_s-T_\infty)^2}{495}a_2$

$$MF2 = \frac{(T_s-T_\infty)(a_1+2a_2T_\infty)}{3} = \frac{a_2(T_s-T_\infty)}{5}$$

$$HF1 = \frac{1}{30}\left[a_o b_o+(a_1 b_o+a_o b_1)T_\infty+(a_2 b_o+a_1 b_1+a_o b_2)T_\infty^{\,2}+(a_2 b_1+a_1 b_2)T_\infty^{\,3}\right.$$

$$\left.+a_2 b_2 T_\infty^{\,4}\right]$$

$$+\frac{(T_s-T_\infty)}{56}\left[a_1 b_o+a_o b_1+2(a_2 b_o+a_1 b_1+a_o b_2)T_\infty+3(a_2 b_1+a_1 b_1)T_\infty^{\,2}+4a_2 b_2 T_\infty^{\,3}\right]$$

$$+\frac{(T_s-T_\infty)^2}{90}\left[a_2 b_o+a_1 b_1+a_o b_2+3(a_2 b_1+a_1 b_2)T_\infty+6a_2 b_2 T_\infty^{\,2}\right]$$

$$+\frac{(T_s-T_\infty)^3}{132}\left[a_2 b_1+a_1 b_2+4a_2 b_2 T_\infty\right]+\frac{a_2 b_2 (T_s-T_\infty)^4}{182}$$

From these two equations two coupled ordinary differential equations are found which can be solved in the ways discussed in chapter 4. The resultant equations are:

$$\frac{d\delta}{dx}\left(\frac{HF1\theta_w\Gamma}{2}\right) = \frac{2\,k_{flo}\theta_w}{\delta} - HF1\Gamma\delta\,\frac{d\theta_w}{dx} + \frac{HF1\theta_w}{2MF1}\,\frac{\mu_o}{\delta} + \frac{\delta g MF2MF1\theta}{2MF1} \tag{A2.9}$$

$$\frac{d\Gamma}{dx}\left(MF1\delta\theta_w\right) = 2MF1\Gamma\delta\,\frac{d\theta_w}{dx} - \frac{4\,k_{flo}\theta_w}{\delta} - \frac{HF1\theta_w}{MF1}\,\frac{\mu_o}{\delta} - \frac{\theta g MF2MF1\theta_w}{2MF1\Gamma} \tag{A2.10}$$

APPENDIX 3

Comparison of Solution Technique for Plane Wall with Work by Miyamoto et al [66]

To compare the solution method in chapter three with the work by Miyamoto and his co-workers [66] both solution techniques must be restricted in some way. For the work presented in chapter three the boundary conditions on the temperature profile are changed to limit the temperature, or heat flux, to a constant value on the side of the plane wall next to the heat source. The work in [66] looks at the axial conduction in the wall, but also provides a solution for the one-dimensional situation, which is the one used for the comparison.

As in chapter three the temperature profile is assumed to be parabolic:

$$T_1 - T_\infty = a + by + cy^2 \qquad \text{(A3.1)}$$

The first boundary condition is a heat balance carried out between the constant temperature, or constant heat flux, on the heat source side and the interface between the wall and the fluid on the heat sink side. The other two boundary conditions are those used previously and show that the temperature excess and the temperature gradient decreases to zero at the edge of the boundary layer.

y=0:

$$-k_w \frac{\partial T}{\partial y} = WT\,(T_o - T_\infty) \quad \text{or} \quad -k_w \frac{\partial T}{\partial y} = Q$$

y=δ:

$$T_1 = T_\infty \qquad \text{(A3.2)}$$

$$\frac{\partial T_1}{\partial y} = 0$$

The resulting temperature profiles are:

constant temperature

$$\frac{T_1 - T_\infty}{T_o - T_\infty} = \frac{(y-\delta)^2}{\frac{2k_w k_1}{WT} + \delta}$$

constant heat flux

$$\text{or} \quad T_1 - T_\infty = \frac{Q(y-\delta)^2}{2\,k_1\,\delta} \tag{A3.3}$$

These temperature profiles can now be substituted into the momentum and heat balances, equations (3.1) and (3.2) in the same way as was done in chapter 3.

For the constant temperature boundary condition the momentum balance and heat balance are the same as before except that the term $2\,k_1/U_o$ is now replaced by $2\,k_1 k_w/WT$ and the temperature difference is in terms of T_o, the constant wall temperature, instead of T_1, the constant heat source temperature. Thus, these two equations can be solved using the same procedure as before.

For the constant heat flux situation the momentum and heat balances can be written:

$$\frac{1}{105}\,\frac{d}{dx}\,(\Gamma^2\Delta) = \frac{g\Delta^2}{6Q^2\beta^3\alpha^2} - \frac{\nu}{\alpha}\,\frac{\Gamma}{\nu} \tag{A3.4}$$

$$\frac{1}{30}\,\frac{d}{dx}\,(\Gamma\Delta^2) = 2 \tag{A3.5}$$

where $\delta = \frac{k_1\Delta}{Q}$, $x = \frac{k_f X}{Q\beta}$, $= \frac{Q\beta\alpha\Gamma}{k_1}$

Equations (A3.4) and (A3.5) represent the starting solutions found in chapter 3 and are solved by assuming solutions of the form:

$$\Delta = Ax^{\alpha}$$

$$\Gamma = Bx^{\beta}$$

Giving

$$\Delta = \left[\left(\frac{48 + 60\ Pr}{Gr}\right) x \right]^{1/5}$$

$$\Gamma = 60 \left(\frac{48 + 60\ Pr}{Gr}\right)^{-2/5} x\ 3/5$$

$$\text{where } Gr = \frac{g\ k_f^{\ 3}}{6Q\beta^3\alpha^2}$$

In the paper by Miyamoto et al [66] the results presented are found using a Prandtl number of 0.7. To compare results with those found using the above equations some assumptions need to be made regarding the physical properties used to obtain a Prandtl number of 0.7. Assuming that the fluid being heated is air at one atmosphere pressure the temperature at which properties are evaluated must be $175^{o}C$.

The notation used in [66] is as follows:

$D = Gd$; d = thickness of plate

G = constant (defined later)

k_s = thermal conductivity of solid

k_f = thermal conductivity of fluid

$L = Gl$; l = height of plate

$$Gr_L = \frac{g\beta(T_o - T_\infty)l^3}{\nu^2} \text{ ; Grashof number}$$

$$G = \left(\frac{g\beta\Delta T}{\nu^2}\right)^{1/5}, \quad \Delta T = T_o - T_\infty \text{ ; for isothermal wall}$$

$$G = \left(\frac{g\beta a_o}{\nu^2 \lambda_f}\right)^{1/4}, \qquad T = \left(\frac{g\beta\Delta_f^3}{\nu^2 q_o^3}\right) \text{ for constant heat flux wall}$$

Figures A3.1, A3.2, and A3.3 correspond to figures 2, 3 and 4 in [66]. For figure A3.1 it is known that the parameter K is 28, Gr is $2.76*10^7$ and that T_o is a constant. For K equal to 28 and knowing the thermal conductivity of air at 175°C the thermal conductivity of the wall is calculated. If the value of L is kept constant at 300 changing the value of D from 5 to 25 to 50 will give the required values for the parameter KL/D (1677, 333 and 167 respectively). Specifying a value of T_o equal to 315°C and T_∞ equal to 20°C a value of 570.0 for G is found (giving a height of 0.16m). Similar calculations provide the physical properties needed to calculate values for the interfacial temperature for the other two figures.

From figures A3.1, A3.2 and A3.3 the comparison between the two methods of calculating the temperature profile at the wall fluid interface is shown. The difference between the two sets of results is minimal when considering the assumptions that are made. The agreement between the two methods shows that the procedure used in chapter 3 provides a good method by which to calculate temperatures, and hence heat flows, for the conjugated system under consideration.

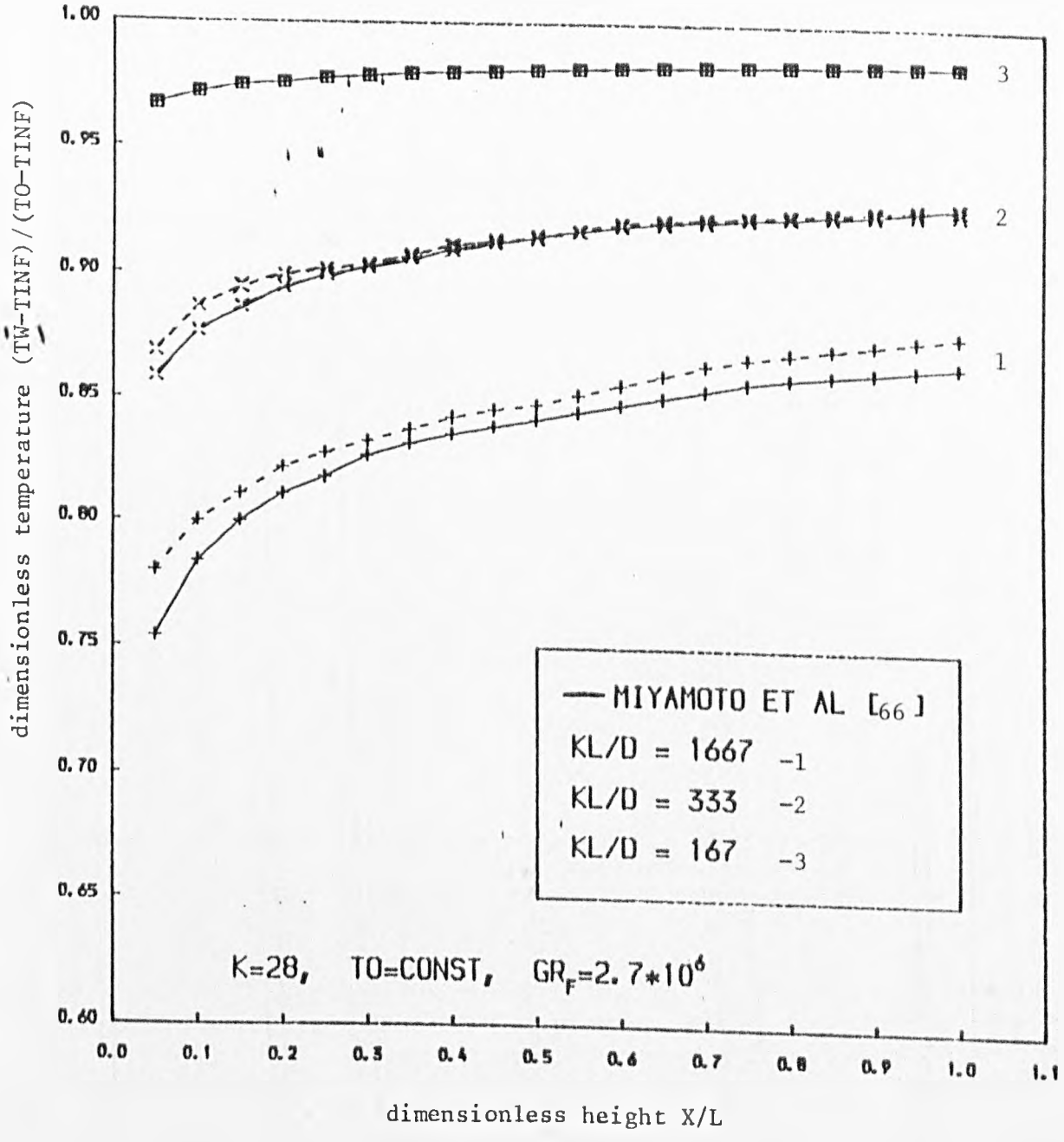

Fig. A3.1 Temperature Profile at Wall

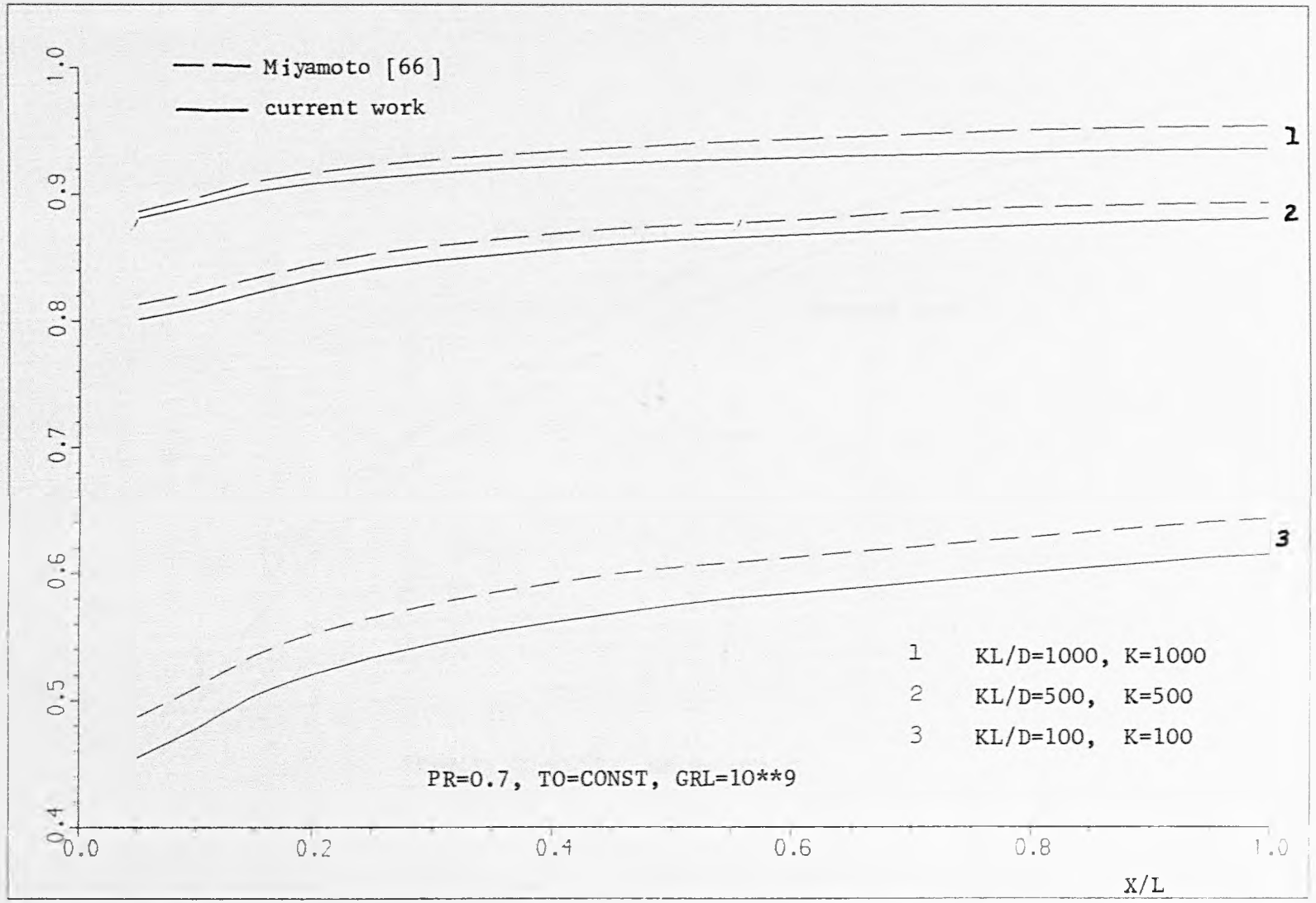

Fig.A3.2 Effect of Parameter KL/D on Wall Temperature

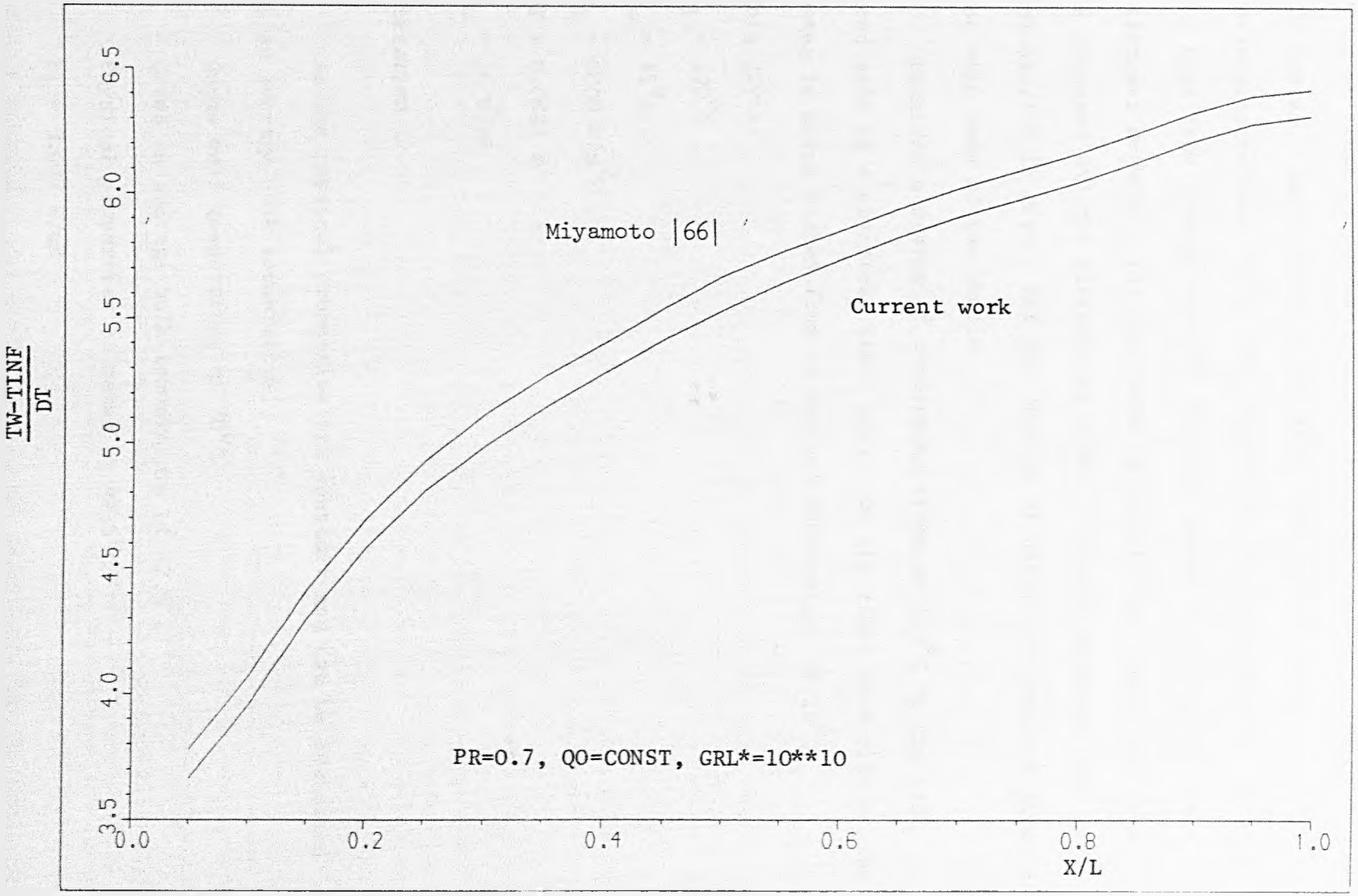

Fig.A3.3 Constant Heat Flow - Interfacial Temperature

APPENDIX 4

Sample of Iterative Calculation to Find the Heat Flow Through a Plane Wal

In chapter 3 a method is given by which the heat flow through a plane vertical wall can be calculated. Usually this heat flow would be found by considering the individual elements which make up the system. These elements are then combined by using a sum of resistance method. It is the purpose of this appendix to calculate the heat flow through exactly the same system but using the two different methods. The resultant calculated heat flows can then be compared and the differences noted. In this appendix only one calculation is given, but the results of other problems are given in the main body of the thesis.

Consider a system of condensing steam at $100^{o}C$ on the left hand side of a stainless steel wall. On the right hand side of the wall water is being heated from an ambient temperature of $15^{o}C$.

This gives:

$T_1 = 100^{o}C$

$T_\infty = 15^{o}C$

$\alpha_1 = 6000\ W/m^2K$

$WT = 0.0034\ m$

$k_w = 16\ W/mK$

Iteration 1

Assume physical properties are constant and can be evaluated at an average bulk temperature.

Guess wall temperature of $70^{o}C$

Gives an average bulk temperature of $42.5^{o}C$

Physical properties of water at $42.5^{o}C$:

$k_1 = 0.637\ W/mK$

$\rho = 990.7\ kg/m$

$Cp = 4.177\ kJ/kgK$

μ = 6.32*10 kg/ms

β = 1.23*10/^{o}C

Considering a height of 0.03m we first need to check that we are operating in the laminar region:

$$Gr_L = \frac{g\beta(T_o - T_\infty)L^3}{(\mu/\rho)^2} = 1.51*10^7$$

$$Pr = \frac{Cp\mu}{k_1} = 4.15$$

$$GrPr = Re = 6.28*10^7$$

Using the correlation for the Nusselt number given by Pohlhausen [11] the heat transfer coefficient on the fluid side can be found:

$$Nu = \frac{0.902\ Pr^{\frac{1}{2}}\ (Gr/4)^{\frac{1}{4}}}{(0.861+Pr)^{\frac{1}{4}}} = 54.16$$

$$a_1 = Nu\ \frac{k_1}{L} = 1134\ W/m^2K$$

By using the idea of the sum of resistances the following expression can be written down, so that the temperature required, that at the wall fluid interface, can be found.

$$T_w = T_\infty + \frac{\frac{1}{\alpha 1}}{\Sigma R}\ (T_1 - T_\infty)$$

From this the temperature at the wall/fluid interface is found to be 74.3^{o}C.

Iteration 2

Assume $T_w = 74^oC$

Average bulk temperature = 44.5^oC

Re-evaluating the physical properties and carrying the same procedure as before gives us a wall temperature of 73.9^oC, which is an acceptable difference between the initial guessed value and the calculated result.

Using 74^oC as the isothermal temperature of the wall we find:

$Gr_L = 1.69*10^7$

$Pr = 4.06$

$Nu = 55.33$

$\alpha_l = 1157\ W/m^2K$

The heat flux is given by:

$$\dot{q} = \alpha_l(T_w - T_\infty) = 1157(74-15)$$

$$\underline{\dot{q} = 68300\ W/m^2}$$

For exactly the same system but using the method proposed here the heat flux is found to be:

$$\underline{\dot{q} = 73700\ W/m^2}$$

This is a difference of 7.9% compared with the result found by the sum of resistance method.

APPENDIX 5

Change in Integral Boundary Layer Equations When Studying a Tapered Fin

For the tapered fin extra care must be taken in deriving the integral boundary layer equations. This is because the co-ordinate system in the fluid and in the fin will be different. Looking at figure A5.1 the diagram of the system is shown, which gives the axes in the fluid and in the fin. The boundary layer equations in the fluid will be the same if the new co-ordinate system is used, except that the acceleration due to gravity will be reduced to g.cosØ. The heat flow out of the fin, when given by the temperature gradient in the fluid, takes into account the slope of the fin surface. Writing a heat balance over an elemental height of the fin, the resulting equation is:

$$-k_s \frac{WT}{H} \frac{\partial T}{\partial x} = -k_s \frac{WT}{H} \times \frac{\partial^2 T}{\partial x^2} - \frac{2H}{\sqrt{H^2 + WT^2/4}} \frac{\partial T}{\partial y} \qquad \text{(A5.1)}$$

subject to the following boundary conditions:

$$\begin{aligned} &x=H \; ; \; -WT/2 < Y < WT/2 \\ &T_s = T_b \\ &x=H \; ; \; y=0 \\ &T_s > 0 \end{aligned} \qquad \text{(A5.2)}$$

As the momentum and heat balances in the fluid are identical to those given in chapter 4 (except for the change in the force due to gravity) they will not be given here and the reader is referred to equation 4.9 and 4.10 in the main text.

The numerical analysis itself must also be changed to account for the increase in length of the fin surface. Each step length is no longer the height of the fin divided by the number of intervals, as the height of the fin is the perpendicular height. Therefore, the stepsize is now $H/\cos\phi(N-1)$, where N is the number of nodes up the fin.

In calculating fin efficiencies the input data is supplied in terms of the height and the fin half angle, rather than the height and the thickness of the fin. Besides this difference the procedure to calculate the fin efficiencies is carried out in exactly the same way as with the rectangular fin.

The advantage of considering a tapered fin as opposed to a rectangular fin arises in the consideration of the fin tip conditions. When developing the theory of the rectangular fin, it was assumed that the fin tip was adiabatic. To ensure that this condition was met the fin thickness had to be kept very small compared with the fin height. This places an artificial limit on the geometry of fins available for calculations. For the tapered fin no such assumption need to be made at the fin tip, so allowing a solution procedure which is applicable to all tapered fins.

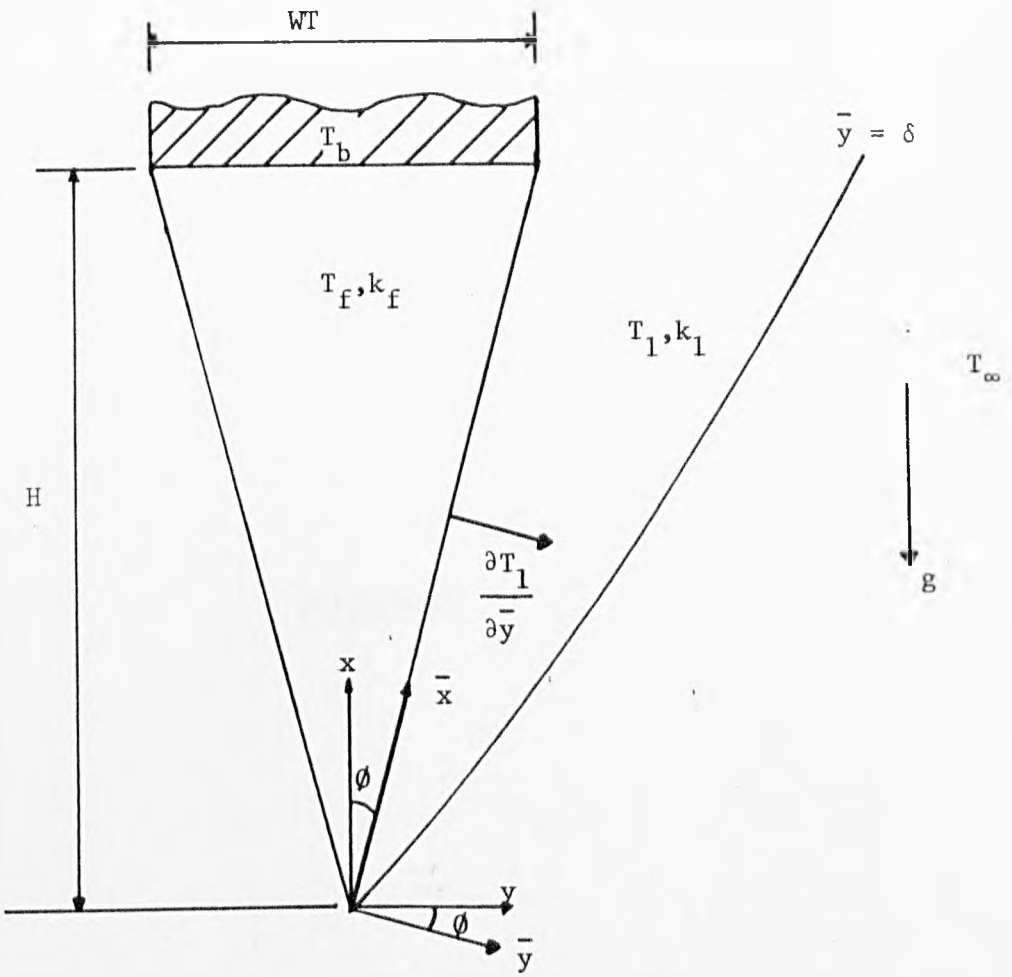

Fig. A5.1 Schematic diagram of tapered fin with co-ordinate system

REFERENCES

1. P.W. Wong, "Mass and Heat Transfer from Circular Finned Cylinders", JIHVE 34 1-28 (1966).

2. P.J. Heggs, P.R. Stones, "The Effects of Dimensions on Heat Flowrate Through Extended Surfaces", J. Heat Transfer, 102, 180-182 (1980).

3. D.R. Harper, W.B. Brown, "Mathematical Equations for Heat Conduction in the Fin of Air-Cooled Engines", NACA Report 158 (1922).

4. K.A. Gardner, "Efficiency of Extended Surfaces", Trans. A.S.M.E. 67, 621-631 (1945).

5. M. Manzoor, "Heat Flow Through Extended Surface Heat Exchangers", Thesis, University of Leeds, (1982).

6. I. Newton, Phil. Trans. Roy. Soc. (London) 22, 824 (1701).

7. L. Graetz, "Uber die Warmeleitungsfahigkeit von Flussigkeiten", Ann. Phys. Chem, 18, 79-99 (1883).

8. L. Prandtl, "Uber Flussigkeitsbeuregung bei sehr kleiner reibung", Proc. 3rd Int. Math. Congr. Heidelberg, (1904), also NACA TM 452 (1922).

9. T. Von Karman, "Uber laminare und turbulente Reibung", N.A.C.A. TM 1092 (1946).

10. E. Schmidt, W. Beckmann, "Das Temperatur-und Geschwindigkeitsfeld von einer warme abgebenden senkrechten platte bei naturlicher konvektion", Forsch Gebeite Ingenieurw , 1, 391 (1930).

284

11. E. Pohlhausen, "Der Warmeaustausch zurischen festen Korpern und Flussigkeiten mit kleiner Reibung und keleiner Warmeleitung", ZAMM 1, 115 (1921).

12. Z.H. Qurshi, B. Gebhart, "Transition and Transport in a Buoyancy Driven Flow in Water Adjacent to a Uniform Flux Surface", Int. J. Heat Mass Transfer, 21, 1467-1479 (1978).

13. T. Fujii et al, "Natural Convection Heat Transfer From a Vertical Plate to Non-Newtonian Sutterby Fluid", Int. Chem. Eng., 17, 729-734 (1972).

14. E.R.G. Eckert, T.F. Irving Jr., J.T. Yan, "Local laminar heat transfer in wedge-shaped passages", Trans. A.S.M.E., 80, p.148 (1958).

15. S.M. Marco, L.S. Han, "A Note on Limiting Nusselt Number in Ducts with Constant Temperature Gradient by Analogy to Thin Plate Theory", Trans. A.S.M.E., 77, 68ff, (1955).

16. L.S. Han, S.G. Lefkowitz, "Constant Cross-Section Fin Efficiencies for Non-Uniform Surface Heat Transfer Coefficient", A.S.M.E., paper 60-WA-41 (1960).

17. S.H. Chen, G.L. Zyskowski, "Steady State Heat Conduction in a Straight Fin with Variable Film Coefficient", A.S.M.E., paper 63-HT-12 (1964).

18. A. Bejan, "Convection Heat Transfer", John Wiley and Sons, New York (1984), p. 32.

19. R. Cheesewright, E. Derokipiotis, "Velocity Measurements in a Natural Convection Boundary Layer", Paper NC31, 7th Int. Heat Transfer Conf., Munich (1982).

20. A. Bejan "Convection Heat Transfer", John Wiley and Sons, New York (1984), p.112.

21. H.B. Squire, Integral Solution published in S. Goldstein ed, "Modern Developments in Fluid Dynamics", Vol. II, Dover, New York, 641-643 (1965).

22. E.R.G. Eckert, T. Jackson, NACA TR no. 1015 (1951).

23. E.R.G. Eckert, "Engineering Relations for Heat Transfer and Friction in High Velocity Laminar and Turbulent Boundary Layer Flow Over Surfaces with Constant Pressure and Temperature", Trans. A.S.M.E. 78, 1273-1283 (1956).

24. K.T. Yang, "Possible Similarity Solutions for Free Convection on Vertical Plates and Cylinders", J. Appl. Mech, 27, 230-236, (1960).

25. J.H. Merkin, "Free Convection Boundary Layer on an Isothermal Horizontal Cylinder", Trans. A.S.M.E. paper 76-HT-16, (1976).

26. E. Schmidt, Z ges Kalte-hd 35, 213 (1928).

27. A. Bejan, "Convection Heat Transfer", John Wiley and Sons, New York (1984), p. 125.

28. S. Ostrach, "An Analysis of Laminar Free Convection Flow and Heat Transfer About a Flat Plate Parallel to the Direction of the Generating Body Force", NACA TN 2635 (1952).

29. F.J. Suriano, K.T. Yang, J.A. Donlon. "Laminar Free Convection Along a Vertical Plate at Extremely Small Grashof Numbers", Int. J. Heat Mass Transfer, 8, 815-831 (1965).

30. K. Kishinami, N. Seki, "Natural Convective Heat Transfer on an Unheated Vertical Plate Attached to an Upstream Isothermal Plate", J. Heat Transfer, 105, 759 (1983).

31. S. Suriano, K.T. Yang, "Laminar Free Convection About Vertical and Horizontal Plates at Small and Moderate Grashof Numbers", Int. J. Heat Mass Transfer, 11, 473-490 (1960).

32. T.Y. Na, I. Pop, "Free Convection Flow Past a Vertical Flat Plate Embedded in a Saturated Porous Medium", Int. J. Engng. Sci. 21, 517 (1983).

33. R. Viskanta, D.W. Lankford, "Coupling of Heat Transfer Between Two Natural Convection Systems Separated by a Vertical Wall", Int. J. Heat Mass Transfer, 24, 1171-1177, (1981).

34. K.E. Hassan, S.A. Mohamed, "Natural Convection From Isothermal Flat Surfaces", Int. J. Heat Mass Transfer, 13, 1874-1886 (1970).

35. G.S.H. Lock, J.C. Gunn, "Laminar Free Convection From a Downward Projecting Fin", J. Heat Transfer, 90, 63-70, (1968).

36. S.S. Kwon, T.M. Kuehn, "Conjugate Natural Convection Heat Transfer From a Horizontal Cylinder with a Long Vertical Longitudinal Fin", Numerical Heat Transfer, 6, 85-102 (1983).

37. A.K. Tolpadi, T.H. Kuehn, "Conjugate Three-Dimensional Natural Convection Heat Transfer From a Horizontal Cylinder with Long Transverse Plate Fins", Numerical Heat Transfer, 7, 319, (1984).

38. H. Darcy, "Les fontaines publiques de la ville de Dijon", Dalmont, Paris (1856).

39. P. Cheng, K.L. Yueng, K.H. Lau, "Numerical Solutions for Steady Free Convection in Confined Geothermal Reservoirs", Proc. 1975 Int. Seminar on Future Energy Production eds. N. Afgen, J.P. Hartnett, 429-448, Hemisphere Publishing Co. (1975).

40. P. Cheng, "Convective Heat Transfer in Porous Layers by Integral Methods" Letters in Heat and Mass Transfer, 5, 243-252 (1978).

41. P. Cheng, W.J. Minkowycz, "Free Convection About a Vertical Plate Embedded in a Porous Medium with Applications to Heat Transfer From A Dike", J. Geophysical Research, 82, 2040-2044 (1977).

42. P. Cheng, "Constant Surface Heat Flux Solutions for Porous Layer Flows", Letters in Heat and Mass Transfer, 4, 119-127 (1977).

43. G.H. Evans, O.A. Plumb, "Natural Convection from a Vertical Isothermal Surface Imbedded in a Saturated Porous Medium", AIAA-ASME Thermophysics and Heat Transfer Conf. Paper 78-HT-55, Palo Alto. Calif. (1978).

44. O.A. Plumb, J.C. Heunefeld, "Non Darcy Natural Convection from Heated Surfaces in Saturated Porous Media", Int. J. Heat. Mass Transfer, 24, 765-768 (1981).

45. J. Bear, "Dynamics of Fluids in Porous Media", An Elseiner, New York (1972).

46. J.Y. Liu, W.J. Minkowycz, P. Cheng, "Conjugate Mixed Convection Heat Transfer Analysis of a Plate Fin Embedded in a Porous Medium", Numerical Heat Transfer, 9, 575-590, (1986).

47. J.Y. Liu, W.J. Minkowycz, P. Cheng, "Conjugated Mixed Convection Conduction Heat Transfer Along a Cylindrical Fin in a Porous Medium", Int. J. Heat Mass Transfer, 29, 769-795, (1988).

48. I. Pop, et al. "Conjugate Heat Transfer from a Downward Projecting Fin Immersed in a Porous Medium", 8th Int. Heat Transfer Conf. San Francisco, 2635-2640, (1986).

49. H. Schuh, "The Solution of the Laminar Boundary Layer Equations for the Flat Plate for Velocity and Temperature Fields for Variable Physical Properties and for the Diffusion Field at High Concentration", NACA TM 1275 (1950).

50. E. Seider, G. Tate, "Heat Transfer and Pressure Drop of Liquids in Tubes", Ind. Engng. Chem. 28, 1429-1436 (1936).

51. C.B. Cohen, E. Reshotker, "Similar Solutions for the Compressible Laminar Boundary Layer with Heat Transfer and Pressure Gradient", NACA Report 1293 (1956).

52. T. Hara, "The Free Convection Flow About a Heated Vertical Plate in Air", Trans. Japan Soc. Mech. Engrs. 20, 517-520 (1959).

53. E.M. Sparrow, J.L. Gregg, "The Variable Fluid Property Problem in Free Convection", Trans. A.S.M.E. 80, 869-886 (1958).

54. W.J. Minkowycz, E.M. Sparrow, "Free Convection Heat Transfer to Steam Under Variable Property Conditions", Int. J. Heat Mass Transfer, 9, 1145-1147 (1966).

55. V.P. Carey, J.C. Mollendorf, "Variable Viscosity Effects in Several Natural Convection Flows", Int. J. Heat Mass Transfer, 23, 995-1091 (1980).

56. A.M. Clausing, S.N. Kempka, "The Influence of Property Variations on Natural Convection From Vertical Surfaces, "Trans. ASME, J. Heat Transfer, 103, 609-612 (1981).

57. A.M. Clausing, "Natural Convection Correlations for Vertical Surfaces including Influences of Variable Physical Properties", Trans. ASME, J. Heat Transfer, 105, 138-143 (1983).

58. A. Bejan, "Convection Heat Transfer", John Wiley and Sons, New York, (1984), p. 110.

59. A.A. Hayday, D.A. Bowles, R.A. McGraw, "Free Convection from a Vertical Plate with Step Discontinuities in Surface Temperature", J. Heat Transfer Trans. ASME, 89, 244-256 (1967).

60. E.M. Sparrow, "Laminar Free Convection on a Vertical Plate with Prescribed Non-Uniform Heat Flux or Prescribed Non-Uniform Temperature, N.A.C.A. TN 3500 (1955).

61. S.B. Sutton, "A Study of Free Convection From a Vertical Plate with Sinusoidal Temperature Distribution", AIAA paper no. 71-988.

62. R. Siegel, "An Analysis of Turbulent and Free Convection from a Smooth Vertical Plate with Uniform Heat Dissipation per Unit Surface Area", G.E. Report R54, GL 89 (1954).

63. R. Siegel, "An Analysis of Turbulent and Free Convection from a Smooth Vertical Plate with Uniform Heat Dissipation Per Unit Surface Area", G.E. Report R54, GL89 (1954).

64. M. Finston, "Free Convection Past a Vertical Plate", Z. Agnew Math. Phys. 7, 527-529 (1956).

65. T.T. Kao, G.A. Domoto, H.G. Elrod, "Free Convection Along a Non-Isothermal Vertical Flat Plate", J. Heat Transfer, 99, 72-78, (1977).

66. M. Miyamoto et al. "Effects of Axial Conduction in a Vertical Flat Plate on Free Convection Heat Transfer", Int. J. Heat Mass Transfer, 23, 1545-1553 (1980).

67. M.D. Kelleher, K.T. Yang, "A Steady Conjugate Heat Transfer Problem With Conduction and Free Convection", Appl. Sci. Res., 17, 249-269 (1967).

68. G.S.H. Lock, R.S. Ko, "Coupling Through a Wall Between Two Free Convection Systems", Int. J. Heat Mass Transfer, 16, 2087-2096 (1973).

69. R. Anderson, A. Bejan, "Natural Convection on Both Sides of a Vertical Wall Separating Fluids at Different Temperatures", J. Heat Transfer Trans. ASME, 102, 630-635 (1980).

70. E.M. Sparrow, J.L. Gregg, "Laminar Free Convection from a Vertical Plate with Uniform Surface Heat Flux", Trans. ASME, 78, 435-440 (1956).

71. J. Gryzcigardis, "Natural Convection from a Vertical Flat Plate in the Low Grashof Number Range", Int. J. Heat Mass Transfer, 14, 162-165 (1971).

72. W.M. Murray, J. Applied Mechanics, 5, A78-80, (1938).

73. F. Harahap, H.N. McManus, Jr. "Natural Convection Heat Transfer from Horizontal Rectangular Fin Arrays", J. Heat Transfer, 89, 32-38 (1967).

74. C.D. Jones, L.F. Smith, "Optimum Arrangement of Rectangular Fins on Horizontal Surfaces for Free Convection Heat Transfer", J. Heat Transfer, 92, 6-10 (1970).

75. M. Miyamoto et al. "Free Convection Heat Transfer from Vertical and Horizontal Short Plates", Int. J. Heat Mass Transfer, 28, 1733-1745 (1985).

76. T. Schulenberg, "Natural Convection Heat Transfer Below Downward Facing Horizontal Surfaces", Int. J. Heat Mass Transfer, 28, 467-477 (1985).

77. K. Stewartson, "On Free Convection From a Horizontal Plate", Z. Agnew, Math. Phys. 9, 276-282 (1958).

78. N.N. Gill, D.W. Zeh, F. Del Casal, Z. Agnew Math Phys. 16, 539 (1965).

79. F.Krieth, "Principles of Heat Transfer", Harper and Row, New York, (1970), p. 15.

80. E.J. Le Fevre "Laminar Free Convection From a Vertical Plane Surface", 9th International Congress on Applied Mechanics, Brussels, paper H68, (1956).

81. B.R. Rich, "An Investigation of Heat Transfer From an Inclined Flat Plate in Free Convection", Trans. ASME, 75, 489-499, (1953).

82. F.S. Bayley, J.M. Owen, A.B. Turner, "Heat Transfer", Nelson, London, p. 39 (1972).

83. B. Gebhart, J. Mollendorf, "Viscous Dissipation in External Natural Convection Flows", J. Fluid Mechanics, 38 (97-107), (1969).

84. B. Sunden, "A Numerical Investigation of Coupled Conduction-Mixed Convection for Rectangular Fins", Proc. Third Int. Conf. on Num. Methods in Laminar and Turbulent Flow", Pineridge Press, 809-819, (1988).

85. B. Sunden, "Conjugate Mixed Convection Heat Transfer From a Vertical Rectangular Fin", Int. Comm. Heat Mass Transfer, 10, 267-276, (1983).

86. I.R. Lloyd, B.M. Sparrow, "Combined Forced and Free Convection Flow on Vertical Surfaces", Int. J. Heat Mass Transfer, 13, 434-438 (1970).

87. R. Anderson, A. Bejan, "Heat Transfer Through Single and Double Vertical Walls in Natural Convection: theory and experiment", Int. J. Heat Mass Transfer, 24, 1611-1670, (1984).

88. C.T. Hsu, P. Cheng, "The Brinkmann Model for Natural Convection About a Semi-Infinite Vertical Flat Plate in a Porous Medium", Int. J. Heat Mass Transfer, 28, 683-697 (1985).

89. P. Cheng, C.L. Ali, "An Experimental Investigation of Free Convection About a Heated Inclined Surface in a Porous Medium", ASME, paper 81-HT-85.

90. S. Mcriet al, "Performance of Counterflow, Parallel Plate Heat Exchangers Under Laminar Flow Conditions", Heat Transfer Engng. 2, 28-38 (1980).

91. E.M. Sparrow, M. Faghri, "Fluid to Fluid Conjugate Heat Transfer for a Vertical Pipe Internal Forced and External Natural Convection", J. Heat Transfer, 102, 402-407, (1980).

92. S. Mori et al "Conjugate Heat Transfer Between Internal Forced and External Natural Convections with Wall Conduction", Canadian J. of Chem. Eng. 64, 216-222 (1986).

93. S.P. Frankel, "Convergence Rates of Iterative Treatments of Partial Differential Equations", Maths Tables Aids Comput. 4, 65-75 (1950).

Paper Presented at I.Chem.E. 11th Annual Research Meeting, Bath, 1984

NATURAL CONVECTION LAMINAR FLOW WITH HEAT TRANSFER THROUGH A VERTICAL PLANE WALL

by C.J.Hoogendoorn, D.B.Ingham and D.A.Gardener,
Department of Chemical Engineering, The University, Leeds LS2 9JT.

1. Introduction

Studies into natural convection heat transfer from a vertical hot plate have been carried out since 1881. In 1930, after the work of E.Schmidt and W.Beckmann [1], E. Pohlhausen showed that, by the introduction of a stream function, the resulting partial differential equation for the stream function could be reduced to an ordinary differential equation by suitable transformations [2]. This equation can then be used to give two further ordinary differential equations which, on solving, allow the temperature and velocity profiles in the boundary layer to be found.

An integral method approximating the exact solution found by Pohlhausen and Ostrach [3] is used for comparison with the results calculated in this investigation.

A wall is heated, on one side, by steam, whilst on the opposite side there is a colder fluid (figure 1). The calculations carried out by Pohlhausen and Ostrach were based on an isothermal plate heating the surrounding fluid. Resistance to the heat flow is now due to the composite effect of the heat transfer coefficient on the steam side, the thermal resistivity of the wall, as well as the resistance on the fluid side, the latter being the only resistance normally considered.

2. Temperature and Velocity Profiles

As in the integral approximation method the temperature profile is assumed to be parabolic:

$$T_f - T_\infty = a\,y + b\,y^2 + c \qquad (1)$$

Boundary conditions:

$$-k_f \frac{\partial T_f}{\partial y} = U\,(T_1 - T_f); \quad y = 0, \quad 0 \leq x \leq \infty \qquad (2)$$

$$T_f = T_\infty \quad ; \quad y = \delta \quad , \quad 0 \leq x \leq \infty \qquad (3)$$

$$\frac{\partial T_f}{\partial y} = 0 \qquad (4)$$

This gives a solution for the temperature profile of:

$$\frac{T_f - T_\infty}{T_1 - T_\infty} = \frac{(y - \delta)^2}{\left(\frac{2k_f}{U} + \delta\right)\delta} \tag{5}$$

The expression for the velocity profile is taken to be the same as in the integral method, that is:

$$v = \Gamma \frac{y}{\delta} \left(1 - \frac{y}{\delta}\right)^2 \tag{6}$$

3. Solution

By carrying out momentum and energy balances over an element across the wall and boundary layer and substituting equations (5) and (6) into the resulting equations gives:

$$\frac{1}{105} \frac{d}{dx} (\Gamma^2 \delta) = \frac{g_x \beta (T_1 - T_\infty) \delta^2}{3\left(\frac{2k_f}{U} + \delta\right)} \quad \to \frac{\Gamma}{\delta} \tag{7}$$

and

$$\frac{1}{30} \frac{d}{dx} \left(\frac{\Gamma \delta^2}{\frac{2k_f}{U} + \delta}\right) = \frac{2\alpha}{\frac{2k_f}{U} + \delta} \tag{8}$$

These equations reduce to those found in the classical method when the te $\frac{2k_f}{U}$ is set equal to zero. Hence when $\frac{2k_f}{U} \ll \delta$, the equations (7) and (8) can be solved as in the classical method.

When $\frac{2k_f}{U} \gg \delta$ the equations can be solved analytically.

This condition, however, is rarely satisfied (except at the base of the wall where $x \to 0$ and consequently $\delta \to 0$).

This investigation is therefore concerned with the case when $\frac{2k_f}{U}$ is of th same order of magnitude as δ .

Under these conditions a solution must be obtained numerically. To facilitate analysis the equations are made non-dimensional:

$$\frac{1}{105} \frac{d}{dX} (V^2 \Delta) = \frac{g_x \beta (T_1 - T_\infty) b^3}{3\alpha^2} \frac{\Delta^2}{1+\Delta} - \frac{\nu}{\alpha} \frac{V}{\Delta} \tag{9}$$

$$\frac{1}{30} \frac{d}{dX} \left(\frac{V\Delta^2}{1+\Delta}\right) = \frac{2}{1+\Delta} \tag{10}$$

Equations (9) and (10) can be reduced to the following coupled differential equations:

$$\frac{d\Delta}{dX} = \frac{1+\Delta}{\Delta V(3+\Delta)}(105Pr + 120) - 105\,Gr_x \frac{\Delta^2}{V^2(3+\Delta)} \qquad (11)$$

$$\frac{dV}{dX} = 105\,Gr_x \frac{\Delta(2+\Delta)}{V(3+\Delta)(1+\Delta)} - \frac{1}{\Delta^2(3+\Delta)}(105Pr(2+\Delta)+60(1+\Delta)) \qquad (12)$$

The solution of these two equations gives the thickness of the boundary layer; and the velocity profile and temperature profile using equations (6) and (5) respectively. The temperature profile of the wall can be found by finding the fluid temperature at y = 0.

The heat flow through the system is given by:

$$\left(\frac{q}{A}\right) = \frac{2k_f . \Delta T}{K + \delta} \qquad (13)$$

4. Results

Equations (11), (12) and (13) have been solved for a number of systems to find the effect of changing:

(a) the fluid being heated;

(b) the heat transfer coefficient on the steam side;

(c) the thickness of the wall.

Changing (c) has very little effect, as the resistance to the heat flow through the wall is negligible compared to that on the fluid side (and sometimes the steam side), so can be ignored.

The greatest deviations from the classical results appear when the resistance to the flow of heat due to the steam side are not negligible compared with the fluid, which is given when the conditions $\frac{2k_f}{U} \ll \delta$ is not met. This can be a result of decreasing (b) to a small value and/or changing the fluid from a gas (high resistance to heat flow as k_f is small) to a liquid (smaller resistance to heat flow as k_f is relatively large).

Figure (2) shows the velocity profile, boundary layer thickness, and a comparison between the classical and numerical heat flows when the fluid is air and there is a high heat transfer coefficient on the steam side.

Figure (3) again has air as the fluid being heated but now there is a low heat transfer coefficient on the steam side.

Figure (4) gives the same curves but for water and a high heat transfer coefficient.

5. Conclusions

Using the classical approach to work out the heat flow through a system appears to be satisfactory when the resistance to that heat flow is on the opposite side from the heating medium. When the resistance to heat flow is equally distributed across the whole system the investigation carried out would indicate a need to develop another approach. At the present the method used is fairly crude and could not be used for quantitative analysis, but it appears to give a guide to when a more sophisticated model is needed.

6. Future Work

The calculations have used a simple one-dimensional heat flow through the system, which will not be true, especially in the case of a liquid.

Average physical properties have been assumed for the fluid. This assumption could be relaxed and the change in the velocity and temperature profiles could be studied as was done by T. Hara [4] when he used a temperature dependent viscosity when calculating these profiles in laminar boundary layers in natural flow.

References

1. Schmidt, E and W. Beckman, "Das Temperatur-und Geschwindigkeitsfeld von einer Warme abgebenden, Senkrechten Platte bei natürlicher Konvektion". Forsch. Ing.-Wes 1, 391, (1930).

2. Polhausen, E., "Der Warmeaustausch zwischen festen Korpern und Flüssigkeiten mit kleiner Reibung und kleiner Warmeleitung", ZAMM, 1, 115, (1921).

3. Ostrach: NACA. T.R. No.1111 (1953).

4. Hara, T. "Heat transfer by laminar free convection about a vertical flat plate with large temperature difference"., Bull. J.S.M.E., 1, 251-254, (1958).

Nomenclature

k = thermal conductivity

g_x = gravitational const. (in x-direction)

Gr_β = modified Grasshof No. $\left(\frac{g_x \beta (T_1 - T_\infty) \kappa^3}{3\alpha^2}\right)$

h = heat transfer coefficient on steam side

Pr = Prandtl No. $\left(\frac{\nu}{\alpha}\right)$

$\frac{q}{A}$ = heat flux

T = temperature

U = overall heat transfer coefficient $\left(\frac{1}{\frac{WT}{K_w} + \frac{1}{h}}\right)$

v = velocity

V = dimensionless velocity term $\left(\frac{k}{\alpha}\,\frac{\Gamma}{\nu}\right)$

WT = thickness of wall

x = height up wall

X = dimensionless height $\left(\frac{x}{k}\right)$

y = distance from wall on fluid side

α = thermal diffusivity

β = coefficient of thermal expansion

δ = boundary layer thickness

Δ = dimensionless boundary layer thickness $\left(\frac{\delta}{k}\right)$

ν = kinematic viscosity

k = ratio of fluid thermal conductivity to overall h.t.c. $\left(\frac{2k_f}{U}\right)$

Γ = const. with dimensions of velocity (equ. (6))

ΔT = $T_1 - T_\infty$

Subscripts

1 steam side

f fluid

w wall

∞ bulk

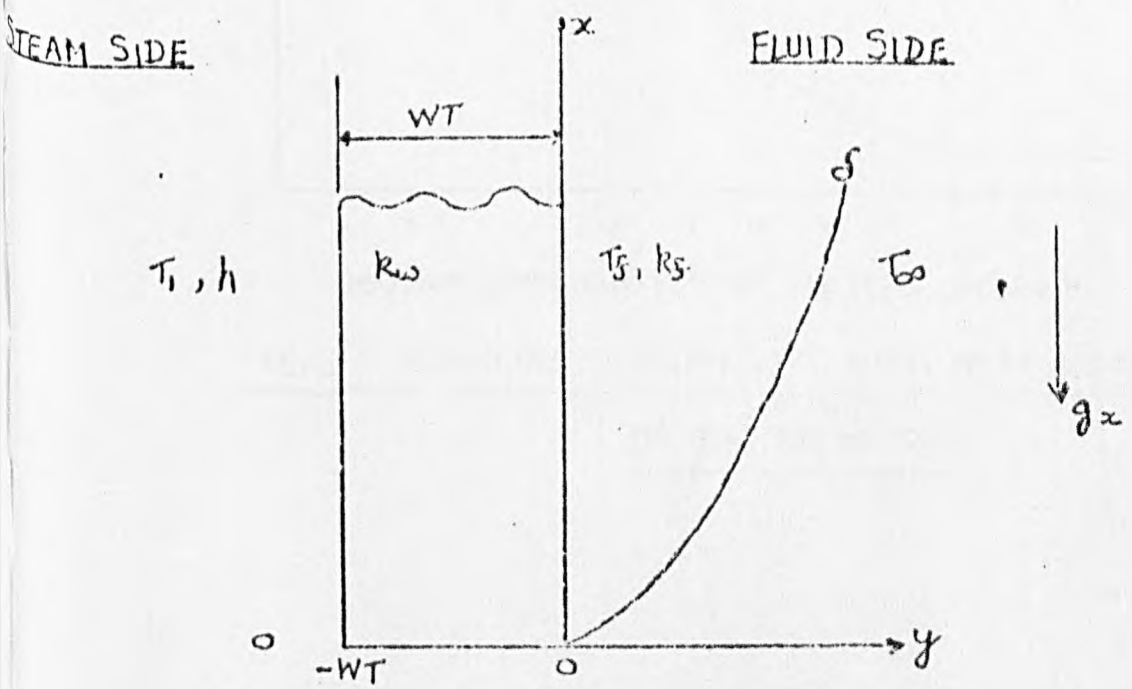

FIG. 1 SCHEMATIC DIAGRAM OF THE SYSTEM INVESTIGATED

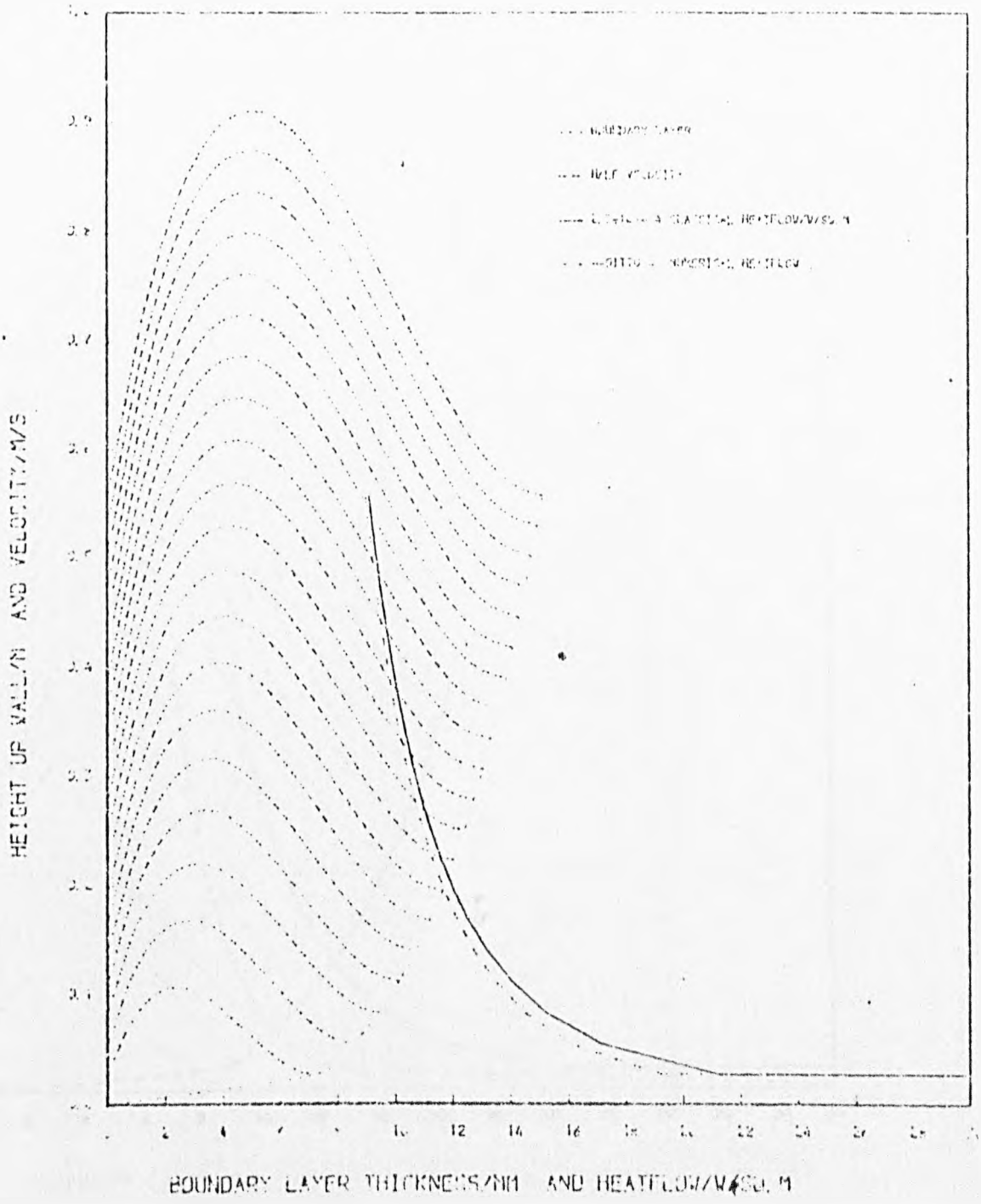

FIG. 2 STEAM/AIR SYSTEM WITH HIGH HEAT TRANSFER COEFFICIENT ON THE STEAM SIDE

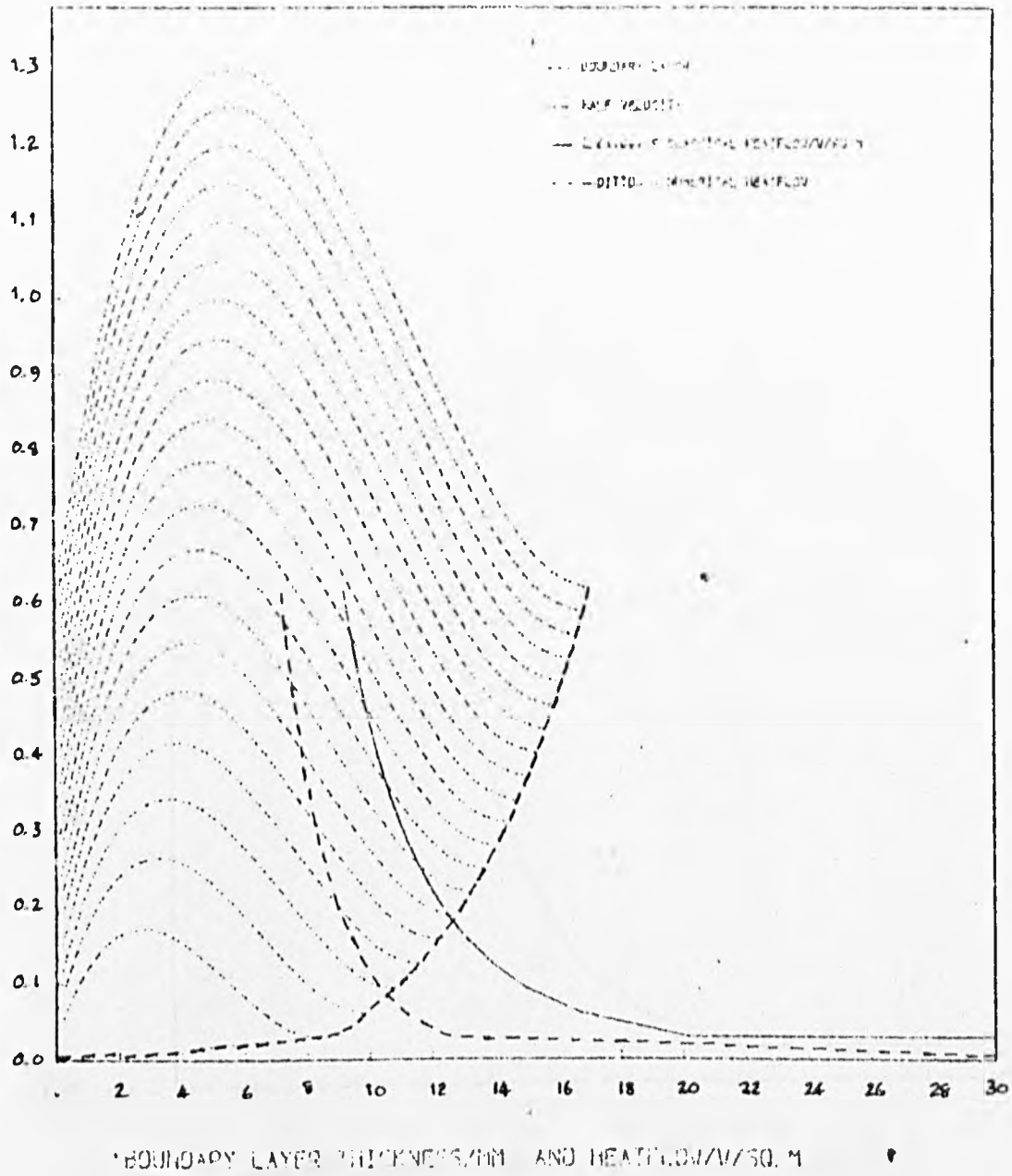

FIG. 5 STEAM/AIR SYSTEM WITH LOW HEAT TRANSFER COEFFICIENT ON THE STEAM SIDE

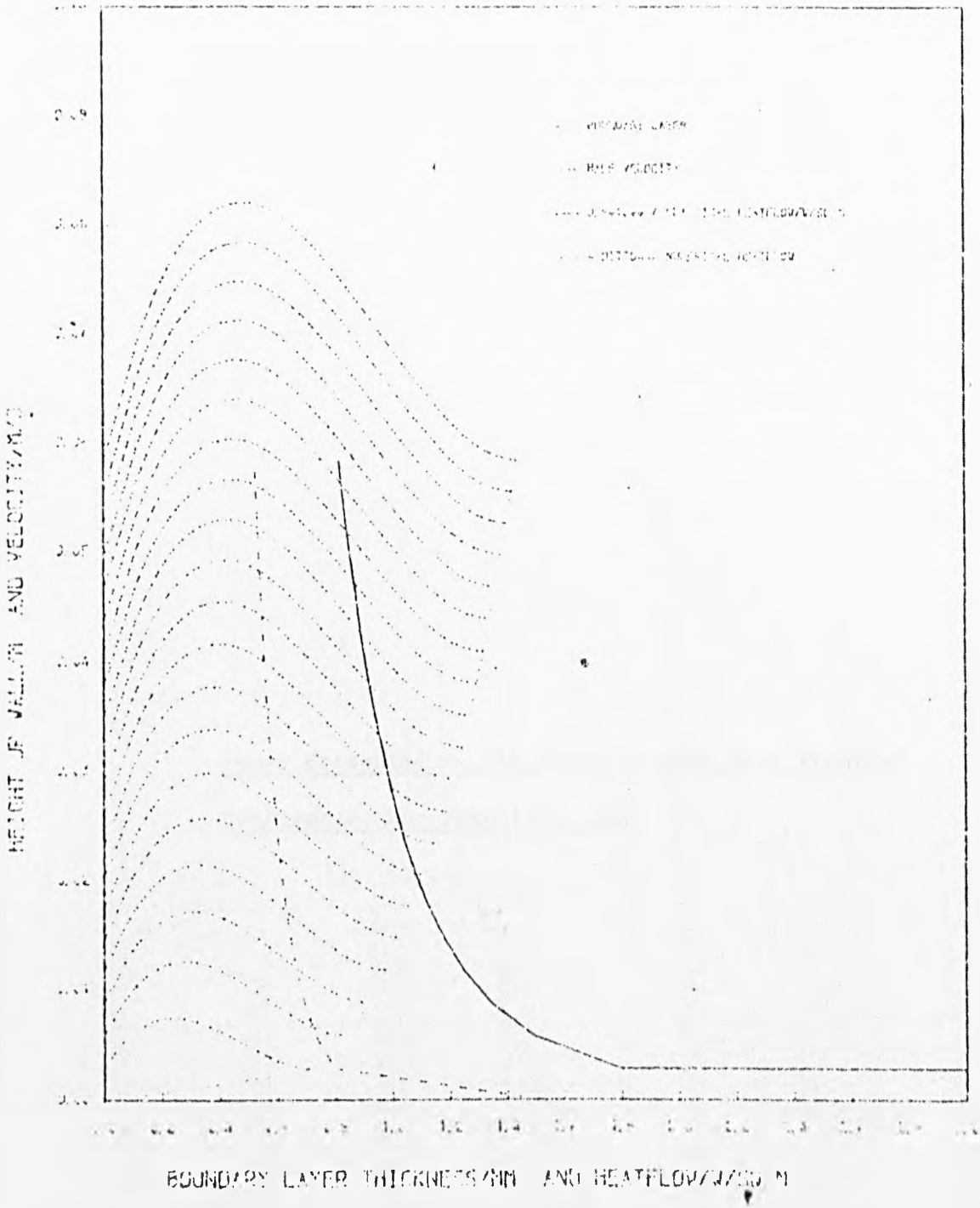

FIG. 4 STEAM/WATER SYSTEM WITH HIGH HEAT TRANSFER COEFFICIENT ON THE STEAM SIDE

Paper Presented at 8th International Heat Transfer Conference, San Francisco, 1986

CONJUGATE HEAT TRANSFER FROM A DOWNWARD PROJECTING FIN IMMERSED IN A POROUS MEDIUM

I. POP, D. B. INGHAM*, P. J. HEGGS** and D. GARDNER**

Faculty of Mathematics, University of Cluj, Romania.
*Department of Applied Mathematical Studies, University of Leeds, England.
**Department of Chemical Engineering, University of Leeds, England.

ABSTRACT

The problem in which a rectangular fin, which is embedded in a saturated porous medium, with only the fin base temperature and ambient fluid temperature prescribed is investigated. Both the mixed and natural convection situations are considered and also the case where the fluid flow opposes the natural flow due to buoyancy. The governing boundary layer equations are expressed in the variables appropriate to the natural convection from a fin at a constant temperature, and the resulting equations are discretised using central differences throughout. A very accurate solution is obtained using the Richardson extrapolation method. It is found that flow reversals occur for $-0.98 < Pe/Ri < 0$ when CCP = 1.0. Increasing the forced convection increases the heat flow from the system whilst surrounding the fin with a saturated porous medium reduces the heat flow as compared with a fin immersed in a free fluid. These results are indicated by a reduction and an increase in the temperature of the fin respectively.

INTRODUCTION

The application and theory of heat transfer by natural convection from finned bodies has now been studied for over half a century, see for example Harper and Brown [1]. However, the conjugate nature resulting from the conduction in the fin and natural convection from the surface of the fin has only been investigated more recently, Lock and Gunn [2]. In a porous medium Cheng and Minkowycz [3] studied the transfer of heat by natural convection from a vertical wall. However no calculations have yet been published in which the effect of conjugate heat transfer from a downward projecting fin in a porous medium has been considered. This is a very important problem in such applications as the extraction of geothermal energy and in the design of insulating systems for energy conservation. The present work attempts to fill this gap by using an improved method of an already well established numerical procedure in solving conjugate mixed convection from a downward projecting fin [4].

Sunden [4] investigated the problem of coupled conduction-mixed convection for rectangular fins. He writes the governing set of parabolic differential equations in finite difference form which he solves using an iterative technique.

Anderson and Bejan [5, 6] have investigated the conjugate heat transfer through an impermeable wall in both the porous medium and the free fluid problem. However, these solutions are only applicable to symmetrical problems in which the Oseen linearization can be used.

Cheng and Minkowycz [3] and Hsu and Cheng [7] consider the heat transfer from a semi-infinite vertical plate which is maintained at a temperature T_w, which is given by,

$$T_w = T_\infty + Ax^\lambda$$

where x is the distance from the leading edge of the plate. Cheng and Minkowycz [3] consider the situation when the fluid may be approximated by the Darcy law whilst Hsu and Cheng [7] use the Brinkman model.

In the present paper we investigate the mixed and free convection from a vertical rectangular fin which extends from a plane wall which is maintained at a constant temperature. Since the temperature of the fin is not known a priori it is necessary to solve the conjugate convection and conduction problem. It is exactly this problem that Sunden solves in the non porous medium. However, Sunden discretises the governing partial differential equations when expressed in scaled cartesian coordinates. Since the boundary layer has zero thickness at the tip of the fin then such a discretisation results in very few mesh points within the boundary layer near the tip of the fin. Hence the solution in this vicinity will be extremely inaccurate. Further since the governing equations are parabolic these inaccuracies are transmitted along the full length of the fin.

In the present paper we use the natural convection similarity variables in order to transform the boundary layer equations into their natural coordinates η and ξ. This choice of variables then allows us to solve both the mixed and natural convection problems with the same basic formulation. This contrasts with the situation in a non porous medium where this is not possible. This formulation has several advantages over that proposed by Sunden [4] - in addition to the increased accuracy due to the location of the mesh points it is easy

to discretise the governing equations using a second order accurate solution everywhere within the domain of integration.

In order to check the solution procedure solutions are first obtained for the same values of the parameters as used by Sunden [4]. The boundary layer equations for the plate fin embedded in a saturated porous medium are solved using the same procedure as for the free fluid situation.

This problem has been solved when the form of the temperature profile is prescribed by Hsu and Cheng [7] using the Brinkman model for the porous medium so that the no slip boundary condition at the wall can be enforced. In this work they give the condition under which the no slip condition can be neglected and this condition is tested here in order to confirm the validity of the present solutions.

THEORY

We consider a rectangular fin of thickness b and length L with a fin base temperature T_b placed in a fluid stream U_∞ as shown in figure 1.

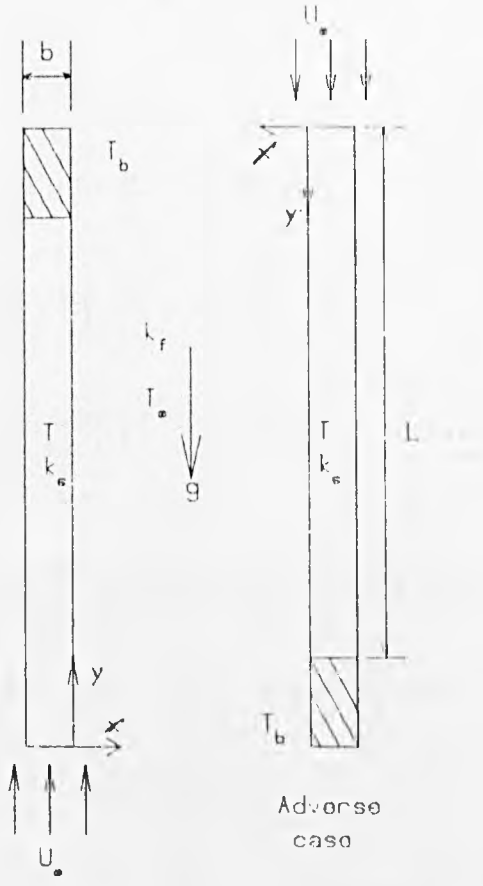

Figure 1 The flow model and coordinate system

The thermal conductivity of the fin is k_s and that of the fluid is k_f. We shall consider the two cases when the gravity force both assists and opposes the forced flow. With the coordinate system as shown in figure 1 the governing equations to be solved are identical in the two cases except for a change in sign in the momentum equation, i.e. the direction of the gravity term in the x' direction.

In practice the fin thickness, b, in relation to the height, L, is small and we shall assume it to be sufficiently small for the fin tip to be considered adiabatic. However, the height of the fin must be small enough for us to be operating in the laminar flow regime. Within the fin one dimensional heat transfer is assumed. Under the Boussinesq approximation and assuming that there is negligible viscous dissipation the boundary layer equations become

$$\frac{\partial u'}{\partial x'} + \frac{\partial v'}{\partial y'} = 0 \qquad (1)$$

$$u' = U_\infty + g\beta(T - T_\infty) \qquad (2)$$

$$u'\frac{\partial T}{\partial x'} + v'\frac{\partial T}{\partial y'} = \alpha\frac{\partial^2 T}{\partial y'^2} \qquad (3)$$

For the fin an energy balance gives

$$\frac{\partial^2 T}{\partial x'^2} + \frac{k_f}{k_s b}\left[\frac{\partial T}{\partial y'}\right]_w = 0 \qquad (4)$$

Equations (1)-(4) have now to be solved subject to the boundary conditions,

$$\left.\begin{aligned} v' &= 0 \\ T_f &= T_w \\ -k_s\frac{\partial T_f}{\partial y'} &= k_s\frac{\partial^2 T_w}{\partial x'^2} \end{aligned}\right\} \quad \text{on } y' = 0,\ x' > 0 \qquad (5)$$

$$u' \to U_\infty,\ T \to T_\infty \quad \text{as } y' \to \infty, \text{ all } x' \le L \qquad (6)$$

$$T_w = T_b \quad \text{on} \quad x' = L \qquad (7)$$

We now introduce the similarity variables which are appropriate to those used in natural convection. This transformation of variables also allows us to solve the forced convection problem easily. However, if the similarity variables

appropriate for forced convection are introduced into the partial differential equations (1)-(4) the resulting equations would contain the parameter Ra/Pe which obviously cannot be used in free convection when Pe → 0. Therefore the variables used in the present analysis are

$$\left.\begin{aligned} \eta &= \frac{y'}{x'} Ra_x^{\frac{1}{4}}, \quad \xi = \frac{x'}{L} \\ \psi &= \alpha\, Ra_x^{\frac{1}{4}}\, f(\eta,\xi) \\ \theta &= \frac{T - T_\infty}{\Delta T}, \quad \Delta T = T_b - T_\infty \\ u' &= \frac{\partial \psi}{\partial y'}, \quad v' = -\frac{\partial \psi}{\partial x'} \\ F &= \frac{\partial f}{\partial \eta} \end{aligned}\right\} \quad (8)$$

On introducting these natural convection similarity variables equation (1) is identically satisfied and the governing equations become

$$F = \frac{\partial f}{\partial \eta} \quad (9)$$

$$F = \frac{Pe_\xi}{Ra_\xi} + \theta \quad (10)$$

$$\xi F \frac{\partial \theta}{\partial \xi} - \frac{1}{2} f \frac{\partial \theta}{\partial \eta} - \xi \frac{\partial f}{\partial \xi} \frac{\partial \theta}{\partial \eta} = \frac{\partial^2 \theta}{\partial \eta^2} \quad (11)$$

$$\frac{\partial^2 \theta_w}{\partial \xi^2} + \frac{CCP}{\xi^{\frac{1}{4}}} \left[\frac{\partial \theta}{\partial \eta}\right]_w = 0 \quad (12)$$

where the parameter CCP is given by

$$CCP = \frac{k_f L\, Ra^{\frac{1}{4}}}{k_s b} \quad (13)$$

Equations (8)-(11) must now be solved subject to the boundary conditions (5) and (6) which can be written in the appropriate variables as

$$f = 0, \ \theta_w = \theta_f, \ k_s \left[\frac{\partial^2 \theta}{\partial \xi^2}\right]_w = -k_f \left[\frac{\partial \theta_f}{\partial \eta}\right]_w \text{ on } \eta = 0 \quad (14)$$

$$F \to 1, \ \theta \to 0 \text{ as } \eta \to \infty \quad (15)$$

$$\theta_w = 1 \text{ on } \xi = 1 \quad (16)$$

In order to solve equations (9)-(12) subject to the boundary conditions (14)-(15) we require the initial profile. This can be obtained by setting $\xi = 0$ in the governing equations which then reduce to

$$F = \frac{df}{d\eta} \quad (17)$$

$$F = \frac{Pe_\xi}{Ra_\xi} + \theta \quad (18)$$

$$\frac{d^2\theta}{d\eta^2} + \frac{1}{2} f \frac{d\theta}{d\eta} = 0 \quad (19)$$

NUMERICAL PROCEDURE

The solution procedure is very similar to that used by Sunden [4] and therefore the full details will not be presented here.

Within the fin the governing equation is discretised using M intervals so that the grid size is $\Delta\xi = 1/M$ and calculations were performed with M = 100, 200 and 400. Within the boundary layer a rectangular grid was used with $\Delta\xi = 1/M$ and $\Delta\eta = \eta_\infty/N$ with all of the results presented in this paper corresponding to N = 80. The value of η_∞ was varied until accurate results were achieved.

A finite difference scheme which is second order accurate over the entire solution domain is derived by using central differencing at all the nodes. Even though we are using a scheme which is second order accurate everywhere the number of nodes required to solve the problem is large due to the inaccuracies which are inherent in the problem at the fin tip.

The solution procedure may be summarised as follows:

1. The parameters k_s, k_f, L, b, Ra_ξ and Pe_ξ are specified.
2. The variation of the wall temperature is guessed. It was found that a parabolic variation was always a reasonable first approximation.
3. The initial profiles at $\xi = 0$ were obtained by solving the ordinary differential equations (17)-(19) subject to the boundary conditions $f(0) = 0$, $\theta(0) = \theta_w$, $\theta(\infty) = 0$. Central difference approximations were used throughout and an iterative procedure employed.
4. Since equation (11) is parabolic a marching procedure, which is similar to the Crank Nicolson scheme, is employed to solve equation (11) whilst central differences are used to discretise equation (9).
5. The temperature gradient $\left[\frac{\partial \theta}{\partial \eta}\right]_{\eta=0}$ is evaluated using a second order approximation.

6. Using equation (12) a new temperature distribution along the fin wall is obtained. It is observed that equation (12) cannot be used at $\xi = 0$ because of the $\xi^{-\frac{1}{2}}$ term. Thus in the first element at the fin tip we need to carry out a separate heat balance. In order to find the heat flow from this surface we perform one integration along this element of surface and equation (12) for this element becomes

$$\frac{\partial \theta_w}{\partial \xi} + CCP \left[\frac{\partial \theta}{\partial \eta}\right]_w (\Delta\xi)^{\frac{1}{2}} = 0 \qquad (20)$$

7. The new temperature variation of the wall is now compared with the previous variation. If the sum of the differences in temperature at corresponding nodes is within some prescribed tolerance then the iteration process is complete otherwise we go back to step 3 and continue. The tolerance was varied but it was found that very accurate results could be obtained with 10^{-3}.

In order to obtain very accurate results the Richardson extrapolation method was employed. This method requires three different solutions using different grid sizes. In this paper we use grid sizes which are in the ratio 1:2:4. Using these three results then the extrapolated result u_e can be obtained from the expression $u = u_e + A(\Delta\xi)^p$ where A and p are unknown constants and u is the physical quantity required.

In setting the size of the solution domain we must ensure that we place the infinite boundary condition sufficiently far from the wall, i.e. the value of η_∞ must be sufficiently large. If this is not done then artificially high values of the velocity and temperature gradients will be obtained. This is because the velocity and temperature are forced to the ambient conditions too quickly, thus resulting in the rapid fall in their values near the wall.

In the case of adverse flow, when U_∞ is sufficiently small, such that neither free nor forced convection dominates, separation may occur. The range of values Pe/Ra for which separation occurs can be found by using the numerical scheme as described above with negative values of Pe/Ra. Separation will first occur at the base of the fin when the upflow due to the natural convection is largest since at this point the temperature difference, and hence the bouyancy force, is greatest.

The numerical method employed here is unable to solve the finite difference equations past the point where the flow reverses as the governing equations are parabolic and a marching procedure has been used. The onset of separation indicates that information is travelling to the node under investigation from the fin tip. If flow reversal occurs along the surface of the fin information concerning the flow is coming from both directions rather than just from the fin tip so the governing equations are singular parabolic partial differential equations and the solution procedure fails.

RESULTS

In order to test whether we are operating within the validity of Darcy's law we investigate the parameter

$$Pn_x = \sqrt{\frac{K^2 g\beta (T_w - T_\infty)}{\nu^2 x}} \qquad (21)$$

as suggested by Hsu and Cheng [7]. The size of Pn_x is a measure of the thickness of the viscous sub-layer as compared with the thermal boundary layer thickness and therefore we require $Pn_x << 1$ for the Darcy law to hold. Clearly near the fin tip, x = 0, Darcy's law is not appropriate but neither is the boundary layer approximation. For the temperature differences of order 10^2 °C we find that the Darcy law may be applied. However Hsu and Cheng [7] did find that even when the viscous sub-layer is significant the effect on the temperature profile acorss the boundary layer is not significant.

Cheng and Ali [8] have shown that Darcian flow can only be observed when the value of the non-Darcian Grashof number, Gr, is less than about 0.03. Using typical values for the constants associated with the porous medium, i.e. the particle diameter, permeability and porosity, we find that for the system considered the non-Darcian Grashof number is 0.002. This means that we are operating well within the limits of the Darcian flow approximations. All the results presented in this paper being based on air at 20°C.

After trying several values of η_∞, the station at which the infinity boundary conditions are enforced, it was found that $\eta_\infty = 10$ was sufficiently large for all values of the parameter CCP. In fact it was observed that the velocity and temperature profiles had effectively reached their ambient values at $\eta = 7$ in most computations performed.

The tolerance used in all the iterative procedures was varied but it was found that a value of 10^{-3} was sufficiently small in order to obtain accurate results. In all cases the tolerance was obtained by evaluating the sum of the absolute differences at all mesh points between two iterations for all quantities being calculated.

Figure 2 shows the temperature profile along the wall for two values of the convection-conduction parameter CCP and for Pe/Ra = 550. Also shown in figure 2 are the results found by Sunden [9] for the non porous problem. These results have also been recalculated by the authors in order to check that both the results of Sunden and the numerical procedure described by the authors in the present paper are accurate.

It should be observed that the value of the parameter Pe/Ra has been chosen such that the

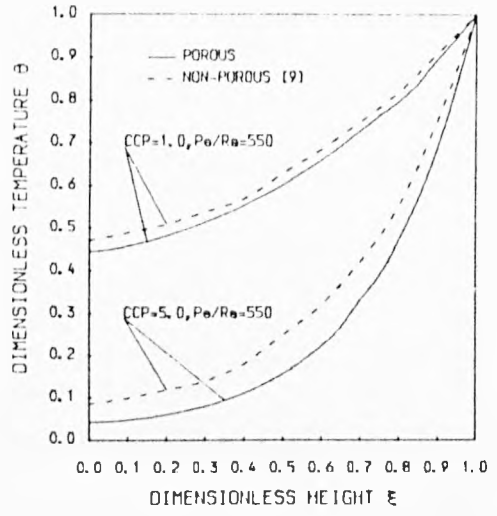

Figure 2. The variation of the temperature at the wall as a function of the distance along the wall for Pe/Ra = 550 and CCP = 1.0 and 5.0.

velocity U_∞ is the same as that given by Sunden. The value of this parameter is, however, significantly different since the Grashof number is based on the product of permeability and length and not just the length.

Figure 3 shows the variation of the temperature on the fin as a function of distance along the fin for two different values of the ambient velocity, one of which is zero and corresponds to natural convection.

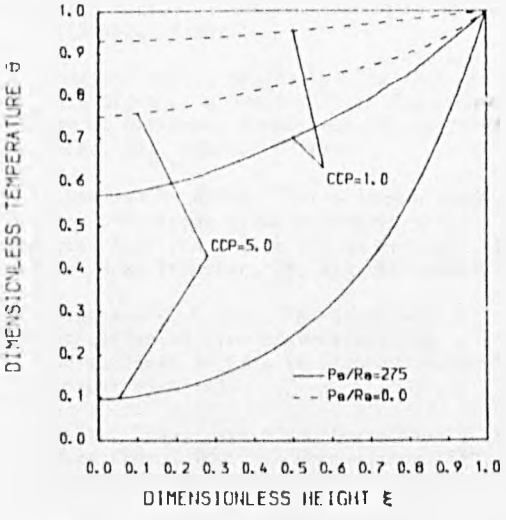

Figure 3. The variation of the temperature at the wall as a function of the distance along the wall for Pe/Ra = 0 and 275 and CCP = 1.0 and 5.0.

CONCLUSIONS

The present numerical method gives general results for a fin which is embedded in a porous medium. The method of solution does not require a form for the temperature profile to be assumed a priori unlike previous similarity solutions [3, 7]. The variables employed are the similarity variables as used when solving the natural convection problem with the fin maintained at a constant temperature. This allows us to solve the mixed and free convection problems using the same formulation.

From the results found we may conclude that,

1. Surrounding a fin in a porous medium, as opposed to a free fluid, decreases the temperature of the fin, see figure 2. This shows that the heat transferred from a fin embedded in a saturated porous medium is more than from an identical fin in a free fluid.
2. The temperature of the fin tip is significantly higher than the ambient fluid, see figures 2 and 3. Therefore if one assumes the fin tip temperature to be that of the ambient fluid inaccurate results will be obtained. Hence it is inappropriate to approximate the conjugate problem with any existing similarity solution.
3. Flow separation occurs only when the value of Pe/Ra is small and negative. This range of values is given by $-0.98 < Pe/Ra < 0$ for CCP = 1.0.

It has been found that the solution procedure is very sensitive to the tolerance imposed on the iterative procedures. This is due to the fact that the partial differential equations are coupled and hence the variables f, F and θ are also coupled. If the tolerance is set too low the solution procedure ends rapidly whilst the errors in the solution for f, F and θ are still oscillating about a high tolerance level. As soon as the tolerance is decreased below this oscillating point errors reduce monotonically and reducing the tolerance still further does not have a significant effect on the results although it does on the computational time.

NOMENCLATURE

CCP convection-conduction parameter $\sqrt{Ra}\,\frac{k_f L}{k_s b}$

d diameter of porous medium

f,F variables defined in equation (5)

g acceleration due to gravity

Gr Grashof number, $g\beta KL(T_b - T_\infty)/\nu^2$

$\hat{G}r$ Modified Grashof number, $\sqrt{K}\beta g(T_w - T_\infty)/\nu^2$

k thermal conductivity

K permeability of medium

L length of fin

Pe Peclet number, $U_\infty L/\nu$

Pe_x local no-slip parameter, $\left[\frac{K^2\beta g(T_w - T_\infty)}{\nu\alpha_{max}}\right]^{\frac{1}{2}}$

Pr Prandtl number, ν/α

Ra Rayleigh number, $g\beta KL(T_b - T_\infty)/(\nu\alpha)$

Re Reynolds number, $U_\infty L/\alpha$

Greek

β coefficient of expansion
η dimensionless coordinate, $y'Ra_x^{\frac{1}{4}}/x'$
ξ dimensionless coordinate, x'/L
θ dimensionless temperature, $(T - T_\infty)/(T_b - T_\infty)$
ψ stream function
λ Forchheimer's coefficient, $1.75d/(150(1 - \varepsilon))$
ε porosity of medium

Subscripts

w wall
f fluid
s solid
∞ ambient

REFERENCES

[1] W. P. Harper and D. R. Brown, "Mathematical Equations for Heat Conduction in the Fins of Air-Cooled Engines". N.A.C.A. Report 158 (1922)

[2] G. S. M. Lock and J. C. Gunn, "Laminar Free Convection from a Downward Facing Fin". Trans ASME J. Heat Transfer, 90, 63-70 (1968).

[3] P. Cheng and W. J. Minkowycz, "Free Convection about a Vertical Flat Plate Embedded in a Porous Medium with Application to Heat Transfer from a Dyke". J. Geophysics Res, 82, 2040-2049 (1977).

[4] B. Sunden, "A Numerical Investigation of Coupled Conduction - Mixed Convection for Rectangular Fins". Proc. Third Int. Conf. on Num. Methods in Laminar and Turbulent Flows, Pineridge Press, 809-819 (1983).

[5] A.Bejan and R. Anderson, "Heat Transfer across a Vertical Impermeable Partition Embedded in a Porous Medium". Int. J. Heat Mass Transfer, 24, 1237-1245 (1981).

[6] R. Anderson and A. Bejan, "Natural Convection on Both Sides of a Vertical Wall Separating Fluids at Different Temperatures". J. Heat Transfer, 102, 630-635 (1980).

[7] C. T.Hsu and P. Cheng, "The Brinkman Model for Natural Convection about a Semi-infinite Vertical Flat Plate in a Porous Medium", Int. J. Heat Mass Transfer, 28, 683-697 (1985).

[8] P. Cheng and C. L. Ali, "An Experimental Investigation of Free Convection about a Heated Inclined Surface in a Porous Medium", ASME paper 81-HT-85.

[9] B. Sunden, "Conjugate Mixed Convection Heat Transfer from a Vertical Rectangular Fin", Int. Comm. Heat Mass Transfer, 10, 267-276 (1983).